Induction, execution and clinical relevance of TNF- and TRAIL-induced necroptosis

Dissertation

zur Erlangung des Doktorgrades

der Mathematisch-Naturwissenschaftlichen Fakultät

der Christian-Albrechts-Universität zu Kiel

vorgelegt von

Susann Voigt

Kiel

2014

Erster Gutachter:	Prof. Dr. Dieter Adam
Zweiter Gutachter:	Prof. Dr. Dr. Thomas C. G. Bosch
Tag der mündlichen Prüfung:	01.07.2014
Zum Druck genehmigt:	01.07.2014

gez. Prof. Dr. Wolfgang J. Duschl, Dekan

Meinem Großvater

Walter Bronkalla
(1932-2011)

I. Table of contents

II. Abbreviations

AAA	ATPases associated with diverse cellular activities
ABC	ammonium bicarbonate
ACN	acetonitrile
ac-zDEVD-afc	benzyloxycarbonyl-Asp-Glu-Val-Asp-7-aminotrifluoromethylcoumarin
ac-zIETD-afc	benzyloxycarbonyl-Ile-Glu-Thr-Asp-aminotrifluoromethylcoumarin
ADAMTS18	a disintegrin and metalloproteinase with thrombospondin motifs 18
AIF	apoptosis inducing factor
ANT	adenine nucleotide translocase
Apaf-1	apoptotic protease activating factor-1
AP-Q	aminopeptidase Q
ASC	apoptosis-associated speck-like protein containing a CARD
A-SMase	acid sphingomyelinase
ATCC	American Type Culture Collection
ATP	adenosine-5'-triphosphate
Bcl-2	B-cell CLL/lymphoma-2
BSA	bovine serum albumin
CARD	caspase activation and recruitment domain
Cas	cellular apoptosis susceptibility
Caspase	cysteine-aspartate protease
CASP8	caspase-8
CAT	catalase
CBPQ	carboxypeptidase Q
CFLAR	caspase 8 and FADD-like apoptosis regulator
CFL-1	cofilin-1
c-FLIP	cellular FLICE-inhibitory protein
CHX	cycloheximide
cIAP	cellular inhibitor of apoptosis protein
CID	collision-induced dissociation
COXIV	cytochrome c oxidase subunit 4
CrmA	cytokine response modifier protein A
Ctr	control
CYLD	cylindromatosis
CypD	cyclophilin D
DAG	diacylglycerol
DAMPs	damage associated molecular patterns
DAPK	death-associated protein kinase
dATP	deoxyadenosine triphosphate
DD	death domain
DESC	transmembrane protease serine 11E
DIABLO	direct inhibitor of apoptosis protein binding protein with low pI
DIE	insulysin
DISC	death inducing signaling complex
DKO	double knock-out
DMF	dimethylformamide
DNML1	dynamin 1-like protein
DPP8	dipeptidyl peptidase 8
DPYL	dihydropyrimidinase-related protein

DPYSL4	dihydropyrimidinase-like 4
DRs	death receptors
Drp-1	dynamin 1-like protein
dsRNA	double-stranded RNA
DTT	dithiothreitol
DUBs	deubiquitinating enzymes
EDAR	ectodysplasin A receptor
ENO1	alpha-enolase
ER	endoplasmatic reticulum
ESI	electrospray ionization
ET	extracellular trap
FA	formic acid
FADD	Fas-associated protein with death domain
FBP2	fructose-1,6-bisphosphatase 2
FCS	fetal calf serum
FFCK	fluorescently labeled N-tosyl-L-phenylalanine chloromethyl ketone-derivative
FH	fumarate hydratase
FLICE	FADD-like IL-1β-converting enzyme
$FLIP_L$	FLICE-like inhibitory protein long isoform
G6P	glucose-6-phosphate
Gas2	growth arrest-specific protein 2
GDIA2	Rho GDP-dissociation inhibitor 2
GFP	green fluorescent protein
GGT1	gamma-glutamyltransferase 1
GLT25D1	glycosyltransferase 25 domain-containing 1
GLUD1	glutamate dehydrogenase 1
GLUL	glutamate-ammonia ligase
HAX-1	HCLS1-associated protein X-1
HB	homogenization buffer
HCD	higher-energy collisional dissociation
HNRNP	heterogeneous nuclear ribonucleoprotein
HPLC	high performance liquid chromatography
HRP	horseradish peroxidase
HSPB1	heat shock protein beta-1
HtrA	high temperature requirement protein A
IAP	inhibitor of apoptosis protein
I-CLIPs	intramembrane-cleaving proteases
IDH1	isocitrate dehydrogenase 1
IEF	isoelectric focusing
IF	immunofluorescence
IFN	interferon
IKK	IκB kinase
IL	interleukin
IMPDH2	inosine-5’-monophosphate dehydrogenase 2
iTRAQ	isobaric tag for relative and absolute quantification
JNK	c-Jun N-terminal kinases
LAMP	lysosome-associated membrane glycoprotein
LARD	lymphocyte-associated receptor of death
LB	lysogeny broth
LC	liquid chromatography
LF	lung fibroblast
LMP	lysosomal membrane permeabilization
LONM	Lon protease 1
LONP1	Lon protease 1
LPS	lipopolysaccharide

LUBAC	linear ubiquitin chain assembly complex
MALDI	matrix-associated laser desorption/ionization
MEF	mouse embryonic fibroblast
MEP1B	meprin β
MLKL	mixed lineage kinase domain-like
MMP3	metalloproteinase 3 or stromelysin-1
MMS	methyl methanesulfonate
MNNG	1-methyl-3-nitro-1-nitrosoguanidine
MOMP	mitochondrial outer membrane permeabilization
MS	mass spectrometry
MSN	moesin
MTT	3-[4,5-dimethylthiazol-2yl]-2,5-diphenylterazolium bromide
M6P	mannose-6-phosphate
NAD	nicotinamide adenine dinucleotide
NADPH	nicotinamide adenine dinucleotide phosphate
Nec-1	necrostatin 1
NEMO	NF-κB essential modulator
NET	neutrophil extracellular trap
NF-κB	nuclear factor-κB
NGFR	nerve growth factor receptor
NIK	NF-κB-inducing kinase
NOD	nucleotide-binding oligomerization domain
Nox1	NADPH oxidase-1
NSA	necrosulfonamide
N-SMase	neutral sphingomyelinase
OPA1	optic atrophy 1
OPG	osteoprotegerin
PAGE	polyacrylamide gel electrophoresis
PAK2	p21 activated kinase 2
PARP	poly (ADP-ribose)-polymerase
PBS	phosphate buffered saline
PCD	programmed cell death
PDIA6	protein disulfide isomerase A6
Pea-15	phosphoprotein enriched in astrocytes 15
PFA	paraformaldehyde
PGAM	phosphoglycerate mutase family member
PHGDH	D-3-phosphoglycerate dehydrogenase
PI	propidium iodide
PKC	protein kinase C
PKM	pyruvate kinase isozymes M1/M2
PKR2	cAMP-dependent protein kinase type II-alpha regulatory subunit
PLA_2	phospholipase A_2
PMPCA	mitochondrial processing peptidase alpha
POD	alkaline phosphatase
PRPF8	pre-mRNA processing factor 8
PSA1	proteasome subunit, alpha type-1
PSMA1	proteasome subunit, alpha type-1
PTPC	permeability transition pore complex
PYGL	glycogen phosphorylase
Rab	Ras-related protein
RHIM	RIPK homotypic interaction motif
RIPK	receptor-interacting serine-threonine protein kinase
RNAi	RNA interference
ROCK-1	Rho-associated, coiled-coil containing protein kinase 1
ROS	reactive oxygen species
RT	room temperature

SDS	sodium dodecyl sulphate
siRNA	small interfering RNA
SM	Smac mimetic/sphingomyelin
Smac	second mitochondria-derived activator of caspases
SMase	sphingomyelinase
SPH	sphingosine 1-phosphate
SPP	signal peptide peptidase
SPPL	signal peptide peptidase-like
S-SMase	secretory sphingomyelinase
STMN1	stathmin
SV40	simian virus 40
TAB	transforming growth factor-β-activated kinase-binding protein
tAIF	truncated apoptosis inducing factor
TAILS	terminal amine isotopic labeling of substrates
TAK1	TAB kinase 1
TARD	tumor necrosis factor-receptor-related apoptosis-mediating protein
TCA	trichloroacetic acid
TFA	trifluoroacetic acid
TFCK	N-tosyl-L-phenylalanine chloromethyl ketone
TLR	Toll-like receptor
TMPRSS11E	transmembrane protease serine 11E
TNF	tumor necrosis factor
TNF-R	TNF-receptor
TOF	time-of-flight
TR3	TNF-receptor-like 3
TRADD	TNF-R1-associated protein with death domain
TRAF2	TNF-R-associated factor 2
TRAIL	TNF-related apoptosis inducing ligand
TRAIL-R	TRAIL-receptor
TRMP	transient receptor potential channels of the melastatin-like family
TRMP7	transient receptor potential cation channel, subfamily M, member 7
TUBA1B	tubulin alpha-1B chain
VDAC	voltage-dependent anion channel
wt	wild-type
YME1L1	YME1-like ATPase
zVAD-fmk	benzyloxycarbonyl-Val-Ala-Asp-fluoromethylketone
2D-PAGE	two-dimensional polyacrylamide gel electrophoresis
2D-DIGE	two-dimensional difference gel electrophoresis

Commonly used abbreviations are not listed.

III. List of Figures

IV. List of Tables

1. Summary

Regulated necrosis is important in many (patho)physiological settings. In contrast to apoptosis, the molecular mechanisms of the induction and execution of regulated necrosis are only marginally understood. This thesis therefore presents detailed analyses of different aspects of regulated necrosis: the characterization of distinct routes to regulated necrosis, the identification of novel proteins involved in the execution of necroptosis and the study of the applicability of tumor necrosis factor (TNF)-related apoptosis inducing ligand (TRAIL)-induced regulated necrosis in clinically relevant systems.

In the first part of the thesis, it is shown that TNF-induced necroptosis and induction of the poly (ADP-ribose)-polymerase (PARP) pathway by DNA-damaging agents such as MNNG represent distinct and independent routes to regulated necrosis. The interruption of the PARP pathway by PARP-1 inhibitors prevented MNNG- but not TNF-induced necroptosis and the genetic interference with JNK kinases and the protease cathepsin D as further components of the PARP pathway did not affect TNF-induced necroptosis. Likewise, the interference with components important for TNF-induced necroptosis such as the kinase RIPK3 did not prevent regulated necrosis through the PARP pathway.

In the course of the work of this doctoral thesis, new components of the execution signaling mechanisms of TNF-induced necroptosis could be discovered. Experiments aimed at the identification of serine protease(s), which appear to be crucial in this pathway, found the serine protease HtrA2/Omi as a promising candidate. Pharmacological inhibition or genetic deletion of HtrA2/Omi protected from TNF-induced necroptosis, further substantiating its functional impact on necroptosis. In addition to HtrA2/Omi, the proteases Lon protease 1, PSA1 and PMPCA were identified as further potential components of the TNF-induced necroptotic pathway. By RNA interference screens using siRNAs targeting all proteases encoded by the human genome, 16 proteases were identified whose down-regulation affects necroptosis in HT-29 cells. The impact of the candidate proteases CYLD, CASP8, DESC, GGT1, DPYL4, PRPF8, MMP3 and CFLAR on TNF-induced necroptosis could be also verified in U-937 cells. Additionally, the comparison of the proteomes of healthy cells or cells undergoing TNF-induced necroptosis via 2D-DIGE in combination with mass spectrometry revealed differentially expressed proteins (TUBA1B, PKM, CFL-1, IMPDH2, PHGDH, CAT) and possible substrates for proteolytic cleavage during necroptosis (moesin, stathmin). Furthermore, it was shown that acid sphingomyelinase (A-SMase) is proteolytically cleaved and activated in TNF-induced necroptosis. Besides the proteolytic regulation of A-SMase, it could be demonstrated that the potentially pro-necroptotic protein PGAM5 is constitutively degraded by yet unknown proteases in healthy cells and that this degradation is blocked upon induction of TNF-induced necroptosis.

Additionally, presenilins, which are parts of the catalytic core of the γ-secretase protease complex, were found to be involved in the execution of necroptosis.

In the third part of the thesis, new and additional information on the potential of TRAIL-induced necroptosis in clinically relevant tumor cell lines of wide-ranging origin was obtained. Eight out of 14 tumor cell lines were spontaneously sensitive to TRAIL-induced regulated necrosis and Smac mimetics could further enhance TRAIL-induced regulated necrosis. Clonogenic survival was reduced in all sensitive and even one resistant cell lines tested and TRAIL synergized with chemotherapeutics in killing resistant cell lines by regulated necrosis. At the molecular level, the obtained data point to a relation of the kinases RIPK3 and MLKL as primary targets for resistance or susceptibility of the analyzed tumor cells to regulated necrosis. Finally, the pharmacological inhibition of the ceramide generating-enzyme A-SMase showed protection against TRAIL- and TNF-induced necroptosis in multiple tumor cell lines, extending the previously established role of ceramide as a pivotal downstream mediator of death receptor-induced regulated necrosis and thus as a potential target for future therapy of cancer patients.

Altogether, the data presented in this thesis substantiate the hypothesis that there are several independent pathways to regulated necrosis. The study provides a more detailed picture of necroptosis with newly identified proteins involved in the execution of necroptosis and it provides evidence that TRAIL-induced regulated necrosis represents a feasible approach for the elimination of tumor cells. In the long term, a better understanding of necroptosis and the distinct pathways of regulated necrosis may help to define potential targets for future therapies for diseases that arise from deregulated necrosis.

1.1 Zusammenfassung

Die regulierte Nekrose stellt einen wichtigen Mechanismus in physiologischen und pathophysiologischen Szenarien dar. Im Gegensatz zur Apoptose sind die Induktions- und Wirkungsmechanismen der regulierten Nekrose nur ansatzweise erforscht. Die vorliegende Arbeit präsentiert daher detaillierte Analysen über relevante Aspekte der regulierten Nekrose: die Charakterisierung verschiedener Wege zur regulierten Nekrose, die Beschreibung neuer Proteine, die an der Ausführung der TNF-induzierten Nekroptose beteiligt sind und die Untersuchung ob TRAIL-induzierte Nekroptose auch in klinisch relevanten Systemen angewendet werden kann.

Die Ergebnisse aus dem ersten Teil dieser Arbeit zeigen, dass die TNF-induzierte Nekroptose und die Induktion der PARP-vermittelten regulierten Nekrose durch DNA-schädigende Agenzien wie MNNG zwei verschiedene und völlig voneinander unabhängige Wege der regulierten Nekrose darstellen. Die Blockierung der PARP-vermittelten regulierten Nekrose durch PARP-1 Inhibitoren verhinderte die MNNG-vermittelte, jedoch nicht die TNF-induzierte regulierte Nekrose. Die genetische Deletion nachgeschalteter Komponenten der PARP-vermittelten regulierten Nekrose (JNK Kinasen oder die Protease Cathepsin D) hatte keinen Effekt auf die TNF-induzierte regulierte Nekrose. Gleichermaßen hatte eine Inhibition der TNF-induzierten Nekroptose durch die Blockierung der für die Nekroptose essentiellen Proteinkinase RIPK3 keine Auswirkung auf die Aktivierung der PARP-vermittelten regulierten Nekrose.

In der vorliegenden Arbeit konnten neue Komponenten der exekutiven Signaltransduktion der TNF-vermittelten Nekroptose identifiziert werden. Experimente zur Identifizierung von Serinproteasen, welche wichtig für die Weiterleitung des nekroptotischen Signals zu sein scheinen, konnten HtrA2/Omi als vielversprechenden Kandidaten identifizieren. Ein Aktivitätsverlust von HtrA2/Omi durch die pharmakologische Inhibition oder genetische Ablation blockierte die TNF-induzierte Nekroptose, was als ein weiterer Beleg für eine wichtige Rolle von HtrA2/Omi in der Nekroptose gewertet werden kann. Neben HtrA2/Omi konnten außerdem die Proteasen Lon protease 1, PSA1 und PMPCA als weitere potentielle Komponenten der TNF-induzierten Nekroptose identifiziert werden. In einem komplementären Ansatz wurden alle im humanen Genom kodierten Proteasen mittels eines „small interfering“ siRNA Screens auf ihre Relevanz in der TNF-induzierten Nekroptose untersucht. In humanen HT-29 Zellen konnten 16 Proteasen ermittelt werden, deren Inhibition Effekte auf die TNF-induzierte Nekroptose zeigte. Die Bedeutung bestimmter Proteasen (CYLD, CASP8, DESC, GGT1, DPYL4, PRPF8, MMP3 und CFLAR) konnte auch in einem weiteren Zellsystem, humanen U-937 Zellen, bestätigt werden. Zusätzlich konnten während des Vergleiches der Proteome von gesunden und nekroptotischen Zellen im 2D-DIGE Verfahren und nachfolgender Massenspektrometrie differenziell exprimierte Proteine (TUBA1B, PKM, CFL-1, IMPDH2, PHGDH, CAT) und mögliche Substratproteine für proteolytische Spaltung (Moesin, Stathmin) in nekroptotischen Zellen

nachgewiesen werden. Weiterhin konnte eine proteolytische Spaltung und die damit verbundene Aktivierung der sauren Sphingomyelinase (A-SMase) während der TNF-induzierten Nekroptose erstmals beschrieben werden. Neben der proteolytischen Aktivierung der A-SMase wurde eine proteolytische Degradierung des potentiell Nekroptose-vermittelnden Proteins PGAM5 in gesunden Zellen durch noch unbekannte Proteasen nachgewiesen. Dieser Abbau von PGAM5 wird durch die Einleitung der Nekroptose gehemmt. Weiterhin wurden Anhaltspunkte gefunden, dass Präseniline, die einen Teil des γ-Sekretase-Komplexes bilden, in der Nekroptose eine Rolle spielen.

Im dritten Teil dieser Arbeit wurden neue und vielversprechende Informationen über die Induktion von nekroptotischen regulierten Zelltod durch TRAIL in klinisch relevanten Tumorzelllinien gewonnen. Acht der 14 untersuchten Zelllinien zeigten eine Sensibilität für nekroptotischen TRAIL-vermittelten Zelltod. Diese Reaktion konnte durch die Zugabe von Smac-nachahmenden Molekülen noch verstärkt werden. Die Behandlung der Tumorzelllinien mit TRAIL ging einher mit dem Verlust der Klonogenität der sensitiven Tumorzelllinien und darüber hinaus auch einer resistenten Tumorzelllinie. Des Weiteren konnte gezeigt werden, dass die gemeinsame Behandlung mit TRAIL und Chemotherapeutika in den meisten resistenten Tumorzelllinien in Synergie regulierte Nekrose induziert. Auf molekularer Ebene zeigten die generierten Daten, dass RIPK3 und MLKL primäre Faktoren für die Resistenz oder Empfindlichkeit einzelner Zelllinien darstellen. Die pharmakologische Inaktivierung des Ceramid-produzierenden Enzyms A-SMase führte ebenfalls zu einer Blockierung der TRAIL- und TNF-vermittelten Nekroptose. Schlussfolgernd stellt Ceramid damit ein Schlüsselmolekül in der Todesrezeptor-vermittelten regulierten Nekrose dar und kann somit als potentielles Zielmolekül für eine zukünftige Therapie von Krebspatienten angesehen werden.

Zusammenfassend untermauern die Ergebnisse der vorliegenden Arbeit die Existenz verschiedener, voneinander unabhängiger Signalwege der regulierten Nekrose. Die vorliegende Studie liefert ein detaillierteres Bild über neu identifizierte Proteine, die in die Prozesse der regulierten Nekrose eingebunden sind und liefert Belege, dass die TRAIL-vermittelte regulatorische Nekrose einen sinnvollen Ansatz für die Eliminierung von Tumorzellen darstellt. Langfristig kann ein verbessertes Verständnis der Nekroptose und der verschiedenen Signalwege der regulierten Nekrose dabei helfen, neue Zielmoleküle zu identifizieren, welche für die Entwicklung zukünftiger Behandlungsstrategien von Krankheiten wichtig sein könnten, die durch deregulierten Zelltod verursacht werden.

2. Introduction

The balance between cell survival and cell death is a fundamental concept in biology, regulating the development and homeostasis of every organism. Already in 1842, the process of natural cell death was described by Carl Vogt. While studying tadpoles and their metamorphosis, he realized that the resorption and replacement of the notochord by the vertebrae must be a physiological process involving the death of certain cells (Vogt, 1842). Programmed cell death (PCD), first described in 1964 by Lockshin and Williams, was defined as an important regulated cellular mechanism (Lockshin and Williams, 1964), likely involved in many human pathologies from viral infections to tumor formation or neurodegenerative diseases. PCD not only influences development: it is also involved in regulating tissue homeostasis by eliminating unwanted and harmful cells (Degterev and Yuan, 2008). Experiments using *Caenorhabditis elegans* unraveled, amongst others, the genetic program of apoptosis (Ellis and Horvitz, 1986). Apoptosis is defined by the induction of PCD through the activation of caspases (Galluzzi *et al.* 2012a), which is the classical and most studied primary route to death in most cell types. Historically, apoptosis was regarded to be the only form of PCD, whereas necrosis was considered to be an accidental, uncontrolled cell death as a consequence of extreme physicochemical stress. However, in the last 20 years, increasing evidence has accumulated showing that PCD can also occur independent from caspases and that different regulated types of necrosis exist. For example, it was shown that caspase inhibition can switch the toxic response evoked by TNF from apoptosis to necrosis (Vercammen *et al.* 1998a). In 2000, Holler and coworkers reported that the death receptor CD95 is, in some cell types, able to trigger necrotic-like cell death. This process is independent of caspases but dependent on both the adaptor protein Fas-associated protein with death domain (FADD) and receptor-interacting serine-threonine kinase 1 (RIPK1; Holler *et al*. 2000). The discovery of chemical inhibitors of necrosis led to the accumulation of additional lines of evidence for regulated types of necrosis (Degterev *et al.* 2005; Sun *et al.* 2012). The mechanisms of necrosis have been intensively investigated, revealing the existence of multiple pathways of regulated necrosis (discussed in detail in chapter 2.2). In the future, a better understanding of these pathways could be directly translated into improved therapies, for e.g., cancer, stroke or neurodegenerative diseases (Degterev and Yuan, 2008; Vandenabeele *et al.* 2010).

2.1 Caspase-dependent programmed cell death – apoptosis

The first study on the biochemical mechanisms of apoptosis was published in 1972 (Kerr *et al.* 1972) and opened the way to explore the relevance of this mode of PCD in fundamental processes such as tissue remodeling, homeostasis and the development of multi-cellular organisms. Apoptosis is characterized by the activation of cysteine-aspartate proteases (caspases). Caspase-dependent PCD (apoptosis) is defined by an ensemble of morphological features, including membrane blebbing, chromatin condensation and DNA cleavage, resulting in the fragmentation of dying cells into

apoptotic bodies (Taylor *et al.* 2008). These apoptotic bodies can be phagocytized by macrophages or neighboring cells, resulting in the uptake of apoptotic corpses without the release of intracellular material into the environment, thereby avoiding an inflammatory response (Savill and Fadok, 2000). In the absence of a phagocytic system, apoptotic bodies lose their integrity which leads to the release of their content into the extracellular microenvironment, resulting in an inflammatory answer. This process is called secondary necrosis.

There are two main pathways of apoptosis, i.e. the extrinsic apoptosis pathway triggered by extracellular inducers and the intrinsic apoptosis pathway initiated mainly by stress factors. In the extrinsic apoptotic pathway, activation of caspases occurs through stimulation of death receptors (DRs) which belong to the TNF-receptor (TNF-R) superfamily. Upon binding of the corresponding ligand and stimulation of the DR, trimerization of the receptor molecules is induced with clustering of their cytoplasmic death domain (DD) and the formation of the death-inducing signaling complex (DISC). Distinct adaptor proteins e.g. TNF-R1-associated protein with death domain (TRADD) and FADD are recruited to the receptor and this interaction results in the recruitment of pro-caspase-8 and -10 to the DISC and subsequently to their auto-catalytical activation. Caspase-8 and -10 in turn proteolytically activate effector caspases such as caspase-3 (Figure 1; Galluzzi *et al.* 2012a) and initiate subsequent steps of proteolytic cleavage of, for example, substrate proteins that participate in cellular blebbing (gelsolin, Rho-associated, coiled-coil containing protein kinase 1 (ROCK-1), p21 activated kinase 2 (PAK2)), determine cell shape (cytokeratin-18, vimentin, growth arrest-specific protein 2 (Gas2) and plectin, fodrin, focal adhesion kinase, cellular apoptosis susceptibility (Cas) proteins or paxillin) or influence nuclear architecture. This altogether leads then to the ordered demise of the cell (Fischer *et al.* 2003). Downstream of caspase-8 activation, apoptosis can occur via two distinct mechanisms. In so-called type I cells, massive auto-proteolytic activation of caspase-8 leads to sufficient activation of subsequent effector caspases, e.g. caspase-3, whereas in type II cells only small quantities of cleaved, active caspase-8 are produced at the DISC. To ensure apoptosis in type II cells, apoptosis is in part dependent on the cleavage of the mitochondrial protein Bid to its truncated form tBid by caspase-8 (Figure 1; Scaffidi *et al.* 1998).

The intrinsic pathway is mainly initiated in response to non-receptor stimuli, including DNA damage, cytokine deprivation, hypoxia, oxidative stress and other types of severe cell stress (Galluzzi *et al.* 2012b). Proteins of the B-cell CLL/lymphoma-2 (Bcl-2) protein family which exhibit pro-survival and pro-apoptotic features control the intrinsic pathway by aggregation of pro-apoptotic Bcl-2 family members (e.g. BAX and BAK). Activated BAX and BAK initiate mitochondrial outer membrane permeabilization (MOMP) which leads to the swelling of mitochondria and to the loss of the mitochondrial inner transmembrane potential. Subsequently, this results in the release of mitochondrial intermembrane space proteins like cytochrome c, Smac (second mitochondria-derived activator of caspase)/DIABLO (direct inhibitor of apoptosis protein (IAP) binding protein with low

pI), HtrA2/Omi (high temperature requirement protein A2), apoptosis inducing factor (AIF) and endonuclease G into the cytoplasm. Cytoplasmic cytochrome c together with deoxyadenosine triphosphate (dATP) and the adaptor protein apoptotic protease activating factor 1 (Apaf-1) form a protein complex named apoptosome (Figure 1). The apoptosome activates the initiator caspase-9 resulting in the cleavage and activation of the effector caspases-3, -6 and -7 (Galluzzi *et al.* 2012a).

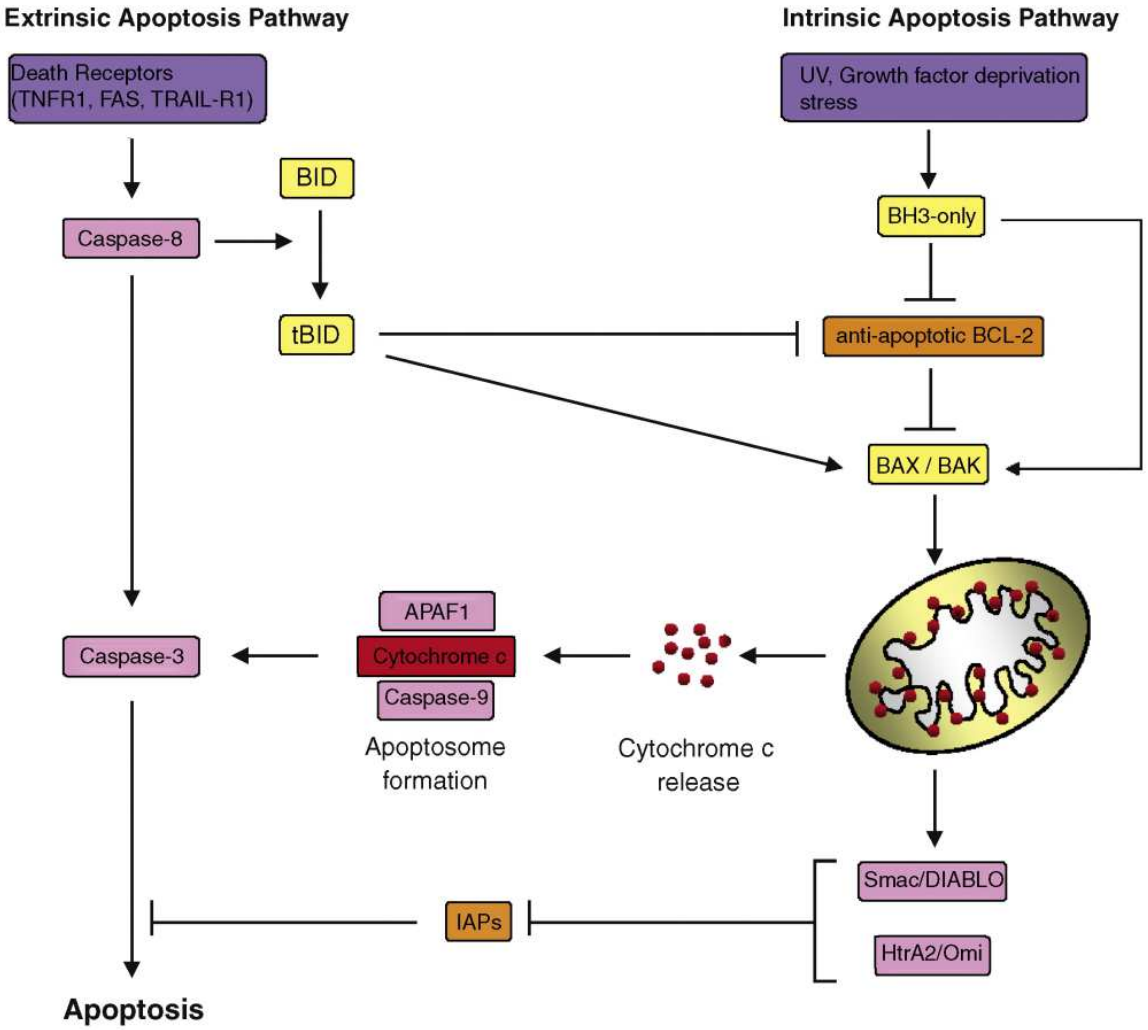

Figure 1: Apoptosis, the caspase-dependent programmed cell death pathway. Apoptosis can be induced by two distinct routes: the extrinsic and the intrinsic apoptosis pathway. The extrinsic apoptotic pathway is induced by binding of cell surface death receptors (TNF-R1, CD95 (or Fas), TRAIL-R1/R2) to their respective ligands. This leads to the activation of initiator caspase-8, which in turn activates the effector caspase-3. Activation of caspase-3 results in cleavage of intracellular proteins and the ordered demise of the cell. On the other hand, the intrinsic apoptotic pathway is induced by UV-irradiation, growth factor deprivation or various other stress stimuli and results in the activation of pro-apoptotic BH3-only Bcl-2-family members. The BH3-only proteins inhibit their anti-apoptotic Bcl-2-family members and release or directly activate the pro-apoptotic proteins BAX and BAK. Once activated, the proteins BAK and BAX promote MOMP and the release of cytochrome c from the mitochondria. The apoptosome, which activates caspase-3, is built by association of cytochrome c, Apaf-1 and caspase-9. In addition to cytochrome c release and MOMP, the factors Smac/DIABLO and HtrA2/Omi are also released from the mitochondria. These proteins promote apoptosis by inhibiting the action of IAPs. In type II cells, the intrinsic and the extrinsic apoptotic pathway are interconnected by Bid. Bid is cleaved by caspase-8 to its truncated form tBid, translocates to the mitochondria where it interacts directly with BAX to promote MOMP and finally apoptosis. **Abbreviations:** apoptotic protease activating factor 1 (Apaf-1), B-cell CLL/lymphoma-2 (Bcl-2), high temperature requirement protein A2 (HtrA2/Omi) inhibitor of apoptosis proteins (IAPs), mitochondrial outer membrane permeabilization (MOMP), second mitochondria-derived activator of caspase / direct IAP binding protein with low pI (Smac/DIABLO), tumor necrosis factor-receptor 1 (TNF-R1), TNF-related apoptosis inducing ligand-receptor (TRAIL-R)
(Scheme was taken from Brenner and Mak (2009) *Curr Opin Cell Biol* 21, p. 872)

To circumvent the accidental activation of the deadly caspase cascade under conditions favoring cell survival, caspases are suppressed by inhibitor of apoptosis proteins (IAPs). During apoptosis, mitochondrial factors are released into the cytosol to, e.g. interfere with IAPs or to trigger DNA fragmentation. The proteins Smac/DIABLO and HtrA2/Omi bind to and neutralize IAPs and thereby release the caspases from the IAPs (Figure 1; Wu *et al.* 2000). Upon induction of apoptosis, the mitochondrial factors AIF and endonuclease G translocate to the nucleus and trigger there large-scale DNA fragmentation in a caspase-independent manner (Sevrioukova, 2011).

Both apoptotic pathways, extrinsic and intrinsic, are functionally linked. Caspase-3 and -8, components of the extrinsic apoptotic pathway, cleave the pro-apoptotic protein Bid (Scaffidi *et al.*, 1998). The truncated form tBid causes then the release of cytochrome c from mitochondria, an important component of the intrinsic pathway, and the subsequent activation of caspase-9 and caspase-3 (Figure 1).

2.2 Caspase-independent programmed cell death – regulated necrosis

While caspase-dependent apoptosis (described above) represents the major physiologic pathway by which PCD is mediated, regulated necrosis can act as a backup system when the apoptotic machinery fails or is inactivated (Leist and Jäättelä, 2001). Cytoplasmic granulation and cellular swelling which culminate in the breakdown of the plasma membrane are morphological features of regulated necrosis. Different cellular stimuli (e.g. TNF, CD95 ligand, TRAIL, double-stranded (ds)RNA, interferon-γ (IFN-γ), ATP depletion, ischemia-reperfusion injury and pathogens) have been shown to induce necrotic PCD (Vanlangenakker *et al.* 2012).

Several modes of regulated necrosis have been already defined based on their underlying signaling pathways, such as ferroptosis, NETosis, ETosis, pyroptosis, pyronecrosis, parthanatos and necroptosis (Vanden Berghe *et al.* 2014). All these processes share morphological hallmarks but are characterized by individual aspects of cell death. For example, ferroptosis depends on intracellular iron and is typically observed in the context of cancer and neurodegeneration (Vanden Berghe *et al.* 2014). The lethal small molecule erastin triggers this unique iron-dependent form of cell death which is morphologically, biochemically and genetically distinct from apoptosis, necrosis and autophagy (Dixon *et al.* 2012). NETosis is a specialized form of neutrophil death occurring with the release of neutrophil extracellular traps (NETs). These NETs are composed of DNA associated with histones, granular, and cytoplasmic proteins enabling neutrophils to immobilize and kill bacteria (Remijsen *et al.* 2011). In addition to neutrophils, other cell types, such as eosinophils, mast cells, and macrophages, can also die by NETosis (Remijsen *et al.* 2011). Therefore, NETosis was re-named as the more generalized term ETosis (Wartha and Henriques-Normark, 2008). Pyroptosis has been described as an atypical death of macrophages and dendritic cells but may also occur in other cell types. Pyroptosis appears as a result from osmotic pressure generated by caspase-1 (but not caspase-3,

the central executioner of apoptosis)-dependent formation of membrane pores and is characterized by the rapid release of cytosolic contents (von Moltke *et al.* 2013). Another necrosis-like cell death process is pyronecrosis and has been described in response to *Shigella flexneri*. Pyronecrosis occurs independently of caspase-1 and -11, but is dependent on the inflammasome-adaptor ASC (apoptosis-associated speck-like protein containing a CARD) and the lysosomal protein cathepsin B (Willingham *et al.* 2007). Parthanatos was named after Thanatos, the personification of death in Greek mythology, and describes a particular mode of regulated necrosis involving the DNA damage-responsive enzyme PARP-1, in particular the (hyper)activation of PARP-1 (Galluzzi *et al.* 2014a). Regulated necrosis is considered as parthanatic when cell death depends on early PARP-1 activation and depletion of nicotinamide adenine dinucleotide (NAD^+), which has a dramatic bioenergetic impact (Chiarugi, 2005). Furthermore, PARP-1 dependent regulated necrosis relies on the release of AIF from the mitochondrial intermembrane space and its translocation to the nucleus (Yu *et al.* 2002; Andrabi *et al.* 2008). Finally, necroptosis represents the currently best understood and molecularly most well characterized form of regulated necrosis. Necroptosis is defined as a RIPK-dependent molecular cascade promoting necrotic-like cell death (Vanden Berghe *et al.* 2014; see 2.2.1) and will be the main focus of the study presented here.

Currently, regulated necrosis is intensively studied and in the focus of scientific interest because induction of regulated necrosis plays a significant role in both physiological settings (e.g. embryonic development) as well as in pathological scenarios (e.g. neurodegeneration). Therefore, the modulation of regulated necrosis may result in novel or additional options for the treatment of patients affected by disorders related to regulated necrosis (Galluzzi *et al.* 2014a; see 2.2.2).

2.2.1 Necroptosis

The term “necroptosis” was introduced in 2005 to describe a mode of regulated necrosis induced by TNF when caspase activity was blocked (Degterev *et al.* 2005). Later, necroptosis was redefined as being dependent on RIPK1 activity (Degterev *et al.* 2008). In the following years, necroptosis was classified as a PCD pathway mediated by signaling components that depend on the functional interactions of RIPK1 with its homolog RIPK3 (Cho *et al.* 2009; He *et al.* 2009; Zhang *et al.* 2009). RIPK3 was proposed to be the major initiator of necroptosis because RIPK3 can also trigger necroptosis independent from RIPK1 (Zhang *et al.* 2009; Upton *et al.* 2010). Later on, in 2012, the substrate of RIPK3 mixed lineage kinase domain-like (MLKL) was discovered as a crucial mediator of necroptosis downstream of RIPK3 (Sun *et al.* 2012). The induction of necroptosis can be inhibited by the RIPK1 inhibitor necrostatin 1 (Nec-1) or the inhibitor necrosulfonamide (NSA) which acts only on human, but not mouse MLKL (Figure 2; Degterev *et al.* 2008; Sun *et al.* 2012).

2.2.1.1 Initiation of necroptosis

The induction of necroptosis can be exemplified by the TNF signaling pathway. Under caspase-inhibitory conditions (e.g. in the presence of caspase inhibitors or virally expressed proteins), TNF induces the recruitment of RIPK1 to the TNF-R1 complex I (described in detail in 2.3.3) where RIPK1 is deubiquitinated by deubiquitinating enzymes (DUBs) such as cylindromatosis (CYLD), A20 or cezanne (Hitomi *et al.* 2008; Shembade *et al.* 2010; Enesa *et al.* 2008). The inhibition of RIPK1 ubiquitination by DUBs or Smac mimetics leads to the formation of a protein complex containing RIPK1 and its homolog RIPK3 which is termed "necrosome" (Figure 2; Declercq *et al.* 2009; Vanden Berghe *et al.* 2014). Both kinases possess an N-terminal kinase domain and a C-terminal RIPK homotypic interaction motif (RHIM) which appears to be critical for the activation of the necrosome (Sun *et al.* 2002; Galluzzi *et al.* 2014a). Recently, it was reported that the RIPK1-RIPK3-necrosome aggregates in microfilament-like complexes mediated by the RHIMs of RIPK1 and RIPK3. These heterodimeric filamentous structures exhibited classical characteristics of β-amyloids and the inhibition of the formation of RIPK1-RIPK3 amyloid-like structures represses the signal transduction of necroptosis (Li *et al.* 2012). The finely regulated crosstalk between RIPK1 and RIPK3 is regulated by phosphorylation of RIPK1 and RIPK3. For example, the autophosphorylation of RIPK1 at serine 161 (S161) and the direct and indirect RIPK3-mediated phosphorylation of RIPK1 generate pro-necroptotic signals (Cho *et al.* 2009; Degterev *et al.* 2008; He *et al.* 2009). The phosphorylation site at S199 of RIPK3 was reported to be a pro-necroptotic phosphorylation target site (Cho *et al.* 2009). Phosphorylation of RIPK3 is crucial for the recruitment of MLKL (Chen *et al.* 2014), a pseudokinase that binds ATP but is catalytically inactive (Sun *et al.* 2012). RIPK3-dependent phosphorylation of MLKL results in c-Jun N-terminal kinase (JNK) activation, reactive oxygen species (ROS) production and the execution of necroptosis (Zhao *et al.* 2012). Human MLKL is phosphorylated by human RIPK3 at threonine 357 (T357) and S358 (Sun *et al.* 2012), whereas mouse MLKL is phosphorylated at positions S345, S347, S352 and T349 by mouse RIPK3 (Figure 2; Xie *et al.* 2013). Wang and coworkers proposed that the phosphorylation of MLKL promotes the activation and association of the mitochondrial protein phosphatase phosphoglycerate mutase family member 5 (PGAM5). PGAM5 in turn recruits the mitochondrial fission factor dynamin-1-like protein (Drp-1) leading to the execution of necroptosis (Wang *et al.* 2012). However, accumulating evidence indicates that both PGAM5 and Drp-1 may be dispensable for the pro-necroptotic effects of MLKL (Galluzzi *et al.* 2014a). Recently, two independent studies demonstrated that MLKL appears to form oligomers upon phosphorylation by RIPK3 and that this results in the re-localization of MLKL to the plasma membrane in the course of necroptotic cell death (Figure 2; Cai *et al.* 2014; Chen *et al.* 2014). However, the existing data are still inconsistent regarding the molecular events of how MLKL regulates necrotic plasma membrane permeabilization and the execution of necroptosis (Galluzzi *et al.* 2014b; see 2.2.1.2).

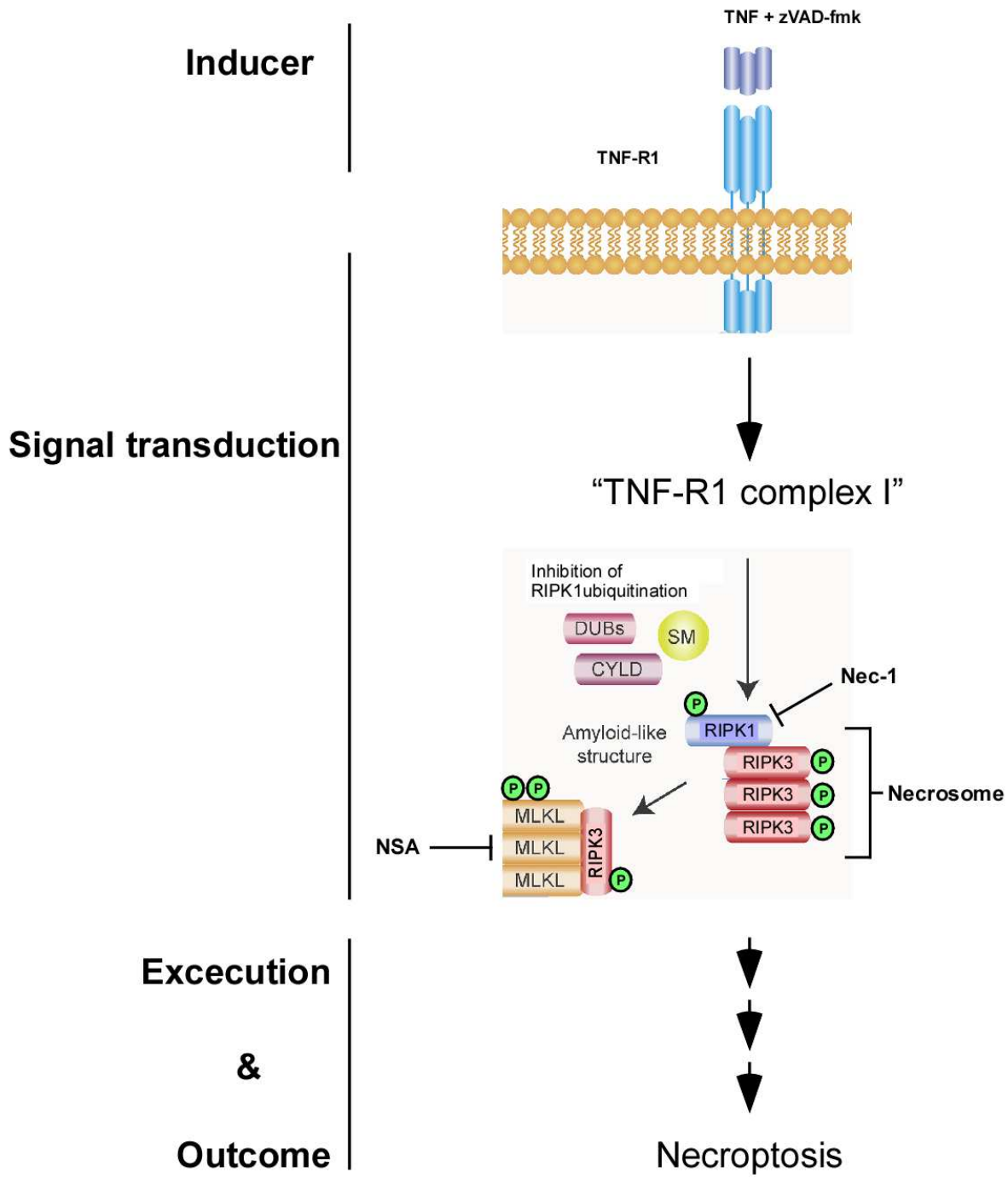

Figure 2: TNF-R1-mediated necroptosis. Necroptosis is induced by TNF (inducer) when caspases are inhibited, e.g. by the pan-caspase inhibitor zVAD-fmk. The signal transduction starts with the assembly of the TNF-R1 complex I and the subsequent deubiquitination of RIPK1 by SMs or DUBs such as CYLD leads to the formation of the necrosome. The necrosome contains phosphorylated and activated RIPK1 and RIPK3 associated in amyloid-like structures. The phosphorylation of RIPK1 and RIPK3 leads to the recruitment of MLKL. MLKL is phosphorylated by RIPK3 and forms oligomers resulting in the re-localization of MLKL to the plasma membrane where it interferes with membrane integrity and induces necroptosis. The assembly of the necrosome culminates in multiple executioner pathways which all lead to necroptosis (outcome). Necroptosis can be blocked by Nec-1 which inhibits RIPK1, and by NSA which blocks human MLKL. **Abbreviations:** cylindromatosis (CYLD), deubiquitinating enzymes (DUBs), mixed-lineage kinase domain-like (MLKL), necrostatin 1 (Nec-1), necrosulfonamide (NSA), phosphorylation (P), receptor-interacting protein kinase (RIPK), Smac mimetic (SM), tumor necrosis factor (TNF), TNF-receptor 1 (TNF-R1).
(Modified from Moriwaki and Chan (2013) *Cytokine Growth Factor* Rev 25, p. 170)

Necroptosis, triggered by the ligation of TNF to the TNF-R1 (Figure 2), is also the most extensively investigated model which will be the main focus of the thesis presented here. Nevertheless, necroptosis can also be triggered by other members of the TNF receptor family, e.g. CD95 (Holler *et al.* 2000); TNF-R2 (Chan *et al.* 2003) and TRAIL-R1 and -R2 (Vercammen *et al.* 1998b; Thon *et al.* 2006; Voigt *et al.* 2014) as well as by Toll-like receptors (TLR) 3 and 4 (Holler *et al.* 2000; Chan *et al.* 2003) and DNA and/or RNA sensors (Kaczmarek *et al.* 2013).

2.2.1.2 Execution of necroptosis

The list of mechanisms implicated in the execution of regulated necrosis is constantly growing, but detailed insights into these mechanisms, and especially those involved in the execution of necroptosis downstream of MLKL are sparse. It is currently unclear whether the execution mechanisms are exclusive for necroptosis or whether they also participate in other modes of regulated necrosis described above (see 2.2). Therefore, this chapter describes common execution mechanisms of regulated necrosis, which may also turn out to be relevant for necroptosis.

The signals required for necroptotic cell death downstream of MLKL remain uncertain. Recent reports show that MLKL forms trimers and translocates to the plasma membrane to facilitate calcium influx in response to TNF-induced regulated necrosis (Cai *et al.* 2014). The transient receptor potential cation channel, subfamily M, member 7 (TRPM7) seems to represent the central voltage-sensitive channel facilitating calcium influx, because blockade of TRPM7 inhibited regulated necrosis (Cai *et al.* 2014). Consequently, the influx of calcium ions into the cytoplasm disrupts osmotic homeostasis leading to the death of the cell (Cai *et al.* 2014). Furthermore, the generation of ROS may be another consequence in response of MLKL activation promoting necroptotic cell death (Moriwaki and Chan, 2013).

The accumulation of ROS during necrotic cell death was discovered even before the discovery of the necrosome (Schulze-Osthoff *et al.* 1992). The kinase RIPK3 links TNF-R1 signaling to metabolic enzymes and the production of ROS by building a complex with glycogen phosphorylase (PYGL), glutamate-ammonia ligase (GLUL), glutamate dehydrogenase 1 (GLUD1), fructose-1,6-bisphosphatase 2 (FBP2), fumarate hydratase (FH), glycosyltransferase 25 domain containing 1 (GLT25D1), and isocitrate dehydrogenase 1 (IDH1). PYGL, GLUL and GLUD1 can directly interact with RIPK3. The knock-down of any of these enzymes reduced TNF-induced accumulation of ROS, correlating with reduced cell death (Zhang *et al.* 2009). GLUL, a cytosolic enzyme that condensates glutamate and free ammonia into glutamine, and GLUD1, a mitochondrial enzyme converting glutamate into α-ketoglutarate, are hyperactivated by RIPK3. This hyperactivation results in increased glutaminolysis and excessive generation of α-ketoglutarate and lactate overproduction (Mates *et al.* 2009). PYGL catalyzes one step of glycogenolysis, the breakdown of glycogen into glucose-1-phosphate and subsequent conversation to glucose-6-phosphate (G6P). G6P stimulates glycolysis

contributing to ROS production and generation of cytotoxic methylglyoxal (Van Herreweghe *et al.* 2002). Altogether, there are several mechanisms by which enhanced glycogenolysis, glycolysis and glutaminolysis can contribute to the respiratory burst that characterizes necrotic cell death. A non-mitochondrial source of ROS is the plasma membrane-associated NADPH oxidase-1 (Nox1). The activation of TNF-R1 signaling rapidly activates Nox1 through RIPK1-dependent signaling, leading to a burst of Nox1-derived ROS (Morgan *et al.* 2008).

Profound depletion of ATP levels triggered by overconsumption of NAD^+ in ADP ribosylation reactions (e.g. by PARP-1 hyperactivation) is a hallmark of some forms of regulated necrosis. In addition to ROS production, mitochondria also contribute to the abrupt decrease in ATP. Temkin and coworkers reported that binding of TNF to TNF-R1 leads to the RIPK1-mediated inhibition of the mitochondrial adenine nucleotide translocase (ANT; Temkin *et al.* 2006) which is an ATP/ADP antiporter. ANT was shown to interact with other mitochondrial proteins like voltage-dependent anion channel (VDAC) and cyclophilin D (CypD) leading to the assembly of a permeability transition pore complex (PTPC; Vanlangenakker *et al.* 2008). Pro-apoptotic and anti-apoptotic members of the Bcl-2 family were also shown to interact with the PTPC (Brenner *et al.* 2000). In response to cytotoxic stimuli such as ROS and cytosolic Ca^{2+} overload, the PTPC rearranges its conformation, allowing the entry of unwanted solutes and water into the mitochondrial matrix, the so-called mitochondrial permeability transition leading to the rupture of the mitochondria and to cell death (Vanlangenakker *et al.* 2008). Mitochondria appear to be important activators of regulated necrosis signals; however, recent studies claimed that mitochondria are dispensable for the execution of necroptosis in response to MLKL activation (Tait *et al.* 2013).

Lysosomal membrane permeabilization (LMP) was also found to contribute to the execution of regulated necrosis (Vanlangenakker *et al.* 2008). During this process, excess ROS production overcomes the antioxidant defenses of the cell leading to the destabilization of other intracellular membranes, e.g. of the endoplasmatic reticulum (ER), mitochondria or lysosomes. LMP can be a consequence of the activation of several signaling pathways. For example, TNF-R1 engagement leads to the activation of cytosolic phospholipase A_2 (PLA_2). PLA_2 is known to generate arachidonic acid which is transformed by lipoxygenase into lipid hydroperoxides. These lipids are characterized by a high membrane-damaging potential (Burke and Dennis, 2009). Another signaling pathway following after TNF binding to TNF-R1 results in the activation of the lysosomal enzyme acid sphingomyelinase (A-SMase) and membranous neutral sphingomyelinases (N-SMase). Both enzymes convert sphingomyelin into ceramide. Ceramide is a substrate for ceramidases, producing sphingosine as an inducer of LMP (Kagedal *et al.* 2001). Of note, ceramide is implicated to play an additional, much more important role in mediating necroptosis elicited by TNF or TRAIL (Strelow *et al.* 2000; Thon *et al.* 2005, Thon *et al.* 2006) which will be the focus of chapter 2.4. Membrane destabilization at the mitochondrial level has multiple consequences like inhibition of ATP synthesis, inner membrane

permeabilization and altered Ca^{2+} buffering (Galluzzi *et al.* 2011). Destabilization of the ER membrane promotes the accumulation of cytosolic Ca^{2+}. As additional inducers of LMP, cytotoxic hydrolases such as Ca^{2+}-dependent calpains (calcium activated neutral proteases) destabilize lysosomal membranes. Calpain-triggered LMP results in the release of cytotoxic lysosomal cathepsins leading to the cytoskeletal protein breakdown and cell death (Vanlangenakker *et al.* 2008).

Proteolysis of regulatory proteins, leading to either activation or inactivation of downstream signaling cascades is a further potential critical execution mechanism during regulated necrosis and especially necroptosis. During apoptosis, hundreds of proteins are specifically cleaved by proteolysis as part of the apoptotic program. The family of caspases is involved in many of these proteolytic events which are essential for the cleavage of substrate proteins, initiation and execution of PCD and thus for the survival and homeostasis of multicellular organisms (Degterev and Yuan, 2008). During regulated necrosis, proteolysis appears to be equally important. For example, necroptosis is negatively regulated by caspase-8 which cleaves and inactivates RIPK1 (Mocarski *et al.* 2011). During regulated necrosis, alternative proteolytic molecules such as lysosomal proteases (calpains, cathepsins and granzymes), serine proteases, the proteasome and metalloproteases might substitute for caspases (Leist and Jäättelä, 2001; Schrader *et al.* 2010). The ability of non-caspase proteases to cleave at least some of the classic caspase substrates implicates that non-caspase proteases might be essential for regulated necrosis. For example, cathepsins are responsible for the translocation of Bax to the mitochondrion in the complete absence of caspase activation (Bidere *et al.* 2003). The cleavage and translocation of Bid as well as the cleavage and release of AIF are cathepsin-mediated events which do not need caspase activity (Lorenzo and Susin, 2007). Similar to cathepsins, calpains can also cleave AIF in the absence of caspases (Lorenzo and Susin, 2007). Moreover, the serine protease granzyme B was shown to cleave and activate Bid to its truncated product gtBid. During regulated necrosis, gtBid translocates to the mitochondrion, integrates into the mitochondrial membrane and thereby releases cytochrome c (Heibein *et al.* 2000). Furthermore, the proteolytic activity of the mitochondrial serine protease HtrA2/Omi has been implicated to mediate necrotic-like cell death of human neutrophils (Blink *et al.* 2004).

Taken together, the above described events like ROS overproduction, mitochondrial dysfunction and proteolysis may play a major role in the execution of regulated necrosis. Besides its suggested role during healthy development, regulated necrosis has been described to additionally trigger pathophysiological alterations, e.g. in stroke, Alzheimer's, Huntington's and Parkinson's disease (Vandenabeele *et al.* 2010).

2.2.2 Regulated necrosis in health and disease

Regulated necrosis has physiological and pathophysiological consequences. Regulated necrosis occurs in vital processes such as regulation of bone growth by participating in the physiological cell death of

chondrocytes (Roach and Clarke, 2000) and in adult tissue homeostasis where colonocytes in the lower regions of intestinal crypts undergo necrotic cell death (Barkla and Gibson, 1999). The homeostasis of T-cell populations is another physiological relevant response (Jäättelä and Tschopp, 2003). Furthermore, regulated necrosis is reported to be relevant for the negative selection of lymphocytes, embryonic removal of interdigital webs, ovulation, termination of immune responses, hyperacute shock in response to TNF, or the autonomous death of activated T-cells (Festjens *et al.* 2006).

As described above, regulated necrosis plays a major role as a backup cell death mechanism, when apoptosis is disabled. For example, viral and bacterial proteins can efficiently suppress caspase activity and thus the cell initiates regulated necrosis as an alternative mechanism to limit viral and bacterial infections (Kaczmarek *et al.* 2013). Studying RIPK3-deficient mice revealed that these mice are more susceptible to viral infection than their wild-type counterparts (Cho *et al.* 2009). In addition, Upton and coworkers demonstrated that the murine cytomegalovirus M45 protein interferes with the necrosome (Upton *et al.* 2010). In summary, these findings support the antiviral and antibacterial properties of necroptosis.

In addition, regulated necrosis has been shown to play a role in many human pathologies like hyperacute shock (Cauwels *et al.* 2003), pancreatitis (He *et al.* 2009; Zhang *et al.* 2009), cerebral and myocardial ischemia-reperfusion injury (Linkermann *et al.* 2013), Crohn's disease (Günther *et al.* 2011), Alzheimer's disease (Lin and Beal, 2006) and photoreceptor cell loss (Viringipurampeer *et al.* 2014). Moreover pathogens such as HIV, vaccinia virus, Shigella and Salmonella (Festjens *et al.* 2006; Cho *et al.* 2009) can destruct cells in a caspase-independent manner. Rapid plasma permeabilization due to necrotic triggers leads to the release of damage associated molecular patterns (DAMPs) from the cell. These necrosis-dependent DAMPs can contribute to sensitization of necroptosis in neighboring cells or modulate the fate of inflammation (Kaczmarek *et al.* 2013).

Genetic studies of knock-out mice revealed that RIPK1-deficient mice are not viable, whereas kinase-dead mutant RIPK1^{D138N} mice are viable (Newton *et al.* 2014). The pharmacological inhibition of RIPK1 with Nec-1 or geldanamycin showed cytoprotective effects *in vitro* (Vandenabeele *et al.* 2010). Moreover, the inhibition of RIPK1 activity *in vivo* attenuates neurodegenerative diseases (Yuan *et al.* 2003), adult brain ischemia (Degterev *et al.* 2005), myocardial infarction (Lim *et al.* 2007) and photoreceptor degeneration of retina disorders (Trichonas *et al.* 2010; Viringipurampeer *et al.* 2014). The genetic deletion of RIPK1 functionally complemented the impaired lymphocyte proliferation in FADD-deficient mice (Zhang *et al.* 2011). This and the above findings are consistent with a critical role for the kinase activity of RIPK1 in pathological cell death. RIPK3 deficient mice displayed reduced pancreatitis (He *et al.* 2009; Zhang *et al.* 2009). The absence of any phenotypic change in unchallenged RIPK3-deficient mice suggests that RIPK3 is not involved in embryogenesis and homeostasis (Newton *et al.* 2014). However, genetic deletion of RIPK3 rescues caspase-8-deficient

mice from early embryonic death, revealing that during development apoptotic regulatory mechanisms counteract RIPK3-dependent necroptosis (Kaiser *et al.* 2011). Genetic deletion of both caspase-8 and RIPK3 lead to progressive lymphoaccumulative disease in adult mice (Oberst *et al.* 2011). These studies clearly demonstrate that apoptotic mechanisms block the necrotic pathway in diverse physiological ways.

2.3 Death receptors

2.3.1 The TNF superfamily

As outlined above, members of the TNF superfamily are central inducers of necroptosis. Cellular processes such as immune responses, cell proliferation, hematopoiesis and cell death are regulated by the family of TNF receptor-related molecules (Aggarwal, 2003). So far, 19 different ligands belonging to the TNF superfamily have been identified. These 19 ligands mediate their cellular response via 29 different receptors all belonging to the TNF receptor superfamily. These receptors have a cysteine-rich domain in the extracellular portion of the receptor (Aggarwal, 2003). Within the members of the TNF-receptor superfamily, DRs have been shown to induce both caspase-dependent as well as caspase-independent pathways leading to PCD (Leist and Jäättelä, 2001). At present, eight members of the DR family have been identified: TNF-R1 (also known DR1/CD120a/p55/p60), CD95 (named also Fas-receptor, DR2, or APO-1), DR3 (also termed as APO-3, lymphocyte-associated receptor of death (LARD), TNF-R-related apoptosis-mediating protein (TARD), WS-1, TNF-receptor-like 3 (TR3), TNF receptor superfamily member 25 (TNFRSF25)), TRAIL-receptor 1 (TRAIL-R1; or APO-2 and DR4), TRAIL-R2 (also known as TRICK2, TNFRSF10B, DR5, KILLER), DR6 (or TNFRSF21), ectodysplasin A receptor (EDAR) and nerve growth factor receptor (NGFR) (Mahmood and Shukla, 2010).

With focus on regulated necrosis, members of the DR family are able to induce cell death independent of caspases. For example, Holler and coworkers showed that activated primary T cells were killed by CD95 ligand in the absence of caspases (Holler *et al.* 2005). Human and murine TRAIL-receptors (TRAIL-R) are also able to induce regulated necrosis (Holler *et al.* 2000; Guo *et al.* 2005; Thon *et al.* 2006). TNF-R1 is as well capable of inducing necroptosis as described above (see 2.2.1.1) and the most extensively investigated model of necroptosis is triggered by the activation of TNF-R1 signaling (Figure 2 and 3).

2.3.2 The death receptor TNF-R1

Two different types of TNF receptors have been characterized. TNF-R1 (also referred to as type I or p55 or p60) is expressed by almost all cell types, whereas TNF-R2 (also known as type II or p75 or p70) was shown to be expressed by endothelial cells as well as by cells of the immune system (Aggarwal and Natarajan, 1996). TNF-R1 belongs to the DR subgroup of the TNF superfamily, whereas TNF-R2 contains no DD. The latter interacts with the adaptor protein TNF receptor-

associated factor-2 (TRAF2) leading to the proteasomal degradation of TRAF2 and inhibition of TNF-R1-induced activation of nuclear factor-κB (NF-κB; Wu *et al.* 2005). In 2009, TRAF1 was shown to inhibit TNF-R2-induced proteasomal degradation of TRAF2 and thereby modifies TNF-R1-TNF-R2 cooperation shifting signaling from apoptosis to proinflammatory NF-κB signaling (Wicovsky *et al.* 2009). Typically, cells expressing TNF-R2 also express TNF-R1 and thereby regulate the balance between cellular survival and cell death. TNF-R1 stimulation usually induces cytokine generation, inflammation, and cell survival, unless the cytotoxic potential of TNF-R1 is unmasked by inhibiting these survival pathways. However, the potential usefulness of TNF in clinical oncology is severely limited by its strong side effects.

2.3.3 The complex signaling pathways of TNF-R1

The balance between pro-survival and pro-cell death signals depends on intracellular interactors of TNF-R1. Additionally, the existence of different protein complexes is very critical to determine which signaling pathway will be induced upon TNF ligation to TNF-R1 (Figure 3). Binding of TNF to TNF-R1 can, for example, induce the formation of a membrane-proximal supra-molecular complex termed "TNF-R1 complex I". Complex I is responsible for the activation of pro-survival signals favoring the canonical pathway of activation of the transcription factor NF-κB and up-regulating anti-apoptotic genes such as A20 and FLICE-like inhibitory protein long isoform ($FLIP_L$) (Micheau and Tschopp, 2003). The ligand-bound TNF-R1 trimers recruit TRADD, RIPK1, cellular (c)IAP1 and cIAP2, TRAF2 and TRAF5 (Micheau and Tschopp, 2003). The cIAP-mediated polyubiquitination of RIPK1 (Bertrand *et al.* 2008) recruits downstream adaptors such as transforming growth factor-β-activated kinase 1 (TAK1), TAK1-binding protein 2 (TAB2) and TAB3 as well as inhibitor of NF-κB kinase (IKK) complex which together trigger the canonical NF-κB activation (Figure 3a). The activation of NF-κB is enhanced by recruitment of the linear ubiquitin chain assembly complex (LUBAC). LUBAC activity results in linear ubiquitination of RIPK1 and the NF-κB essential modulator (NEMO) protein (Walczak, 2011).

Upon endocytosis of TNF-R1, the TRADD-dependent "TNF-R1 complex IIa" is generated by a rearrangement of the molecular composition of complex I (Figure 3b). Here, the dissociation of RIPK1 from TNF-R1 by CYLD-mediated deubiquitination (O'Donnell *et al.* 2007; Hitomi *et al.* 2008) is crucial for the transition from complex I to the lethal complex II which has also been termed DISC. Complex IIa is composed of pro-caspase-8 and $FLIP_L$ heterodimers as well as TRADD and FADD. Upon activation of caspase-8 several substrates including Bid and caspase-3 are activated. RIPK1, RIPK3 and CYLD are cleaved by the caspase-8/$FLIP_L$ heterodimer leading to their inactivation, thereby preventing necroptosis (Lin *et al.* 1999; Feng *et al.* 2007) and instead leading to execution of caspase-dependent apoptosis (Figure 3b and see 2.1).

When cIAPs are inhibited, through for example Smac/DIABLO, a distinct signaling cascade occurs (Vanlangenakker *et al.* 2011a). Here, the degradation of cIAPs reduces the canonical NF-κB activation of complex I (Bertrand *et al.* 2008). This leads to an up-regulation of NF-κB-inducing kinase (NIK) and facilitates non-canonical NF-κB signaling (Figure 3d; Varfolomeev *et al.* 2007). Moreover, a TRADD-independent cytosolic complex is supposed to be formed between non-ubiquitinylated RIPK1, RIPK3, FADD and the caspase-8/FLIPL heterodimer. This second lethal complex II is referred to as RIPK1-dependent complex IIb or "ripoptosome" (Figure 3e; Feoktistova *et al.* 2011). The ripoptosome is necessary but not sufficient to induce cell death because caspase-8 activity is controlled by c-FLIP (Feoktistova *et al.* 2011). Similar as described for complex IIa, RIPK1 and RIPK3 are inactivated through cleavage mediated by caspase-8/$FLIP_L$ heterodimers, leading to the induction of apoptosis by the release of caspase-8 homodimers.

However, the deletion of FADD or caspase-8 as well as inhibition of caspase-8 by cytokine response modifier protein A (CrmA), a potent viral inhibitor of caspase-8 or pharmacologically with zVAD-fmk can lead to the formation of the necrosome, a pro-necrotic complex (Vercammen *et al.* 1998a; Holler *et al.* 2000). This complex is comprised of and dependent on active RIPK1-RIPK3 and MLKL (Figure 3c and Figure 2; Vandenabeele *et al.* 2010; see chapter 2.2.1.1). Whether FADD or TRADD are strictly required to assemble the necrosome remains unclear.

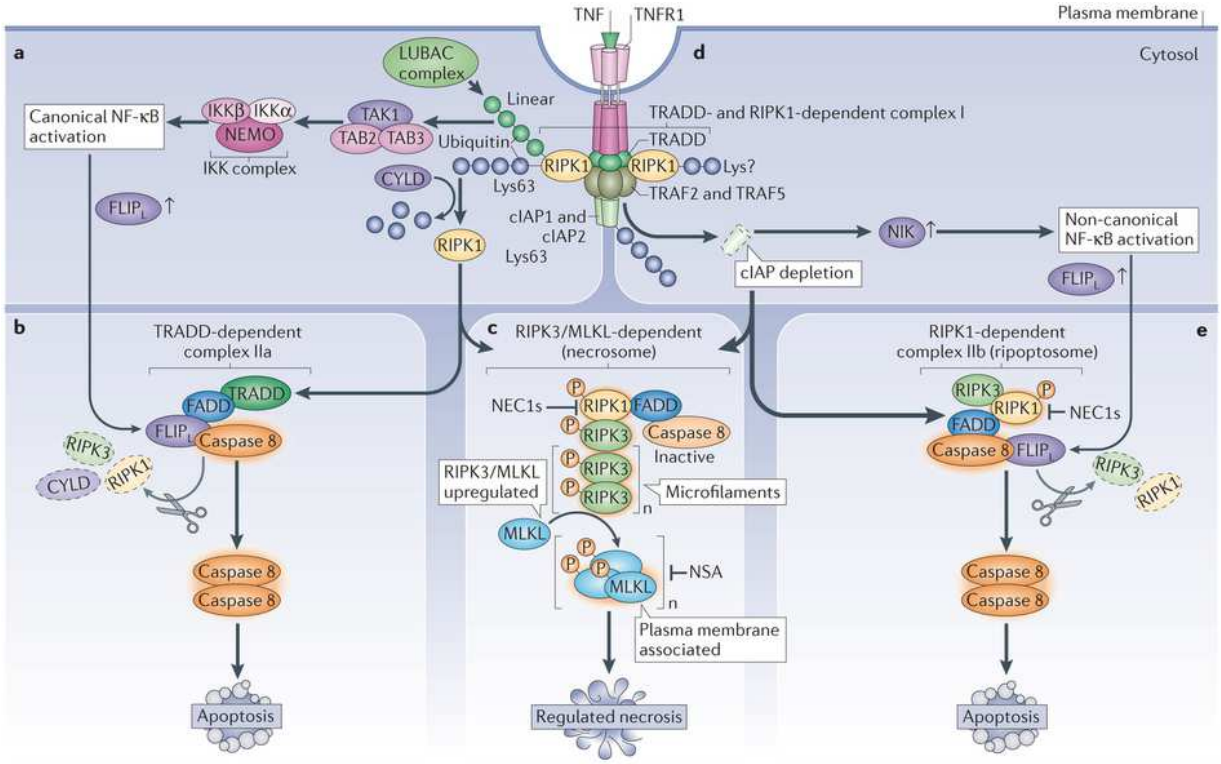

Figure 3: TNF-R1-mediated signaling pathways. Stimulation of TNF-R1 by the TNF ligand results in **(a)** the recruitment of TRADD, RIPK1, cIAP1, cIAP2, TRAF2 and TRAF5 and in the assembly of complex I. cIAP1 and cIAP2 in turn poly-ubiquitinylate RIPK1, allowing recruitment of the TAK1-TAB2/3 complex as well as the IKK/NEMO complex. The assembly of this complex leads to the activation of the canonical NF-κB pathway which is enhanced by the recruitment of the LUBAC. **(b)** TRADD-dependent complex IIa is built after de-ubiquitination of RIPK1 by CYLD, allowing RIPK1 to dissociate from the plasma membrane. Here, RIPK1 interacts with TRADD, FAAD, pro-caspase-8 and FLIP. Pro-caspase-8 and $FLIP_L$ cleave and inactivate RIPK1, RIPK3 and CYLD (dashed ovals) to inhibit necroptosis. Homodimerized, active caspase-8 in turn activates executioner caspases resulting in apoptosis. **(c)** When caspase-8 is inactive, the RHIM domains of RIPK1 and RIPK3 associate in RIPK1-RIPK3 amyloid-like microfilaments (necrosome). The phosphorylation of RIPK1 and RIPK3 leads to the recruitment of MLKL which can be inhibited by NSA. The RIPK3/MLKL-dependent complex initiates regulated necrosis. **(d)** However, when cIAPs are inhibited by Smac mimetics, RIPK1 is not ubiquitinated. This leads to an up-regulation of NIK and the activation of the non-canonical NF-κB pathway. **(e)** In the absence of cIAPs, a RIPK1-dependent complex IIb (ripoptosome) comprised of RIPK1, RIPK3, FADD and $FLIP_L$-caspase-8-homodimers is formed. As in **(b)** RIPK1 and RIPK3 are inactivated and apoptosis is induced. **Abbreviations:** cIAP (cellular inhibitor of apoptosis protein), CYLD (cylindromatosis), FADD (Fas-associated death domain), FLIP (FLICE-like inhibitory protein), IKK (inhibitor of NF-κB), LUBAC (linear ubiquitin chain assembly complex), MLKL (mixed lineage kinase domain-like), NEC1s (necrostatin 1), NEMO (NF-κB essential modulator), NF-κB (nuclear factor-κB), NIK (NF-κB-inducing kinase, NSA (necrosulfonamide), RHIM (RIP homotypic interaction motif), RIPK (receptor-interacting protein kinase), SMAC (second mitochondria-derived activator of caspase), TAB2 (TAK1 binding protein 2), TAK (transforming growth factor-β-activated kinase), TRADD (TNF receptor-associated death domain), TRAF (TNF receptor-associated factor), TNF (tumor necrosis factor), TNF-R1 (TNF-receptor 1).
(Adapted from Vanden Berghe *et al.* (2014) *Nat Rev* 15, p. 138)

2.3.4 The death receptors TRAIL-R1 and TRAIL-R2

The ligand TRAIL was first cloned and characterized in 1995 (Wiley *et al.* 1995). TRAIL is a type II transmembrane protein belonging to the TNF superfamily. Five receptors are able to bind TRAIL (Wang and El-Deiry, 2003). In humans, TRAIL-R1 and TRAIL-R2 are capable of inducing PCD through their DD. Both receptors have cysteine-rich repeats facilitating TRAIL binding. TRAIL also binds to the decoy receptor TRAIL-R3 (also known as DcR1, LIT, TRID) and TRAIL-R4 (also termed as DcR2, TRUNDD). However, in their cytoplasmic domains, both receptors completely or partially lack a DD and are therefore unable to induce apoptosis. For this reason, TRAIL-R3 and TRAIL-R4 are regulators rather than inhibitors of TRAIL-mediated PCD (Merino *et al.* 2006). Osteoprotegerin (OPG), the fifth and soluble receptor, has a rather low affinity to the ligand TRAIL. It was suggested that the function of OPG and TRAIL is linked to bone metabolism (Emery *et al.* 1998). To date, only one mouse receptor is known, which is homologous to the human TRAIL-R2 (Wu *et al.* 1999).

In contrast to TNF, TRAIL has emerged as a most promising molecule for cancer therapy due to its ability to selectively induce apoptosis in tumor cells without affecting normal cells (Walczak *et al.* 1999). For example, the treatment of patients with human agonistic TRAIL-R antibodies Mapatumumab and Lexatumumab can induce apoptosis and have been employed for selective cancer therapy (Pukac *et al.* 2005; Ashkenazi and Herbst, 2008). Similar to TNF-R1, TRAIL-R1 and TRAIL-R2 are able to induce regulated necrosis independently of their apoptotic capabilities when apoptosis induction fails or is inhibited (Holler *et al.* 2000; Guo *et al.* 2005; Thon *et al.* 2006). In contrast to TNF-R1 induced necroptosis, a comprehensive picture of the signaling pathways of regulated necrosis induced by TRAIL-R1 or TRAIL-R2 is currently lacking. In 2006, the capacity of mTRAIL-R2 to induce necroptosis has been demonstrated (Thon *et al.* 2006). Moreover, cells over-expressing acid ceramidase, an enzyme which degrades the second messenger ceramide, showed an increased resistance to regulated necrosis elicited by TRAIL (Thon *et al.* 2006). TRAIL-induced necroptosis results in the increase of intracellular ceramide levels in murine L929, NIH3T3 and human Jurkat T cells (Voigt, Bachelor Thesis, 2009). To this end, the induction of regulated necrosis by TRAIL may represent a novel and additional option for the elimination of tumor cells, and the second messenger ceramide seems to play a crucial role in regulated necrosis distinct from apoptosis signaling elicited by TRAIL and TNF (see below).

2.4 Acid sphingomyelinase and its product ceramide

2.4.1 Biological role and function of ceramide

As described above, the lipid ceramide plays a crucial role in mediating regulated necrosis. Ceramide is an important second messenger and a structural membrane component and involved in multiple biological processes, such as apoptosis, differentiation and cell growth, or bacterial and viral pathogenesis (Kolesnick and Krönke, 1998). This pro-apoptotic mediator is generated in response to various stimuli including ionizing radiation, chemotherapy and by the DRs TNF-R1, CD95 and TRAIL receptors (Figure 4). Ceramide can be produced in mammalian cells either by the *de novo* synthesis in the ER, by the hydrolysis of sphingomyelin to ceramide mediated by sphingomyelin-specific forms of phospholipase C, called sphingomyelinases (SMases) or by the activity of cerebrosidases. The activity of ceramidases, sphingomyelin synthases or glucosylceramide synthases is required for further processing of ceramide. The catabolic pathway of ceramide is controlled by the activity of SMases which hydrolyze the phosphodiester bond of sphingomyelin yielding ceramide and phosphocholine. The cleavage of ceramide at the amino bond resulting in sphingosine and a free fatty acid is catalyzed by ceramidases and the reversion by ceramide synthases (Figure 4). Ceramide and its metabolites have been shown to influence various cellular processes, including angiogenesis, apoptosis, autophagy, differentiation, infection, inflammation, migration, proliferation, protein trafficking and senescence (Pettus *et al.* 2002; Gulbins and Li, 2006). For example, ceramide-rich membrane domains may serve as sorting locations for membrane receptors, inhibitors and other membrane components involved in signaling (Gulbins *et al.* 2004). At present, the molecular details, involved in preferential sorting and receptor clustering at the ceramide-rich membrane domains, remain unknown. The concept of temporal organization of the signaling platform by a specific receptor was first shown for CD95. Clustering of CD95 at the plasma membrane amplifies the initial signaling and activation of caspase-8 (Grassmé *et al.* 2003). In addition, ceramide also directly interacts with and regulates cathepsin D (Heinrich *et al.* 1999), phospholipase A_2 (Huwiler *et al.* 2001), kinase suppressor of Ras (Zhang *et al.* 1997), ceramide-activated protein phosphatases (Saddoughi *et al.* 2013), and protein kinase C isoforms (Huwiler *et al.* 1998). Furthermore, ceramide regulates the activity of the potassium channel Kv1.3 (Gulbins *et al.* 1997) and calcium release-activated calcium channels (Samapati *et al.* 2012). Apart from this, ceramide molecules can form channels in the outer mitochondrial membrane, which might contribute to the induction of cell death (Siskind and Colombini, 2000).

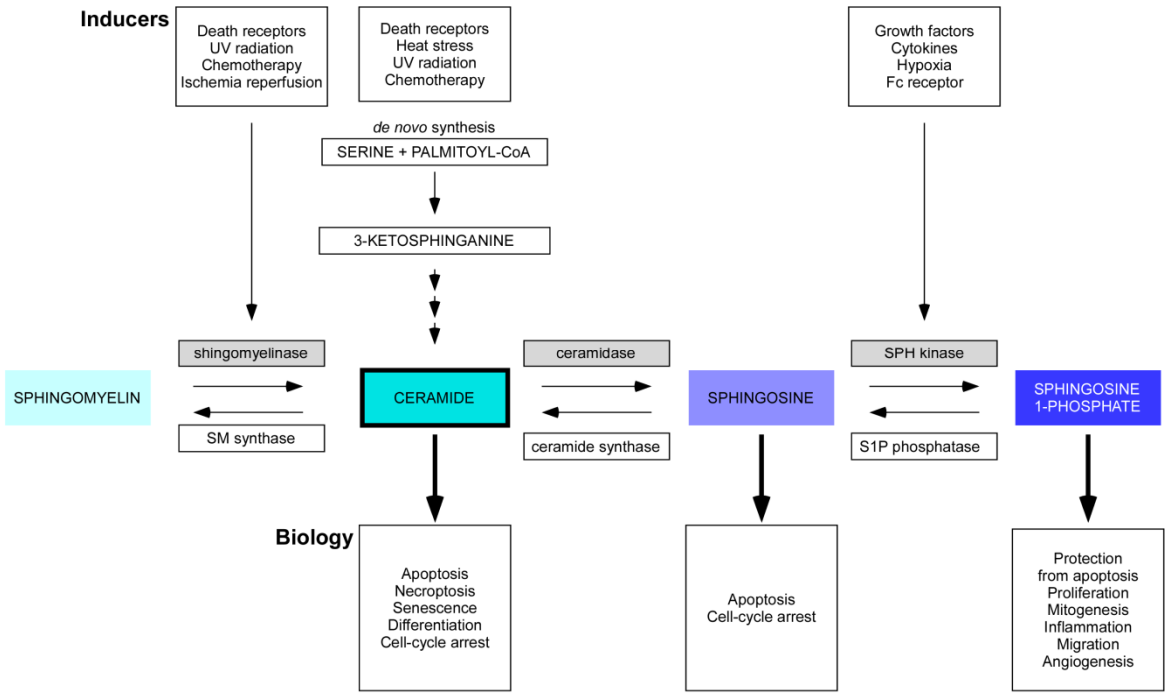

Figure 4: Regulation of ceramide levels and its biological role. Ceramide levels are controlled by the activity of a variety of enzymes that synthesize and catabolize ceramide. The breakdown of sphingomyelin to ceramide is hydrolyzed by sphingomyelinases. SM synthase clears ceramide by synthesizing sphingomyelin. The condensation of serine and palmitoyl-CoA by serine palmitoyltransferase initiates the *de novo* pathway. 3-ketosphinganine is then reduced, N-acetylated and desaturated by addition of a 4-5 *trans* double bond in a series of enzymatic steps, resulting in the generation of ceramide. Ceramidases cleave ceramide at the amide bond, leading to sphingosine and a free fatty acid. Sphingosine 1-phosphate is generated by sphingosine kinase. A number of stimuli can induce the production of ceramide and its metabolites (upper boxes) and results in biological effects (lower boxes). **Abbreviations:** sphingomyelin (SM), sphingosine (SPH), sphingosine 1-phosphate (S1P)
(Modified from: Pettus *et al.* (2002) *Biochim Biophys Acta* 1585, p. 115, and Hannun YA and Obeid LM (2008) *Nat Rev Mol Cell Biol* 9, p. 140)

2.4.2 Biological functions and activation of acid sphingomyelinase

SMases are considered to be the most important enzymes in the pathway of ceramide signal transduction (Kolesnick and Krönke, 1998). There are five types of SMases known, all are defined by their pH optimum: plasma membrane-bound neutral sphingomyelinase (N-SMase-1), N-SMase-2, N-SMase-3, and endo-lysosomal acid sphingomyelinase (A-SMase) and a secreted form of A-SMase (S-SMase).

Acid sphingomyelinase (A-SMase) is an endo-lysosomal protein that hydrolyzes sphingomyelin to ceramide and phosphocholine at an acidic pH optimum. Several A-SMase isoforms have been identified, although only one transcript has been reported to be catalytically active (Rhein *et al.* 2012). Two types of the metallo-enzyme A-SMase are described based on the common protein precursor and direct activation by zinc ions (Schissel *et al.* 1998). The lysosomal A-SMase is partially depending on Zn^{2+}, because the enzyme is exposed to cellular Zn^{2+} during trafficking to lysosomes and in lysosomes. Hence, lysosomal A-SMase is zinc ion-saturated and does not require exogenous Zn^{2+} ions. In contrast to lysosomal A-SMase, the secretory A-SMase (S-SMase) requires exogenous Zn^{2+} for full activity and is released extracellularly (Schissel *et al.* 1998).

Maturation of A-SMase from its initial 75-kDa pre-pro form involves multiple proteolytic processing steps (Hurwitz *et al.* 1994). Using pulse-chase labeling experiments, the maturation of A-SMase was unraveled. The processing of the initial 75-kDa pre-pro form of A-SMase to the 72-kDa pro-form was seen within 3 h of chase and the formation of the mature 70-kDa form was apparent after 4 to 8 h (Hurwitz *et al.* 1994). The primary mechanism of targeting A-SMase to the lysosome is the mannose-6-phosphate (M6P) receptor system (Ferlinz *et al.* 1997) because fibroblasts with mutations in enzymes of the M6P machinery showed enhanced A-SMase secretion (Takahashi *et al.* 2006).

In humans, mutations in the *SMPD1* gene (the gene product is A-SMase) result in the lysosomal storage disorder Niemann-Pick disease type A or B. Patients suffering from type A exhibit rapid neurodegeneration that leads to early death of the patient (2-3 years of age). In contrast to type A, Niemann-Pick disease type B is a milder form and is characterized by hepatosplenomegaly, pulmonary insufficiency and cardiovascular disease (Simpson *et al.* 2010). The different clinical outcome of Niemann-Pick disease types A and B are likely due to differences in the amount of residual, functional A-SMase activity (Schuchmann, 2010). Patients with Niemann-Pick disease accumulate sphingomyelin and other lipids, including cholesterol and gangliosides, leading to many cellular abnormalities (Scandroglio *et al.* 2008).

The regulation of A-SMase and the underlying molecular mechanisms involving post-translational modifications as well as proper trafficking signals are only partially characterized. It was shown that in addition to initial cleavage, the enzyme can be further processed to a protein with a size of 57 kDa (Hurwitz *et al.* 1994). Here, proteases, in particular caspases, have been suggested to regulate A-SMase activity (Brenner *et al.* 1998; Edelmann *et al.* 2011). Brenner and coworkers demonstrated in initial studies that caspase inhibition (by ac-YVAD-chloromethylketone or transient CrmA transfection) prevents A-SMase activation by CD95 (Brenner *et al.* 1998). Further studies reported that TNF triggers the interaction of the TNF-R1 with caspase-7. This interaction results in receptor internalization and rapid formation of endosomes (Edelmann *et al.* 2011). The receptor containing endosomes fuse with lysosomes resulting in multivesicular bodies bringing lysosomal A-SMase into close contact with caspase-7. Caspase-7 was shown to cleave the 72-kDa pro-form into the 57-kDa A-SMase fragment and thereby activating the enzyme (Edelmann *et al.* 2011). Similar activation mechanisms of A-SMases by stimuli other than TNF are presently unknown. Additionally, cytosolic protein kinase C (PKC) δ-mediated phosphorylation of A-SMase at serine 508 can cause activation of A-SMase (Zeidan and Hannun, 2007). Furthermore, the second messenger diacylglycerol (DAG) was shown to be able to activate PKC as well as A-SMase (Schütze *et al.* 1992). The activity of A-SMase is also dependent on glycosylation, as there are six predicted N-glycosylation sites in the A-SMase polypeptide chain. However, only five are used for glycosylation (asparagine 86 (N86), N175, N335, N395, N520; Ferlinz *et al.* 1997). Mutation of N520 caused the impaired secretion of S-SMase in addition to a complete loss of activity, presumably resulting from defective trafficking (Hurwitz *et al.*

1994; Ferlinz *et al.* 1997). The glycosylation pattern also determines trafficking of the enzyme because only M6P glycosylation permits binding to M6P receptors. The M6P receptors target then the enzyme to lysosomes (Schissel *et al.* 1998).

The translocation of A-SMase to the plasma membrane is triggered, for example, by CD95 and TRAIL-R2, or by infection with *Pseudomonas aeruginosa*, *Neisseria gonorrhoeae*, *Staphylococcus aureus* or rhinovirus (Stancevic and Kolesnick, 2010). It was demonstrated that A-SMase resides in secretory lysosomes that are mobilized upon stimulation to fuse with the cell membrane and that the t-SNARE protein syntaxin-4 is required for the translocation of A-SMase (Perrotta *et al.* 2010). Another study showed that dysferlin is required for translocation of these vesicles (Han *et al.* 2012). The translocation of A-SMase leads to the fusion of secretory lysosomes with the plasma membrane resulting in exposure of A-SMase to the membrane extracellular leaflet of the cell. The hydrolysis of sphingomyelin to ceramide at the plasma membrane results in the formation of lipid microdomains as described in 2.4.1.

Apart from receptor-mediated activation, A-SMase can be activated by receptor-independent stimuli, like irradiation, UV-light, heat, oxidative stress or chemotherapeutic agents (Hannun and Obeid, 2008). Irradiation induces A-SMase activation in intact bovine aortic endothelial cells (Haimovitz-Friedmann *et al.* 1994). Experiments with A-SMase-deficient mice revealed that endothelial cells lacking A-SMase were entirely resistant to apoptotic cell death. Moreover, lymphoblasts from patients with Niemann-Pick disease were completely resistant to radiation-induced apoptosis (Santana *et al.* 1996). In Jurkat cells, it was shown that there are two distinct mechanisms for A-SMase activation. On the one hand, caspases were required and on the other hand, UV-C and ionizing radiation induced caspase-independent A-SMase activation (Rotolo *et al.* 2005). This then leads to the accumulation of ceramide-rich platforms, indicating that these membrane platforms may be responsible for irradiation-induced cell death. However, at present it is still not known how these stimuli can exactly activate A-SMase.

It is generally accepted that A-SMase plays a central role in cellular responses, including non-receptor mediated signals, infection with various pathogens, ligation of DRs to their respective ligands, and chemotherapeutic drugs (Gulbins and Li, 2006). Ceramide, generated by A-SMase, appears to be also involved in necroptosis. It was shown that ceramide is involved in necroptosis induced by the DR TNF-R1 in murine L929 fibrosarcoma cells, NIH3T3 fibroblasts and human Jurkat T-cells (Strelow *et al.* 2000; Thon *et al.* 2005). Furthermore, it could be shown that ceramide plays a role in TRAIL-induced necroptosis in murine L929, NIH3T3 fibroblasts and human Jurkat T cells, but that it is less pronounced than in necroptosis induced by the cytokine TNF (Thon *et al.* 2006; Voigt, Bachelor Thesis, 2009). Furthermore, TRAIL-induced necroptosis is effective to eliminate various types of human-derived tumor cells mediated by ceramide production (Voigt *et al.* 2014).

Despite the multitude of studies implicating the A-SMase and ceramide pathway in apoptosis, many important questions regarding the roles and regulation of A-SMase during necroptosis remain unanswered. For example, the molecular mechanism(s) of A-SMase regulation under caspase blocking conditions, as well as the cellular pathways involved in regulating A-SMase trafficking, localization and activity, are at present unresolved.

3. Aims of the presented dissertation

The specific and detailed knowledge of apoptotic signaling has resulted in the targeted design and development of new drugs. This suggests that a comparably detailed functional and structural analysis of regulated necrosis signaling pathways holds similar therapeutic potential. To this end, the work plan for this thesis was divided into three major parts dealing with different aspects of regulated necrosis and especially necroptosis. The main goals were to unravel different molecular aspects of the distinct induction (1; chapter 5.1) and execution (2; chapter 5.2) mechanisms of regulated necrosis and necroptosis, thereby providing a basis for further translation into new therapeutically options (3; chapter 5.3) for, e.g. the elimination of tumor cells or for diseases that are caused by inappropriate induction of regulated necrosis.

(1) As described above, it has been proposed that regulated necrosis can be induced by several molecular pathways. One key question was therefore whether individual pathways such as necroptosis and PARP-1-induced regulated necrosis depend on common execution mechanisms as part of an interacting network. First, the induction of regulated necrosis by TNF or DNA-alkylating agents such as 1-methyl-3-nitro-1-nitrosoguanidine (MNNG) or methyl methanesulfonate (MMS) will be analyzed morphologically and at the molecular level conducting caspase activity assays and measurements of intracellular ATP levels in different model cell lines for necroptosis. These model cell lines were either described earlier or will be characterized in the course of the study. Second, the interruption of the PARP pathway by PARP-1 inhibitors and genetic interference with JNK and cathepsin proteases as further components of the PARP pathway will be addressed to understand the molecular mechanisms underlying both modes of regulated necrosis. Third, the role of the kinase RIPK3 for initiation and execution of both pathways will be investigated. This will give an overview on potential differences between signaling in necroptosis and PARP-1-induced regulated necrosis and thus may provide first answers to the recently raised question whether there is one core program or several independent pathways of regulated necrosis which are important for the future design of therapeutic strategies targeting components of regulated necrosis.

(2) Moreover, exploring in more detail the contribution of common executioner mechanisms in regulated necrosis and especially necroptosis could validate, challenge and disentangle the current view of the different execution mechanisms of regulated necrosis (see 2.2.1.2). In apoptosis, cleavage of proteins by caspases is essential for the initiation and execution of PCD and thus for the survival and homeostasis of multicellular organisms (Degterev and Yuan, 2008). As described above, proteolysis appears to be equally important in regulated necrosis, but the underlying mechanisms rely on alternative and yet marginally characterized proteolytic events. The second and main purpose of the dissertation aims to further define the role of proteolysis in the regulation of death receptor-mediated regulated necrosis/necroptosis. High throughput techniques as well as proteomic approaches will be

employed to identify known or unknown proteases and their substrates participating in necroptosis. One aim will be the identification of new or known serine proteases and their substrates that appear to be crucial in necroptosis by employing affinity-labeling of potential candidates with an active-site-directed inhibitor derivate. As a complementary approach, it is planned to screen all 585 proteases encoded by the human genome using an RNA interference (RNAi) approach to define their relevance in necroptosis. Subsequently, the immunomagnetic enrichment of necroptotic TNF-R1-containing vesicles in combination with proteomic technologies will be conducted to isolate proteolytic substrates and to further examine the signaling pathway of necroptosis within the cell. Then, it is planned to characterize the proteases and potential substrates identified with the above utilized methods with regard to their relevance in TNF- and TRAIL-induced regulated necrosis. As a secondary goal, the proteolytic maturation and activation of A-SMase will be investigated during TNF-induced necroptosis by conventional Western blot analysis and enzymatic activity measurements. Furthermore, it is planned to identify the exact cleavage site of mature, active A-SMase to provide information about the so far unknown protease that possibly cleaves A-SMase in a caspase-independent manner.

(3) The third part of the thesis will provide new and additional information on the potential of ceramide-mediated necroptosis in clinically relevant tumor cell lines. A panel of tumor cell lines will be analyzed with regard to their sensitivity towards necroptotic stimuli. Successively, the role of possible effector proteins of the signaling cascade will be investigated by pharmacological inhibitor studies of relevant signaling components. Since TRAIL selectively eliminates tumor cells without affecting normal cells, the effectiveness of the induction of necroptosis through TRAIL will be in the focus of this part of the study.

In summary, the study should provide a better understanding of the initial and subsequent steps of regulated necrosis and especially necroptosis, with the intention to provide a basis for further translation into new therapeutic options for, e.g. elimination of apoptotic-resistant tumors or diseases that are caused by inappropriate induction of regulated necrosis.

4. Materials and Methods

4.1 Materials

4.1.1 Technical equipment

Company	Equipment
AB SCIEX, Darmstadt, Germany	AB SCIEX GPS software, Version 3.6, build 332 MALDI targets (Opti-TOF, 384 Well Insert) MALDI-TOF/TOF 5800, 4000 Series Explorer Software
BD Biosciences, Heidelberg, Germany	FACSCalibur flow cytometer Software: BD CellQuest™ Pro V. 4.0.2 PRIMARIA™ cultureware 5 mL polystyrene round-bottom FACS tubes Plastipak™ 1 ml syringe
Beckman Coulter, Krefeld, Germany	TL-100 Ultracentrifuge, SW32 rotor Ultra centrifuge XL-800, SW60Ti rotor Ultra clear™ Centrifuge Tube, 11 x 60 mm
Biometra, Göttingen, Germany	Rocking platform WT12
Bio-Rad, Munich, Germany	Gene Pulser™ X Cell Mini PROTEAN® System Casting Stand Glass plates 1.0 mm, 10-well comb Power Pac 3000 protein blotting cell Smart SpecTM 3000 spectrometer
Branson Ultrasonics, Danbury, CT, USA	W-450 sonication device
Carl Roth, Karlsruhe, Germany	Microscope slides
Dionex, Idstein, Germany	Acclaim PepMap100 C-18 column UltiMate 3000 RS Nano/Cap System
Duran Group, Mainz, Germany	Conical glass tubes
Eppendorf, Hamburg, Germany	Bench-top centrifuge (5415D) Refrigerated centrifuge (5417R) Thermomixer compact
GE Healthcare, Munich, Germany	Ettan DALTsix large vertical electrophoresis system HiTrap™ Protein G HP 1mL columns Hyperfilm™ Hypercassette™ 18 x 24 cm Molecular Dynamic Personal Densitometer SI Software: PDSI Scanner Control V5.03 Typhoon Trio imager Software: Image Master 6.0, DeCyder 6.5

Company	Equipment
GFL, Wunstorf, Germany	Water bath 1003 Shaker 3033
Gilson, Middleton, WI, USA	Minipuls 3 casing pump Pipettes (10, 20, 200 and 1000 µL)
Greiner Bio-One, Frickenhausen, Germany	Serological pipettes (1, 5, 10, 25 and 50 mL) 15 and 50 mL tubes
Heraeus, Osterode, Germany	Drying oven T6760 Lamin Air HA2472GS Megafuge 1.0 (R) Minifuge RF
Hirschmann Laborgeräte, Eberstadt, Germany	Pipetus-Accu
HOOCK, Kiel, Germany	Magnetic device: HOKImag 1
Lonza Group, Basel, Switzerland	Amaxa® Nucleofector™ Device
Merck, Darmstadt, Germany	High-performance thin layer chromatography plates
MSE, London, UK	Soniprep 150 (ultrasonic disintegrator)
Nerbe Plus, Winsen/Luhe, Germany	'V' bottom 96-well plates
Nikon, Düsseldorf, Germany	DS-5M-L1 Digital Sight Camera System
Panasonic, Wiesbaden, Germany	Lumix DMC-FS10 digital camera
PeqLab Biotechnologie, Erlangen, Germany	NanoDrop® photospectrometer ND-1000 Software: ND-100 v. 3.7.9
Sarstedt (DESAGA), Nümbrecht, Germany	Chromatography chamber 1 mL non-pyrogenic serological pipette
Sigma Zentrifugen, Osterode, Germany	Refrigerated centrifuge (6K10)
Sterilin, Caerphilly, UK	40 x 6 mm round base test tube (RT15)
Tecan Group, Männedorf, Germany	Freedom Evo 200 robotic platform Infinite M200 ELISA Microplate Reader, Software: i-Control 1.3
Thermo Scientific, Waltham, MA, USA	Cell culture incubator 3336 Multidrop cell dispenser Orbitrap LTQ Velos mass spectrometer Proteome Discoverer software (version 1.3 and 1.4): Sequest, Mascot and MS Amanda SpeedVac centrifuge
VWR International GmbH, Darmstadt, Germany	1.5 x 3 mm silicone tubing 4 x 6 mm silicone tubing

Company	Equipment
Wheaton, Millville, NY, USA	15 mL tissue grinder, dounce
Zeiss, Göttingen, Germany	Axiovert 10 microscope Axiovert 135 microscope Axioskop 510 laserscanning microscope Software: AIM LSM Image Browser

4.1.2 Chemicals and reagents

Unless otherwise stated all basic chemicals were purchased by Merck (Darmstadt, Germany) and Sigma-Aldrich (Munich, Germany).

Company	Product
Alexis Biochemicals, Lörrach, Germany	Super*Killer*TRAIL™
AppliChem, Darmstadt, Germany	Click-RPMI cell culture medium
Axon, Groningen, The Netherlands	Olaparib (PARP-1 inhibitor)
Bachem, Heidelberg, Germany	zVAD-fmk ac-zDEVD-AFC ac-zIETD-AFC
BASF Bioresearch, Ludwigshafen, Germany	hTNF
BD Biosciences, Heidelberg, Germany	Streptavidin-PE Bacto-tryptone
Biochrom, Berlin, Germany	10 X Trypsin/EDTA L-glutamine PBS FCS
Biomol, Hamburg, Germany	N-[L-3-trans-(propylcarbamoyl)-oxirane-2-carbonyl]-L-Ile-L-Pro methyl ester (CA-074 Me)
Bio-Rad, Munich, Germany	Flamingo™ Fluorescent gel stain Mini-PROTEAN TGX Precast Gels
Cambrex, East Rutherford, NJ, USA	Sea Plaque agarose
Cell Signaling Technology, Danvers, MA, USA	LumiGLO® chemiluminiscent substrate
ChemieTek, Indianapolis, IN, USA	Birinapant (Smac mimetic)
Fermentas, St. Leon-Rot, Germany	PageRuler™ protein marker
GE Healthcare, Munich, Germany	CyDyes DeStreak Rehydration solution GammaBind G-sepharose

Company	**Product**
Granovita, Heimertingen, Germany	Milk powder
Hartmann Analytic GmbH, Braunschweig, Germany	N-methyl-[^{14}C]-sphingomyelin
ICT, Bloomington, MN, USA	FLISP™ Serine Protease Detection Assay Kit
Imgenex, San Diego, CA, USA	FAM-Phe-CMK SerPase™ Kit
Invitrogen, Darmstadt, Germany	GIBCO® RPMI 1640 and DMEM cell culture medium Freestyle™ 293 Expression Medium Lysotracker® Red DND 99 ProLong® Gold antifade reagent with DAPI Protein G, Alexa Fluor® 488 conjugate
Life Technologies, Darmstadt, Germany	Opti-MEM® medium siPORT™ Amine Transfection Agent
Lonza Group, Basel, Switzerland	Amaxa® Cell line Nucleofector™ Kit V
Macherey-Nagel, Düren, Germany	Porablot nitrocellulose membrane
Miltenyi Biotec, Bergisch-Gladbach, Germany	Protein G micro beads Streptavidin micro beads
PAA Laboratories, Pasching, Austria	Accutase Sodium pyruvate G418-sulphate
PeptaNova, Sandhausen, Germany	$(Z\text{-}LL)_2$-ketone
PeqLab Biotechnologie, Erlangen, Germany	peqGOLD agarose
Promega, Madison, WI, USA	Cell Titer-Glo® Luminescent Cell Viability Assay
Qiagen, Hilden, Germany	Plasmid Maxi Kit
R&D Systems, Minneapolis, MN, USA	Fluorokine® Biotinylated Human TNF-α Kit
Roche, Mannheim, Germany	Complete Mini and Maxi – protease inhibitor cocktail Pefabloc SC®
Serva, Heidelberg, Germany	Acrylamide/bis-Solution TEMED Trypan blue solution Albumin bovine fraction V, pH 7.0 Sequencing-grade trypsin Yeast extract
TCI, Zwijndrecht, Belgium	1-methyl-3-nitro-1-nitrosoguanidine (MNNG) 3-aminobenzamide (3-AB; PARP-1 inhibitor)

Company	Product
Thermo Scientific, Waltham, MA, USA	BCA Protein Assay Kit BSA standard Coomassie based reagent Zeba™ Spin Desalting Columns 7K
Tocris Bioscience, Ellisville, MO, USA	PJ-34 (PARP-1 inhibitor)
Zinsser Analytic, Frankfurt a.M., Germany	Liquid scintillator fluid Aquasafe 300 plus

4.1.3 Plasmids and siRNAs

The plasmid pEF6.V5/His.aSMase^{wt} (referred to as V5-A-SMase throughout this thesis) coding for a human V5-tagged version of full-length A-SMase was obtained from Yusuf A. Hannun (Department of Biochemistry and Molecular Biology, Charleston, SC, USA) and described previously (Zeidan and Hannun, 2007). The transfection vector BMGneo harboring a neomycin resistance cassette was described earlier (Karasuyama and Melchers, 1988) and was used for stable transfection of pEF6.V5/His.aSMase^{wt} into L929Ts cells (see 4.2.2.4). Plasmids coding for Fc-tagged TNF variants based on the expression vectors pCR™ 3 (TNF60-Fc) and pdg105 (TNFwt-Fc) were obtained from Harald Wajant (University Würzburg, Germany) and used to produce the fusion proteins TNF60-Fc and TNFwt-Fc (see 4.2.14.3). The transfection-ready DNA of a myc-DDK-tagged ORF clone of *Homo sapiens* phosphoglycerate mutase family member 5 (PGAM5, NM: 001170543.1) in a pCMV6-entry vector was purchased from OriGene (catalog number: RC201678, Rockville, MD, USA), used for stable transfection of L929Ts cells and is referred to as PGAM5-FLAG throughout this thesis. The expression plasmids pPPHβ and pPPHβ E90A were a gift from Christoph Becker-Pauly (Christian-Albrechts-University, Kiel, Germany) and described earlier (Eldering *et al.* 1997). These plasmids were used to transiently express wild-type meprin β or an inactive meprin β mutant (E90A).

Table 1: List of all siRNAs used.

Product	Description	Catalogue number	Company
siGENOME Human **CASP8**	mixture of four siRNAs targeting caspase-8	M-003466-05	Thermo Scientific, Waltham, MA, USA
siGENOME Human **CFLAR**	mixture of four siRNAs targeting caspase 8 and FADD-like apoptosis regulator (CFLAR) (also known as c-FLIP, I-FLICE)	M-003772-06	Thermo Scientific, Waltham, MA, USA
siGENOME Human **CYLD**	mixture of four siRNAs targeting cylindromatosis (turban tumor syndrome) protein	M-004609-01	Thermo Scientific, Waltham, MA, USA
Silencer® Select Human **DNM1L**	individual siRNA targeting dynamin 1-like protein (alias DRP1)	S19560	Life Technologies, Darmstadt, Germany
Silencer® Select Mouse **Dnm1l**	individual siRNA targeting dynamin 1-like protein (alias DRP1)	S92135	Life Technologies, Darmstadt, Germany

Product	Description	Catalogue number	Company
siGENOME Human **DPYSL4**	mixture of four siRNAs targeting dihydropyrimidase-like 4 (other known aliases: Crmp3, Drp-4)	M-008504-00	Thermo Scientific, Waltham, MA, USA
siGENOME Human **GGT1**	mixture of four siRNAs targeting gamma-glutamyltransferase 1	M-005884-02	Thermo Scientific, Waltham, MA, USA
Silencer® Select Human **HTRA2**	validated siRNA targeting HtrA (high temperature requirement protein A) serine peptidase 2 or Omi stress-regulated endoprotease (HtraA2/Omi)	S654	Life Technologies, Darmstadt, Germany
Silencer® Human Druggable Genome siRNA **library**	Version 3 covering 23,349 human genes with 3 individual siRNAs targeting 7,783 human genes	4391844	Life Technologies, Darmstadt, Germany
siGENOME Human **LONP1**	individual siRNA targeting Lon protease 1	D-003979-01	Thermo Scientific, Waltham, MA, USA
siGENOME Human **MEP1B**	individual siRNA targeting meprin A beta alias PPH beta or Mep1β	D-005942-01	Thermo Scientific, Waltham, MA, USA
Silencer® Select Human **MLKL**	individual siRNA targeting mixed lineage kinase domain-like protein	42942	Life Technologies, Darmstadt, Germany
Silencer® Select Mouse **Mlkl**	individual siRNA targeting mixed lineage kinase domain-like protein	S92950	Life Technologies, Darmstadt, Germany
siGENOME Human **MMP3**	mixture of four siRNAs targeting matrix metalloproteinase 3 (stromelysin 1)	M-005968-03	Thermo Scientific, Waltham, MA, USA
Silencer® **Negative Control**	control #1 siRNA with no significant sequence similarity to mouse or human genes	AM4611	Life Technologies, Darmstadt, Germany
siGENOME **Non-Targeting** siRNA Pool # 1	pool of 4 non-targeting siRNAs, control for experiments with siGENOME reagents	D-001206-13	Thermo Scientific, Waltham, MA, USA
Silencer® Select Human **PGAM5**	individual siRNA targeting phosphoglycerate mutase family member 5 (serine/threonine phosphatase)	S46938	Life Technologies, Darmstadt, Germany
Silencer® Select Mouse **Pgam5**	individual siRNA targeting phosphoglycerate mutase family member 5 (serine/threonine phosphatase)	S91079	Life Technologies, Darmstadt, Germany
siGENOME Human **PMPCA**	individual siRNA targeting mitochondrial processing peptidase alpha	D-008734-02	Thermo Scientific, Waltham, MA, USA
siGENOME Human **PRPF8**	mixture of four siRNAs targeting pre-mRNA processing factor 8	M-012252-02	Thermo Scientific, Waltham, MA, USA
siGENOME Human **PSMA1**	individual siRNA targeting proteasome subunit, alpha type-1	D-010123-01	Thermo Scientific, Waltham, MA, USA

Product	Description	Catalogue number	Company
Silencer® Select Human **RIPK1**	validated siRNA targeting receptor-interacting serine/threonine kinase 1	S16653	Life Technologies, Darmstadt, Germany
siGENOME Human **RIPK3**	validated siRNA targeting receptor-interacting serine/threonine kinase 3	D-003534-01	Thermo Scientific, Waltham, MA, USA
Silencer® Select Human **RIPK3**	individual siRNA targeting receptor-interacting serine/threonine kinase 3	S21741	Life Technologies, Darmstadt, Germany
siGENOME Human **TMPRSS11E**	mixture of four siRNAs targeting transmembrane protease serine 11E (DESC1)	M-005847-02	Thermo Scientific, Waltham, MA, USA
Silencer® Select Human **TNFRSF1A**	validated siRNA targeting TNF-R1	S14266	Life Technologies, Darmstadt, Germany
siGENOME Human **YME1L1**	individual siRNA targeting YME1-like ATPase (presenilin associated metalloprotease)	D-006103-02	Thermo Scientific, Waltham, MA, USA

4.1.4 Antibodies

Table 2: List of all applied primary and secondary antibodies and their working dilutions.

Target and clone	Used dilution	Article number	Company
primary antibodies:			
α-Actin, C-11	1:10,000	sc-1615	Santa Cruz Biotechnology, Heidelberg, Germany
β-Actin, AC-15	1:10,000	A1978	Sigma-Aldrich, Munich, Germany
A-SMase	1:1,000	#3687	Cell Signaling Technology, Danvers, MA, USA
Caspase-7, E22	1:1,000	Ab32522	Abcam, Cambridge, UK
cleaved Caspase-7, D198	1:1,000	#9491	Cell Signaling Technology, Danvers, MA, USA
Caspase-8, IC12, human Caspase-8, murine	1:1,000 1:1,000	#9746 #4927	Cell Signaling Technology, Danvers, MA, USA
COXIV	1:10,000	#4850	Cell Signaling Technology, Danvers, MA, USA
Drp-1, H-300	1:1,000	sc-32898	Santa Cruz Biotechnology, Heidelberg, Germany
FLAG, M2	1:1,000	035K6196	Sigma-Aldrich, Munich, Germany
HtrA2/Omi, E55	1:1,000	ab32092	Abcam, Cambridge, UK
IgG_1 fluorescence control	1:5	349040	BD Biosciences, Heidelberg, Germany
JNK1, G151-333	1:1,000	554286	BD Biosciences, Heidelberg, Germany
JNK2, A-7	1:1,000	sc-271133	Santa Cruz Biotechnology, Heidelberg, Germany
Lamp-1	1:500	611043	BD Biosciences, Heidelberg, Germany
Lamp-1, supernatant	1:100	1D4B	DSHB, Iowa City, IA, USA
Lamp-2, CD107b, H4B4	1:1,000	SBA-9840-01	Southern Biotech, Birmingham, AL, USA
MLKL	1:1,000	SAB2103620	Sigma-Aldrich, Munich, Germany

Target and clone	Used dilution	Article number	Company
primary antibodies:			
PARP-1	1:1,000	#9542	Cell Signaling Technology, Danvers, MA, USA
PGAM5, K-16	1:1,000	sc-161156	Santa Cruz Biotechnology, Heidelberg, Germany
Rab5	1:1,000	#3547	Cell Signaling Technology, Danvers, MA, USA
Rab5	1:300	sc-598	Santa Cruz Biotechnology, Heidelberg, Germany
RIPK1	1:1,000 or 1:100	610459	BD Biosciences, Heidelberg, Germany
RIPK3, human	1:1,000	PAB0287	Abnova, Heidelberg, Germany
RIPK3, murine	1:1,000	PRS2283	Sigma-Aldrich, Munich, Germany
TNFα	1:1,000	sc-8301	Santa Cruz Biotechnology, Heidelberg, Germany
TNF-R1	1:1,000	sc-8436	Santa Cruz Biotechnology, Heidelberg, Germany
TRAIL-R1, HS101	1:100	ALX-804-297	Alexis Biochemicals, Lörrach, Germany
TRAIL-R2, HS201	1:100	ALX-804-298	Alexis Biochemicals, Lörrach, Germany
V5	1:5,000	P/N 46-0705	Invitrogen, Darmstadt, Germany
secondary antibodies:			
biotin rat anti-mouse IgG_1	1:50	553441	BD Biosciences, Heidelberg, Germany
donkey anti-rabbit Alexa Fluor® 555 IgG (H+L)	1:200	A-31572	Life Technologies, Darmstadt, Germany
goat anti-mouse Alexa Fluor® 555 IgG (H+L)	1:200	A-31572	Life Technologies, Darmstadt, Germany
goat anti-mouse IgG2b-horseradish peroxidase (HRP)	1:2,500	sc-2062	Santa Cruz Biotechnology, Heidelberg, Germany
secondary antibodies, alkaline phosphatase (POD)-coupled	1:10,000		Jackson Immuno Research Laboratories, West Grove, PA, USA

4.1.5 Cell lines

The murine fibrosarcoma cell line L929Ts is a TRAIL-sensitive sub line of the L929 cell line derived in the laboratory of Dieter Adam (Christian-Albrechts-University, Kiel, Germany) and has been described earlier (Thon *et al*. 2006). L929sA cells were kindly provided by Peter Vandenabeele (Ghent University, Ghent, Belgium) and have been described previously (Vanhaesebroeck *et al.* 1992). Wild-type and RIPK3-deficient mouse embryonic fibroblasts (MEFs) as well as murine NIH3T3 cells naturally expressing RIPK3 have been previously described (Sosna, Voigt *et al*. 2014). Cells deficient for RIPK3 expression and transfectants stably expressing murine green fluorescent protein (GFP) fusions to wild-type or kinase-defective murine RIPK3 in the vector pEGFP-N1 (Takara Bio Inc., Mountain View, CA, USA) were generated and provided by Francis Ka-Ming Chan (University of Massachusetts Medical School, Worcester, MA, USA), together with human Jurkat I42 acute leukemia T cells deficient for FADD but additionally stably transfected with TNF-R2 (Chan *et*

al. 2003). Hamster embryonic kidney cells constitutively expressing the simian virus 40 (SV40) large T antigen (HEK293T), MCF-7, HeLa, L929ATCC and wild-type Jurkat cells (clone E6-1) were obtained from the American Type Culture Collection (ATCC, Manassas, VA, USA). Immortalized MEFs deficient for caspase-7 expression and their wild-type counterparts were kindly provided by Stefan Schütze (Christian-Albrechts-University, Kiel, Germany). These MEFs were originally generated by Richard Flavell (Yale School of Medicine, New Haven, CT, USA). MEFs lacking SPPL2a or SPPL2b or SPPL2a/b and wild-type cells as control were generated and kindly provided by the group of Bernd Schröder (Christian-Albrechts-University, Kiel, Germany). Presenilin-1/2-deficient MEFs were a gift from Paul Saftig (Christian-Albrechts-University, Kiel, Germany) and have been described (Herreman *et al.* 1999). Immortalized wild-type and JNK1/JNK2 double-deficient MEF were a kind gift from Roger Davis (University of Massachusetts Medical School, Worcester, MA, USA). Wild-type, cathepsin D-deficient, and cathepsin D-deficient MEF stably transfected with the pro-cathepsin D cDNA have been previously described (Heinrich *et al.* 2004). Primary lung fibroblasts from JNK1- and JNK2-deficient mice and their wild-type littermate controls were prepared in the laboratory of Dieter Adam (Christian-Albrechts-University, Kiel, Germany). Human gall bladder adenocarcinoma (Mz-ChA-1), pancreatic adenocarcinoma (Colo357, PancTu-I, Panc89, A818-4, Pt45P1), gastric adenocarcinoma (MKN-28) and non-small cell lung carcinoma (KNS-62) cell lines have been described (Egberts *et al*. 2007; Sipos *et al.* 2003; Kurdow *et al.* 2005; Juhl *et al.* 1997). The leukemia-derived U-937, CCRF-CEM, pancreatic BxPC-3, colorectal HT-29, ovary adenocarcinoma SK-OV-3 and malignant melanoma-derived SK-MEL-28 cancer cells were originally obtained from ATCC and were, as well as Mz-ChA-1, Colo357, PancTu-I, Panc89, A818-4, Pt45P1, MKN-28 and KNS-62, a gift from Holger Kalthoff (Christian-Albrechts-University, Kiel, Germany). HEK293T and all MEFs were cultivated in DMEM supplemented with 10 % (v/v) FCS, 50 µg/mL penicillin and streptomycin each and 50 µM β-mercaptoethanol in 0.9 % (w/v) NaCl. Mz-ChA-1, KNS-62, U-937 and HT-29 were maintained in RPMI 1640 medium supplemented with 10 % (v/v) heat-inactivated FCS and 1 mM sodium pyruvate. L929, NIH3T3 and Jurkat cells were cultivated in a mixture of Click's/RPMI 1640 medium (50/50 % (v/v)), supplemented with 10 % (v/v) heat-inactivated fetal calf serum (FCS), 2 mM L-glutamine, 50 µg/mL penicillin and streptomycin. All described cell lines were maintained in a humidified incubator containing 5 % (w/v) CO_2 at 37 °C.

For passaging, cells were detached, using phosphate buffered saline (PBS) supplemented with 0.5 % (v/v) trypsin and 0.2 % (v/v) EDTA every two to four days and re-seeded in fresh medium. For functional assays (to preserve the integrity of cell surface molecules), cells were alternatively detached with accutase. For long-term storage, cell lines were re-suspended in FCS with 10 % (v/v) DMSO and frozen in liquid nitrogen.

4.2 Methods

4.2.1 Cytotoxicity assays

4.2.1.1 Trypan blue staining

To determine the amount of dead cells (when measuring ceramide levels), cells were pelleted and re-suspended in PBS. An aliquot of the cell suspension was added to the same volume of 0.4 % (v/v) trypan blue staining solution and applied onto a Neubauer counting chamber. Live cells with an intact cell membrane did not absorb trypan blue and were scored separately from dead (blue) cells.

4.2.1.2 Measurement of intracellular ATP levels

The loss of intracellular ATP was measured as a marker for cell death. Intracellular ATP content was determined with the Cell-Titer GLO® Assay Kit following the instructions of the manufacturer.

4.2.1.3 Crystal violet staining

For determination of cell viability by crystal violet staining, cells were seeded onto flat-bottom 96-well plates. After stimulation as indicated in the figure legends, adherent cells were washed twice with PBS and stained with crystal violet solution (0.5 % (w/v) crystal violet, 4 % (w/v) formaldehyde, 30 % (v/v) ethanol, and 0.17 % (v/v) NaCl) for 10 min at 37 °C. The staining solution was carefully washed away with tap water and the cells were dried at 50 °C for 1 h. Stained cells were dissolved in 33 % (v/v) acetic acid and the absorbance of the staining was measured in a microplate reader at 570 nm.

4.2.1.4 Propidium iodide staining

For flow cytometric analysis of cell death (e.g. loss of membrane integrity), cells were seeded in 12-well plates at 70 % confluence. Suspension cell lines (U-937 and Jurkat T cells) were stimulated immediately whereas adherent cells were left to attach over night. After treatment, adherent (detachment with accutase) and detached cells were collected followed by centrifugation at 400 x g for 5 min at 4 °C. The cell pellet was washed once in cold PBS/5 mM EDTA, resuspended in PBS/EDTA containing 2 µg/mL propidium iodide (PI), and analyzed for loss of membrane integrity on a FACSCalibur flow cytometer at red fluorescence.

For every flow cytometric measurement, 10,000 cells were examined and cellular debris was excluded from the analysis. All values for loss of membrane integrity were calculated as 100 % minus PI-negative intact, alive cells to account for disintegrated dead cells that have lost their PI staining again due to diffusion.

4.2.2 Clonogenic survival assays

The analysis of clonogenic survival of cells was carried out as described by Franken and coworkers (Franken *et al.* 2006). Briefly, after treatment, 1,000 viable cells were re-suspended in RPMI 1640 supplemented with 10 % FCS and 1 mM sodium pyruvate and plated into 6-well plates, cultured for 7 days, and stained with crystal violet staining solution (see 4.2.1.3) for 10 min at 37 °C. The remaining staining solution was washed away and plates were dried at 50 °C. Colony formation (>10 cells) was determined from pictures taken with a digital camera (Lumix DMC-FS10, Panasonic, Wiesbaden, Germany). Non-adherent U-937 cells were alternatively analyzed for their ability to form colonies in soft agarose by mixing treated cells with 2 mL of 0.4 % (w/v) Sea Plaque agarose in RPMI 1640 supplemented with 10 % FCS and 1 mM sodium pyruvate. This cell suspension was then transferred into a 6-well plate containing 3 mL of a 1 % (w/v) peqGOLD agarose underlayer in complete medium in each well. Cells were incubated for 7 days at 37 °C. Again, colony formation (>10 cells) was determined from pictures taken with a digital camera. For this purpose, cells were stained with 1 mL of 3-[4,5-dimethylthiazol-2yl]-2,5-diphenyltetrazolium bromide (MTT; 2.5 mg/mL in PBS) for 2 h at 37 °C to allow metabolization of MTT to blue MTT-formazan.

4.2.3 Transfection

All used constructs and siRNAs are listed in 4.1.3.

4.2.3.1 Nucleofection

L929Ts cells were transfected with 150 pmol siRNA using the Amaxa® Cell line Nucleofector™ kit V according to manufacturer's instruction. Briefly, 1 x 10^6 cells per transfection were pelleted and re-suspended in 100 µL room temperature (RT) solution V. The cell suspension was combined with either 150 pmol siRNA or 10-20 µg DNA and transferred into a cuvette. The transfection was applied with Nucleofector® Program T-20 and cells were gently transferred into 6-well plates containing pre-warmed media for 24-72 h.

HT-29 cells were transfected as above using the Amaxa® Cell line Nucleofector™ kit R according to the manufacturer's standardized protocols.

4.2.3.2 Electroporation

U-937, HEK293T and L929Ts cells were transfected using electroporation with an electroporation device from Bio-Rad. Depending on the purpose of the transfection, 2-10 x 10^6 cells were pelleted and dissolved in 200 µL cell specific medium without supplements and mixed with the desired siRNA (150 pmol) or DNA (10 µg). The mixture was transferred into a 0.2 µm pre-warmed cuvette and placed into the electroporation device. The parameters for electroporation were optimized for each cell line and depicted in table 3.

Table 3: Electroporation settings for U-937, HEK293T and L929Ts cells.

Cell line	Settings
U-937	155 V 1000 µF resistance [Ω]: ∞
HEK293T	110 V pulse length: 25 ms
L929Ts	280 V 960 µF resistance [Ω]: ∞

4.2.3.3 Reverse transfection with siPORT™ Amine Transfection Agent

The transfection with siPORT™ Amine Transfection Agent is polyamine-based and was utilized for HT-29 cells. For reverse transfections, 3 x 10^3 cells were utilized per transfection reaction in 96-well plates. For 12-well plates, 3 x 10^4 cells were used per transfection. For each 96-well plate transfection reaction, 9.4 µL OptiMEM® reduced serum media and 0.6 µL siPORT™ Amine solution (1:16 (v/v)) was incubated for 10 min at RT. Meanwhile, 2 µM siRNA (1 µL) was diluted in 9 µL OptiMEM®. After incubation, diluted siRNA and siPORT™ Amine solution were mixed and incubated for further 10 min and thereafter placed in 96-well (for viability assay; see 4.2.1.2) or 12-well plates (volumes were ten times multiplied respectively; for further Western blot analysis see 4.2.11) before the cell suspension was added. After 72 h post-transfection, either cellular extracts were prepared or cells were stimulated as indicated.

For each transfection reaction, the efficiency of the down-regulation was analyzed by Western blot analysis either for the protein of interest or control siRNAs.

4.2.3.4 Stable transfection of L929Ts cells

Stable transfection of L929Ts cells with pEF6.V5/His.aSMase^{wt} or myc-DDK-tagged PGAM5 was performed either by nucleofection or electroporation (see 4.2.3.1 and 4.2.3.2). The expression plasmid of PGAM5 already contains a neomycin resistance cassette, whereas pEF6.V5/His.aSMase^{wt} does not. Cells were transfected with 10 µg PGAM5-FLAG or a mixture of 2 µg of BMGNeo and 20 µg of V5-A-SMase plasmid. The transfected cells were transferred into fresh complete media over night. Further cultivation of transfected cells was performed in 14 cm cell culture plates at 1:5 (v/v) dilution in fresh media supplemented with 1 mg/mL G418 to select resistant transfectants. After approximately two weeks of cultivation with routine media change, cell colonies were visible. These sub clones were detached with sterile filter paper pieces soaked with PBS supplemented with 0.5 % (v/v) trypsin and 0.2 % (v/v) EDTA and transferred into 6-well plates. The cell clones were expanded and analyzed via Western blot for stable expression of the desired protein.

4.2.4 High-throughput RNA interference screen procedure with HT-29 cells

For a high-throughput RNA interference (RNAi) screen, the Silencer Human Druggable Genome siRNA Library V3 was used. From this siRNA library the respective 560 genes encoding protease siRNAs were selected and transferred to 96-well plates generating a human protease siRNA library. HT-29 cells (3,000 cells per well in 96-well plates) were reverse-transfected with three individual siRNAs per target gene (final concentration: 20 nM) using siPORT™ Amine Transfection Agent (see 4.2.3.3) and a multidrop cell dispenser (Freedom Evo 200 robotic platform). After 72 h, cells were stimulated for 20 h with TNF, zVAD-fmk and cycloheximide (CHX) or left unstimulated and intracellular ATP levels were measured (see 4.2.1.2). The experimental set up is depicted in Figure 5.

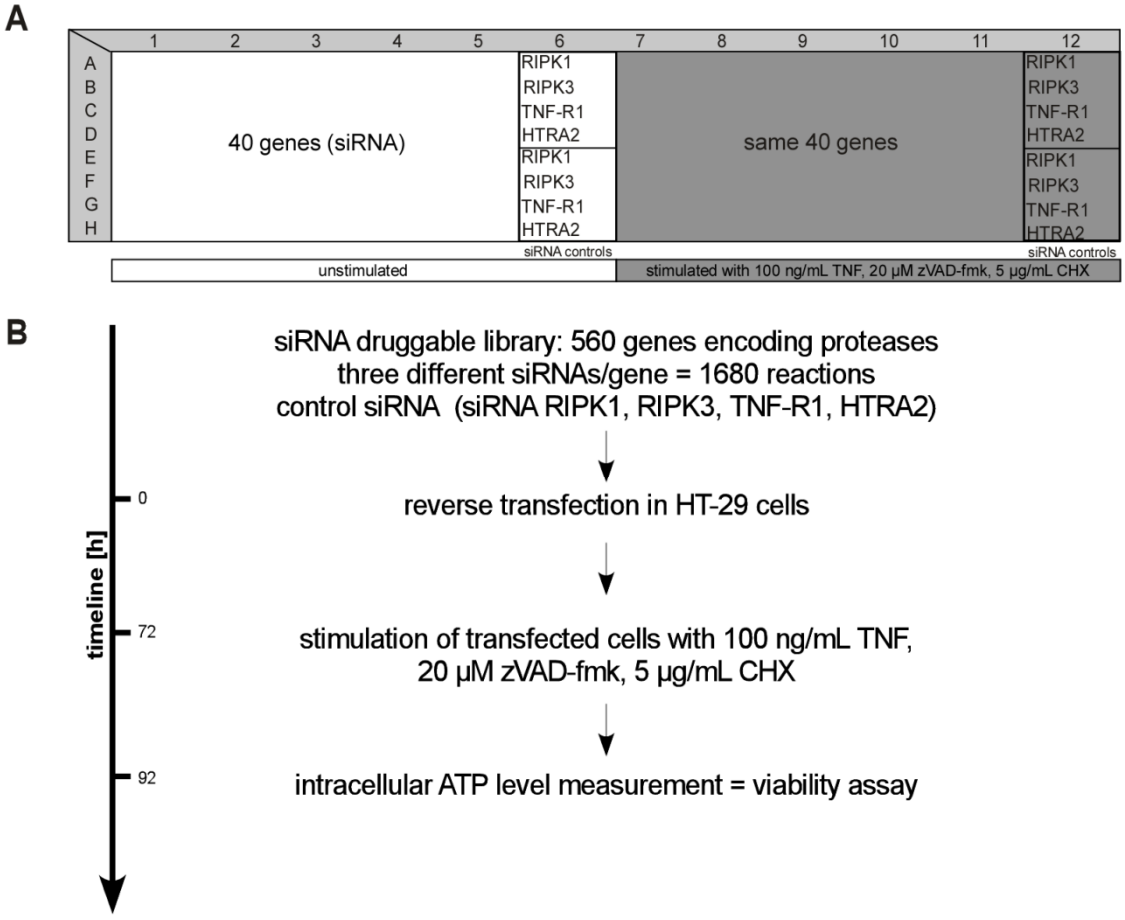

Figure 5: High-throughput siRNA screen for proteases participating in necroptosis. (A) The pipetting scheme for a Tecan Freedom Evo 200 robotic device and **(B)** the schematic diagram of the first screen is shown. HT-29 cells were reverse transfected with protease siRNA. After 72 h, necroptosis was induced by 100 ng/mL TNF, 20 µM zVAD-fmk and 5 µg/mL CHX. ATP levels were measured 20 h after stimulation. The complementary siRNA screen was performed in collaboration with the group of Philip Rosenstiel (Christian-Albrechts-University, Kiel, Germany).
Abbreviations: adenosine-5'-triphosphate (ATP), cycloheximide (CHX), high temperature requirement protein A2 (HTRA2), receptor-interacting serine-threonine protein kinase (RIPK), tumor necrosis factor (TNF), TNF-receptor 1 (TNF-R1), benzyloxycarbonyl-Val-Ala-Asp-fluoromethylketone (zVAD-fmk).

For data analysis, values of all plates were color-coded and manually inspected for systematic bias (e.g. row or rim effects) and/or inappropriate knock-down efficiency (i.e. the viability of either RIPK3 or TNF-R1 siRNA-transfected controls was less than twofold of the overall median calculated for each plate). Plates that did not meet these criteria were repeated before further analysis. Stimulation intensities (fold induction) were calculated by dividing unstimulated through stimulated treatment. Individual fold inductions were normalized to the median of the corresponding 96-well plate. Genes with normalized fold-induction values ≥ 1.5 or ≤ -1.5 were considered to be candidate genes (hits).

The described RNAi screen was performed in collaboration with Gunnar Jacobs (PopGen, Kiel, Germany) and the group of Philip Rosenstiel (Christian-Albrechts-University, Kiel, Germany).

4.2.5 Staining of cell surface molecules

4.2.5.1 Internalization studies of TNF-R1

The cell surface expression of TNF-R1 was detected by fluorescence based labeling of the receptor and flow cytometric analysis. U-937 cells were centrifuged at 100 x g for 10 min and washed twice with PBS. Cells were re-suspended in PBS to a final concentration of 4 x 10^6 cells/mL and cooled down to 4 °C. 50 µL of the washed and cold cell suspension was pre-incubated with zVAD-fmk or dynasore as indicated in the figure legends. After pre-incubation, cells were incubated with 400 ng ligand TNF60-Fc for 1 h on ice. Internalization of TNF60-Fc bound TNF-R1 complexes was achieved by incubation of the cell suspension at 37 °C for various time-points. The reaction was stopped by immediately cooling down on ice. To stain the receptor/ligand complexes still retained at the cell surface, the cell suspension was incubated with 1 µg of Protein G-Alexa Fluor® 488 for at least 30 min at 4 °C in the dark. Thereafter, cells were washed twice with 1 x RDF1 buffer (provided by the TNFα Kit from R&D) to minimize background staining and to remove unreacted Protein G-Alexa Fluor® 488. Cells were fixed in 0.2 mL of 3 % (w/v) paraformaldehyde (PFA) in PBS for final flow cytometric analysis at green fluorescence.

For control, the fluorescence of cells was measured which were incubated with Protein G-Alexa Fluor® 488 alone.

4.2.5.2 Cell surface staining of TRAIL receptors

To detect cell surface expression of TRAIL receptors (DR4 and DR5), a total of 4.5 x 10^5 U-937 cells were collected in a 'V'-bottom 96-well assay plate, washed once with washing buffer containing 1 % (w/v) bovine serum albumin (BSA) and 0.1 % (v/v) NaN_3 in PBS and centrifuged at 200 x g for 4 min at 4 °C. The cells were incubated with 10 µg/mL anti-TRAIL-R1 or anti-TRAIL-R2 mouse monoclonal antibodies in washing buffer for 1 h at 4 °C in a humidified chamber, washed twice with ice-cold washing buffer and incubated with anti-mouse biotin-conjugated secondary antibodies for one additional h at 4 °C. After two washing steps, cells were incubated with phycoerythrin-conjugated

streptavidin for further 15 min at 4 °C, washed twice and fixed in 150 µL PBS containing 1 % (w/v) PFA and transferred into 0.6 mL flow cytometric tubes. Samples were stored at 4 °C for further flow cytometric analysis.

For control, the fluorescence of cells was measured which were incubated with iso-type matched antibodies IgG_1 and incubated with anti-mouse biotin-conjugated secondary antibodies and phycoerythrin-conjugated streptavidin.

4.2.6 Caspase activity assay

Measurement of caspase-3 and -8 activities was based on the reaction of the enzymes with a specific fluorogenic substrate. Following treatment, adherent and detached cells were collected and lysed in a lysis buffer (10 mM HEPES pH 7.4, 142 mM KCl, 5 mM $MgCl_2$, 1 mM EGTA, 0.2 % (v/v) NP40, 1 mM dithiothreitol (DTT), 2 mM Pefabloc). Cytosolic extracts equilibrated with 1 mM dATP and 10 µM cytochrome c for 1 h at 30 °C (to activate caspases) served as positive control. To measure caspase-3 activity, 100 µM ac-zDEVD-afc (benzyloxycarbonyl (ac)-Asp-Glu-Val-Asp-7-aminotrifluoromethylcoumarin (afc)) diluted in 100 µL caspase buffer containing 20 mM Pipes pH 7.2, 100 mM NaCl, 10 mM DTT, 1 mM EDTA, 0.1 % (w/v) CHAPS and 10 % (w/v) sucrose was added to 10 µL cytosolic extracts (5-20 µg protein, depending on the enzymatic activity) and incubated at 37 °C for distinct time-points. For measuring caspase-8 activity, 100 µM ac-z-IETD-afc (ac-Ile-Glu-Thr-Asp-afc) was added to the caspase buffer. The release of afc was measured as emission at 505 nm upon excitation at 405 nm using a fluorimeter equipped with a thermo stated microplate reader.

4.2.7 Intracellular ceramide quantification

For measurement of ceramide generation, 1 x 10^7 cells per treatment and time-point were seeded onto 14 cm culture plates. After treatment, the supernatant and already detached cells were collected and the reaction was stopped by washing cells with ice-cold PBS. Adherent cells were detached by treatment with accutase, collected, and pooled with the supernatant followed by centrifugation at 400 x g for 5 min at 4 °C. The cell pellet was re-suspended in PBS and the cell number was counted (see 4.2.1.1). After counting, cells were washed twice in PBS and pelleted for either storage at -80 °C or immediate processing.

Lipid extraction with methanol/chloroform was performed at 4 °C according to the method of Bligh and Dyer (1959). Briefly, the cell pellet was re-suspended in 2 mL autoclaved Milli-Q water and 4 mL methanol (1:2 (v/v)) and transferred into a 14 mL conical glass tube. Subsequently, the mixture was homogenized with an ultrasonic disintegrator for 16 x 5 sec with 10 sec intervals between each sonication step. After sonication, 2 mL chloroform were added and the samples were again homogenized for 16 x 5 sec as described above. Samples were centrifuged for 10 min at 2,800 x g.

The upper phase was transferred into a 40 mL conical glass tube with 3 mL autoclaved Milli-Q water and 6 mL chloroform (1:2 (v/v)). For re-extraction, the lower and interphase were supplemented with 1 mL autoclaved Milli-Q water and 4 mL methanol (1:4 (v/v)), immediately sonicated for a second cycle as described above and centrifuged at 2,800 x g for 10 min. The resulting supernatant was pooled with the separately stored upper phase from the previous step and again centrifuged at 2,800 x g for 10 min. After centrifugation, the resulting lower organic phase - containing the extracted lipids - was transferred to a new glass tube and evaporated under 1 bar N_2 at 37 °C. Dried lipids were re-suspended in a mixture of chloroform/methanol (9:1 (v/v); recommended amount: 50 µL for a total of 1 x 10^7 cells). In parallel, for chromatographic separation of the lipids, thin layer chromatography plates were pre-run with chloroform/methanol (2:1 (v/v)) and dried for at least 30 min at 80 °C. The chromatography chamber was equilibrated with a solvent containing dichloromethane/acetic acid/methanol (100:5:2 (v/v)) for 1 h at RT. 50 µL of each sample and ceramide standards (1 nM, 2.5 nM and 5 nM; mostly composed of N-stearoylsphingosine) were diluted in chloroform/methanol (9:1 (v/v)), and applied onto the plate. The plate was run in the chromatography chamber with dichloromethane/acetic acid/methanol until the migration front had arrived at 1 cm below the upper end of the plate. After chromatography, the plate was dried for 10 min at 180 °C. For charring of the resolved lipids, the plate was submerged into a bath of 10 % (v/v) copper sulphate and 8 % (v/v) ortho-phosphoric acid for 15 sec at RT, dried for 2 min at 100 °C and charred by heating to 180 °C until lipid bands became visible. The plate was scanned and analyzed using the Molecular Dynamic Personal Densitometer SI and the program ImageQuant 5.2. Different ceramide species containing ester-linked fatty acids with 16 and 18 carbon atoms were identified by comparison with the applied co-migrating ceramide standards.

4.2.8 A-SMase activity assay

The measurement of A-SMase activity in cell lysates was described previously (Edelmann *et al*. 2011). Briefly, cells were detached with accutase, cooled down with cold medium and pre-incubated with zVAD-fmk and various stimuli indicated in the figure legends. After pre-incubation, the cell suspension was incubated with 100 ng/mL TNF for 1 h and internalization was induced by switching the temperature from 4 °C to 37 °C for a specific time kinetic. Internalization was stopped by washing cells twice with ice-cold PBS. Cell pellets were stored at -80 °C.

Prepared samples were kindly analyzed for A-SMase activity by Supandi Winoto-Morbach (Christian-Albrechts-University, Kiel, Germany). Concisely, cell pellets were washed twice with PBS and diluted in A-SMase assay buffer (250 mM sodium acetate, 1 mM EDTA, 0.1 % (v/v) Triton X-100, pH 5.0) and lysed by sonication for 4 x 1 sec on ice. The A-SMase activity was measured using N-methyl-[^{14}C]-sphingomyelin (0.5 µCi/mL, 0.55 Ci/mmol) as a radioactively labeled substrate. A range from 0.5-2 µg of protein was incubated with the substrate for 2 h at 37 °C in a total volume of 50 µL. Radioactivity of enzymatically liberated radioactive phosphocholine was extracted with

750 µL chloroform/methanol (2:1 (v/v)) and 250 µL of autoclaved Milli-Q water. The radioactive aqueous phase was mixed with liquid scintillator (Aquasafe 300 plus) and measured in a β-counter.

4.2.9 Preparation of cellular extracts

After removal of the supernatant, adherent cells were washed once with pre-warmed PBS and harvested after detaching with trypsin/EDTA in PBS or accutase. Detached cells were pelleted by centrifugation at 400 x g for 5 min at RT and washed twice with cold PBS. Suspension cells were immediately pelleted by centrifugation as described above and washed twice with cold PBS. Cells were lysed for 10 min on ice in cold TNE lysis buffer (50 mM Tris pH 8.0, 150 mM NaCl, 1 % (v/v) NP-40, 3 mM EDTA) supplemented with 10 µg/mL of a protease inhibitor cocktail. Lysates were centrifuged at 20,000 x g at 4 °C and the supernatants were stored at -20 or -80 °C until further analysis.

4.2.10 Protein quantification

Protein concentrations were measured using either the sensitive BCA-Protein Assay Kit according to the manufacturer's instructions or alternatively, a ready to use Coomassie Blue G-250 based reagent. Here, 1 mL of staining solution was mixed with 1-5 µL cellular extracts and incubated for 5 min in a polystyrene cuvette (10 x 4 x 45 mm). Absorbance was measured at 595 nm with a spectrometer. BSA was used as a standard (working range = 0.2 to 1.0 mg/mL).

4.2.11 SDS-PAGE and Western blot analysis

For one-dimensional separation of proteins by sodium dodecyl sulphate-polyacrylamide gel electrophoresis (SDS-PAGE), gels were either purchased ready-to-use from Bio-Rad or poured according to standard protocols (Laemmli, 1970). Samples were diluted in 5 X sample buffer (10 % (v/v) β-mercaptoethanol, 125 mM Tris-HCl pH 6.8, 4 % (w/v) SDS, 20 % (v/v) glycerol, 0.02 % (w/v) bromophenol blue) to a final volume of 25 µL and denatured by boiling for 3 min at 100 °C. After loading the samples onto the gel, a constant electric current of 25 mA per gel was applied for 1 h at RT. The separated proteins were then transferred by wet blotting at 4 °C according to standard procedures (Harlow and Lane, 1988). Afterwards, the blotted membrane was placed in blocking buffer (5 % (w/v) milk-powder in PBS and 0.1 % (v/v) Tween 20) for 1 h at RT under constant gentle agitation. Proteins were detected by incubation with specific primary antibody (see table 2) over night at 4 °C. Excess of primary antibody was removed washing with PBST (PBS with 0.1 % (v/v) Tween 20). Subsequently, POD or HRP-conjugated secondary antibodies (1:10,000 diluted in blocking buffer) were added for 60 min at RT under constant rocking. Followed by further washing steps with PBST, the membrane was developed using LumiGLO™ Western blotting reagent. The reactive proteins were detected by exposure on an X-ray film for 10 seconds to 60 min. For densitometric analysis, the X-ray film was scanned and analyzed using the program ImageJ (Wayne Rasband, National Institutes of Health, Bethesda, MD, USA).

4.2.12 Two-dimensional PAGE (2D-PAGE)

To increase the resolution of a one-dimensional PAGE, proteins were alternatively separated in two dimensions by isoelectric focusing (IEF) prior to conventional SDS-PAGE. After harvesting, cells were lysed as described before (4.2.9). If needed, protein precipitation was done by addition of 10 % (v/v) trichloroacetic acid (TCA) to the protein lysate and incubation for 30 min on ice, followed by centrifugation at 10,000 x g at 4 °C for 20 min. After removal of the supernatant, the pellet was washed with ice-cold acetone and the sample was again centrifuged. The supernatant was removed, the pellet was air dried and re-suspended in 2D-lysis buffer (7 M urea, 2 M thiourea, 30 mM Tris pH 8.5, 4 % (w/v) CHAPS).

The two-dimensional gel electrophoresis was principally performed as described (O'Farrel, 1975) with technical assistance by Melanie Nebendahl and Benjamin Schönbeck (Christian-Albrechts-University, Kiel, Germany). Briefly, the supernatant containing the solubilized proteins was recovered after centrifugation for 20 min at 20,000 x g at 4 °C. Proteins (250 µg) were centrifuged at 180,000 x g, 4 °C for 20 min, diluted in 2D-lysis buffer, and applied by cup-loading onto 24 cm non-linear pH 3-11 IPG gel strips (re-hydrated in DeStreak Solution for 10 h at RT) for approximately 65 kVh. The second dimension, separating the proteins by their mass, was performed on 26 x 20 cm large 12.5 % (w/v) SDS gels after reduction and alkylation using the Ettan DALTsix large vertical electrophoresis system. The gel was mounted on a non-backed gel frame and scanned on a Typhoon Trio imager. Subsequently, the gels were fixed with 40 % (v/v) ethanol and 10 % (v/v) acetic acid for at least 5 h and stained for proteins over night with Flamingo™ Fluorescent gel stain and scanned at red fluorescence. The obtained images were analyzed using Image Master 6.0 software. Protein spots were selected depending on the experimental setup and were picked using the Ettan spot picker unit equipped with a 2 mm picking head and further prepared for mass spectrometry (MS) analysis (see 4.2.14).

4.2.13 Two-dimensional difference gel electrophoresis (2D-DIGE)

The 2D-DIGE method was utilized to compare two samples, labeled with fluorescent dyes, to see changes in protein abundance, expression and differential cleavage within one gel. This technique is based on the above described 2D-PAGE and was described first in 1997 (Unlü *et al*.). For 2D-DIGE analysis, either whole cell lysates or magnetically enriched receptor containing vesicles were used whose preparation is described in section 4.2.15.4.

The 2D-DIGE technique was kindly performed by Melanie Nebendahl and Benjamin Schönbeck (Christian-Albrechts-University, Kiel, Germany) essentially as described before (Schmidt *et al*. 2009). Protein samples prepared in other buffer systems were either de-salted using Zeba™ Spin Desalting Columns (74 kDa MWco) or immediately diluted in 2D-lysis buffer. The supernatant was removed after centrifugation for 20 min at 20,000 x g at 4 °C. The same amount of protein per sample

(maximum 50 µg) was labeled with 400 pmol of the fluorescent dyes Cy 3 or Cy 5 in dimethylformamide (DMF, pH 8.5) for 30 min in the dark on ice. The reaction was stopped by quenching the labeling reaction with 1 µL 10 mM lysine for 10 min on ice. The differentially labeled samples were pooled with the same amount of unlabeled protein of each sample, centrifuged at 180,000 x g, 4 °C for 20 min and further processed as described in 4.2.12.

The in-gel fluorescence was scanned on a Typhoon Trio imager to detect Cy 3 and Cy 5 specific emission. The detection of differentially labeled protein spots was performed using *in silico* analyses tools included in the DeCyder 6.5 software. To stain whole separated proteins, the gel was stained with Flamingo™ Fluorescent gel stain and again mounted on a non-backed gel frame, scanned and analyzed using Image Master 6.0 software. Differentially labeled spots were picked using the Ettan spot picker unit equipped with a 2 mm picking head and further processed as described in the next section.

In order to verify that the picked spots had been picked from their correct locations, all 2D-gels were scanned again after the picking procedure.

4.2.14 In-gel tryptic digestion and MALDI-TOF/TOF MS analysis

Picked gel spots were washed with ultra-pure water, 50 mM ammonium bicarbonate (ABC) in 50 % (v/v) methanol, 70 % (v/v) acetonitrile (ACN), and dehydrated in pure ACN. The gel pieces were dried by evaporation of ACN in a SpeedVac centrifuge and rehydrated with 100 ng porcine sequencing-grade trypsin in 25 mM ABC at 37 °C over night. For peptide extraction, 20 µL of 0.1 % (v/v) trifluoroacetic acid (TFA) in ACN was added and the samples were sonicated for 15 min. The supernatant was collected and the gel spots were again incubated with 20 µL of 0.1 % (v/v) TFA in ACN for 10 min. Both supernatants were combined and dried in a SpeedVac centrifuge. The samples were reconstituted in 0.8 µL MALDI matrix solution containing 3.2 mg/mL α-cyano-4-hydroxycinnamic acid in 65 % (v/v) ACN/0.1 % (v/v) TFA and spotted onto MALDI targets (Opti-TOF; 384 Well Insert).

MS measurements and analysis thereof was performed by members of the Systematic Proteomics and Bioanalytic Unit of the Christian-Albrechts-University (Kiel, Germany), especially by Bart van den Berg, Tomas Koudelka and Andreas Tholey.

Spectra were acquired on an AB SCIEX MALDI-TOF/TOF 5800 mass spectrometer in positive ion mode. For MS measurements, 2,000 shots were accumulated in the mass range of 800 – 4,000 m/z. Default calibration was performed using 4700 Proteomics Analyzer Standard Kit, while MS measurements were calibrated internally using trypsin, matrix and contaminant peaks (842.509, 877.034 and 2,807.315 m/z) and smoothed using a FFT Poison-Denoise algorithm. Precursor selection for tandem MS/MS analysis was achieved using the 4000 Series Explorer Software (AB SCIEX) with

acquisition of the 20 most intense precursors (S/N > 20) beginning with the strongest first. All MS/MS spectra were acquired with 1 KV collision energy at ambient air (CID medium: 1.25 x 10^{-6} Torr) using 3,000 laser shots per precursor. MS/MS post processing involved smoothing using the Savitsky-Golay algorithm with 7 points across the peak and a polynomial order of 4. For peptide identification, MALDI-TOF/TOF MS/MS raw files were searched using AB SCIEX GPS software (Version 3.6, build 332) with the following pre-filter settings: only peaks within a mass range from 60 Da to the precursor mass minus 35 Da and S/N ratio above 10 were used. Spectra were searched with Mascot against the Swissprot database (downloaded 15.02.2011) using either *Homo sapiens* as a taxonomy filter (20,254 sequences) with precursor tolerance of 30 ppm or *Mus musculus* as a taxonomy filter (16,345 sequences) and precursor tolerance of 50 ppm and the following parameters for both: MS/MS tolerance - 0.3 Da; two missed cleavages allowed. Oxidation (M) was set as variable modification, while carbamidomethylation (C) was set as fixed modification. Proteins were considered identified when either two peptides were identified with a confidence interval ≥ 99 % ($p < 0.01$) or three peptides ≥ 95 % ($p < 0.05$).

4.2.15 Protein enrichment and analysis

4.2.15.1 Immunoprecipitation

For immunoprecipitation, 1 mg cellular extracts from stimulated L929Ts cells over-expressing V5-A-SMase were incubated with 2 µg anti-V5 monoclonal antibodies over night on ice. The immune complexes were incubated with 20 µL GammaBind G-sepharose for 1 h at 4 °C with constant shaking and were washed three times with TNE lysis buffer at 450 x g for 5 min at 4 °C. The immunoprecipitated proteins were diluted in 2 X sample buffer (see 4.2.11) and boiled for 3 min at 100 °C and analyzed by SDS-PAGE. The gel was fixed with 40 % (v/v) ethanol and 10 % (v/v) acetic acid for at least 5 h and stained for proteins over night with Flamingo™ Fluorescent gel stain and scanned at red fluorescence on a Typhoon Trio imager for red fluorescence. The obtained image was analyzed using Image Master 6.0 software. Protein bands were labeled with the help of the spot picking device for selecting native and cleaved protein bands for further MS analysis via electrospray ionization (ESI; see below).

4.2.15.2 Electrospray ionization

The method described below was kindly performed by Tomas Koudelka (Christian-Albrechts-University, Kiel, Germany).

For in-gel labeling and digestion, bands corresponding to native and cleaved A-SMase were excised from the Flamingo™ stained SDS-PAGE gel, cut into 2 mm^3 gel pieces and de-stained using 50 mM HEPES (pH 8.0), 30 % (v/v) ACN in 50 mM HEPES with shaking. Gel pieces were dried down after incubation with ACN using vacuum centrifugation for 15 min. The samples were reduced using 10 mM DTT in HEPES for 45 min at 56 °C and the free cysteine residues alkylated using

55 mM iodoacetamide in HEPES for 30 min in the dark at RT. Prior to labeling, gel pieces were washed with 50 mM HEPES and then dehydrated by incubating samples for 15 min with ACN followed by 15 min of vacuum centrifugation. Free amino groups (N-terminus and lysine residues) were labeled by incubating samples with 30 mM formaldehyde and 15 mM sodium cyanoborohydride at 25 °C over night. Any excess reagent was quenched by the addition of 100 mM ABC for 30 min. Gel bands were further de-stained as described above but with HEPES exchanged for ABC. Samples were digested with either trypsin or chymotrypsin (50 ng) at 37 °C over night. Digested peptides were extracted using 1 % (v/v) formic acid (FA), 50 % (v/v) ACN in 1 % (v/v) FA and 100 % (v/v) ACN. Samples were dried in a vacuum centrifuge and re-suspended in 3 % (v/v) ACN in 0.1 % (v/v) TFA. To eliminate potential protein carryover samples were acquired by running the lower molecular weight protein bands first followed by the higher molecular weight bands. In addition, 1-2 wash runs were performed between measurements.

Nano-high performance liquid chromatography (HPLC)-mass spectrometry was performed on a Dionex U3000 nano-LC system coupled online to an Orbitrap LTQ Velos mass spectrometer. Samples were desalted for 6 min (Acclaim PepMap100 C-18, 300 µm I.D. x 5 mm, 5 µm, 100 Å) at a flow rate of 30 µL/min using 3 % (v/v) ACN, 0.1 % (v/v) TFA. An Acclaim PepMap100 C-18 column (75 µm I.D. x 150 mm, 3 µm, 100 Å) was used for analytical separation at a flow rate of 300 nL/min using buffers A (0.05 % w/v FA) and B (80 % (v/v) ACN and 0.04 % (w/v) FA). The elution used gradient steps of 5-12 % B (6-7 min), 12-55 % B (7-42 min) and 55-90 % B (42-47 min) followed by an isocratic wash (90 % B, 47-57 min) and column re-equilibration (5 % B, 57-70 min). MS scans were acquired in the mass range of 300 to 2000 m/z at a resolution of 60,000. The five most intense signals were subjected to collision-induced dissociation (CID) and higher-energy collisional dissociation (HCD) fragmentation using a dynamic exclusion of 120 sec and a repeat count of 3 MS/MS. For this, the following parameters were applied: minimum signal intensity: 1000, isolation width: 3.0 Da, charge state: ≥2, HCD resolution: 7500, normalized collision energy of 35 and 40 for CID and HCD, respectively.

For database searching, HCD and CID MS spectra were searched separately using various database search algorithms via the Proteome Discoverer software (version 1.3 and 1.4): Sequest, Mascot and MS Amanda against the reviewed and canonical mouse database (downloaded 13.03.2013) with common contaminants (http://www.thegpm.org/crap/), peptide-N-glycosidase F (P21163), ribonuclease (P61824), and human A-SMase (P17405) appended to the database (16,737 sequences). Data were searched with 7-10 ppm MS tolerance and a 0.5 Da and 0.02 Da fragment tolerances for CID and HCD spectra, respectively. For samples digested with trypsin, spectra were searched with semi-Arg-C specificity with a maximum of two-missed cleavages allowed, while samples digested with chymotrypsin were searched with either semi-chymotryptic specificity (three-missed cleavages allowed) or no-enzyme specificity. Carbamidomethylation of cysteine residues (+ 57.021 Da) and

dimethylation on lysine (+28.031 Da) were set as fixed modifications while oxidation (+ 15.995 Da) on methionine residues and dimethylation (+28.031 Da) on the N-terminus were set as dynamic modifications.

4.2.15.3 Purification of TNF ligands

For the production of TNF ligands, 2 x 10^6 HEK293T per transfection cells were transiently transfected with 10 µg TNF-ligand DNA via electroporation (see 4.2.3.2). After electroporation, cells from three parallel transfections were pooled into 100 mL pre-warmed antibiotic free FreeStyle® medium and cultivated over night in an incubator with 5 % (w/v) CO_2 at 37 °C. The next day, 50 µg/mL penicillin and 50 µg/mL streptomycin were added. After two days of cultivation, the supernatant was collected, sterile filtrated and supplemented with 10 µg/mL of a protease inhibitor cocktail. The cells were further cultivated with fresh FreeStyle® medium containing 50 µg/mL penicillin and streptomycin each and 1 mg/mL G418 to select for transfected cells. After three more days of cultivation, the supernatant was collected, sterile filtrated and supplemented with 10 µg/mL of a protease inhibitor cocktail. Both supernatants were pooled and stored at 4 °C until further enrichment of the soluble ligands with a Hi Trap™ Protein G HP 1 mL column. The ligands were purified according to the manufacturer's protocols. The protein concentration of the purified ligands was measured using BCA Protein Assay and the biological activity of TNFwt-Fc or TNF60-Fc was always tested in cytotoxicity assays using L929Ts cells (see 4.2.1.4).

4.2.15.4 Preparation of magnetically labeled TNF receptors and isolation of TNF receptor magnetic fractions

A system based on ligand-specific immunomagnetic labeling of cell surface receptors for purification and characterization of TNF receptor magnetic fractions was utilized via a free-flow magnetic chamber (HOKImag 1, invented by Tchikov and Schütze, 2008; now manufactured by HOOCK GmbH, Kiel). The method was recently described (Tchikov *et al*. 2014). This immunomagnetic separation was continuously advanced throughout this doctoral thesis and therefore three different homogenization procedures were used (A-C, see below). Preparations were either analyzed by Western blot or by 2D-DIGE analysis with technical assistance from Vladimir Tchikov and Jürgen Fritsch (Christian-Albrechts-University, Kiel, Germany; contributions are indicated in the figure legends).

For the cultivation and preparation of cells, human U-937 and murine L929Ts cells were grown to 70 % confluence. For detachment, adherent L929Ts cells were incubated with PBS/3.5 mM EDTA for 10 min at 37 °C. Subsequently, cells were collected with a cell scraper, pooled, centrifuged at 400 x g for 5 min at 4 °C and 1 x 10^8 cells per time-point were diluted in 1 mL ice-cold PBS. U-937 cells (1 x 10^9) were washed once with cold PBS at 100 x g for 10 min at 4 °C and diluted in 1 mL PBS. The following preparation was performed permanently at 4 °C unless otherwise stated. U-937 cells were

pre-treated with 50 µM zVAD-fmk for 30 min. TNF receptors on the surface of L929Ts or U-937 cells were labeled either with 100 ng/mL TNFwt-Fc (L929Ts cells) or TNF60-Fc (U-937 cells) by incubation for 20 min. Thereafter, 25 µL of protein G magnetic beads was mixed with 1 mL of the cell suspension for another 1 h (for preparation of whole cell lysates for 2D-DIGE analysis this step was excluded). Unbound magnetic beads were washed at 350 x g with PBS. Synchronized internalization of the TNF receptors was induced by adding 5 mL pre-warmed media without supplements, shifting the incubation temperature from 4 °C to 37 °C followed by incubation at 37 °C for indicated time-points. The reaction was stopped by adding 30 mL ice-cold PBS. Cells were pelleted by centrifugation at 250 x g for 4 min and washed once with homogenization buffer (HB; 15 mM HEPES, 250 mM sucrose and 0.5 mM $MgCl_2$ at pH 7.4). For homogenization, three different methods were used: (A) ultra-sonication, (B) mechanical homogenization using a douncer device and subsequent removal of mitochondria from the samples by iodixanol density barrier centrifugation (done with the help of Jürgen Fritsch) or (C) mechanical homogenization with glass beads (done by Vladimir Tchikov).

A) The cell pellets were re-suspended in 1 mL HB supplemented with 10 µg/mL protease inhibitor cocktail and 12.5 units benzonase, lysed at 4 °C using a Branson W-450 sonication device equipped with a cup-resonator. The cells were sonicated for 15 sec (duty cycle: constant, output control: 2.5) and centrifuged for 4 min at 600 x g. The supernatant was collected and the pellet was again sonicated as above and pooled with the collected supernatant. The homogenate was centrifuged at 600 x g for 5 min. Subsequently, approximately 850 µL of the supernatant were either loaded to the HOKImag 1 device or further prepared without magnetic particles as whole cell lysates for 2D-DIGE analysis.
B) Alternatively, homogenization was performed mechanically using douncer devices to induce shear forces. The cell pellets were re-suspended in 1 mL HB supplemented with 10 µg/mL protease inhibitor cocktail and transferred to two 15 mL dounce tissue grinders performing mechanical homogenization with 5 strokes each. The homogenate was centrifuged at 1,500 x g for 5 min, the supernatant was collected and the remaining pellet was again homogenized. The supernatant and homogenate were pooled and centrifuged. After centrifugation, the resulting post-nuclear supernatant was carefully overlaid on top of 750 µL of a 16 % (v/v) iodixanol solution on the bottom of a 4 mL centrifuge tube. Subsequently, samples were centrifuged at 150,000 x g for 1 h in a swing-out rotor (SW60Ti) without brake. The fraction with light organelles (milky ring) was collected for magnetic separation as described below and the fraction at the bottom of the tube (referred to as mitochondrial fraction) was collected for further Western blot analysis.
C) Homogenization using a homogenization device with glass beads was described previously (Tchikov and Schütze, 2008). The samples were incubated with glass beads on a vortex device for 5 min before the homogenate was centrifuged and the remaining pellet again

homogenized. After repeating the homogenization procedure three times, supernatants were collected, pooled and subjected to magnetic separation.

The post-nuclear supernatant obtained by either of the above methods was submitted to magnetic separation of TNF-R1 magnetic fractions in the magnetic separation device HOKImag 1. Hereby, the magnetically labeled material was soaked in free-flow plastic tubes of 5 mm in diameter and 0.1 mm thin walls which were placed in the magnetic gap serving as column connected to a peristaltic pump. After incubation of the lysate in the magnetic field for 1-2 h, the column was washed with approximately 30 mL HB. This flow-through suspension was collected and is referred to as non-magnetic fraction throughout this doctoral thesis. The magnetic TNF-R1-containing membrane fractions were eluted using 0.5 mL HB and a plunger of a 1 mL syringe and sedimented at 20,000 x g for at least 30 min. The subsequent analysis of the membrane fractions was either conducted by conventional Western blot or 2D-DIGE analysis following MALDI-TOF/TOF analysis.

4.2.16 Microscopy

4.2.16.1 Documentation of cell morphology

For visualization of cell morphology, images from unfixed cells were taken using an Axiovert 10 microscope and a DS-5M-L1 digital sight camera system.

4.2.16.2 Immunofluorescence analysis of suspension cells

For immunofluorescence (IF) analysis of TNF receptor localization in human cells, U-937 cells were attached onto coverslips and surface receptors were stained with a ligand/Protein G-Alexa Fluor® 488-complex. For this, HCl-pre-treated glass coverslips were washed twice with PBS and coated with a 1:5 (v/v) dilution of poly-L-lysine/PBS for 30 min at 37 °C. The coverslips were again washed twice with PBS and 1 x 10^6 U-937 cells were seeded onto the coated coverslips to allow adherent growth for 30 min at 37 °C. The coverslips with attached cells were pre-incubated with 50 µM zVAD-fmk for 30 min at 37 °C. After pre-incubation, coverslips were cooled down on ice and washed once with ice-cold PBS. Meanwhile, 400 ng TNF60-Fc was incubated with 0.5 µL/slide Protein G-Alexa Fluor® 488 in the dark at RT for 1 h. For surface labeling of TNF-R1, 100 µl of the ligand/fluorochrome mixture was incubated with one coverslip in a humidified dark chamber at 4 °C for 1 h. Then, the coverslips were washed twice with cold PBS. To permit receptor internalization, the coverslips were incubated at 37 °C for indicated times in 2 mg/mL TRITC-Dextran diluted in RPMI 1640 media without supplements. After stopping internalization with cold PBS, the cells were fixed with 4 % (w/v) PFA for 40 min at 4 °C. After two washes with PBS, coverslips were mounted in ProLong Gold Antifade plus DAPI mounting medium onto slides. Slides were dried and kept dark at RT until analysis by confocal laser scanning microscopy.

4.2.16.3 Immunofluorescence analysis of adherent cells

For IF analysis of TNF-R1 localization in murine cells, 1 x 10^5 L929Ts cells were attached to coverslips over night. Coverslips with attached cells were placed on ice to cool down and washed once with ice-cold PBS. In parallel, 400 ng TNFwt-Fc ligand was incubated with 0.5 µL Protein G-Alexa Fluor® 488 in the dark. Further processing was performed as described in 4.2.16.2.

For analysis of the co-localization of TNF-R1 with other proteins of interest, L929Ts cells were seeded onto HCl pre-treated glass coverslips to allow adherent growth over night. The cells were incubated with 100 ng/mL biotinylated TNF in combination with 240 ng/mL streptavidin Alexa Fluor® 488 (Kit from R&D Systems) for 1 h on ice. To allow receptor internalization, coverslips were transferred into pre-warmed media and incubation was carried out at 37 °C for defined times indicated in the figure legends. The reaction was stopped by replacing medium with ice-cold PBS and the coverslips were washed twice with ice-cold PBS. For fixation, coverslips were incubated with freshly prepared 4 % (w/v) PFA in PBS for 30 min on ice. Fixed cells were washed with PBS, permeabilized 20 min with 0.1 % (w/v) saponin/ 0.2 % (w/v) BSA in PBS and washed again with PBS. The specific primary antibodies (see table 2) were diluted in PBS and incubated with the coverslips for 1 h in a humidified chamber at 4 °C. Coverslips were then washed two times with PBS and incubated with Alexa Fluor® 555-conjugated specific secondary antibodies (1:200 in PBS) for 1 h at 4 °C in the dark. After two washes with PBS, the coverslips were mounted in mounting medium as described before (4.2.16.2), dried and kept dark at RT until analysis by confocal laser scanning microscopy.

4.2.17 Transformation of *E. coli* and plasmid purification

For the transformation of a plasmid into bacteria, 100 µL chemically competent *Escherichia coli* XL1 blue (prepared in the laboratory of Dieter Adam, Christian-Albrechts-University, Kiel, Germany) and 10 ng of plasmid DNA were incubated on ice for 30 min. After a temperature shift to 42 °C for 45 s, cells were transferred into 1 mL pre-warmed SOC medium (2 % (w/v) Bacto-tryptone, 0.5 % (w/v) yeast extract, 10 mM sodium chloride, 0.25 mM potassium chloride pH 7.0) and incubated at 37 °C for 45 min with continuous shaking at 250 rpm. Afterwards, cells were plated on lysogeny broth (LB) agar plates (1 % (w/v) Bacto-tryptone, 0.5 % (w/v) Bacto-agar, 1.5 % (w/v) yeast extract, 10 mM sodium chloride) with 1 mg/mL ampicillin or kanamycin. Cells containing the ampicillin/kanamycin resistance-encoding plasmid were able to grow over night at 37 °C. Colonies visible on the plates were inoculated in 5 mL LB medium (1 % (w/v) Bacto-tryptone, 0.5 % (w/v) yeast extract, 170 mM sodium chloride pH 7.2) with 1 mg/mL ampicillin/kanamycin at 37 °C and 250 rpm for approximately 4 h. This pre-culture was transferred to 200 mL fresh LB medium containing 1 mg/mL antibiotic over night at 37 °C and 250 rpm. Plasmid purification was conducted using the Qiagen Plasmid Maxi Kit according to manufacturer's instructions. Quantification of plasmid DNA was performed using a NanoDrop® spectrometer.

4.2.18 Statistical analysis

When experiments were performed at least with three technical replicas, results are shown as means +/- standard deviation. For determination of statistical significance (at least three independent experiments), Student's t-test was employed when comparing controls versus one treatment regime assuming differences in standard deviation (statistical analysis program: Excel 2010). A *P* value of $\leq$ 0.05 was considered statistically significant.

5. Results

New model cell lines to study regulated necrosis: U-937 and HT-29 cells

The most extensively studied model cell line for regulated necrosis initiated by the ligands TNF or TRAIL is the murine fibroblast cell line L929 (Strelow *et al.* 2000; Thon *et al.* 2005, 2006; Sosna and Voigt *et al.* 2013; Sosna, Voigt *et al.* 2014). In addition, cell systems such as murine NIH3T3 and human Jurkat T cells have been previously characterized regarding their ability to undergo regulated necrosis (Thon *et al.* 2005, 2006; Sosna and Voigt *et al.* 2013; Sosna, Voigt *et al.* 2014). To extend the repertoire of characterized human cell lines undergoing regulated necrosis, two further cell lines, HT-29 and U-937 were studied with regard to their ability to undergo necroptosis elicited by TNF or TRAIL. Subsequently, it was intended to use them as model systems in studies to identify proteases and protease substrates which protect from or enhance TNF- and TRAIL-induced regulated necrosis.

In a first set of experiments, U-937 cells were analyzed for the presence of the corresponding cell surface death receptors TRAIL-R1, and TRAIL-R2. A corresponding analysis for TNF-R1 was not performed, since almost every cell type in the human body, with the exception of red blood cells, is known to express TNF-R1 (Aggarwal and Natarajan, 1996). As shown in Figure 6A, U-937 cells highly express TRAIL-R2. TRAIL-R1 was only marginally expressed, similar to results obtained in HT-29 cells which also express high levels of TRAIL-R2 and low levels of TRAIL-R1 (Voigt, Master Thesis, 2010). Furthermore, the ability of TNF as well as TRAIL to induce regulated necrosis was determined in HT-29 and U-937 cells. Cell death was measured by flow cytometric analysis of propidium iodide (PI) fluorescence, an indicator for loss of membrane integrity. Since treatment with both cytokines, TNF and TRAIL, activates caspase-dependent apoptosis in most cell systems, the inhibition of caspases is required when studying necroptosis. Therefore, TNF or TRAIL was always used in combination with the broad spectrum caspase inhibitor zVAD-fmk to suppress any caspase activity. If required, the protein biosynthesis inhibitor cycloheximide (CHX) was added to additionally sensitize the cells towards cell death (Holler *et al.* 2000). As shown in Figure 6B, both U-937 and HT-29 cells showed a clear sensitivity to TNF/zVAD/CHX- or TRAIL/zVAD/CHX-induced cell death. The pharmacological inhibition of necroptosis by Nec-1 (Degterev *et al.* 2008) protected both cell lines from TNF- and TRAIL-induced cell death, demonstrating that U-937 and HT-29 cells indeed undergo necroptosis when treated with TNF/zVAD/CHX or TRAIL/zVAD/CHX. Morphological analysis revealed that both cell lines displayed an exclusively necrotic cellular morphology when treated with TNF/zVAD/CHX or TRAIL/zVAD/CHX, in contrast to the apoptotic membrane blebbing seen in controls for apoptosis (TNF/CHX or TRAIL/CHX treatment, Figure 6C).

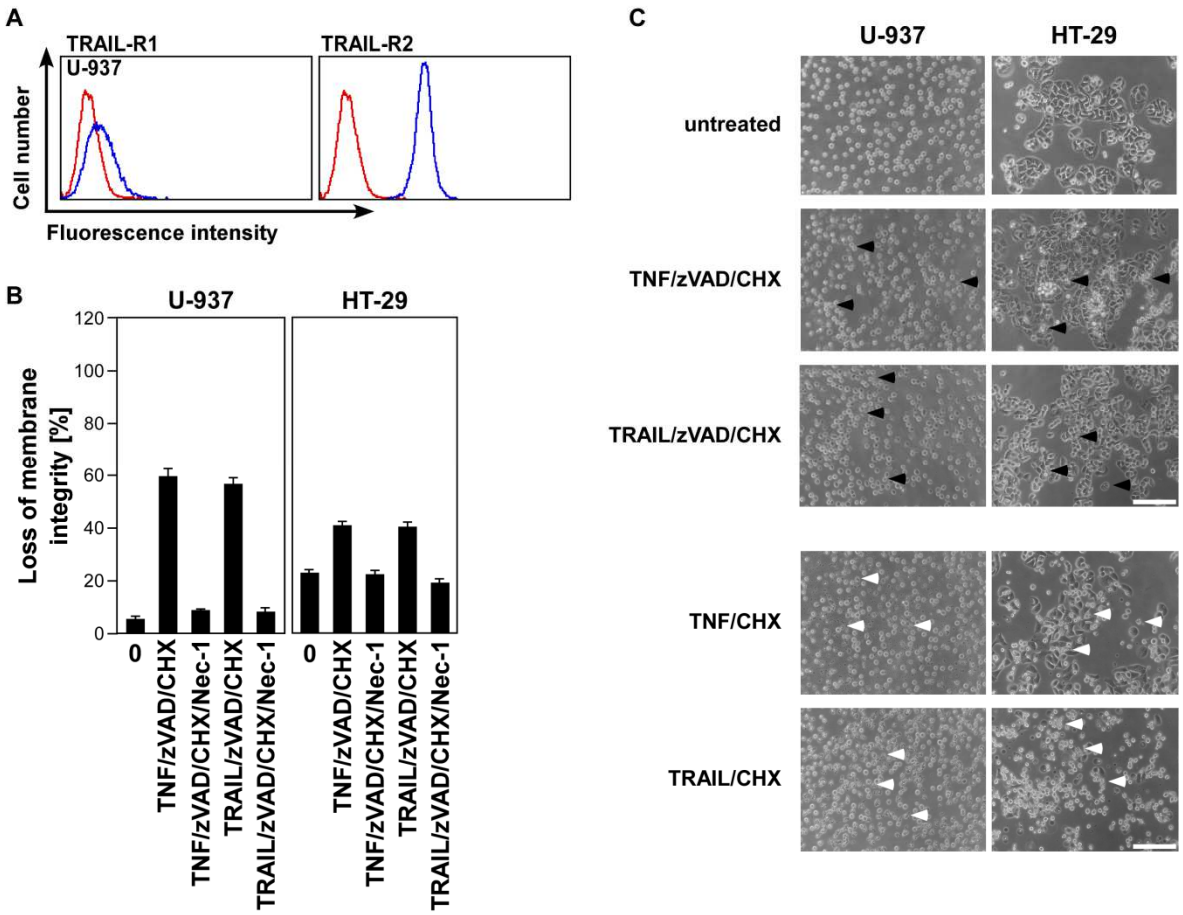

Figure 6: Treatment with TNF/zVAD/CHX or TRAIL/zVAD/CHX elicits necroptosis in U-937 and HT-29 cells. (A) Flow cytometric analysis of cell surface expression of TRAIL-R1 and TRAIL-R2. Blue lines: specific monoclonal antibodies for the respective receptors, red lines: isotype matched control antibodies. Representative results of one out of two experiments performed are shown. 10,000 cells were analyzed for each measurement. **(B)** Cells were treated with 100 ng/mL TNF or TRAIL in combination with 20 µM (HT-29) or 50 µM (U-937) zVAD-fmk and non-toxic concentrations of CHX (U-937: 0.1 µg/mL; HT-29: 5µg/mL). After 24 h, loss of membrane integrity was measured as a marker for cell death by flow cytometric analysis of PI-negative and -positive cells. The error bars represent the standard deviation (SD) of two independent experiments with three measurements each. **(C)** Micrographs show the necrotic cellular morphology (black arrows). U-937 and HT-29 cells were stimulated for 8 h with TNF/zVAD/CHX or TRAIL/zVAD/CHX to induce necroptosis as in **(A)** or as a control without zVAD-fmk to induce apoptosis (white arrows). The micrograph of U-937 cells stimulated with TRAIL/CHX was taken after 5 h stimulation because of the high cell death rate. Scale bar: 100 µm.

Subsequently, further hallmarks of necroptosis were investigated in U-937 cells. During caspase-dependent apoptosis, the mature 116-kDa PARP-1 protein is inactivated by caspase-3-mediated cleavage, resulting in an 89-kDa PARP-1 cleavage product (Lazebnik *et al*. 1994). To provide additional evidence that TNF/zVAD/CHX elicits necroptosis rather than caspase-dependent apoptosis, U-937 cells were left untreated or stimulated with TNF/zVAD to induce necroptosis. As a positive control to induce apoptosis, cells were treated with TNF alone. As shown in Figure 7A, the 89-kDa cleavage product was not detected in U-937 cells undergoing necroptosis in response to TNF/zVAD, only in TNF-treated, apoptotic cells. To further verify that caspases were not activated during TNF/zVAD treatment, activation of caspase-3 and -8 was determined directly by measuring the cleavage of the fluorogenic substrates zDEVD-afc (caspase-3 substrate) or zIETD-afc (caspase-8 substrate). As can be seen in Figure 7B, TNF/zVAD did not activate caspase-3 and -8, whereas the TNF-treated apoptotic control did (black triangles, Figure 7B), demonstrating that PCD induced by

TNF/zVAD was caspase-independent. For HT-29 cells, identical results had been obtained during independent studies in the laboratory (Sosna, Voigt *et al*. 2014; Voigt *et al.* 2014).

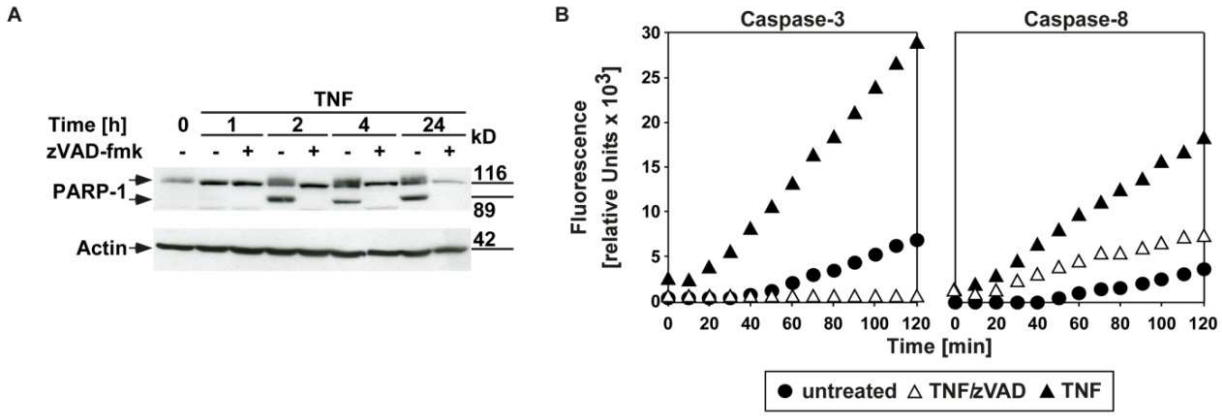

Figure 7: Characterization of necroptosis elicited by TNF in U-937 cells. (A) Cellular extracts were prepared after U-937 cells were treated with 100 ng/mL TNF and 50 µM zVAD-fmk or with TNF alone (to induce apoptosis) for the indicated time-points. Western blots were generated from whole cell lysates incubated with an antibody detecting the full length (116 kDa) and the apoptotic cleavage fragment of PARP-1 (89 kDa). Arrows indicate the position of the full-length protein and the 89 kDa cleavage product (present only in apoptotic lysates treated with TNF alone). **(B)** U-937 cells were left untreated or were stimulated for 4 h as above. Subsequently, activation of caspases-3 and -8 was determined in 1 µg cellular extracts by measuring cleavage of the fluorogenic substrates (zDEVD-afc and zIETD-afc) over 120 min.

Since in previous studies ceramide had been identified as an important mediator of regulated necrosis (Thon *et al.* 2005), the impact of ceramide on TNF- and TRAIL-induced necroptosis was also investigated in U-937 and HT-29 cells. As shown in Figure 8, TNF/zVAD/CHX as well as TRAIL/zVAD/CHX treatment resulted in an accumulation of intracellular ceramide in both cell lines.

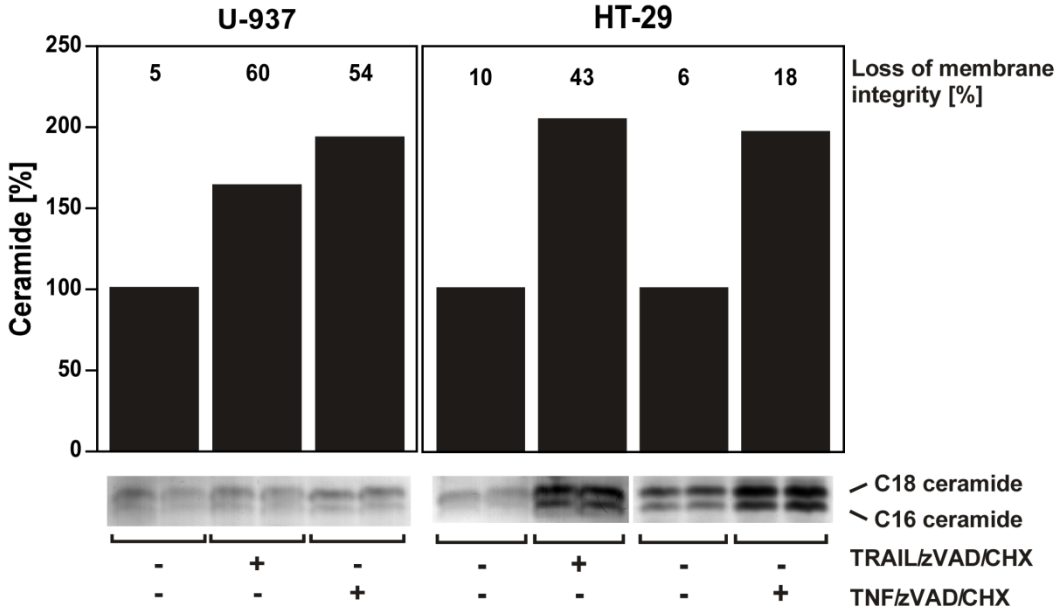

Figure 8: Intracellular ceramide levels of U-937 and HT-29 cells increase in response to treatment with TNF/zVAD/CHX or TRAIL/zVAD/CHX. Cells were left untreated or stimulated with 100 ng/mL TRAIL or TNF with 20 µM (HT-29) or 50 µM (U-937) zVAD-fmk and 0.1 µg/mL (U-937) or 5 µg/mL (HT-29) CHX for 8 h (U-937) or 24 h (HT-29) before intracellular ceramide levels were determined in duplicate by means of thin layer chromatography with subsequent charring. Original data from the chromatography plate (C16 and C18 ceramide species) are shown below the diagram. Trypan blue staining was in parallel performed to measure loss of membrane integrity and is shown above the bar graphs. Data show representative results of two independent experiments.

Conclusion: U-937 and HT-29 cells can undergo necroptosis

The above described observations implicate that human HT-29 cells as well as U-937 cells can undergo necroptosis elicited by either TNF or TRAIL. U-937 cells showed typical hallmarks of necroptosis, similar to previous studies in HT-29 cells (Sosna, Voigt *et al.* 2014; Voigt *et al.* 2014). Furthermore, U-937 and HT-29 cells showed an increase in ceramide levels when treated with TNF/zVAD/CHX and TRAIL/zVAD/CHX, suggesting that ceramide may act as a mediator of necroptosis also in these human tumor-derived cell lines. Because of the results obtained here, U-937 and HT-29 cells were used for further experiments throughout this thesis.

5.1 TNF and PARP-1 elicit distinct routes to regulated necrosis

TNF and MNNG can kill cells by regulated necrosis

Murine fibrosarcoma L929 cells die exclusively by regulated necrosis when treated with TNF (Vercammen *et al.* 1998a; Strelow *et al.* 2000; Thon *et al.* 2005). In response to DNA-alkylating agents such as MNNG, it was reported that L929 cells also die by necrosis rather than by apoptosis (Yu *et al.* 2002; Xu *et al.* 2006). To validate that TNF and MNNG do not elicit caspase-dependent apoptosis in L929 cells, caspase-3 activity measurements were conducted as an indicator for caspase-dependent apoptosis through both the extrinsic and the intrinsic pathway. As shown in Figure 9A, three L929 sublines (TRAIL-sensitive L929Ts cells, L929 cells obtained from ATCC (L929ATCC) and TNF-hypersensitive L929sA cells) did not display any caspase-3 activity after treatment with TNF or MNNG. Accordingly, unlike TNF/CHX-treated positive controls, none of the three L929 sublines showed membrane blebbing after TNF or MNNG stimulation, which is a morphological hallmark of apoptosis (Figure 9B). Therefore, both TNF and MNNG induce cell death through necrotic pathways rather than through apoptosis in the three L929 cell lines utilized for the study presented here.

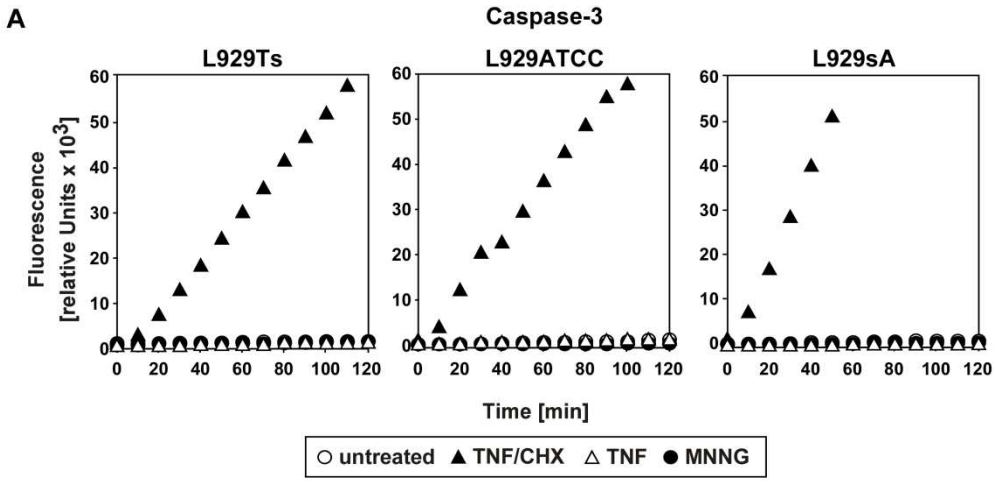

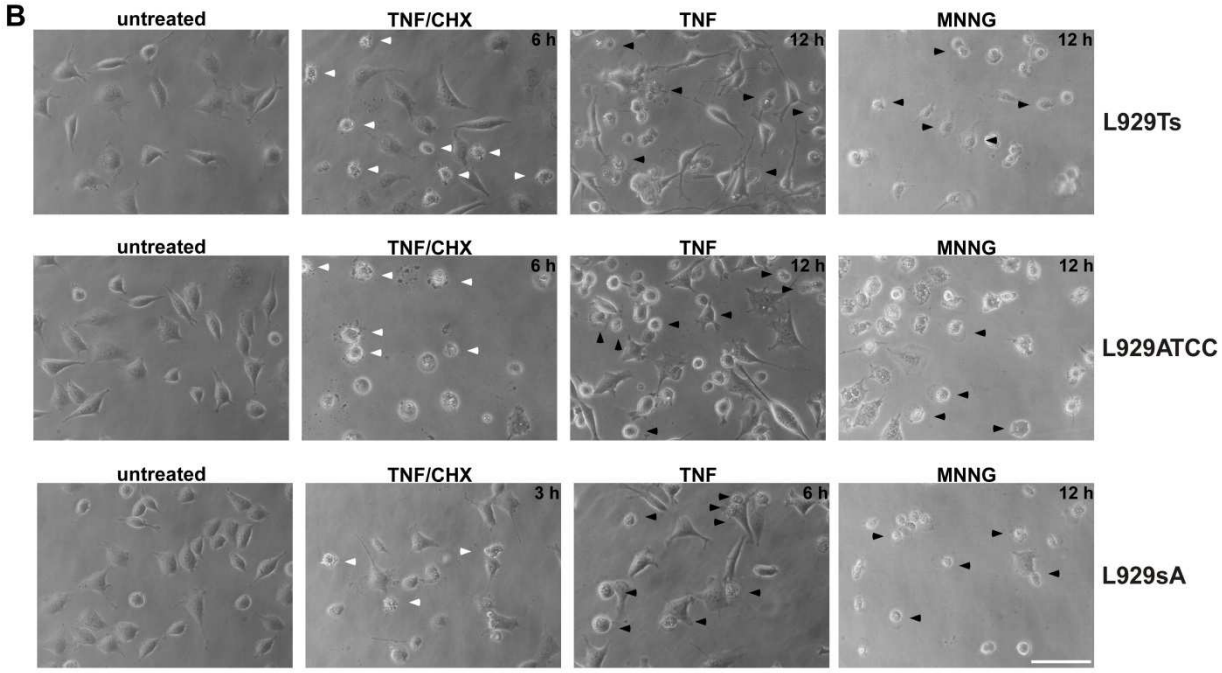

Figure 9: TNF and MNNG elicit regulated necrosis in L929 cells. (A) L929Ts, L929ATCC and L929sA cells were left untreated or were treated with 100 ng/mL TNF for 5 h, or were treated with 0.5 mM MNNG for 15 min and were then incubated with fresh medium without MNNG for another 5 h. Cells treated with 100 ng/mL TNF and 2 µg/mL CHX served as a positive control for induction of apoptosis. Subsequently, activation of caspase-3 was determined in 1 µg of cellular extract by measuring cleavage of the fluorogenic substrate zDEVD-afc over 120 min. **(B)** Micrographs show the morphology of the cells treated as above for the indicated time-points. White arrows mark cells that show apoptotic membrane blebbing after treatment with TNF/CHX. Black arrows indicate necrotic-like morphology of cells in response to TNF or MNNG. Scale bar: 100 µm.

MNNG but not TNF causes rapid activation of the PARP pathway

The activation but not the cleavage of PARP-1 is required for necroptosis (Sosna, Voigt *et al.* 2014). Interestingly, observations that had been obtained during independent studies in the laboratory show that TNF and MNNG activate PARP-1 with distinct kinetics (Sosna, Voigt *et al.* 2014). Hyperactivation of PARP-1 results in a rapid depletion of intracellular NAD^+ levels (Yu *et al.* 2002) and, as a direct consequence, also in the depletion of intracellular ATP levels (Vandenabeele *et al.* 2010). Therefore, ATP levels were compared to the progression of cell death after treatment with TNF or MNNG. In the three L929 sublines, MNNG treatment caused a rapid depletion of intracellular ATP levels within 1 h. Furthermore, the rapid loss of ATP clearly occurred earlier than the loss of membrane integrity (which was measured as a marker for cell death), proving that MNNG treatment induces a rapid activation of PARP-1 (Figure 10A). This was in contrast to TNF-induced necroptosis, where ATP levels decreased at later time-points and concurrently with cell death (Figure 10A), suggesting that the depletion of ATP levels is rather an accompanying factor of TNF-induced cell death than an initial inducer of necroptosis. To further corroborate the distinct activation of PARP-1 after MNNG or TNF treatment, the repertoire of cell lines was extended to Jurkat and HT-29 cells, yielding essentially the same results as in the three L929 sublines (Figure 10B).

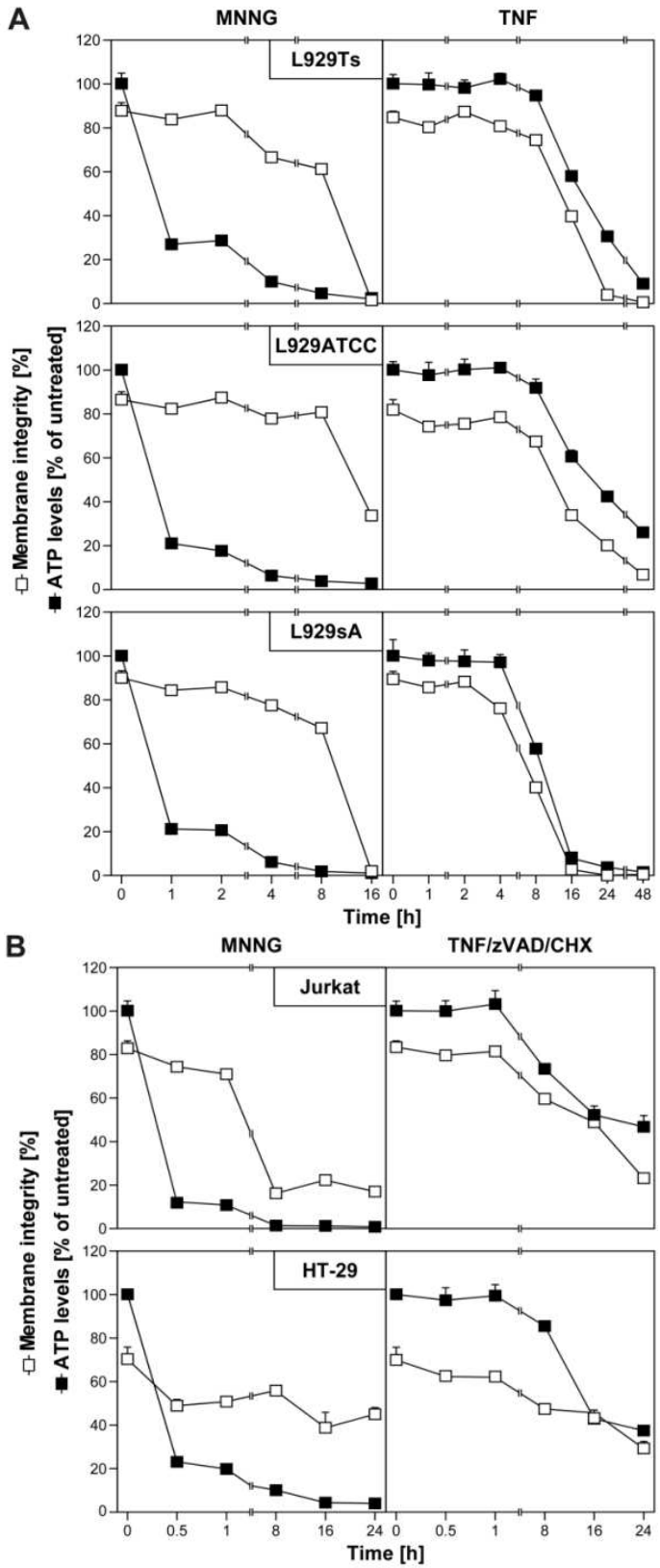

Figure 10: MNNG but not TNF(/zVAD/CHX) induces rapid ATP depletion. (A) L929Ts, L929ATCC and L929sA cells were stimulated with 100 ng/mL TNF, or with 0.5 mM MNNG for 15 min and subsequent incubation with fresh medium without MNNG for the indicated time-points. Subsequently, their intracellular ATP content and loss of membrane integrity (as a marker of cell death) were analyzed. **(B)** HT-29 and Jurkat cells were stimulated with MNNG as above, or with 100 ng/mL TNF with addition of 20 µM (HT-29) or 50 µM (Jurkat) zVAD-fmk and 2 µg/mL (Jurkat) or 5 µg/mL (HT-29) CHX. Subsequently, intracellular ATP levels and loss of membrane integrity were measured at the indicated time-points. For better comparison and for clarity of presentation, the percentage of intact, large PI-negative cells that still retain their membrane integrity is shown. Representative data from one out of two experiments are shown and error bars indicate the SD from three measurements.

In summary, the late depletion of intracellular ATP levels during TNF-induced necroptosis implicates that individual components of the PARP pathway are activated as a secondary consequence during necroptosis rather being the cause of necroptotic cellular disintegration. This is in contrast to the rapid depletion of ATP following PARP-1 activation by DNA-alkylating agents such as MNNG, suggesting that TNF-induced necroptosis and the hyperactivation of PARP-1 represent two distinct routes to regulated necrosis.

Inhibition of the PARP pathway does not protect from TNF-induced necroptosis

To unravel the role of the PARP pathway in TNF-induced necroptosis, the impact of pharmacological inhibitors of PARP-1 was analyzed in L929Ts cells, murine NIH3T3 fibroblasts, and in human Jurkat and HT-29 cells. The PARP-1 inhibitors 3-AB, PJ-34 and olaparib impaired MNNG-induced regulated necrosis, but not TNF-induced necroptosis in any of the four cell lines analyzed (Figure 11), suggesting that inhibition of PARP-1 activation does not protect from TNF-induced necroptosis. However, PJ-34, as the only exception, reduced TNF-induced necroptosis in L929Ts cells. This effect was not seen with any other PARP-1 inhibitor used in this study. Moreover, two independent studies reported unspecific activities of PJ-34 (Madison *et al.* 2011; Antolin *et al.* 2012), indicating that the observed effect in L929Ts cells is most likely unspecific.

In the laboratory, additional results were obtained substantiating that the inhibition of the PARP pathway does not protect from TNF-induced necroptosis. For example, PARP-1 down-regulation by RNA interference in L929Ts and Jurkat cells resulted in reduced MNNG-induced regulated necrosis whereas TNF-induced necroptosis was not affected. Moreover, PARP-1-deficient MEFs displayed a clear protection from MNNG-, but not TNF-induced regulated necrosis (Sosna, Voigt *et al.* 2014).

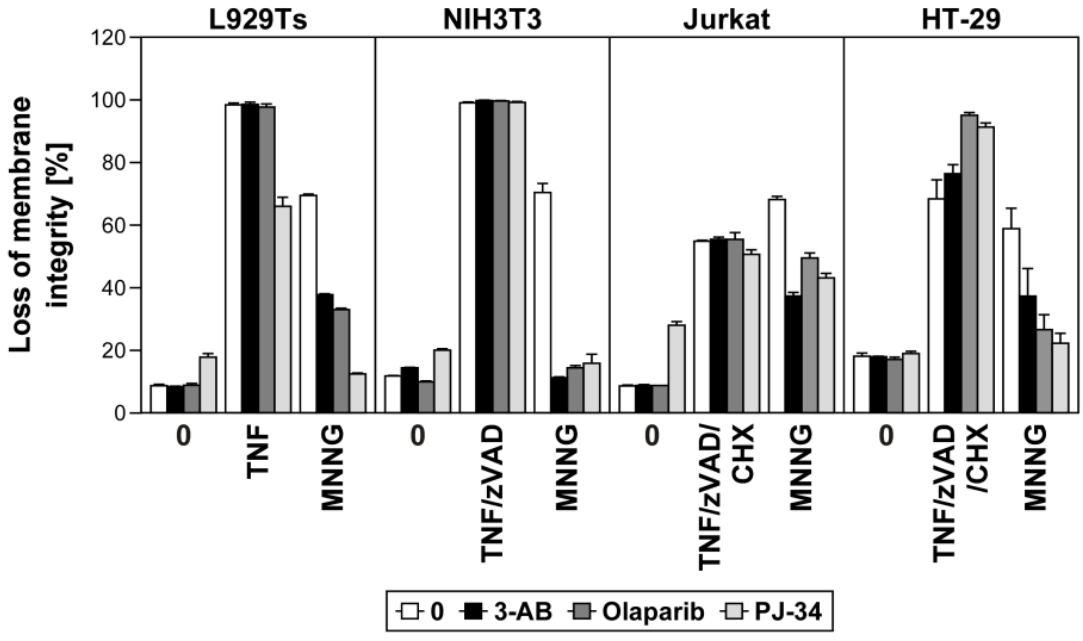

Figure 11: PARP-1 inhibitors affect MNNG-induced regulated necrosis but not TNF-induced necroptosis.

Figure 11: continued. Necroptosis was induced in L929Ts, NIH3T3, Jurkat and HT-29 cells in the absence or presence of the PARP1-inhibitors 3-AB (2.5 mM), olaparib (L929: 1 µM; NIH3T3, Jurkat: 50 nM; HT-29: 2 µM) or PJ-34 (20 µM) by treatment with 100 ng/ml TNF for 24 h (L929Ts, HT-29), 16 h (NIH3T3) or 20 h (Jurkat) with addition of 20 µM (NIH3T3, HT-29) or 50 µM (Jurkat) zVAD-fmk and 2 µg/ml (Jurkat) or 5 µg/ml (HT-29) CHX. In parallel, cells were treated with 1 mM MNNG for 15 min and further incubated for 16 h with fresh medium with or without addition of 3-AB, olaparib or PJ-34. Subsequently, loss of membrane integrity was analyzed by flow cytometry. Representative data from one out of two experiments are shown. The error bars represent the SD of three parallel measurements.

The hyperactivation of PARP-1, the resulting depletion of intracellular NAD^+ and ATP pools, mitochondrial dysfunction and AIF translocation also involves the activation of JNK (Vandenabeele *et al.* 2010). To further elucidate the involvement of JNK in necroptosis, TNF-induced necroptosis was analyzed after pharmacological inhibition of JNK or in a direct genetic approach using primary lung fibroblasts from JNK1- or JNK2-deficient and immortalized MEFs from JNK1/JNK2 double-deficient mice. The inhibition of JNK with the specific JNK inhibitor III did not protect L929Ts cells from TNF-induced necroptosis, even at concentrations at which the JNK inhibitor III itself induced cytotoxicity (Figure 12A). Similar to the pharmacological inhibition, in the direct genetic approach, neither primary lung fibroblasts from JNK1- or JNK2-deficient nor MEFs from JNK1/JNK2 double-deficient mice were protected from TNF-induced necroptosis (Figure 12B). The obtained results suggest that JNK do not participate in TNF-induced necroptosis, which is in contrast to their reported role in the PARP pathway (Xu *et al.* 2006).

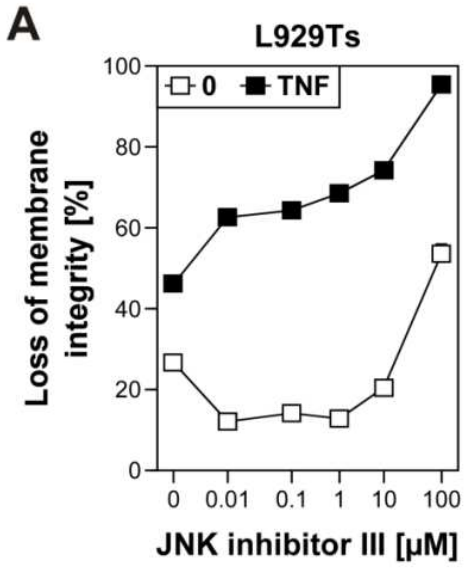

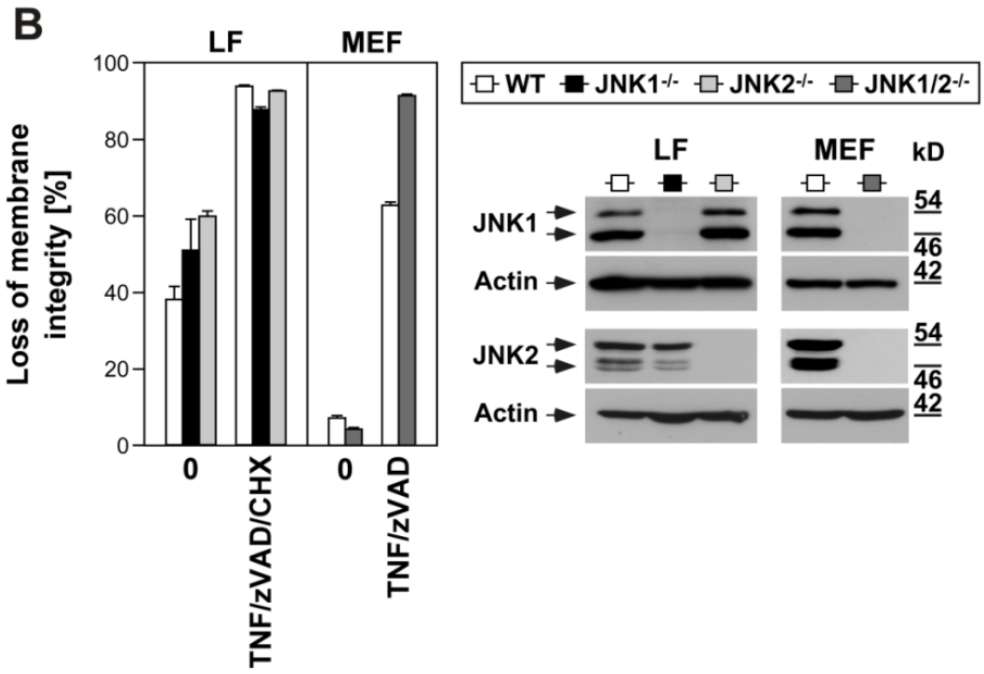

Figure 12: JNK do not participate in TNF-induced necroptosis. (A) L929Ts were left untreated or were treated with 100 ng/mL TNF for 16 h in the presence of increasing concentrations of JNK inhibitor III. Loss of membrane integrity was analyzed by flow cytometry in triplicates. **(B) Left panel:** Primary lung fibroblasts (LF) from wild-type (WT), JNK1- (JNK1 $^{-/-}$) and JNK2-deficient (JNK2 $^{-/-}$) mice or immortalized MEFs from JNK1/JNK2 double-deficient (JNK1/2 $^{-/-}$) mice were left untreated or were treated with 100 ng/mL TNF and 20 µM zVAD-fmk in the presence or absence of 2 µg/mL CHX for 18 h. Loss of membrane integrity was analyzed by flow cytometry. The error bars represent the SD of three parallel measurements. **Right panel:** Control Western blots were performed to verify presence or absence of endogenous JNK1 and/or JNK2. Actin served as a loading control.

Cathepsin and calpain proteases are further components of the PARP pathway (Artus *et al.* 2010). During TNF-induced necroptosis, caspase inhibitors, like zVAD-fmk, but neither individual nor combined application of inhibitors for calpain or cathepsin proteases affect the death response (Vercammen *et al.* 1998a, Thon *et al.* 2005, 2006). This is in line with results obtained in the study presented here analyzing proteolytic events during necroptosis, because treatment of U-937 cells with inhibitors of the cysteine proteases cathepsin L (zFF-fmk), cathepsin B/L (zFA-fmk) as well as the broad spectrum calpain/cysteine protease inhibitor E-64 did not protect from TNF-induced necroptosis (see 5.2.1; Figure 15A). Furthermore, wild-type and cathepsin D-deficient MEFs showed no differences in the necroptotic response to TNF/zVAD/CHX (Figure 13). Cathepsin D-deficient MEFs were not protected from MNNG-induced regulated necrosis, identical to their wild-type counterparts or to cathepsin D-deficient MEFs ectopically re-expressing cathepsin D (Figure 13), suggesting that cathepsin D plays no role in either TNF-induced necroptosis or the PARP pathway.

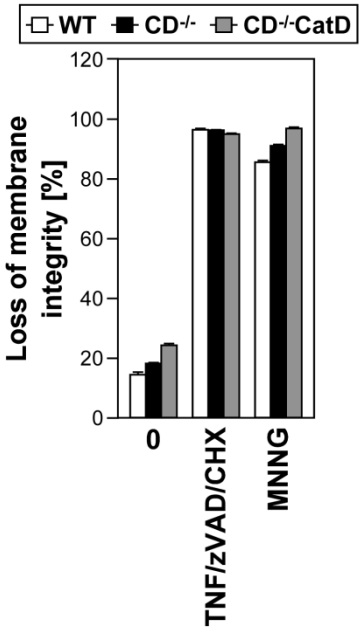

Figure 13: Cathepsin D plays no role in either TNF-induced necroptosis or the PARP pathway. Wild-type (WT), cathepsin D-deficient (CD $^{-/-}$), and CD $^{-/-}$ MEFs stably retransfected with the pro-cathepsin D cDNA (CD $^{-/-}$CatD) were incubated for 14 h with 100 ng/mL TNF in combination with 20 µM zVAD-fmk and 5 µg/mL CHX or with 1 mM MNNG for 30 min and further incubated for 16 h with fresh medium without MNNG. Subsequently, loss of membrane integrity was determined by flow cytometry. Representative data from one out of three experiments are shown and error bars indicate the SD from three measurements.

Altogether, the experiments obtained in the study presented here suggest that TNF-induced necroptosis is not affected by inhibition of PARP-1 and components of the PARP pathway.

Inhibition of necroptosis does not protect from PARP-1-induced regulated necrosis

In a reverse approach, the effect of the inhibition of one crucial component of TNF-induced necroptosis on the PARP pathway was analyzed. RIPK3 is such a crucial mediator of necroptosis. For this purpose, L929Ts, NIH3T3 cells naturally expressing RIPK3 and HEK293T, MCF-7 and HeLa cells which lack endogenous RIPK3 expression were analyzed for their ability to undergo TNF-induced necroptosis and PARP-induced regulated necrosis. In line with the crucial functions of RIPK3 in necroptosis, L929Ts and NIH3T3 were sensitive to TNF/zVAD-induced necroptosis whereas HEK293T, MCF-7 and HeLa cells were resistant to TNF/zVAD/CHX treatment (Figure 14). In contrast to necroptosis, both MNNG and MMS, a distinct DNA-alkylating agent and activator of PARP-1 (Gassmann *et al.* 2012), uniformly induced loss of membrane integrity in all analyzed cell lines (Figure 14). Further results obtained in the laboratory substantiate that RIPK3 and also RIPK1 have no essential functions in the PARP pathway (Sosna, Voigt *et al.* 2014).

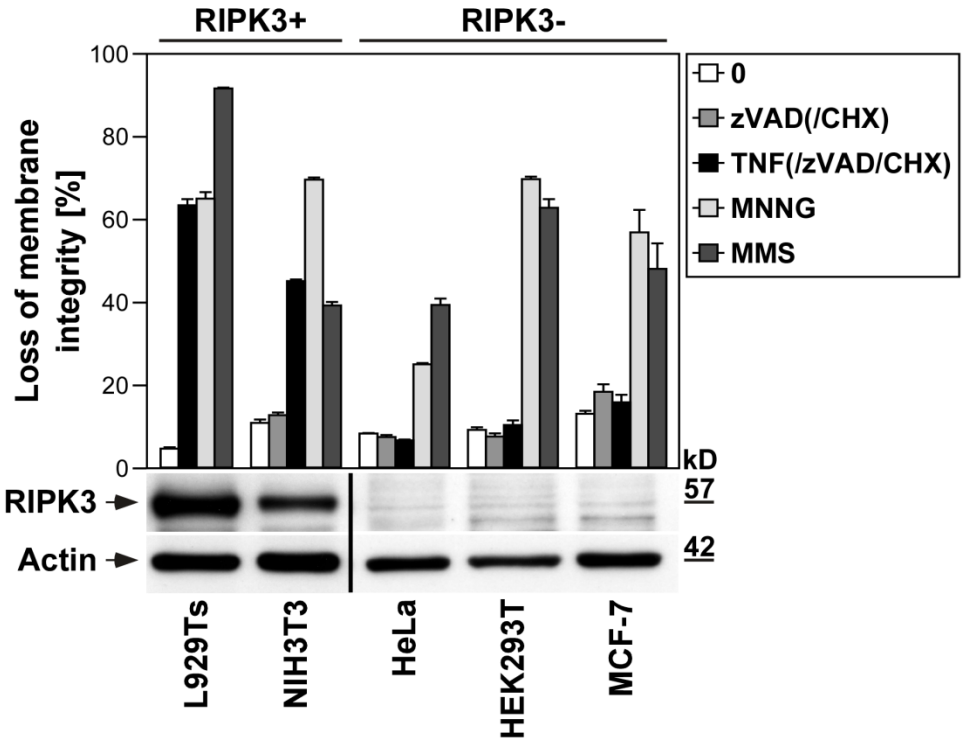

Figure 14: RIPK3 is a crucial mediator of TNF-induced necroptosis, but not in the PARP pathway. RIPK3-positive (L929Ts, NIH3T3) or RIPK3-negative (HEK293T, MCF-7, HeLa) were treated with 100 ng/mL TNF with addition of 20 µM (NIH3T3) or 50 µM (293T, MCF-7, HeLa) zVAD-fmk and 1 ng/mL (293T) or 0.25 µg/mL (MCF-7, HeLa) non-toxic CHX for 24 h or with 0.5 mM MNNG or 25 mM MMS for 15 min and further incubated for 16 h with fresh medium without MNNG or MMS. Treatment with zVAD/(CHX) alone served as a control. Loss of membrane integrity was determined by flow cytometry. Representative data from one out of three experiments are shown and error bars indicate the SD from three measurements.

Conclusion: TNF and PARP-1 induce distinct routes to regulated necrosis

In this part of the study, the two most extensively studied models of regulated necrosis (necroptosis and PARP-induced regulated necrosis) were analyzed and revealed that TNF and MNNG can induce regulated necrosis in L929 sublines, HT-29, Jurkat, NIH3T3, HeLa, HEK293T and MCF-7 cells. The depletion of intracellular ATP levels occurs late during TNF-induced necroptosis, implicating that individual components of the PARP pathway are activated as a secondary consequence during necroptosis rather being the cause of necroptotic cellular disintegration. This was in contrast to the rapid depletion of ATP following PARP-1 activation by MNNG. Moreover, PARP-1 inhibition did not alter TNF-induced necroptosis, whereas the MNNG-induced PARP pathway was blocked. The interference with further components of the PARP pathway revealed that JNK as well as cathepsin D have no role in TNF-induced necroptosis. On the other hand, interference with components of the necroptosis pathway (e.g. RIPK3) did not alter the PARP pathway, suggesting that TNF-induced necroptosis and PARP-1-mediated regulated necrosis represent two distinct routes to necrotic PCD. Further results performed in the laboratory substantiate this hypothesis (Sosna, Voigt *et al.* 2014).

5.2 Proteolysis is crucial for the regulation of TNF-induced necroptosis

In regulated necrosis, proteolysis of regulator proteins appears to be an important execution mechanism among others as described in section 2.2.1.2, but the participating proteases and the underlying molecular mechanisms are only marginally characterized. Therefore, in work described in this chapter, the focus was put on the identification of new proteins participating in the proteolytic regulation during necroptosis primarily induced by TNF/(zVAD/(CHX)). To this end, three different approaches were utilized: (a) identification of proteases whose inhibition blocks necroptosis, especially serine proteases sensitive to TFCK (N-tosyl-L-phenylalanine chloromethyl ketone; formerly abbreviated TPCK; section 5.2.1), (b) RNAi screens to identify proteases which, when down-regulated, affect TNF-induced necroptosis (section 5.2.2) and (c) detection of new or known proteins cleaved during necroptosis by immuno-magnetic enrichment of TNF-R1-containing magnetic vesicles in combination with proteomic technologies, e.g. 2D-DIGE and MALDI-TOF/TOF analyses (section 5.2.3). Furthermore, the analysis of the proteolytic degradation of the potentially pro-necroptotic protein (d) PGAM5 and the characterization of the proteolytic maturation/activation of (e) A-SMase during necroptosis was addressed and described in sections 5.2.4 and 5.2.5. In the last section (5.2.6) of this part of the presented thesis, the investigation of the role of other peptidases such as presenilin and the presenilin homologue signal-peptide-peptidase-like (SPPL) during TNF-induced necroptosis was investigated.

5.2.1 Identification of HtrA2/Omi, PSA1, PMPCA and Lon protease as TFCK-sensitive proteases mediating necroptosis

Inhibition of serine proteases, but not metalloproteases, cathepsin or calpain/cysteine proteases protect cells from TNF-induced necroptosis

In order to investigate which class of proteases substitute for caspases during regulated necrosis, the effects of different protease inhibitors on TNF-induced necroptosis were investigated in murine (L929Ts, NIH3T3) and human cell lines (U-937, HT-29, Jurkat ATCC and Jurkat I42). In line with previous findings (Thon *et al*. 2005, Sosna and Voigt *et al*. 2013; Sosna, Voigt *et al.* 2014) and as shown in Figure 15A, inhibitors of the cysteine proteases cathepsin L (zFF-fmk), cathepsin B/L (zFA-fmk) as well as the broad spectrum calpain/cysteine protease inhibitor E-64 did not protect U-937 cells from TNF-induced necroptosis. Surprisingly, the cathepsin B inhibitor Ca-074Me showed protection from necroptotic cell death in U-937 cells. This, however, was not observed in other cell lines (Sosna and Voigt *et al*. 2013) or with any of the other cysteine protease inhibitors studied here. It was shown that the inhibitor Ca-074Me abrogated staurosporine-induced necrotic cell death in leukemia cells and that this is independent of its inhibitory effect on cathepsin B (Mihalik *et al.* 2004). Moreover, the same group reported that the inhibitor Ca-074Me has a cathepsin B-independent target that plays a role in necroptosis upstream of lysosomal breakdown (Dunai *et al.* 2012) which may explain the protective effect of Ca-074Me on TNF-induced necroptosis in U-937 cells.

Furthermore, pharmacological inhibition of acid proteases (aspartyl peptidases) by pepstatin A showed no decrease in the death response to TNF but rather enhanced necroptosis (Figure 15A). In summary, these results demonstrate that calpain/cysteine and aspartate proteases are not required for TNF-induced necroptosis. Treatment of U-937 cells with the proteasome inhibitor MG-132 did not prevent the cells from TNF/zVAD-induced necroptosis (Figure 15A). It was also investigated whether TNF-induced necroptosis is regulated by metalloproteinases. The broad-spectrum inhibitors of matrix metalloproteinases, GM6001 and marimastat, neither protected murine L929Ts cells, NIH3T3 cells nor human U-937 cells from TNF-induced necroptosis (Figure 15B), additionally arguing against a role of metalloproteinases as well as the proteasome and in this form of PCD.

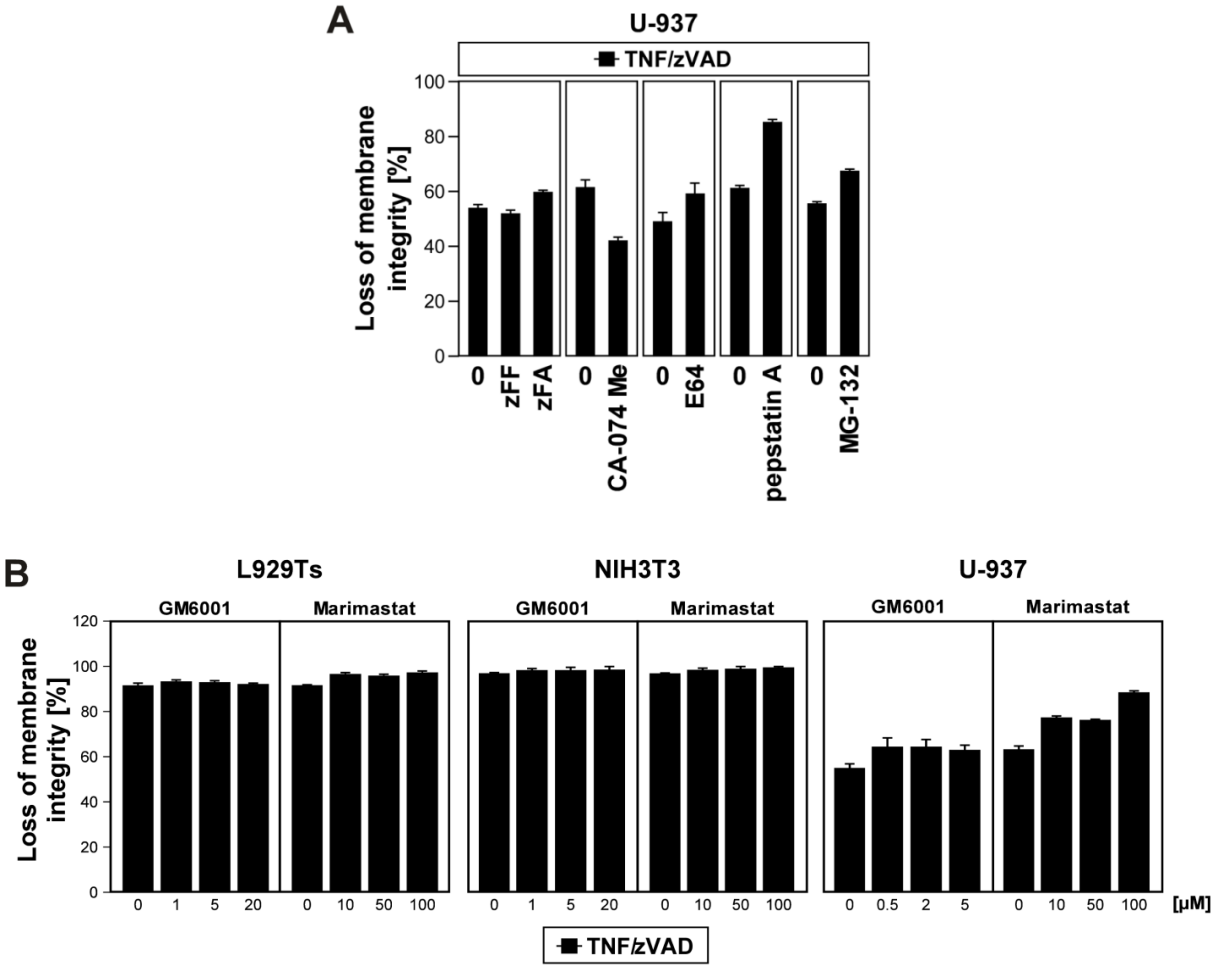

Figure 15: Inhibition of cathepsin or calpain/cysteine proteases and metalloproteases does not protect U-937 cells from TNF-induced necroptosis. (A) U-937 cells were pre-incubated for 2 h with 1 µM z-FF-fmk, 5 µM zFA-fmk or in separate experiments with 1 µM Ca-074Me, 20 µM E64, 0.1 µM MG-132 in combination with 50 µM zVAD-fmk and subsequent addition of 100 ng/mL TNF for 24 h before cell death was analyzed. For pepstatin A incubation, cells were pre-incubated for 24 h with or without 100 µM pepstatin A followed by incubation with or without 100 ng/mL TNF and 50 µM zVAD-fmk for 24 h. Subsequently, loss of membrane integrity was measured by flow cytometry. **(B)** L929Ts, NIH3T3 and U-937 cells were pre-incubated for 2 h with GM6001 and marimastat as indicated and subsequent addition of 100 ng/mL TNF and 20 µM (L929Ts, NIH3T3) or 50 µM (U-937) zVAD-fmk before cell death was analyzed. The diagrams show the percentage of 10,000 analyzed cells losing their membrane integrity. Representative data from one out of two experiments are shown and error bars indicate the SD from three measurements.

In a next set of experiments, the effect of TFCK, an inhibitor of chymotrypsin-like serine proteases, on TNF-induced necroptosis was investigated. As shown in Figure 16, TFCK significantly protected murine L929Ts and NIH3T3 cells from TNF-induced necroptosis. Moreover, TFCK significantly protected Jurkat cells and its subline I42 as well as HT-29 and U-937 cells from necroptosis elicited by TNF (Figure 16). Similar results were obtained with the treatment of Nec-1, suggesting that TFCK can block TNF-induced necroptosis (Figure 16). Taken together, these results show clearly that serine proteases participate in TNF-induced necroptosis in a cell type- and species-independent manner, whereas inhibition of metalloproteinases, calpain/cysteine and aspartate proteases had no major impact in this specific form of regulated necrosis.

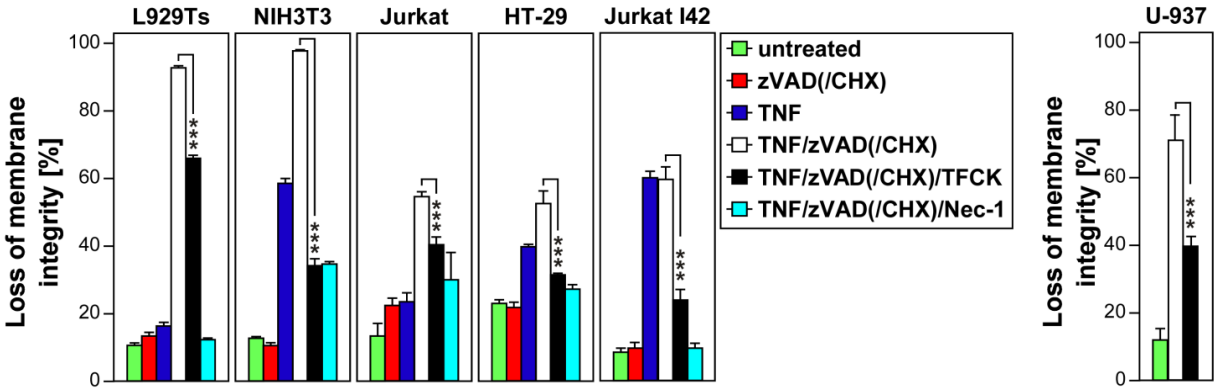

Figure 16: TFCK-specific serine proteases have an impact on TNF-induced necroptosis. Cells were stimulated with or without 100 ng/mL TNF for 5 (L929Ts), 6 (Jurkat I42), 16 (NIH3T3, HT-29), 20 (Jurkat) or 24 h (U-937) with optional addition of 20 (L929Ts, NIH3T3, HT-29, Jurkat I42) or 50 µM (Jurkat, U-937) of the pan-caspase inhibitor zVAD-fmk, 2 (Jurkat) or 5 µg/mL (HT-29) CHX and 50 (L929Ts, NIH3T3, U-937) and 25 µM (Jurkat, Jurkat I42, HT-29) TFCK, or 50 µM necrostatin 1 (Nec-1; to inhibit necroptosis). Subsequently, the cells were analyzed for loss of membrane integrity by means of PI staining and flow cytometry. Asterisks indicate statistical significance (t-test), *** $P \leq 0.001$. Representative data from three experiments are shown and error bars indicate SD from three parallel measurements.

Identification of HtrA2/Omi, PSA1 and PMPCA as TFCK-sensitive proteases mediating necroptosis

To identify the TFCK-sensitive serine protease(s) responsible for TNF-dependent regulated necrosis, a previously employed approach aiming to affinity-label only a subset of proteases and subsequent identification of proteins by means of MS (Egger *et al*. 2007) was adapted. In an initial experiment, L929Ts cells were treated with TNF/zVAD in the presence of cell-permeable active-site-directed fluorescently labeled TFCK-derivative (FFCK) to identify serine proteases activated during TNF-induced necroptosis. Micrographs in Figure 17A show the necrotic-like morphology of cells treated with TNF/zVAD in comparison to TNF/zVAD/FFCK-treated cells, the latter being protected from necroptosis induced by TNF. Already after 30 min of incubation with FFCK, all cells were completely labeled with FFCK (Figure 17B). After 5 h of incubation (a timeframe expected to be sufficient to activate the relevant serine protease(s)), lysates from the cells were prepared and separated by SDS-PAGE. Fluorescence analysis revealed bands only in extracts from cells treated with FFCK but not in extracts from control cells demonstrating successful FFCK-labeling of the treated cells and no background staining in untreated cells (Figure 17C).

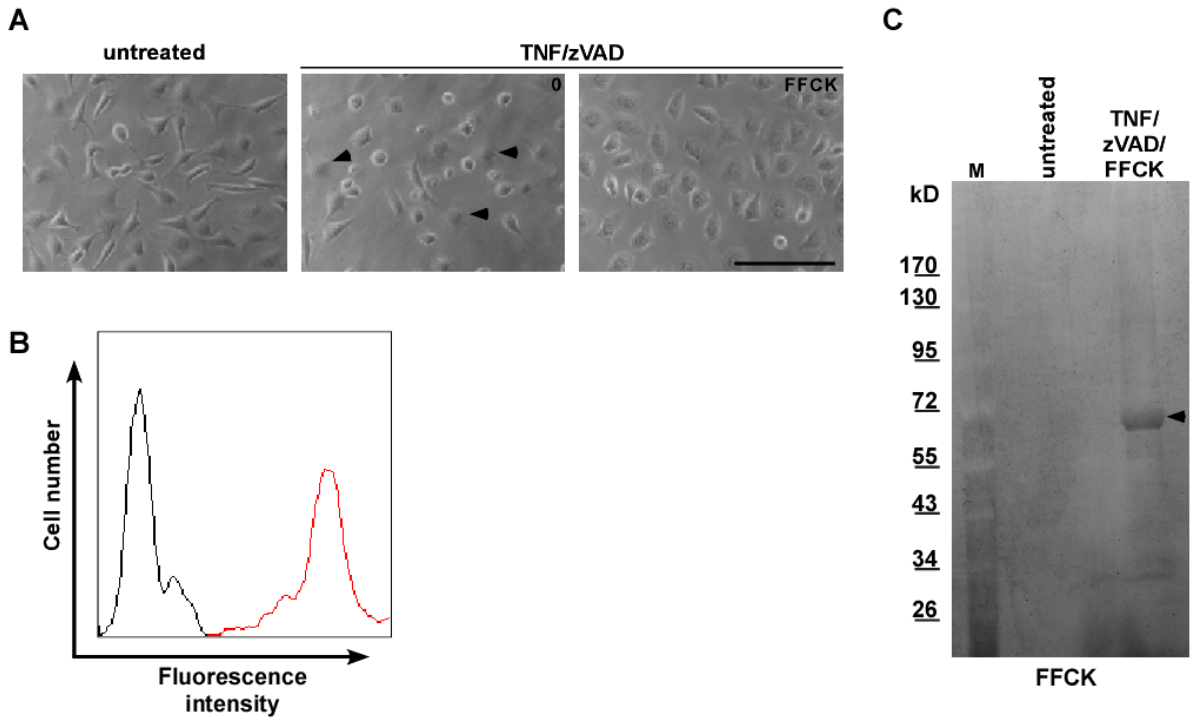

Figure 17: Labeling of L929Ts cells with a fluorescent active-site-directed serine protease inhibitor (FFCK). L929Ts cells were either left untreated, treated with 100 ng/mL TNF and 20 µM zVAD-fmk or additionally with 50 µM fluorescent TFCK-derivate (FFCK) for 5 h. **(A)** Micrographs show the morphology of unstimulated and stimulated cells. Scale bar: 100 µm. Black arrows mark necroptotic cells. **(B)** Flow cytometric analysis of L929Ts cells. Red line: Cells stimulated with TNF/zVAD/FFCK as in **(A)**, black line: untreated control cells. 10,000 cells were analyzed for each measurement. **(C)** Cytosolic extracts of cells treated as in **(A)** were separated with technical assistance by Jürgen Fritsch (Christian-Albrechts-University, Kiel, Germany) on a 6 - 15 % (v/v) gradient SDS gel, and bands (black arrow) were visualized with a scanner at green fluorescence. M: protein size marker.

To increase the resolution of the FFCK-labeled bands found in the one dimensional SDS gel (Figure 17), cellular extracts labeled with FFCK were analyzed by 2D-PAGE. L929Ts cells were treated with TNF/zVAD and CHX (to enhance necroptosis) for 5 h in the presence of FFCK. Lysates were separated by 2D-PAGE. Subsequent scanning for fluorescent signals revealed 128 fluorescently labeled protein spots (Figure 18). The labeled protein spots were analyzed by MS, 80 were identified with high and 28 with lesser confidence. As described in 4.2.14 proteins were considered identified when either two peptides were identified with a confidence interval $\geq$ 99 % ($p < 0.01$) or three peptides $\geq$ 95 % ($p < 0.05$). Due to non-specific background binding of FFCK, most of the 108 identified proteins turned out to be non-proteases. However, in this first screen, the mitochondrial serine protease high temperature requirement protein A2/Omi stress regulated endoprotease (HtrA2/Omi; Q9JIY5) was identified with high confidence (Figure 18). The identification of HtrA2/Omi met strict criteria of the MASCOT database search. Therefore, and because HtrA2/Omi has been associated with both caspase-dependent apoptosis as well as caspase-independent regulated necrosis (Vande Walle *et al.* 2010), this serine protease was considered a promising candidate.

Furthermore, in the same experiment, the mitochondrial-processing peptidase subunit alpha (PMPCA; Q9DC61) was identified which did not meet the high confidence criteria, but at least met the first filtering criteria. Experiments to determine the biological relevance of PMPCA and its potential association with necroptosis are described in section 5.2.2. The remaining identified proteins were non-proteases (data not shown). This might be due to the reported variety of pro- and anti-apoptotic effects of the chymotrypsin-like serine protease inhibitor TFCK (King *et al.* 2004; Rokhlin *et al.* 2004).

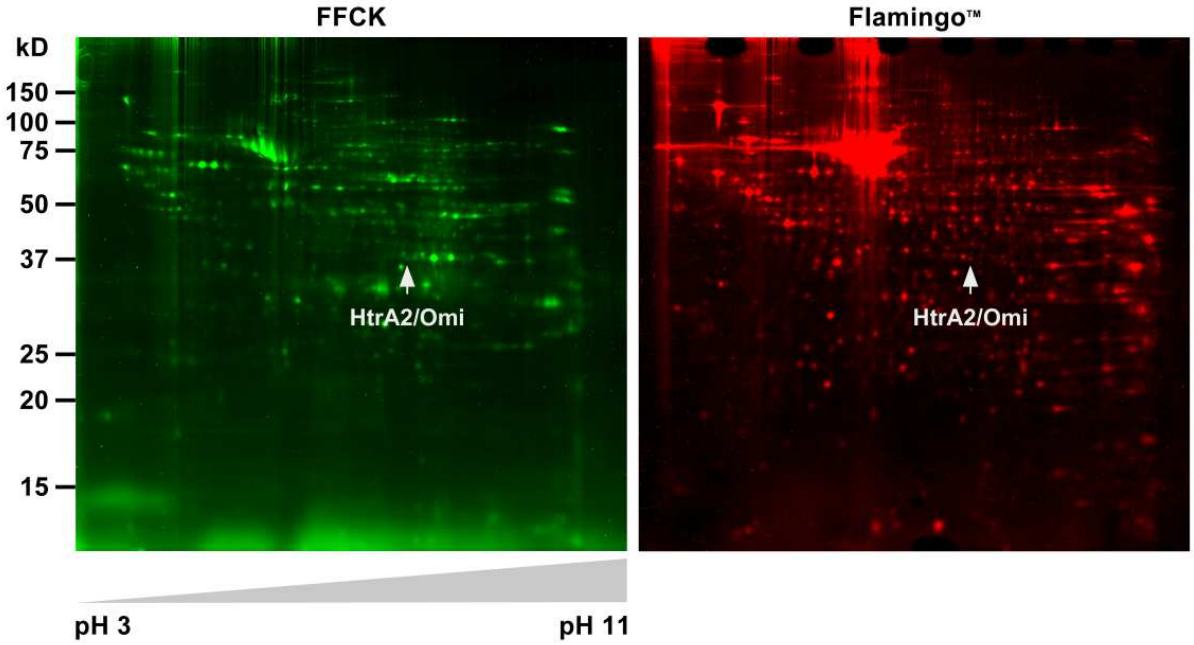

Figure 18: HtrA2/Omi is a candidate serine protease involved in necroptosis. L929Ts cells were stimulated with 100 ng/mL TNF, 20 µM zVAD-fmk and 2 µg/mL CHX in combination with 50 µM fluorescent TFCK-derivate (FFCK) for 5 h. Subsequently, cell lysates were separated by 2D gel electrophoresis and analyzed for protein spots labeled by FFCK (left panel, green), or for all separated protein spots by staining with Flamingo™ Fluorescent gel stain (right panel, red). The protein spots were subsequently identified by mass spectrometry. HtrA2/Omi is indicated by arrows. The preparation of the 2D gel was performed in collaboration with the group of Ottmar Janssen (Christian-Albrechts-University, Kiel, Germany) and MALDI-TOF/TOF analyses of the isolated fluorescently labeled protein spots were performed in collaboration with the group of Andreas Tholey (Christian-Albrechts-University, Kiel, Germany).

To additionally identify candidate proteases which may be activated at earlier time-points, the screen with murine L929Ts cells was repeated and cellular extracts of cells treated with TNF/zVAD/FFCK for 30 min were additionally analyzed. The 2D gel from lysates after 30 min stimulation revealed 157 fluorescently labeled spots which were isolated and identified by MS. In this screen, 71 proteins were identified with high and 20 proteins with lesser confidence. From the proteins with lesser confidence a part of the multicatalytic proteinase complex proteasome was identified with 9 peptide counts. This proteasome subunit alpha type-1 (PSMA1 or PSA1; Q9R1P4) was recently described to be involved in sensitization of bortezomib-resistant leukemia cells (Fang *et al.* 2012) and was therefore considered a promising candidate for further research purposes (see 5.2.2). The remaining identified proteins were non-proteases (data not shown).

Identification of the ATP-dependent Lon protease as a TFCK-sensitive protease mediating necroptosis

The screen for serine-proteases was extended to a cell line of human origin, i.e. Jurkat I42. This Jurkat subline is deficient for FADD and stably transfected with TNF-R2 (Chan *et al*. 2003) and thus susceptible to TNF-mediated cell death in the absence of CHX. Cells were treated with TNF/zVAD to induce necroptosis and labeled with FFCK for 30 min and 5 h. MS analysis of 145 proteins labeled with FFCK from 30 min and 5 h lysates revealed 88 proteins with high and 16 with lesser confidence. In this screen, the mitochondrial ATP-dependent protease Lon (LONM; P36776) was identified in lysates from cells treated with TNF/CHX/zVAD/FFCK for 30 min, albeit with low confidence (Figure 19). The remaining identified proteins from lysates obtained after 30 min and 5 h stimulation were non-proteases (data not shown). Since the mitochondrial ATP-dependent Lon protease has been already associated with tumorigenesis mediated by the generation of ROS (Cheng *et al.* 2013), it was further analyzed as well (see section 5.2.2).

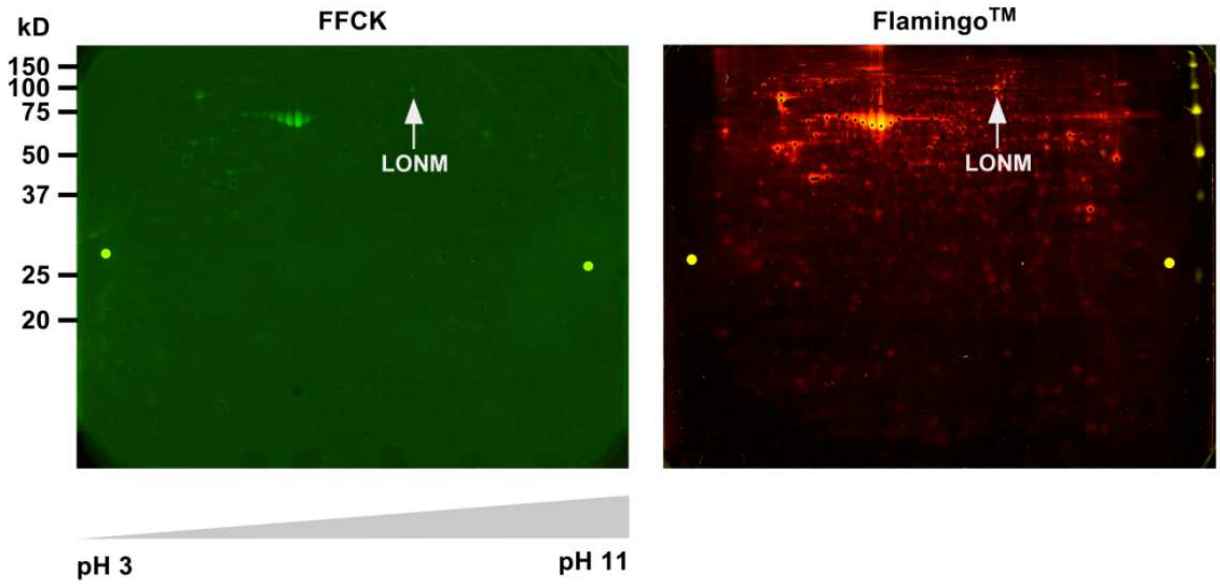

Figure 19: Identification of the mitochondrial ATP-dependent protease Lon as a candidate serine protease involved in necroptosis. Jurkat I42 cells were stimulated with 100 ng/mL TNF, 20 µM zVAD-fmk in combination with 50 µM FFCK for 30 min. Subsequently, lysates from cells were separated by 2D gel electrophoresis and analyzed for protein spots labeled by FFCK (green). The labeled protein spots were subsequently isolated and identified by mass spectrometry. Lon protease (LONM) is indicated by the white arrows. The right picture shows the protein load (Flamingo™ staining for proteins; red) after excision of green fluorescent protein spots. The preparation of the 2D gel was performed in collaboration with the group of Ottmar Janssen (Christian-Albrechts-University, Kiel, Germany) and MALDI-TOF/TOF analyses of the isolated fluorescently labeled protein spots were performed in collaboration with the group of Andreas Tholey (Christian-Albrechts-University, Kiel, Germany).

The TFCK-sensitive serine protease HtrA2/Omi regulates necroptosis

As described above, the identification of HtrA2/Omi met strict criteria of the MASCOT database search. Therefore, and because HtrA2/Omi has been associated with both caspase-dependent apoptosis as well as caspase-independent regulated necrosis (Vande Walle *et al*. 2010), this serine protease was considered a promising candidate. To investigate whether HtrA2/Omi was indeed involved in the execution of TNF-induced necroptosis, the activity of HtrA2/Omi was blocked by pharmacological inhibition with the specific inhibitor Ucf-101 (Cilenti *et al.* 2003). Treatment with Ucf-101 resulted in protection of L929Ts, NIH3T3, Jurkat ATCC, Jurkat I42 and U-937 cells from TNF-induced necroptosis (Figure 20A). However, HT-29 cells showed only marginal protection from TNF/zVAD/CHX treatment when incubated with Ucf-101 (Figure 20A). This might be explained by the fact that other serine proteases might substitute for HtrA2/Omi in a cell-type-specific manner. Notably, in L929Ts cells treated for 5 h with TNF/zVAD, the combination of Ucf-101 and TFCK did not confer a stronger protection from necroptosis (Figure 20B). This observation suggests that both inhibitors (Ucf-101 and TFCK) were acting via the same signaling pathway or even both may target HtrA2/Omi.

Since pharmacological inhibitors might have non-specific effects, MEFs derived from HtrA2/Omi-deficient mice were used for further characterization of HtrA2/Omi in necroptosis. MEFs deficient for HtrA2/Omi were fully protected from TNF-induced necroptosis (Figure 20C), validating the results with Ucf-101. Taken together, the above described observations confirm that the serine protease HtrA2/Omi is indeed a key mediator of TNF-induced necroptosis.

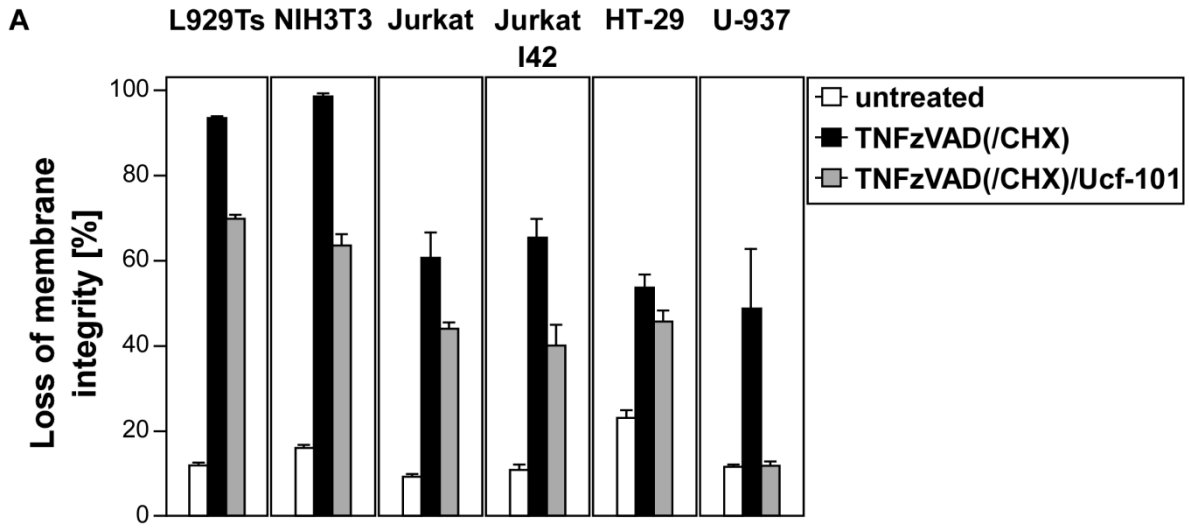

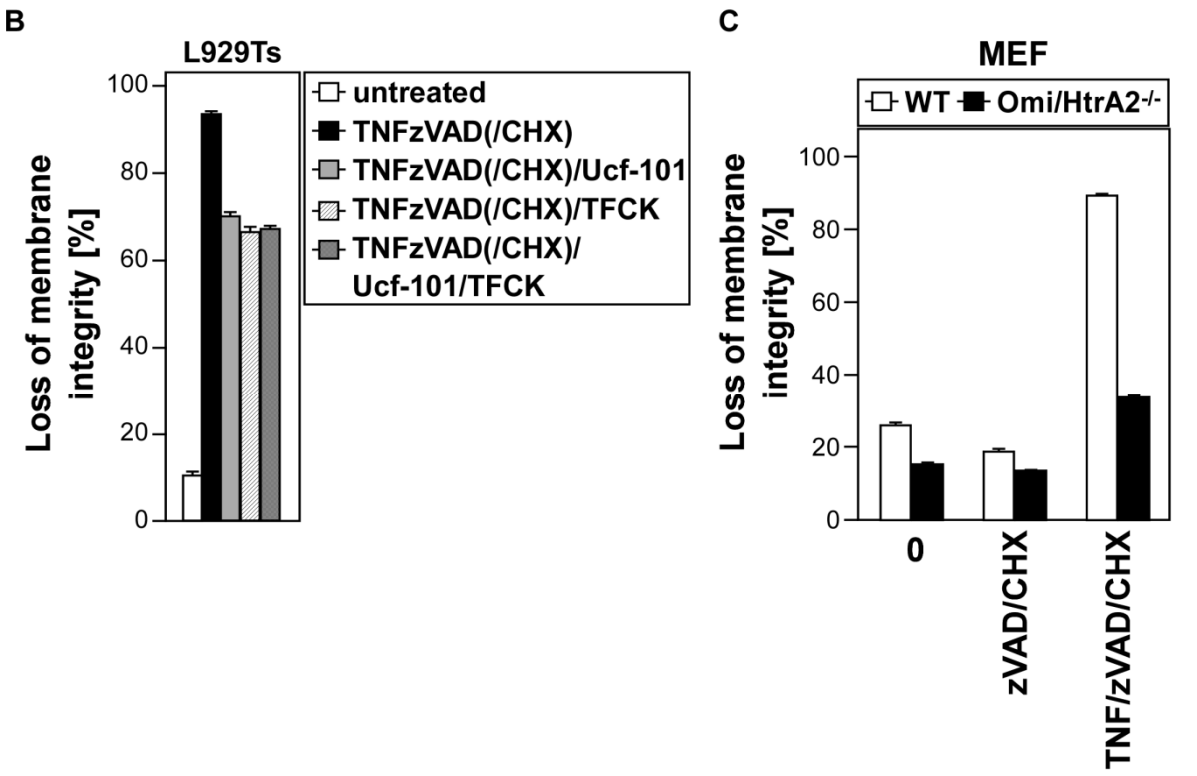

Figure 20: The serine protease HtrA2/Omi mediates TNF-induced necroptosis. (A) Cells were left untreated, or were pretreated for 2 h with 25 µM (Jurkat ATCC, Jurkat I42) or 50 µM (L929Ts, NIH3T3, HT-29, U-937) of Ucf-101 and further incubated for 5 (L929Ts, U-937), 6 (Jurkat I42), 16 (NIH3T3, HT-29), 20 (Jurkat ATCC) or 24 h (U-937) with 100 ng/mL TNF, 20 µM (L929Ts, NIH3T3, HT-29) or 50 µM (Jurkat ATCC, Jurkat I42, U-937) zVAD-fmk and 2 µg/mL (Jurkat ATCC, U-937) or 5 µg/mL (HT-29) CHX before cell death was analyzed by measuring loss of membrane integrity. **(B)** L929Ts cells were left untreated or were pretreated with either 50 µM Ucf-101, 50 µM TFCK or a combination of both as above, followed by stimulation with TNF/zVAD/CHX as outlined above. At the end of the incubation time cells were analyzed as above. **(C)** Wild-type (WT) and HtrA2/Omi-deficient MEFs were stimulated with 100 ng/mL TNF, 20 µM zVAD-fmk and 1 µg/mL CHX or with zVAD/CHX alone for 16 h before cell death was measured by flow cytometry. The diagrams show the percentage of 10,000 analyzed cells losing their membrane integrity. Representative data from one out of two experiments are shown and error bars indicate the SD from three measurements.

Conclusion: HtrA2/Omi is a key component of TNF-mediated necroptosis and PSA1, PMPCA and Lon protease are TFCK-sensitive proteases potentially mediating necroptosis

Using multiple murine and human cell systems, it could be shown that inhibition of serine proteases by TFCK, but not inhibition of metalloproteases, cathepsin or calpain/cysteine proteases protects from TNF-induced necroptosis, suggesting that serine proteases are crucial for TNF-induced necroptosis. To identify the corresponding TFCK-sensitive serine protease(s), necroptosis was induced in L929Ts or Jurkat I42 cells to activate the relevant proteases in the presence of an active-site-directed fluorescently labeled TFCK-derivative. The labeled proteins were resolved by 2D-PAGE, followed by analysis via MALDI-TOF-MS and HtrA2/Omi was identified as the most promising candidate (see Sosna and Voigt *et al.* 2013). The importance of HtrA2/Omi in necroptosis was validated by showing that pharmacological inhibition or genetic deletion of HtrA2/Omi fully protects from TNF-induced necroptosis. In the proteomic screen for TFCK-sensitive proteases that participate in necroptosis, three further candidates were identified: Lon protease 1, PSA1 and PMPCA. These proteases were investigated with regard to their exact function in the signaling pathways of necroptosis after manual

transfection of HT-29 and U-937 cells with the specific siRNA which is shown in the following section of the study.

5.2.2 RNAi screen to identify proteases that regulate necroptosis

Identification of candidate proteases participating in necroptosis in a robotic high-throughput RNAi screen

To identify proteases which protect from or enhance regulated necrosis, a complementary siRNA screen of all proteases encoded by the human genome was performed in collaboration with the group of Philip Rosenstiel (Christian-Albrechts-University, Kiel, Germany), who provided the siRNA library as well as the instrument-based structure, expertise and performed the robotic part of the screens.

The screen was performed using the human colorectal adenocarcinoma cell line HT-29. The setup of the screen was related to previous work from Lipinski *et al.* (2012) identifying mediators of intracellular nucleotide-binding oligomerization domain-2 (NOD2) receptor signaling. The Silencer Human Genome siRNA library, Version 3 covering 21,687 human genes with 3 individual siRNAs per gene (65,061 siRNAs in total) was used to identify proteases potentially involved in TNF-induced necroptosis. The experimental set up is depicted in Figure 5A and 5B and is described in section 4.2.4. For control of transfection efficacy, control siRNAs targeting known regulators of necroptosis (i.e. RIPK1, RIPK3 as well as TNF-R1) were added to the screen. The down-regulation of these control proteins significantly reduced the sensitivity of HT-29 cells to TNF-induced necroptosis (Figure 21A). Down-regulation of HtrA2/Omi served as an internal negative control, since it was shown that down-regulation of HtrA2/Omi does not affect TNF-induced necroptosis (Sosna and Voigt *et al.* 2013; Figure 21A). Of note, the importance of HtrA2/Omi in necroptosis was validated by showing that pharmacological inhibition or genetic deletion of HtrA2/Omi fully protects from TNF-induced necroptosis (see 5.2.1).

In the initial screen, 21.25 % of all single siRNA hits passed the threshold (normalized fold-induction values ≥ 1.5 or ≤ -1.5). To further narrow down the list and to minimize false positives, the effects of down-regulation of the three individual siRNAs per gene were compared. The following rules for positive candidate genes were defined: (a) genes that were represented by two or three siRNAs above the fold-induction threshold, and (b) genes with a single siRNA above the fold-induction threshold and with two other siRNAs pointing in the same direction as the single siRNA passing the threshold. Using these rules, 7 proteases were found that conformed to criterion (a), with the strongest effectors being caspase-8, cylindromatosis (CYLD) and CFLAR (c-FLIP). Furthermore, 33 proteases met the criteria for (b). In total, the first robotic screen identified 40 proteases which, when down-regulated, caused increased (37 %) or reduced sensitivity (63 %) to TNF-induced necroptosis (Figure 21B and Supplementary Table S1).

A second robotic screen was performed using the 40 candidates meeting the described criteria (Figure 21B and Supplementary Table S1) and the same positive and negative controls. After analysis of the results, the list of candidates was narrowed down to 10 proteases with pronounced (and six candidates with less pronounced) effects, again identifying CASP8, CYLD and c-FLIP as the strongest effectors (Table 4).

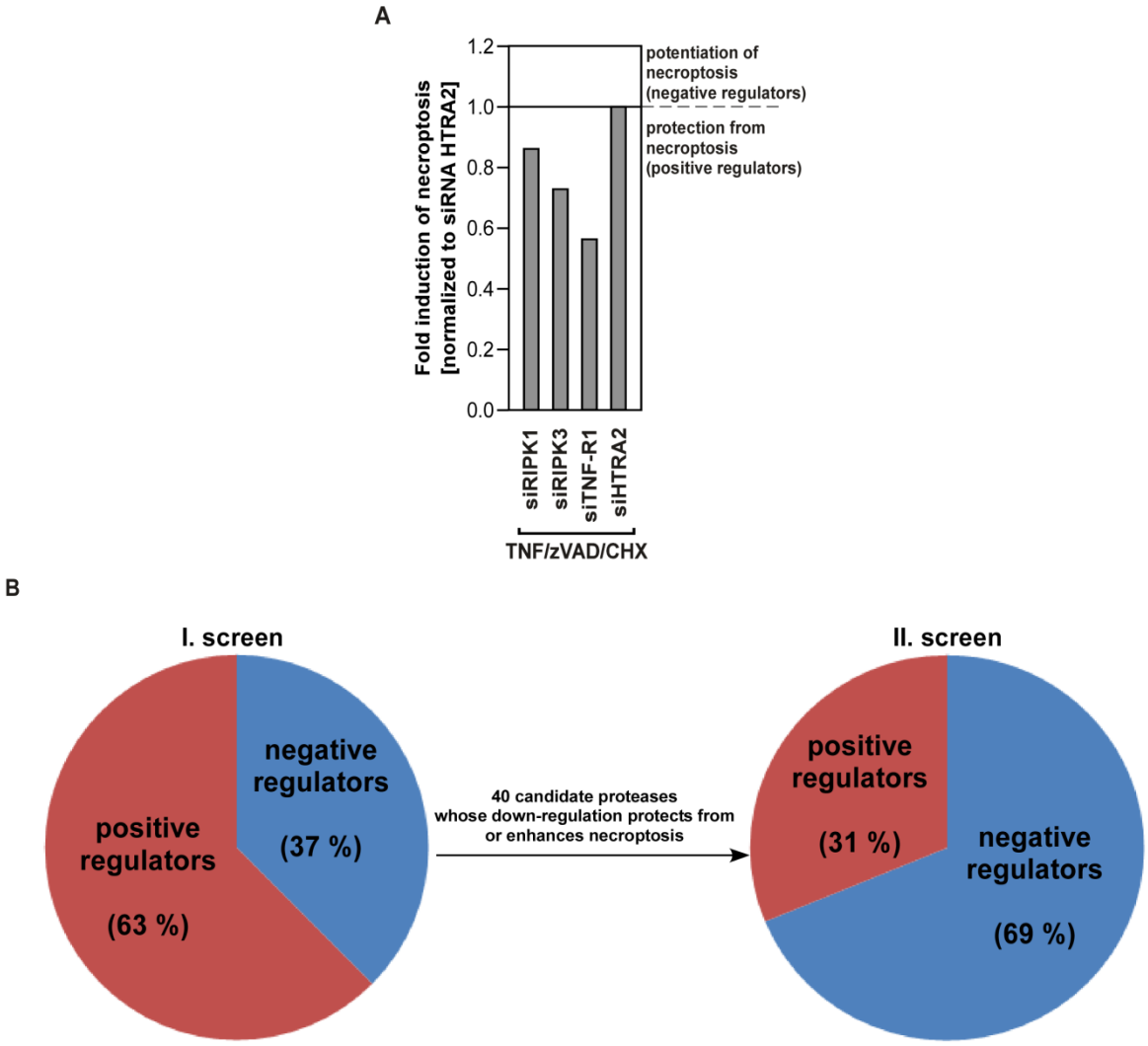

Figure 21: High-throughput siRNA screen for proteases participating in necroptosis. (A) Exemplary control experiment using HT-29 cells transfected with either positive control siRNA (RIPK1, RIPK3, TNF-R1) or HTRA2 siRNA (all 20 nM). After 72 h, necroptosis was induced by addition of 100 ng/mL TNF, 20 µM zVAD-fmk and 5 µg/mL CHX. ATP levels were measured 20 h after stimulation. Fold induction values were calculated by means of normalization of viability to control siRNA of HTRA2. **(B)** In the first screen, a total of 40 candidates met the fold induction threshold and were re-screened in a second screen yielding 16 candidate hits. Candidates were divided into positive (down-regulation decreases cell death after TNF/zVAD/CHX stimulation compared to control transfected cells) and negative regulators (enhancement of cell death after down-regulation). The complementary siRNA screen was performed in collaboration with the group of Philip Rosenstiel (Christian-Albrechts-University, Kiel, Germany).

Table 4: Proteases identified to have a positive or negative effect on TNF-induced necroptosis. These 16 proteases meet the criteria for candidate proteases. Citations linking these proteases to programmed cell death (PCD) are listed in the last column. For all proteases identified, the related reference sequence number from the National Center of Biotechnology Information and their individual accession number are listed.

Protease	Abbreviation	Reference sequence	Accession Number	Link to PCD
A disintegrin and metalloproteinase with thrombospondin motifs 18	ADAMTS18	NM_199355	Q8TE60	-
Aminopeptidase Q	AP-Q	NM_173800	Q6Q4G3	-
ATP-dependent zinc metalloprotease YME1L1	YME1L1	NM_139312	Q96TA2	Stiburek *et al.* 2012
Carboxypeptidase Q	CBPQ	NM_016134	Q9Y646	-
Caspase-8	CASP8	NM_001228	Q14790	Kaczmarek *et al.* 2013
CasperFLIP	CFLAR	NM_003879	O15519	Kaczmarek *et al.* 2013
Cylindromatosis protein	CYLD	NM_015247	Q9NQC7	Kaczmarek *et al.* 2013
Dihydropyrimidinase-related protein 3	DPYL3	NM_001387	Q14195	-
Dihydropyrimidinase-related protein 4	DPYL4	NM_006426	Q14531	Kimura *et al.* 2011
Dipeptidyl peptidase 8	DPP8	NM_197960	Q6V1X1	-
Gamma-glutamyltranspeptidase 1	GGT1	NM_005265	P19440	Boonyanugomol *et al.* 2012
Insulysin	DIE	NM_004969	P14735	-
Meprin 1 beta	MEP1B	NM_005925	Q16820	Carmago *et al.* 2002
Pre-mRNA-processing-splicing factor 8	PRPF8	NM_006445	Q6P2Q9	Tapia-Vieyra *et al.* 2005
Stromelysin-1	MMP3	NM_002422	P08254	Sternlicht *et al.* 1999
Transmembrane protease serine 11E	DESC	NM_014058	Q9UL52	Viloria *et al.* 2007

Manual validation of candidate proteases and TFCK-sensitive proteases in HT-29 cells

Subsequently, candidates with a published link to PCD (Table 4) were selected and analyzed for their potential to enhance or decrease TNF-induced necroptosis. The third screen was performed manually using newly obtained and independent siRNA pools or individual siRNAs (see Table 1) for the 10 candidates to exclude off-target effects of the formerly utilized siRNAs.

Again, positive (RIPK3, TNF-R1) and negative controls (commercial non-targeting siRNA and HTRA2 siRNA) were present in every experiment. Transfected HT-29 cells, where RIPK3 and TNF-R1 was down-regulated showed decreased TNF-induced necroptosis whereas cell death was not prevented by HTRA2-specific siRNA transfection (Figure 22A). Moreover, lysates of siRNA-transfected HT-29 cells were analyzed by Western blot and showed successful down-regulation of representative positive (RIPK3), negative (HTRA2) controls and exemplarily the candidate protease caspase-8 (CASP8; Figure 22B).

The list of candidate siRNA genes was extended by three further candidates (PMPCA, PSA1 and LONM; see section 5.2.1) which were identified during the proteomic screen for TFCK-sensitive proteases participating in regulated necrosis. Down-regulation of the proteases DESC, GGT1, PRPF8 and CFLAR resulted in increased cell death. Down-regulation of CASP8 and CYLD on the other hand resulted in decreased cell death (Figure 23). The remaining candidates from the siRNA screen (MMP3, MEP1B, YME1L1) showed only marginal effects towards TNF-induced necroptosis when compared to control transfected and treated HT-29 cells. Likewise, the transfection of HT-29 cells with siRNAs for LONM, PSA1 and PMPCA did not result in enhanced or decreased TNF-induced necroptosis (Figure 23). This lack of effects may result from an insufficient reduction of proteolytic activity by incomplete down-regulation which might not yet be sufficient to inhibit or enhance the

death response. To further analyze the effects of the candidate proteases, pharmacological inhibitory studies and direct genetic approaches will be required.

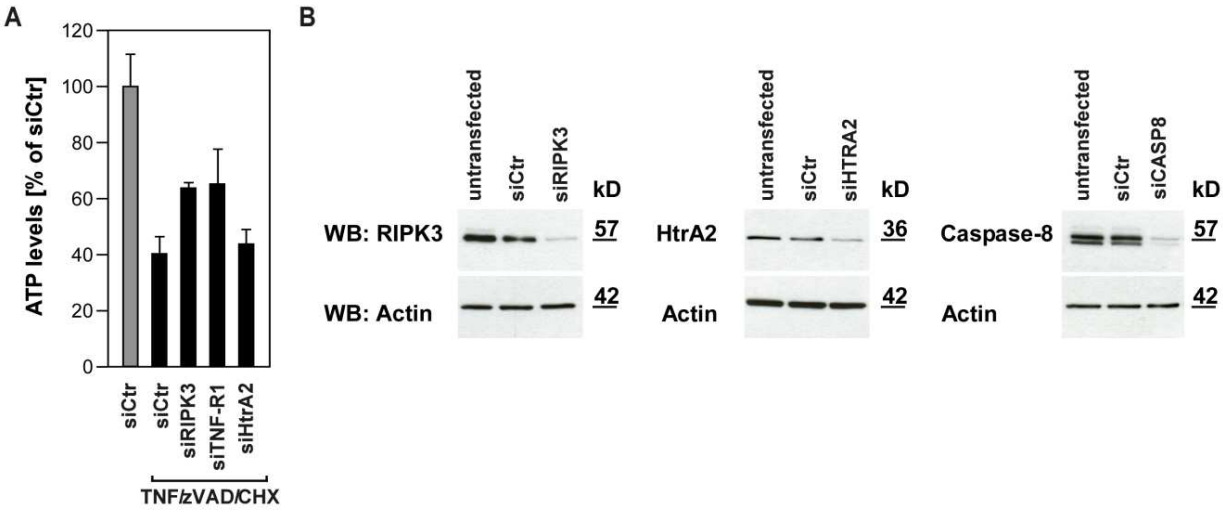

Figure 22: Exemplary control experiment for the validation of candidate proteases in HT-29 cells. (A) Intracellular ATP measurement of HT-29 cells transfected with siRNAs specific for either human RIPK3, TNF-R1 (internal positive control), HTRA2 (negative control) or control siRNA (siCtr). After 72 h, cells were treated with 100 ng/mL TNF, 20 µM zVAD-fmk and 5 µg/mL CHX before intracellular ATP levels were determined after 20 h of stimulation. Error bars show the respective SD from five parallel measurements. **(B)** Control Western blots of transfected (siRIPK3, siHTRA2 and siCASP8) but untreated cells were performed to verify down-regulation of the endogenous proteins. Detection of actin served as a loading control. Here, the diagram and Western blot analysis show one representative experiment which was performed for each siRNA transfection independently.

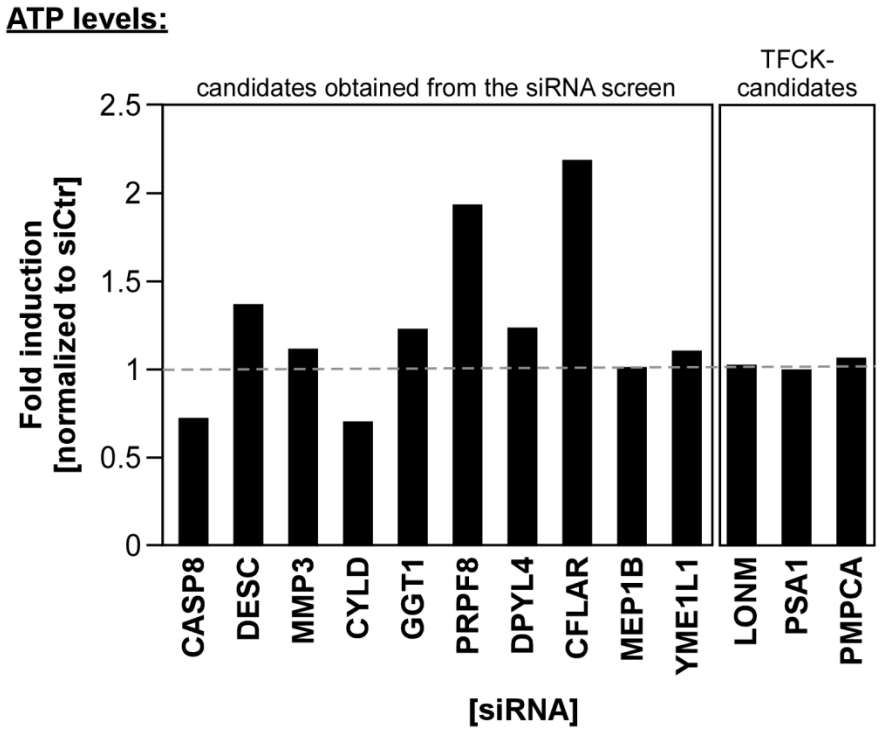

Figure 23: Validation of 13 candidate proteases in HT-29 cells. The specific siRNA of the 10 candidates identified from the siRNA screen (two separate experiments) and of the three candidates from the TFCK-screen were transfected into HT-29 cells and stimulated with 100 ng/mL TNF, 20 µM zVAD-fmk and 5 µg/mL CHX for 20 h. Data show relative viability units of HT-29 cells normalized to cells transfected with control siRNA. Experiments were repeated three times (CASP8, DESC, MMP3, CYLD, GGT1, PRPF8, DPYL4, CFLAR) or four times (MEP1B, YME1L1, LONM, PSA1, PMPCA).Values above the grey line indicate candidates whose down-regulation potentiates necroptosis or below the grey line indicate candidates that possibly protect from necroptosis when down-regulated.

Manual validation of candidate proteases and TFCK-sensitive proteases in U-937 cells

The validation of candidate proteases was extended to an additional human cell line (U-937 cells) and flow cytometry was performed in parallel to ATP level measurements to measure loss of membrane integrity as an additional read-out for cell death (Figure 24A,B). Control transfections (RIPK3, TNF-R1 and HTRA2 as negative control siRNAs) were present in every experiment and revealed essentially the same trends as observed in HT-29 cells (Figure 24C,D). The transfection of siRNAs targeting the candidate proteases DESC, MMP3, CFLAR and PMPCA showed increased loss of intracellular ATP indicating increased cell death (Figure 24A). In addition, these cells showed an increased loss of membrane integrity as measured by the incorporation of PI (Figure 24B). U-937 cells transfected with siRNA targeting GGT1, PRPF8, DPYL1 and PSA1 likewise showed an increase in cell death compared to cells transfected with negative control siRNA (Figure 24B). Remarkably, an increase in ATP level was detected in cells transfected with PRPF8 siRNA which is in contrast to the flow cytometric measurement (Figure 24A,B). As one possible explanation for this result, the increase in ATP levels might be due to cell death unrelated effects because two independent studies reported that intracellular levels of ATP can vary in response to cell death unrelated stimuli (Hahn-Windgassen *et al.* 2005; Galluzzi *et al.* 2011). As a result, measurement of loss of membrane integrity was additionally performed to validate the effects of down-regulation of candidate proteases. Cell death levels of cells with down-regulated CASP8, CYLD and MEP1B were decreased when determined by detection of ATP levels (Figure 24A). This was also true for CYLD siRNA transfected U-937 cells determined by PI-staining (Figure 24B). However, CASP8 and MEP1B siRNA transfected U-937 cells showed no decrease in loss of membrane integrity, suggesting that the measured ATP depletion occurred earlier than the onset of cell death. Down-regulation of LONM and YME1L1 showed no effect in both approaches (Figure 24A,B).

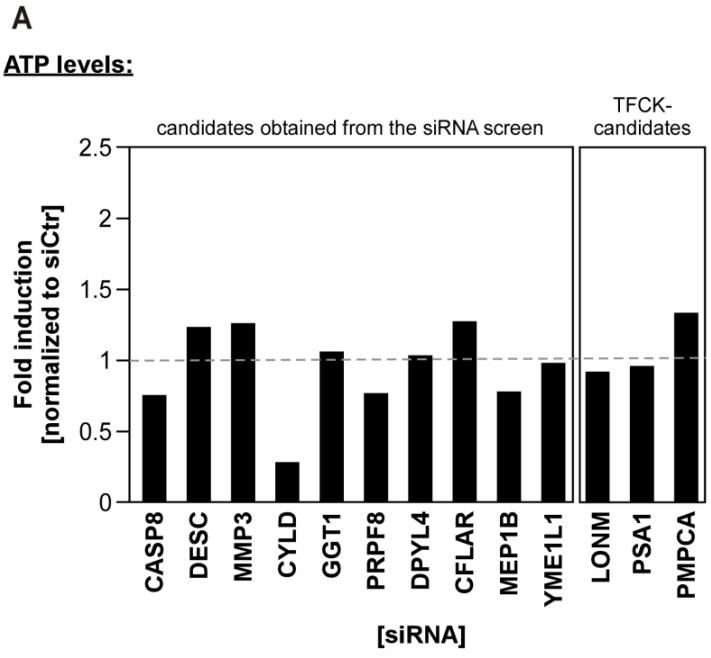

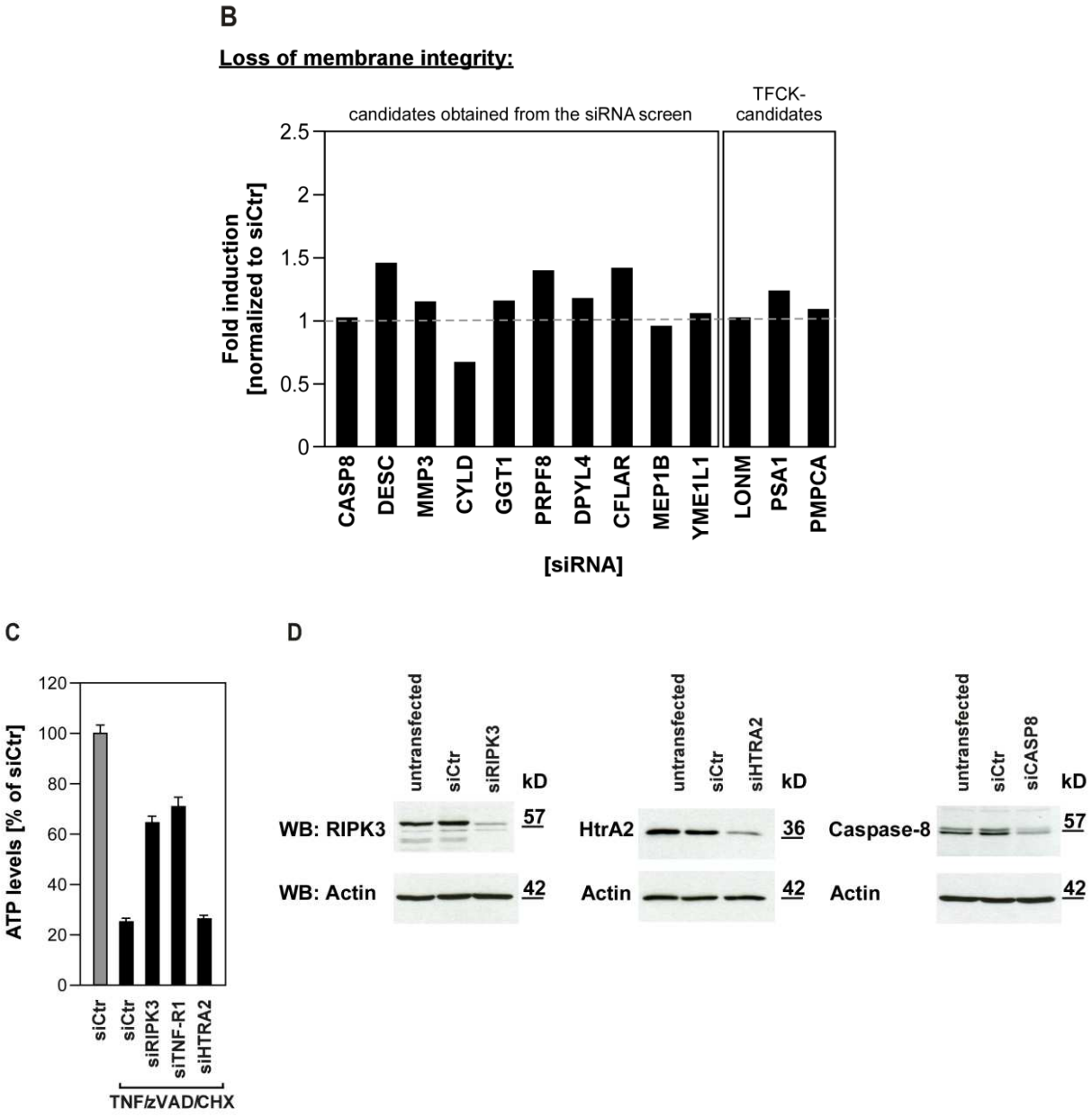

Figure 24: Validation of 13 candidate proteases in U-937 cells. (A-B) siRNAs of the 10 candidates identified from the siRNA screen were transfected into U-937 cells for 48 h. Subsequently, cells were stimulated with 100 ng/mL TNF, 50 µM zVAD-fmk and 0.1 µg/mL CHX for 24 h. Data show relative viability units of U-937 cells normalized to cells transfected with control siRNA either **(A)** measured by intracellular ATP levels or **(B)** by flow cytometry measuring PI-positive cells. Experiments were repeated twice (CASP8, DESC, MMP3, CYLD, GGT1, PRPF8, DPYL4, CFLAR) or three times (MEP1B, YME1L1, LONM, PSA1, PMPCA). Values above the grey line indicate candidates whose down-regulation potentiates necroptosis or below the grey line indicate candidates that possibly protect from necroptosis when down-regulated. **(C)** Exemplary control experiment showing intracellular ATP measurement of U-937 cells transfected with siRNAs specific for either human RIPK3, TNF-R1 (internal positive control), HTRA2 (negative control) or control siRNA (siCtr). After 48 h, cells were treated with 100 ng/mL TNF, 50 µM zVAD-fmk and 0.1 µg/mL CHX before intracellular ATP levels were determined after 24 h of stimulation. Error bars show the respective SD from five parallel measurements. **(D)** Control Western blots of transfected (siRIPK3, siHTRA2 and siCASP8) but untreated cells were performed to verify down-regulation of the endogenous proteins. Detection of actin served as a loading control. Here, the diagram and Western blot analysis show one representative experiment which was performed for each siRNA transfection independently.

The role of meprin β during TNF- and TRAIL-induced necroptosis

Meprin β (MEP1B), as among 4 other metalloproteases (DPYSL4, PRPF8, MMP3, YME1L1), was identified during the siRNA screen as a candidate protease possibly involved in TNF-induced necroptosis (Table 4). In initial experiments to further investigate the role of MEP1B in necroptosis, HT-29 cells were transiently transfected with plasmids encoding wild-type MEP1B or a proteolytically inactive MEP1B mutant (E90A). Cells were stimulated with TNF/zVAD/CHX or TRAIL/zVAD/CHX to induce necroptosis. Measuring loss of membrane integrity as well as ATP levels revealed that transient overexpression of MEP1B in HT-29 cells leads to increased cell death rates after treatment with TNF/zVAD/CHX when compared to non-transfected cells (Figure 25). This effect was only marginally seen in cells treated with TRAIL/zVAD/CHX, suggesting differences in the signal transduction pathways of TNF- and TRAIL-induced necroptosis. Treatment of cells with TNF/zVAD/CHX or TRAIL/zVAD/CHX in combination with Nec-1 was performed as a control and verified that transfected HT-29 cells indeed undergo necroptosis (Figure 25). Interestingly, cells expressing the inactive MEP1B mutant also showed increased cell death levels after stimulation with TNF as well as TRAIL/zVAD/CHX (Figure 25). In conclusion, the analysis of MEP1B function suggests that the catalytic activity of MEP1B has protective effects in TNF-induced necroptosis. Nevertheless, these preliminary data should be substantiated by loss of gene function studies and by studying the effects of MEP1B-specific inhibitors in future experiments.

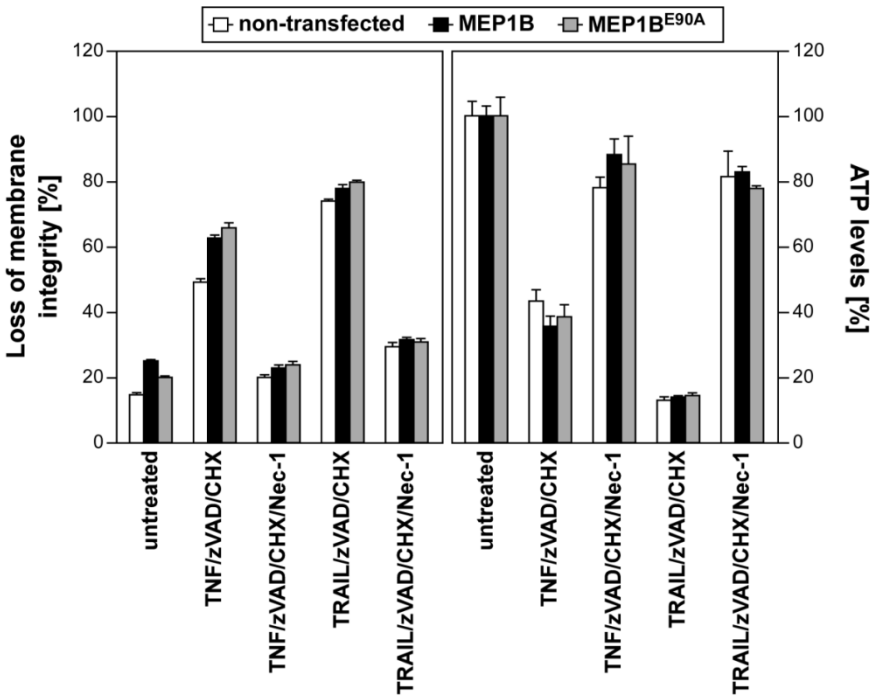

Figure 25: Role of MEP1B during necroptosis. HT-29 cells were transiently transfected with wild-type MEP1B or an inactive MEP1B mutant (MEP1B^{E90A}) for 72 h before cell death was induced by treatment with either 100 ng/mL TNF or TRAIL in combination with 20 µM zVAD-fmk and 5 µg/mL CHX. The addition of 50 µM Nec-1 to TNF/zVAD/CHX- or TRAIL/zVAD/CHX-treated cells served as a control for necroptosis. After 20 h, cell death was analyzed by measuring loss of membrane integrity (left) and decrease of intracellular ATP levels (right). One out of three experiments is shown. Error bars indicate the SD from three parallel measurements.

Conclusion: Five novel proteases enhance necroptosis upon down-regulation

In a complementary siRNA screen of all proteases encoded by the human genome, caspase-8 (CASP8), CYLD and c-FLIP (CFLAR), proteins that represent key regulators of necroptosis, were identified, confirming the functionality of the screen. Subsequently, a second robotic screen was performed using the siRNAs of the 40 best candidates and again identifying CASP8, CYLD and CFLAR as the strongest effectors. The second screen narrowed down the list of candidates to 10 proteases with pronounced and six candidates with less pronounced effect. In a third, manually performed screen, it could be confirmed that the candidates (CASP8, CYLD, CFLAR, DESC, MMP3, GGT1, PRPF8 and DPYL4) affect necroptosis upon down-regulation in HT-29 as well as U-937 cells as two independent human systems for necroptosis. However, the precise role of these proteases in cell death, and in particular, in necroptosis is still unknown. The down-regulation of MEP1B did not affect necroptosis in HT-29 and U-937 cells, but studies of HT-29 cells transiently transfected with plasmids encoding MEP1B showed increased cell death rates in TNF-induced necroptosis, suggesting a possible role of MEP1B during TNF-induced necroptosis.

5.2.3 Identification of new proteins that are cleaved or differentially expressed during necroptosis as potential candidate regulators of necroptosis

After binding to its ligand TNF, the internalization of the activated TNF-R1 is an essential prerequisite for recruiting the DISC to the TNF-R1 and the initiation of pro-apoptotic signaling. Subsequently, TNF-R1-containing vesicles fuse with endosomal compartments containing further signaling molecules, leading to the formation of multivesicular bodies which are capable of mediating apoptosis (Schneider-Brachert *et al*. 2004). To analyze such TNF-R1-containing vesicles, an immuno-magnetic separation procedure has been utilized in previous studies (Tchikov *et al.* 2014). In order to enrich and identify proteins recruited to or cleaved in the vicinity of the TNF-R1, this immuno-magnetic separation procedure was adapted for the isolation of TNF-R1-containing vesicles under necroptotic conditions.

The ligands TNF60-Fc and TNFwt-Fc can induce necroptosis in U-937 and L929Ts cells

Before TNF-R1-containing vesicles can be enriched with the above described immuno-magnetic separation, the TNF-R1 must be prelabeled with Fc-tagged TNF-ligands coupled to Protein G magnetic nanoparticles (see 4.2.15.4). In order to test the biological activity of the purified Fc-tagged TNF-ligands (Figure 26A; see 4.2.15.3), loss of membrane integrity was measured using murine L929Ts and human U-937 cells treated either with commercially available TNF or TNFwt-Fc or TNF60-Fc in combination with zVAD-fmk to induce necroptosis (Figure 26B). Although human TNF and murine TNF are very homologous, human TNF binds only to murine TNF-R1 (Ameloot *et al.* 2001). Therefore, the human TNFwt-Fc ligand was used to trigger necroptosis via TNF-R1 in murine L929Ts cells. Because TNFwt-Fc would bind to both human TNF-R1 and TNF-R2 (Tartaglia *et al.*

1993) in human U-937 cells, these cells were analyzed using the ligand TNF60-Fc which binds exclusively to the human TNF-R1. As shown in Figure 26B, both cell lines displayed the same levels of cell death after treatment with either TNF or the specific TNF-Fc ligands. Therefore, the Fc-tagged ligands were used for further studies analyzing TNF-R1 internalization and magnetically enriched TNF-R1-containing vesicles.

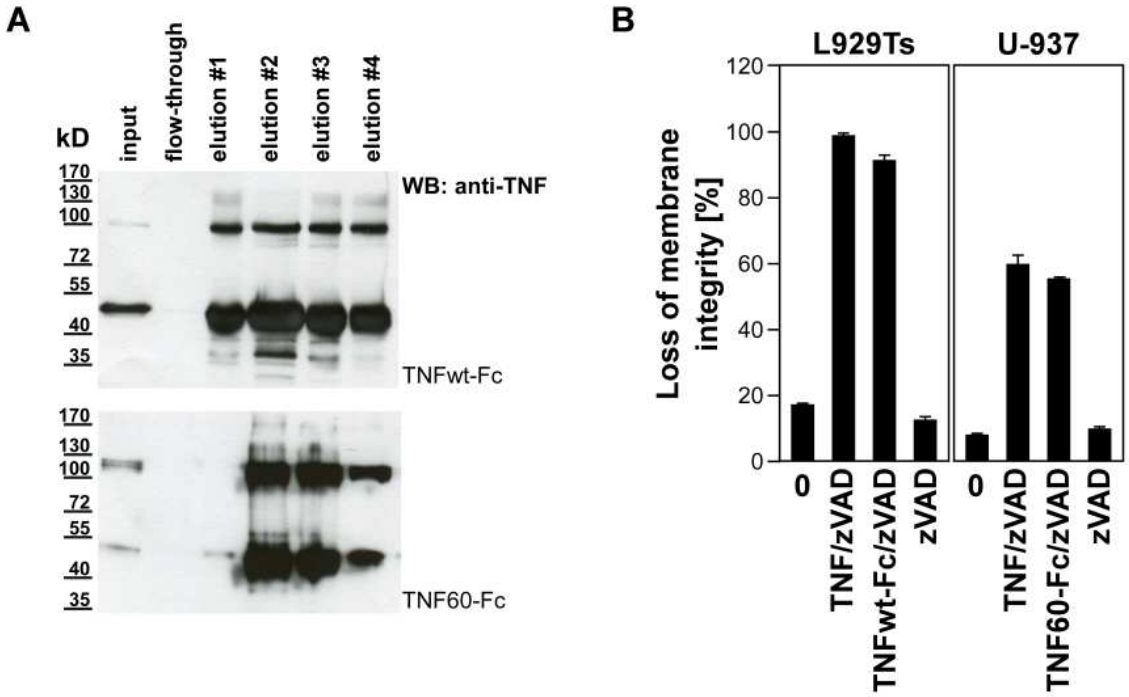

Figure 26: Biological activity of TNF ligands. (A) HEK293T cells were transfected with plasmids encoding for TNFwt-Fc or TNF60-Fc and the TNF-ligands were purified as described in 4.2.15.3. The supernatant of transfected HEK293T cells (input), the different elution fractions (#1-#4) with the respective TNF ligand and the flow-through of the Protein G column were separated on a 10 % SDS-gel. The Western blot shows either TNFwt-Fc **(upper panel)** or TNF60-Fc **(lower panel)** protein levels detected with anti-TNF antibodies. **(B)** Loss of membrane integrity was measured after 24 h of stimulation with either commercially available TNF (100 ng/mL) or 100 ng/mL TNFwt-Fc or TNF60-Fc in combination with 20 µM (L929Ts) or 50 µM (U-937) zVAD-fmk using flow cytometry. Representative data show three parallel measurements and the experiment was repeated three times. Error bars indicate the SD from three parallel measurements.

TNF-R1 is internalized upon induction of necroptosis

Next, it was analyzed whether TNF-R1 internalization upon induction of necroptosis occurred in the same manner as after induction of apoptosis. For this purpose, U-937 cells were incubated with TNF60-Fc with (to induce necroptosis) or without zVAD-fmk (to induce apoptosis) either on ice to block endocytosis or at 37 °C for various time-points to permit internalization. After the time-points indicated in Figure 27A, cell surface-associated ligands were labeled and the fluorescence intensity was measured by flow cytometry. Increasing the temperature to 37 °C resulted in a decrease of fluorescence intensity first detected after 5 min and proceeding for up to 60 min (Figure 27A,B; apoptosis). Cells pre-incubated with zVAD-fmk also showed a loss of fluorescence intensity (Figure 27A,B; necroptosis). To confirm that the loss of the fluorescence signal was due to the internalization of the TNF-R1, cells were incubated with TNF60-Fc/zVAD and an inhibitor of dynamin-dependent

endocytosis (dynasore). As shown in Figure 27C, the decrease in fluorescence intensity and therefore the internalization of TNF60-Fc was almost completely blocked by dynasore, confirming that TNF-R1 is internalized during necroptosis.

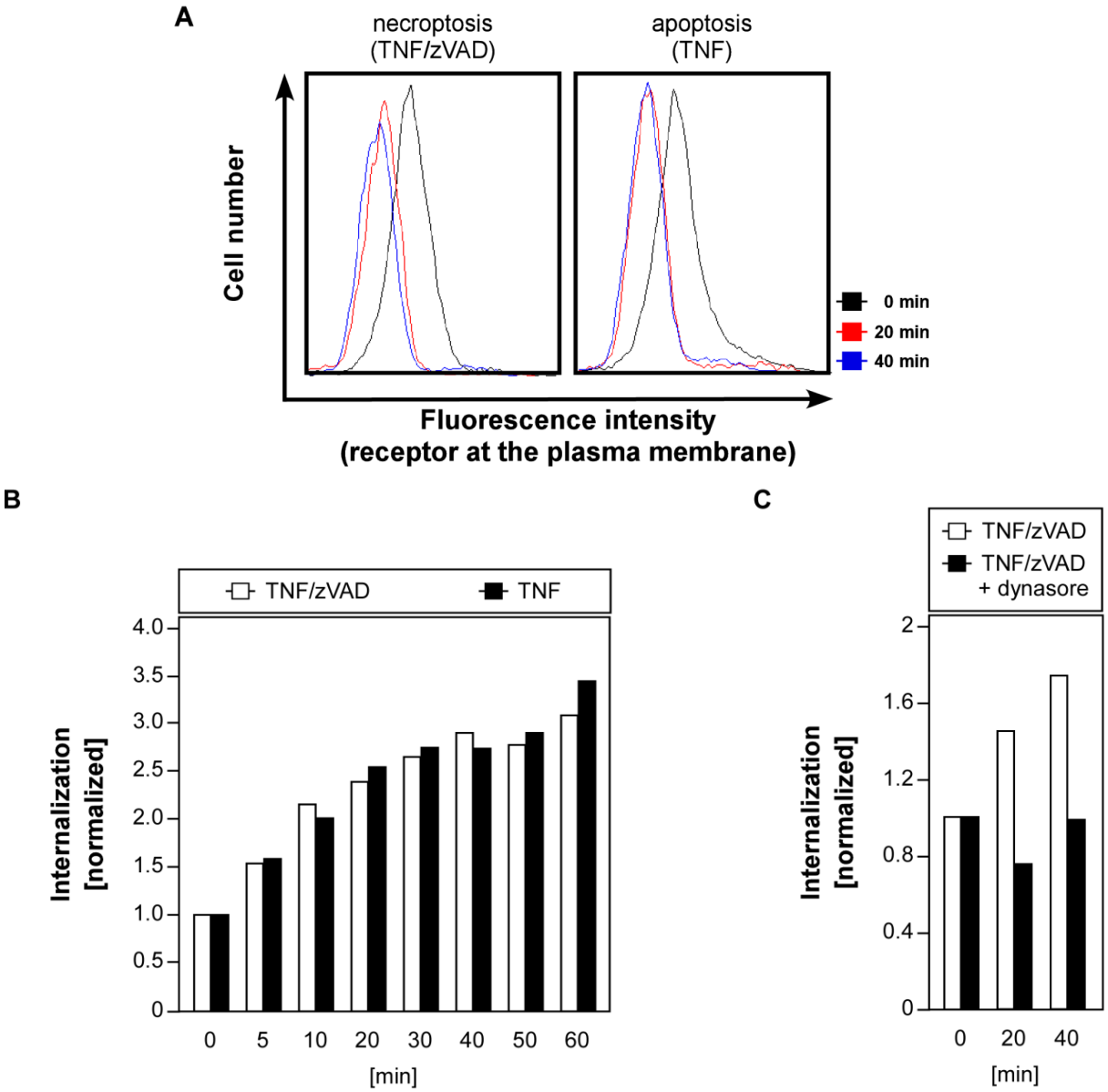

Figure 27: Determination of TNF-R1 internalization by flow cytometry. (**A**) U-937 cells were treated with 100 ng/mL TNF60-Fc without (induction of apoptosis) or with pre-treatment with 50 µM zVAD-fmk (to induce necroptosis). Cells were kept on ice (0 min; black) or internalization was induced by shifting the cells to 37 °C for 5, 10, 20 (red), 30 and 40 min (blue) of internalization. TNF-R1 remaining on the cell surface of U-937 cells was labeled using Protein G-Alexa Fluor® 488. The fluorescence intensity was measured by flow cytometry. The graphs representing cells measured after 5, 10, 30, 50 and 60 min are not shown for clarity of presentation. **(B)** The entire time kinetic was used for calculation of the internalization rate normalized to cells kept on ice (0 min). The graph compares the internalization rate of cells undergoing necroptosis (white bars) or apoptosis (black bars). **(C)** U-937 cells were pre-treated with 50 µM zVAD-fmk as above with or without 50 µM dynasore. Cells were subsequently treated with 100 ng/mL TNF60-Fc to induce necroptosis for 20 and 40 min respectively. In all experiments, 10,000 cells were analysed for each measurement. One representative experiment out of four is shown.

Subsequently, the internalization capacity of murine TNF-R1 after induction of necroptosis was analyzed in L929Ts cells by confocal microscopy. For this purpose, cells were labeled with

biotinylated TNF in combination with streptavidin Alexa Fluor® 488 and counterstained for the endosomal marker Ras-related protein 5 (Rab5). Of note, L929 cells die exclusively by regulated necrosis when treated with TNF (Vercammen *et al.* 1998a; Strelow *et al.* 2000; Thon *et al.* 2005), therefore, no addition of zVAD-fmk was required. Cells kept on ice (0 min) showed clear labeling of TNF-R1 on the cell surface, and no TNF-R1 appeared to be internalized. After 15 min incubation at 37 °C and induction of necroptosis, a small fraction of Rab5-positive endocytic vesicles also contained labeled TNF-R1. The number of Rab5 positive, TNF-R1-containing vesicles increased further at later time-points (Figure 28), confirming the internalization of TNF-R1 during TNF-induced necroptosis.

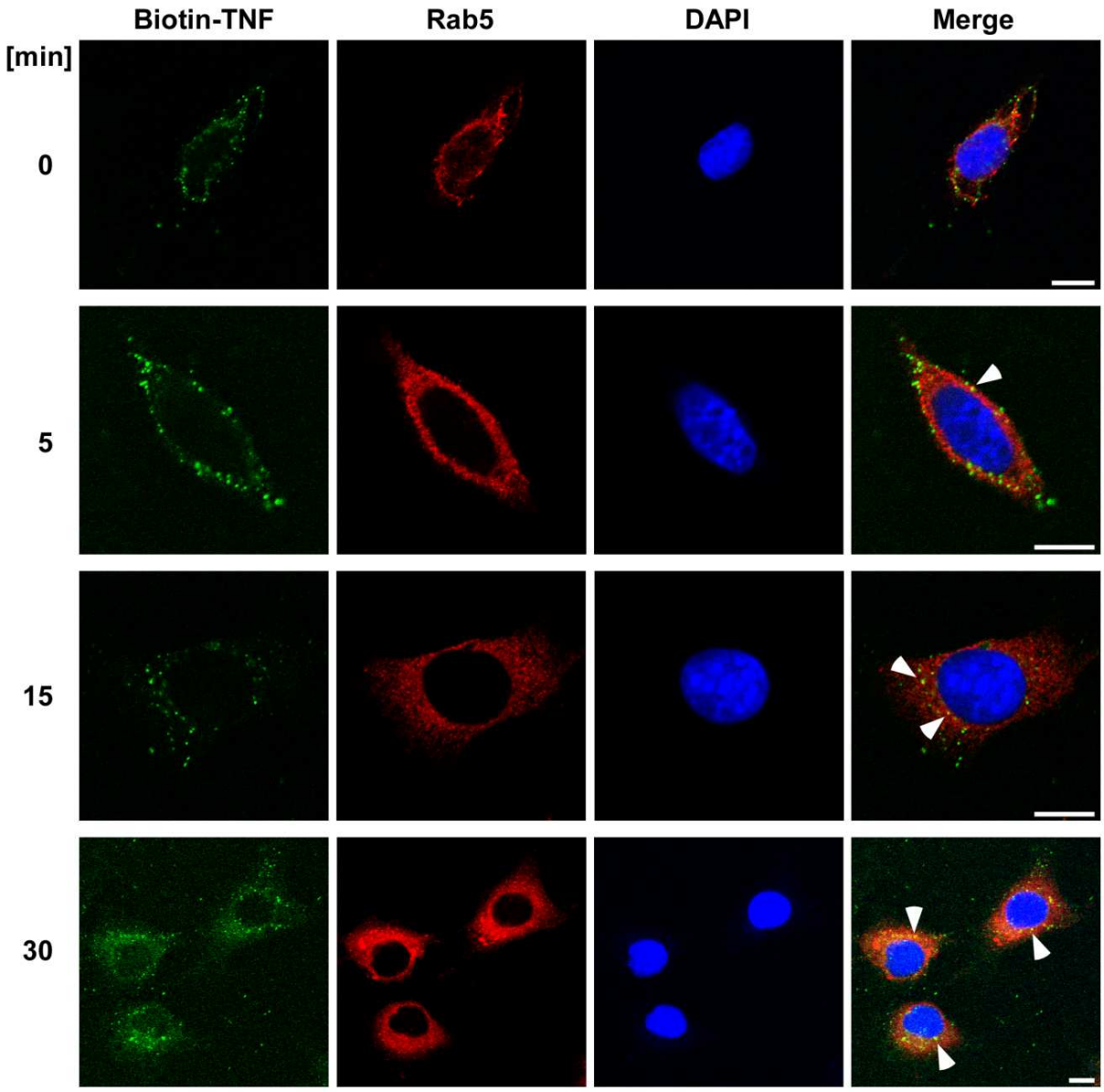

Figure 28: TNF-R1 is internalized upon induction of necroptosis. L929Ts cells were incubated with Biotin-TNF (100 ng/mL) in combination with streptavidin Alexa Fluor® 488 (green) at 37 °C for the indicated time-points. Subsequently, cells were stained with rabbit-**α**-Rab5 antibodies followed by Alexa Fluor® 555-donkey-**α**-rabbit antibodies to stain Rab5 (red) and the nuclei was stained with DAPI (blue) as described in section 4.2.16.3. A co-localization is indicated by yellow staining and representative events were marked with white arrows. Scale bar: 100 µm.

Furthermore, the interaction of internalized TNF-R1 and RIPK1 as a crucial mediator of necroptosis was analyzed by intracellular co-localization studies. In L929Ts cells, RIPK1 was localized in the cytoplasm. After internalization of the TNF-R1 labeled with Biotin-TNF/streptavidin Alexa Fluor® 488, intracellular co-localization with RIPK1 (10 min; Figure 29) was observed, suggesting that after internalization, the TNF-R1 gets in close contact to RIPK1 as a requirement for induction of necroptosis.

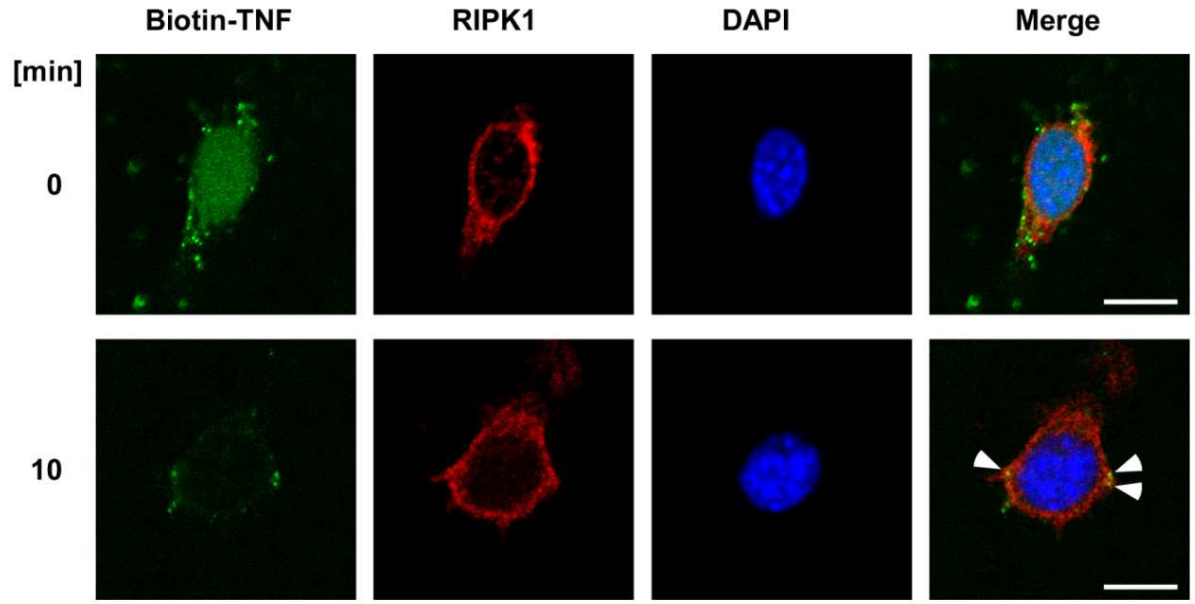

Figure 29: Stimulation with TNF leads to co-localization of internalized TNF-R1 with RIPK1. L929Ts cells were stimulated with 100 ng/mL biotinylated TNF (Biotin-TNF) in combination with streptavidin Alexa Fluor® 488 (green) for 10 min at 37 °C. Nuclei were stained with DAPI (blue) and RIPK1 was stained using mouse-**α**-RIPK1 antibodies and goat-**α**-mouse Alexa Fluor®555 (red) as described in section 4.2.16.3. White arrows indicate intracellular co-localization which is indicated by yellow staining (merge). Scale bars: 10 µm.

To investigate the localization of TNF-R1 after TNF-ligand induced necroptosis with the above described TNF-Fc ligands, L929Ts cells were labeled with TNFwt-Fc in combination with Protein G-Alexa Fluor® 488. The internalization was performed in medium with the fluid phase marker TRITC-Dextran to study endocytosed vesicles. Before internalization was started (0 min), cells showed clear labeling of TNF-R1 on the cell surface, and no TNF-R1 appeared to be internalized. After internalization was started (37 °C), simultaneous immunofluorescence detection of endocytic vesicles and TNF-R1 revealed a time-dependent appearance of TRITC-Dextran-labeled endocytic vesicles containing labeled TNF-R1 (Figure 30A). The observation of TRITC-Dextran vesicles containing labeled TNF-R1 confirmed that TNFwt-Fc treatment and thus induction of necroptosis leads to the internalization of murine TNF-R1 into endocytic vesicles.

In U-937 cells, the simultaneous detection of endocytic vesicles (TRITC-Dextran positive) and labeled TNF-R1 was not possible because the labeling of cells with TRITC-Dextran revealed no signal. Nevertheless, before internalization was started (0 min), cells showed clear labeling of TNF-R1 on the cell surface. After internalization was started (37 °C), the intensity of labeled TNF-R1 was increased

within the cell (Figure 30B). These clusters of TNF-R1 were present already after 10 min of internalization and at later time-points, indicating that TNF-R1 is also internalized into endocytic vesicles in U-937 cells.

The above results demonstrated the biological activity of the TNF-Fc ligands and that TNF-R1 is internalized upon induction of necroptosis into endocytic vesicles, providing the basis for subsequent isolation of the, necroptotic TNF-R1-containing vesicles with the described immuno-magnetic separation procedure, and thus for the identification of proteins recruited into or cleaved at the vicinity of the TNF-R1 during necroptosis.

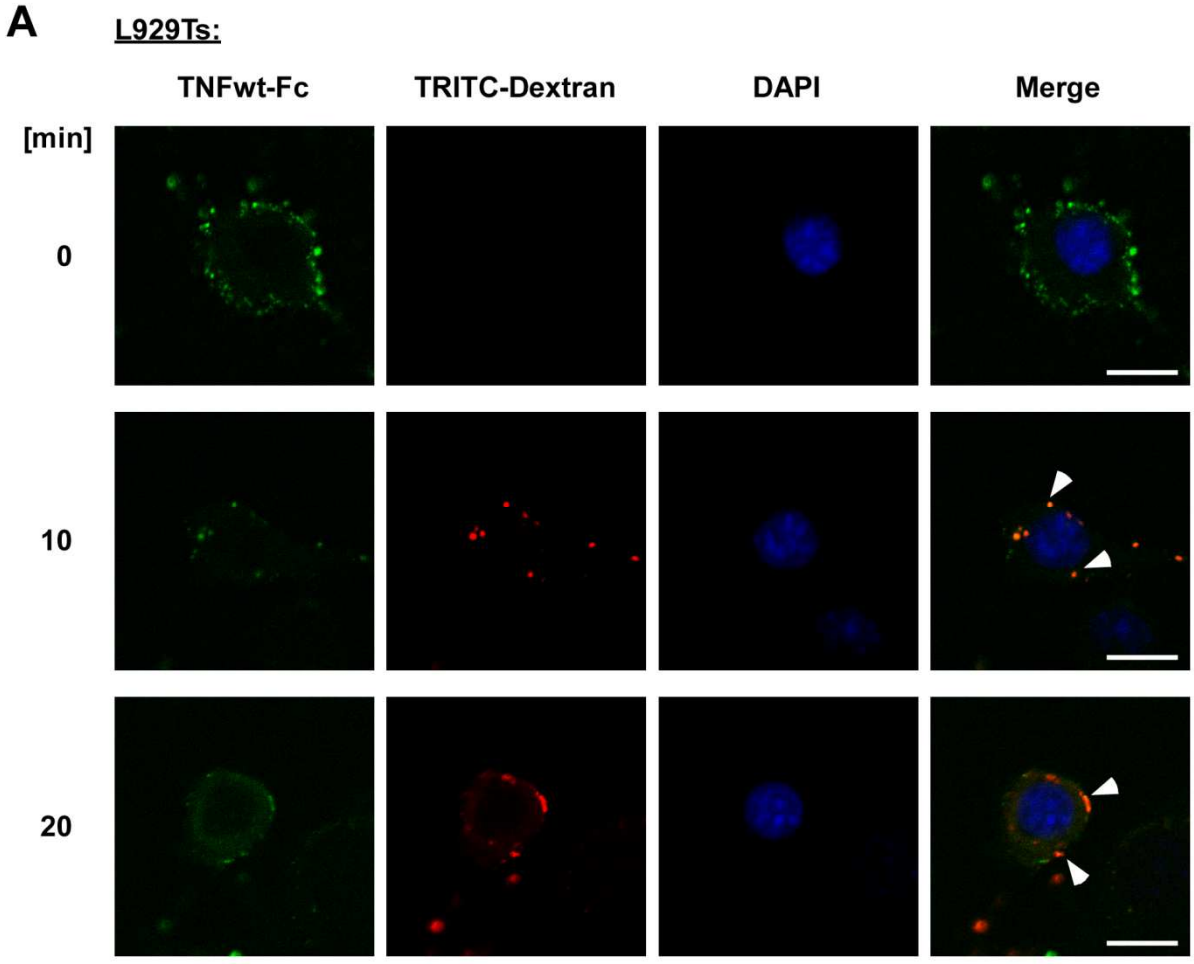

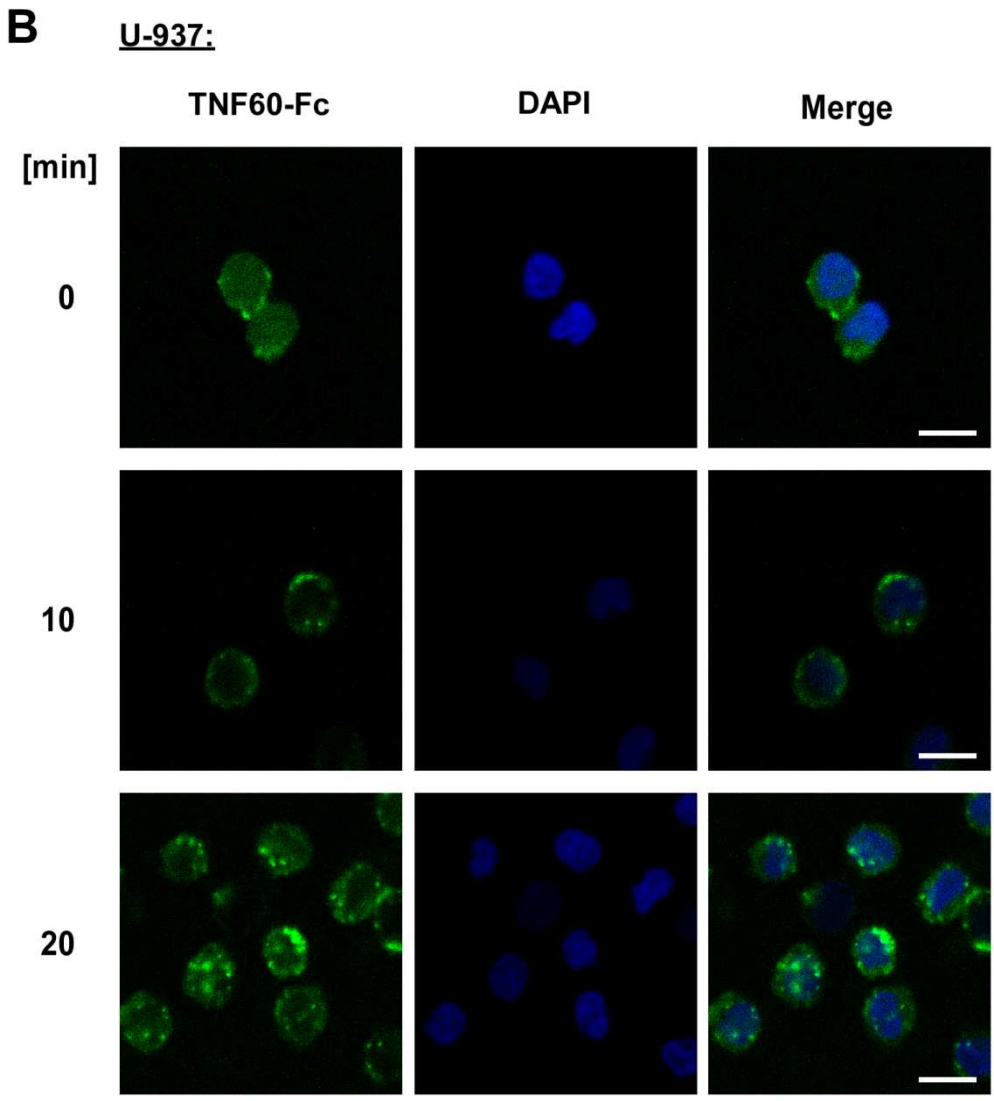

Figure 30: Immunofluorescence of TNF-R1-localization. (A) L929Ts cells were pre-incubated with 20 µM zVAD-fmk for 30 min and further 1 h with TNFwt-Fc/Protein G-Alexa Fluor® 488 (green) on ice. Cells were kept on ice (0 min) or internalization was induced by incubating cells at 37 °C in the presence of the fluid phase marker TRITC-Dextran (red) for the indicated time-points. White arrows indicate fusions of endocytosed vesicles with labeled TNF-R1 which is indicated by yellow staining (merge). **(B)** U-937 cells were pre-incubated with 50 µM zVAD-fmk for 30 min and followed by 1 h incubation with TNF60-Fc/Protein G-Alexa Fluor® 488 (green) on ice. Cells were kept on ice (0 min) or internalization was induced by incubating cells at 37 °C in the presence of the fluid phase marker TRITC-Dextran for the indicated time-points. The labeling of U-937 cells with TRITC-Dextran revealed no signal and is therefore not shown. Nuclei were stained with DAPI (blue). Scale bar: 10 µm.

Characterization of necroptotic TNF-R1-containing vesicles in L929Ts cells

As a prerequisite for the identification of proteins cleaved during TNF-mediated necroptosis by 2D-DIGE analysis, the magnetically isolated vesicles had first to be characterized at the protein level to confirm the successful enrichment of TNF-R1-containing vesicles. For this purpose, the TNF-R1 of L929Ts cells was labeled with TNFwt-Fc and magnetic Protein G-coupled micro-beads in the presence of zVAD-fmk on ice. TNF-R1 internalization was induced for 10 to 40 min and lysates were prepared as described in 4.2.15.4. Subsequently, the magnetic fractions containing potential internalized TNF-R1 vesicles were isolated, subjected to SDS-PAGE and analyzed by Western blot (Figure 31). As shown in Figure 31A, the commercially available antibody directed against human TNF-R1 detected the receptor in the fractions from murine cells only poorly. Since detection of TNF-R1 is essential for quantification of the magnetic fractions, densitometry analyses were performed to quantify the enrichment of TNF-R1-containing vesicles (Figure 31A, lower panel). Western blot analysis additionally revealed that the adaptor protein RIPK1 was accumulated in the receptor containing vesicles after 10 min of internalization, in line with the necroptotic character of the TNF-R1-containing vesicles. Moreover, vesicles from different time-points of TNF-R1 internalization contained the marker protein of early endosomes, Rab5, as well as the lysosome-associated membrane glycoprotein 1 (LAMP-1; Figure 31A), showing that the TNF-R1 was localized in multivesicular bodies. As an independent verification of these findings, Figure 31B shows a time kinetic of magnetic fractions prepared and measured by means of conventional Western blot which was performed by Vladimir Tchikov (Christian-Albrechts-University, Kiel, Germany). In this experiment, Western blot analysis of TNF-R1 demonstrated the successful enrichment of internalized magnetically labeled TNF-R1-containing vesicles, because isolated magnetic fractions contained increasing amounts of Rab5 and accumulated the lysosomal protein LAMP-1 with increasing time. As shown in Figure 31B, TNF stimulation accumulated both RIPK1 and RIPK3 to the TNF-R1-containing magnetic vesicles with rapid and transient kinetics, as expected after the induction of necroptosis. Furthermore, no cleavage of caspase-7 and -8 was detected (Figure 31B), consistent with the fact that caspases are not activated (and thus not cleaved) during necroptosis. Due to consistently low protein yield during large scale isolation and enrichment of TNF-R1 magnetic fractions, 2D-DIGE analyses of magnetic TNF-R1-containing vesicles from L929Ts cells were not conducted.

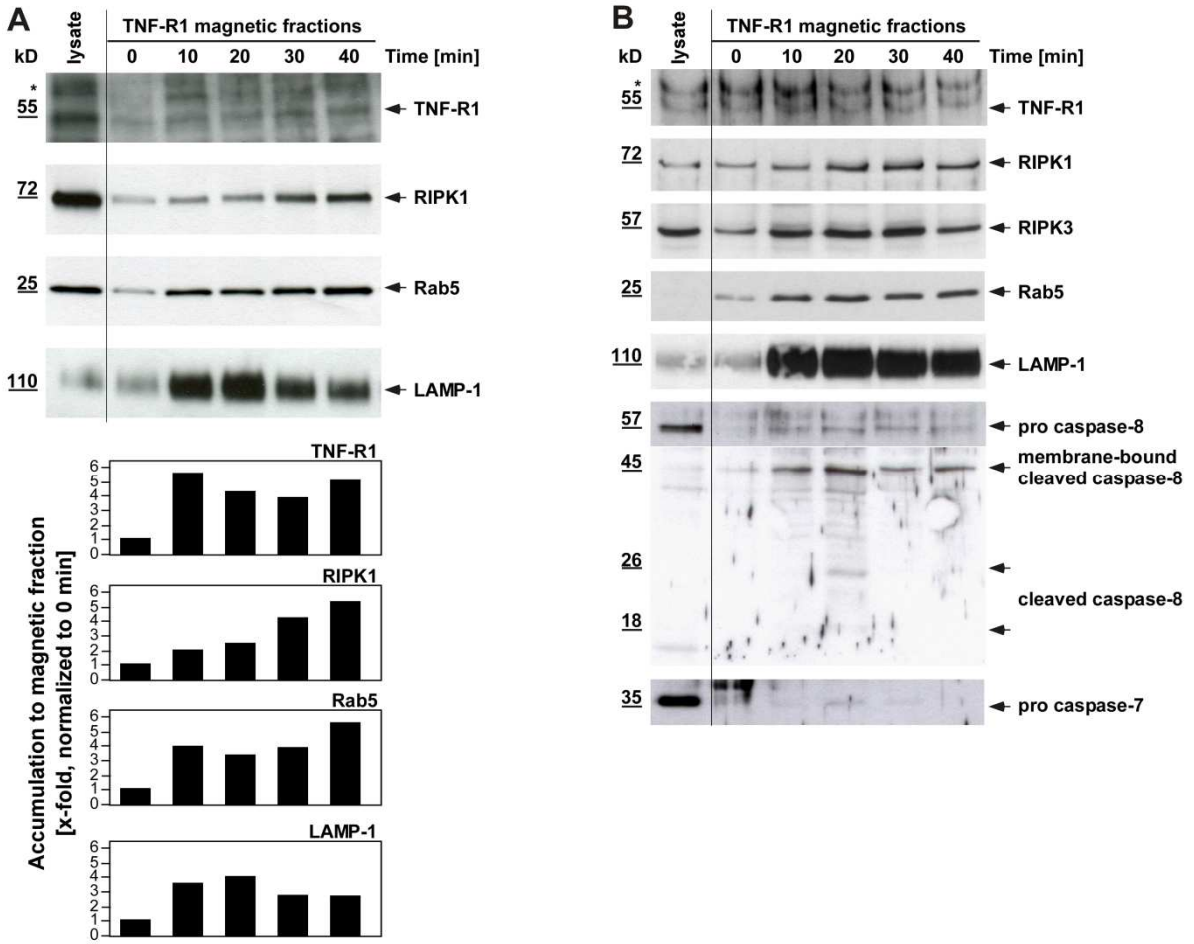

Figure 31: TNF-dependent accumulation of proteins to necroptotic TNF-R1 magnetic fractions. (A) Magnetic fractions harboring TNF-R1-containing vesicles were derived from L929Ts cells after stimulation with 100 ng/mL TNFwt-Fc for the indicated times. 3 µg of protein were immunoblotted for presence/accumulation of endogenous TNF-R1, RIPK1, as well as Rab5 and LAMP-1 as endosomal and lysosomal markers, respectively. Untreated protein cell extracts were used as control (lysate). A quantitative analysis of the x-fold accumulation of the above analyzed proteins is shown below. Values are normalized to 0 min. **(B)** In an independent experiment, the magnetic fractions were prepared and measured by means of conventional Western blot by Vladimir Tchikov (Christian-Albrechts-University, Kiel, Germany). Here, protein load was adjusted to achieve equal signal intensity of TNF-R1 and thus of equal amounts of TNF-R1-containing vesicles. The TNF-R1-containing vesicles were immunoblotted for accumulation of endogenous RIPK1, RIPK3, as well as Rab5 and LAMP-1 and presence of endogenous pro-caspase-7 and -8 and cleaved caspase-8. Asterisk: unspecific band.

Characterization of necroptotic TNF-R1-containing vesicles in U-937 cells

In addition to L929Ts cells, magnetic fractions from human U-937 cells were analyzed. To this end, TNF-R1-containing magnetic fractions were isolated by a two-step procedure including negative selection against mitochondria (described in Tchikov *et al.* 2014), to enhance the purity of the preparation. U-937 cells were pre-incubated with zVAD-fmk to inactivate caspases together with TNF60-Fc and Protein G-coupled micro beads for 1 h at 4 °C prior to internalization at 37 °C. Internalization was stopped immediately (0 min) or after 5 to 60 min. Preparation of mitochondria-free TNF-R1 magnetic fractions was performed with the help of Jürgen Fritsch (Christian-Albrechts-University, Kiel, Germany). Isolated magnetic TNF-R1 complexes were analyzed by Western blot for signature proteins of distinct intracellular compartments.

Consistent with the above results from L929Ts cells, the protein Rab5 as a marker for early endosomes showed low expression levels at 0 min but was accumulated to the magnetic TNF receptor fractions at 20 min and remained there up to 60 min (the latest time-point measured; Figure 32). The lysosome-associated membrane protein LAMP-2 was detectable already at 0 min and showed increased protein levels after 20 min, indicating that the TNF-R1-containing vesicle fuse early with lysosomal compartments. Likewise, RIPK3 accumulated to the TNF-R1-containing vesicles at 20 min in parallel to increased Rab5 and LAMP-2 protein levels (Figure 32). As a consequence of the negative selection against mitochondria, the mitochondrial marker protein cytochrome c oxidase subunit 4 (COXIV) was not present in the magnetic fractions (Figure 32).

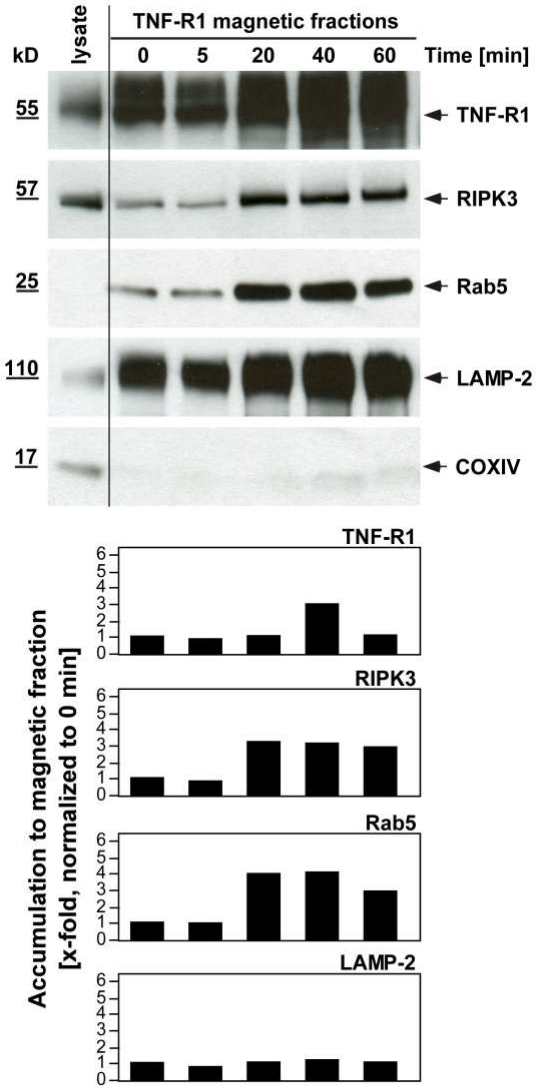

Figure 32: TNF-dependent accumulation of proteins to the necroptotic TNF-R1 magnetic fractions isolated from U-937 cells. Magnetic fractions harboring TNF-R1-containing vesicles were derived from U-937 cells after stimulation with 100 ng/mL TNF60-Fc and 50 µM zVAD-fmk for the indicated times. A two-step procedure to separate contaminating mitochondria was performed as described in 4.2.15.4 and with technical assistance of Jürgen Fritsch (Christian-Albrechts-University, Kiel, Germany). Subsequently, 3 µg of proteins were immunoblotted for presence/accumulation of endogenous TNF-R1, RIPK3, as well as Rab5, LAMP-2 and COXIV as endosomal, lysosomal and mitochondrial markers, respectively. Untreated protein cell extracts were used as control (lysate). A quantitative analysis of the x-fold accumulation of the above analyzed proteins is shown below. Values are normalized to protein levels at 0 min.

Proteome analysis of soluble proteins after induction of necroptosis

To identify proteins differentially expressed or cleaved during TNF-induced necroptosis, a 2D-DIGE approach was used. This form of gel electrophoresis overcomes limitations in traditional electrophoresis because changes in protein abundance between untreated and treated samples can be compared simultaneously. In an initial experiment, all soluble proteins were extracted from U-937 cells stimulated with TNF60-Fc and zVAD-fmk on ice (0 min) and 20 min at 37 °C. Protein extracts from cells stimulated for 20 min were labeled with the fluorescent dye Cy 3, and control extracts were labeled with the fluorescent dye Cy 5 and separated by 2D-PAGE. After gel electrophoresis, the gel was scanned and the detection of differentially labeled protein spots was performed using *in silico* analysis tools as described in 4.2.13. A total of 142 differentially expressed protein spots with at least 1.2-fold increased or decreased protein levels were identified. The appropriate threshold was set and calculated by the utilized software. After 20 min of TNF60-Fc/zVAD stimulation, 77 (3.8 % of total spots) protein spots showed a higher expression, whereas 65 protein spots (3.2 % of total spots) showed a lower expression than in control cellular extracts. All differentially expressed protein spots were analyzed by means of MALDI-TOF/TOF, and 30 proteins were identified with high confidence. The identified proteins were classified based on their x-fold increased or decreased protein levels (Appendix Table S2). In the repetition of the above experiment, 89 differentially expressed protein spots were detected. For 29 protein spots (1.5 % of total spots) an increased expression after 20 min TNF/zVAD stimulation was detected whereas 60 proteins spots (3 % of total spots) showed decreased levels compared to untreated samples.

Furthermore, comparing these two independent 2D-DIGE experiments, one protein, namely cofilin-1 (CFL-1; P23528) was consistently found to be increased in cellular extracts isolated from cells treated for 20 min with TNF60-Fc/zVAD. Protein spots which were consistently decreased were tubulin alpha-1B chain (TUBA1B; P68363) and pyruvate kinase isozymes M1/M2 (PKM; P14618). Several proteins were found to have inconsistently increased or decreased protein levels in the two experiments. These include stathmin (STMN1; P16949), heterogeneous nuclear ribonucleoprotein K (HNRNPK; P61978), cAMP-dependent protein kinase type II-alpha regulatory subunit (PKR2; P13861), heterogeneous nuclear ribonucleoproteins A2/B1 (HNRNPA2B1; P22626) and A1 (HNRNPA1; P09651), Rho GDP-dissociation inhibitor 2 (GDIA2; P52566) and heat shock protein beta-1 (HSPB1; P04792). The proteins HSPB1, HNRPK and PKM showed alterations in their isoelectric points, possibly a result of post-translational modification or the presence of different isozyme species.

As the most promising candidate, although having inconsistently increased or decreased protein levels in the two experiments, the protein stathmin was identified in one experiment in two distinct protein spots of different molecular weight. One of the spots had a molecular weight corresponding to the predicted molecular weight of the full-length protein whereas the other spot had a smaller molecular weight (Figure 33; Table S2), pointing to a possible proteolytic cleavage during necroptosis.

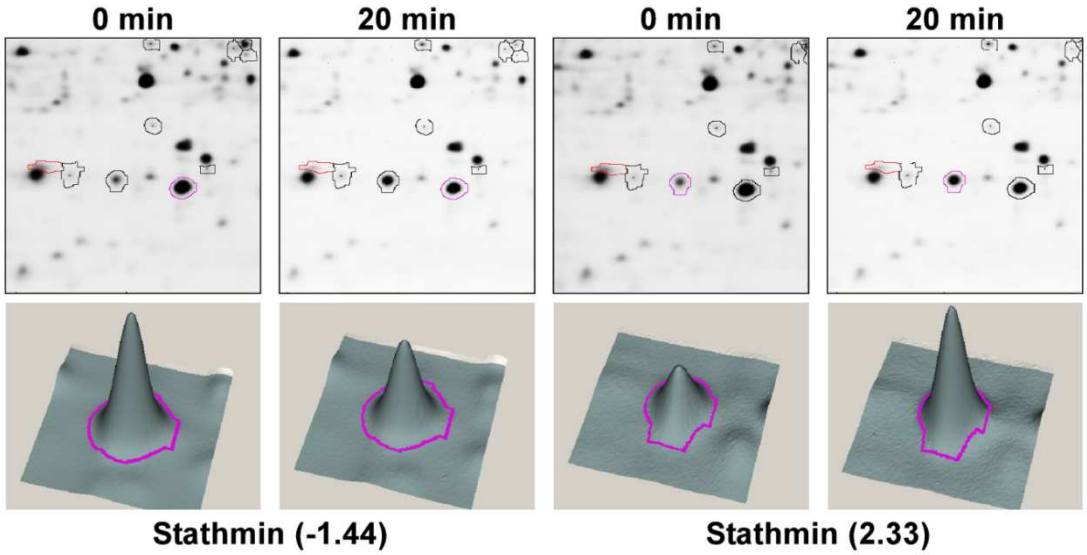

Figure 33: Stathmin was identified by 2D-DIGE analysis and is potentially cleaved during TNF-induced necroptosis. Example of the protein stathmin identified in two spots with different mass potentially indicating proteolytic cleavage events. 3D views of stathmin are shown (individual spots marked by a violet boundary; average ratio of expression in brackets). The 2D-DIGE experiment was performed with technical assistance of Melanie Nebendahl and Benjamin Schönbeck (Christian-Albrechts-University, Kiel, Germany). The mass spectrometry analysis of isolated proteins was performed by Tomas Koudelka (Christian-Albrechts-University, Kiel, Germany).

Proteome analysis of isolated TNF-R1-containing vesicles after induction of necroptosis

To identify additional candidate proteins that are cleaved in U-937 cells after induction of necroptosis with TNF60-Fc/zVAD, a second 2D-DIGE approach was carried out, this time with enriched magnetic TNF-R1-containing vesicles to enrich and identify proteins accumulated into or cleaved merely at the vicinity of the TNF-R1. For this purpose, in a first experiment, magnetically enriched TNF-R1-containing vesicles of U-937 cells stimulated with TNF60-Fc/zVAD for 0 and 20 min were isolated without depletion of mitochondria and compared by 2D-DIGE as described above for soluble proteins. An initial Western blot of total cell lysates, magnetic TNF-R1 fractions and the remaining non-magnetic flow through showed increased protein levels of the marker proteins Rab5 and LAMP-1 in the magnetic fraction, demonstrating the successful enrichment of TNF-R1 endocytic vesicles (Figure 34). Furthermore, no caspase-7 was detected in TNF-R1 magnetic fractions, but caspase-7 was detected in the non-magnetic flow through, consistent with the fact that caspases are not activated and thus not recruited to the TNF-R1 during necroptosis. The lipase A-SMase was shown to be involved in necroptosis (Thon *et al.* 2005) and therefore, the presence of cleaved and thus activated A-SMase was also investigated. However, cleaved A-SMase was not found in the TNF-R1 magnetic fractions

(Figure 34) but in the non-magnetic flow through, suggesting that A-SMase is not a part of the TNF-R1 signaling complex in necroptosis.

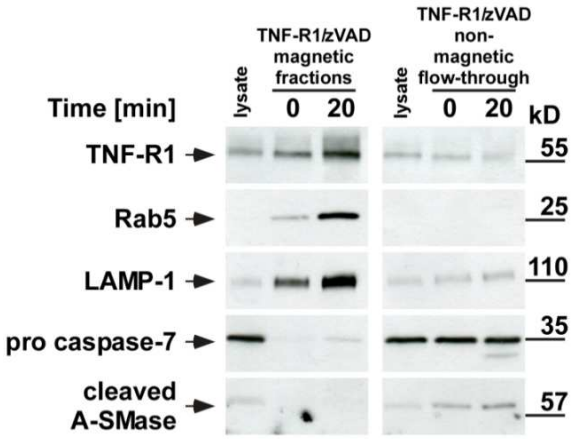

Figure 34: Characterization of magnetically isolated TNF-R1-containing vesicles prior to 2D-DIGE analysis. Magnetic fractions harboring TNF-R1-containing vesicles were derived from U-937 cells after stimulation with 100 ng/mL TNF60-Fc and 50 µM zVAD-fmk on ice (0 min) or for 20 min at 37 °C. Subsequently, 3 µg of protein of each magnetic fraction were immunoblotted for presence/accumulation of endogenous TNF-R1, Rab5, LAMP-1, pro caspase-7 and cleaved A-SMase. Rab5 and LAMP-1 were detected as endosomal and lysosomal marker, respectively. Untreated protein cell extracts were used as control (lysate). The non-magnetic flow-through was also analyzed.

In the subsequent 2D-DIGE analysis, 252 differentially expressed protein spots with at least 1.2-fold increased or decreased protein levels were identified. Protein spots which showed decreased/increased intensities of either Cy 3 or Cy 5 (Figure 35) were analyzed by MALDI-TOF/TOF. The mass spectrometric analysis identified 21 proteins with increased and 25 with decreased protein levels in the fraction of U-937 cells treated with TNF60-Fc/zVAD for 20 min (Table S3). The protein moesin (MSN; P26038) was identified as differentially expressed in magnetic TNF-R1 fractions of both experiments and one of the spots analyzed had a molecular weight smaller than the theoretical molecular weight of the full length protein (Figure 35), suggesting that moesin is cleaved during induction of necroptosis.

A search of the Swissprot database revealed that 27 % of the identified proteins were of mitochondrial origin, indicating that the membranes contained in the magnetic fractions might form contact sites with mitochondria and thereby interact with each other. The resulting heterogeneous membrane fractions might interfere with the identification of non-mitochondrial regulated candidate proteins of lower protein abundance. Therefore, prior to a new 2D-DIGE experiment, the magnetic TNF-R1 fractions were subjected to density-gradient centrifugation to avoid mitochondria contaminations (with technical assistance of Jürgen Fritsch, Christian-Albrechts-University, Kiel, Germany). A Western blot analysis of the TNF-R1/zVAD magnetic fractions was performed to validate the purity of the preparations and showed no mitochondrial protein COXIV expression (Figure 36A). The mitochondria free preparations were also subjected to 2D-DIGE analysis as described above. The 2D-DIGE analysis resulted in 112 spots with differentially expressed proteins. The spots with at least 1.5-fold increased or decreased protein levels were identified (Figure 36B). The protein spots were again analyzed by MALDI-TOF/TOF. The mass spectrometric analysis identified 6 proteins with increased

and 4 proteins with decreased levels in the fraction containing TNF-R1 vesicles which were isolated from cells stimulated with TNF60-Fc/zVAD for 20 min (Table S3).

Comparing these two different 2D-DIGE experiments (Figure 35 and 36B; Table S3), two dehydrogenases (inosine-5'-monophosphate dehydrogenase 2 (IMPDH2; P12268) & D-3-phosphoglycerate dehydrogenase (PHGDH; O43175)) were consistently found to be increased in TNF-R1 fractions isolated from cells treated 20 min with TNF60-Fc/zVAD. The peroxisome enzyme catalase (CAT; P04040) showed lower expression in both 2D-DIGE experiments (Table S3). Protein-disulfide-isomerase A6 (PDIA6; Q15084) and alpha-enolase (ENO1; P06733) showed differential expression patterns in the two independent 2D-DIGE experiments, possibly due to inter-gel variations. The protein spots of ENO1 showed alterations in their isoelectric points, possibly a result of post-translational modification or the presence of different isozyme species. The above identified proteins are involved in either regulating the energy metabolism of a cell (IMPDH2, PHGDH, PDIA6, CAT) or they are components of the cytoskeleton (ENO1, MSN), suggesting that during necroptosis, a change in the energy metabolism as well as a reorganization of the cytoskeleton occurs.

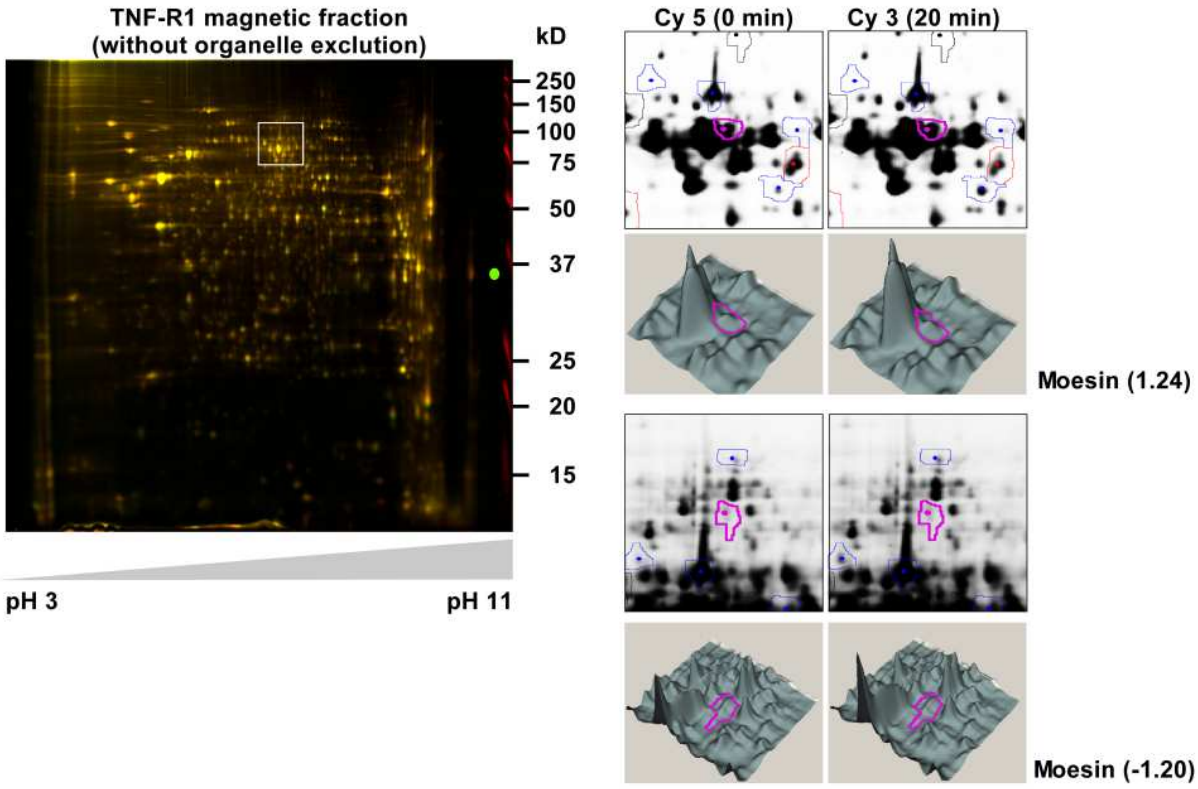

Figure 35: 2D gel and examples of spots identified after TNF60-Fc/zVAD stimulation in isolated TNF-R1 magnetic fractions. Left panel: 2D gel analysis of magnetic fractions harboring TNF-R1-containing vesicles were derived from U-937 cells after stimulation with 100 ng/mL TNF60-Fc and 50 µM zVAD-fmk on ice (0 min, labeled with Cy 5, red) or for 20 min (labeled with Cy 3, green) at 37 °C. The threshold was set to 1.2 (change in protein expression). Similar protein spots (yellow in the overlay): 1189 (82.5 %), increased protein spots (green): 149 (10.3 %) and decreased protein spots (red): 103 (7 %). Differentially expressed proteins were isolated and analyzed by mass spectrometry. The white square indicates the position of the enlarged pictures on the right. **Right panel:** Example of the protein moesin identified in two spots with different mass potentially indicating proteolytic cleavage events. 3D views of Moesin are shown (individual spots marked by a violet boundary; average ratio of expression in brackets). The 2D-DIGE experiment was performed with technical assistance of Melanie Nebendahl and Benjamin Schönbeck (Christian-Albrechts-University, Kiel, Germany). The mass spectrometry analysis of isolated proteins was performed by Tomas Koudelka (Christian-Albrechts-University, Kiel, Germany).

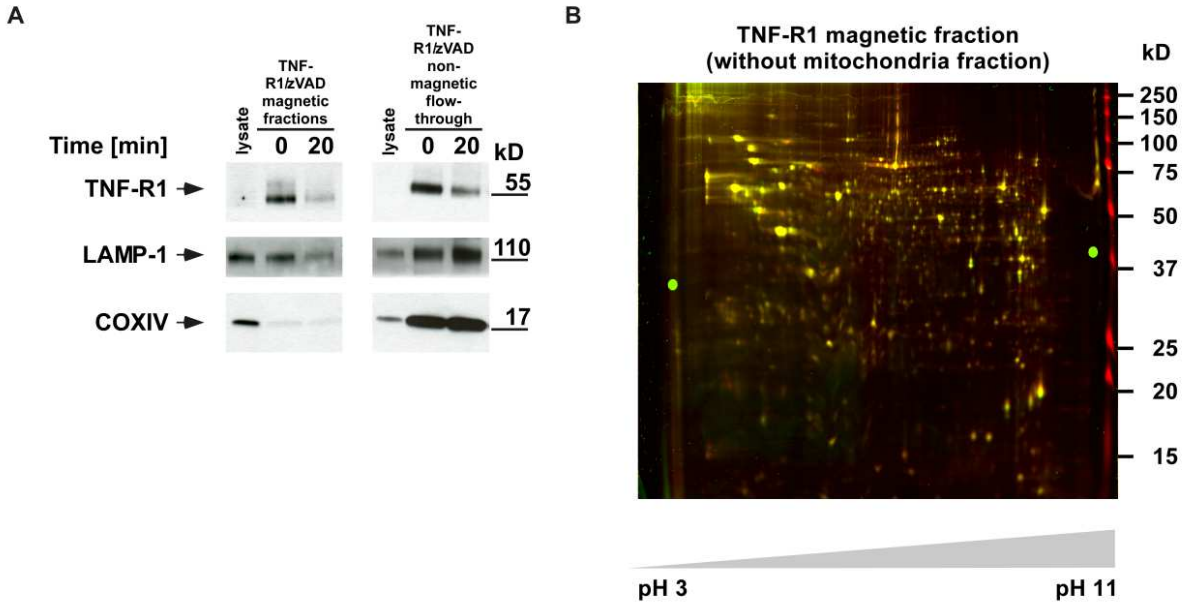

Figure 36: Western blot of mitochondria-free necroptotic TNF-R1 magnetic and non-magnetic fractions and 2D-DIGE analysis of the magnetic fractions. (A) Magnetic fractions harboring TNF-R1-containing vesicles were derived from U-937 cells after stimulation with 100 ng/mL TNF60-Fc and 50 µM zVAD-fmk on ice (0 min) or for 20 min at 37 °C. A two-step procedure to remove contaminating mitochondria was performed as described in 4.2.15.4 and with technical assistance of Jürgen Fritsch (Christian-Albrechts-University, Kiel, Germany). Subsequently, 3 µg of proteins of each magnetic fraction were immunoblotted for presence/accumulation of endogenous TNF-R1, LAMP-1, and COXIV. LAMP-1 and COXIV were detected as lysosomal or mitochondrial marker, respectively. Untreated protein cell extracts were used as control (lysate). The non-magnetic flow-through was analyzed in parallel. **(B)** 2D gel analysis of magnetic fractions harboring TNF-R1-containing vesicles were derived from U-937 cells after stimulation with 100 ng/mL TNF60-Fc and 50 µM zVAD-fmk on ice (0 min, labeled with Cy 5, red) or for 20 min (labeled with Cy 3, green) at 37 °C. A two-step procedure to remove contaminating mitochondria was performed as described in 4.2.15.4 and with technical assistance of Jürgen Fritsch (Christian-Albrechts University, Kiel, Germany). The threshold was set to 1.5 (change in protein expression). Similar protein spots (yellow): 1116 (90.9 %), increased protein spots (green): 57 (4.6 %) and decreased protein spots (red): 55 (4.5 %). Differentially expressed proteins were isolated and analyzed for their origin by mass spectrometry. The 2D-DIGE experiment was performed with technical assistance of Melanie Nebendahl and Benjamin Schönbeck (Christian-Albrechts-University, Kiel, Germany). The mass spectrometry analysis of isolated proteins was performed by Tomas Koudelka (Christian-Albrechts-University, Kiel, Germany).

All proteins identified in this study are listed in the appendix (Table S2 and S3).

Conclusion: Proteins are differentially expressed and cleaved during the execution of necroptosis

Taken together, the 2D-DIGE analysis of soluble proteins and magnetically enriched TNF-R1-containing vesicles identified new proteins with a possible participation in the proteolytic regulation of necroptosis. The analysis resulted in differentially expressed proteins (TUBA1B, PKM, CFL-1, IMPDH2, PHGDH, CAT) whose up- or down-regulation results in the regulation or breakdown of the energy metabolism during necrotic cell death. Furthermore, components of the cytoskeleton (MSN, STMN1) were identified as possible substrate proteins for proteolytic cleavage, suggesting a proteolytically induced reorganization of the cytoskeleton during necroptosis.

5.2.4 The potentially pro-necroptotic protein PGAM5 is constitutively degraded in healthy cells

Necroptosis critically relies on the signaling molecule mixed lineage kinase domain-like (MLKL; Sun *et al.* 2012, Wu *et al.* 2013). It was proposed that MLKL promotes regulated necrosis upon phosphorylation by RIPK3 by PGAM5 and Drp-1, leading to mitochondrial fragmentation (Wang *et al.* 2012). To clarify whether the proteins MLKL, PGAM5 and Drp-1 are also involved in TNF-induced necroptosis, the murine cell line L929Ts and the human cell line HT-29 were analyzed after down-regulation of the above mentioned proteins by RNAi. Down-regulation of PGAM5 and Drp-1 had no effect on TNF-induced necroptosis although protein expression was clearly decreased in Western blots (Figure 37). In contrast, the down-regulation of MLKL reduced TNF-induced necrotic cell death, although the down-regulation could not be confirmed by Western blot due to specificity problems of the antibody used for this experiment. In summary, the results shown in Figure 37 identified MLKL as a mediator of TNF-induced necroptosis. This is in line with recent studies (Galluzzi *et al.* 2014b). Based upon the obtained results, an essential role of Drp-1 and PGAM5 in necroptosis could not yet be confirmed. As one possible explanation, the reduction of PGAM5 and Drp-1 protein levels may have been insufficient to affect TNF-induced necroptosis.

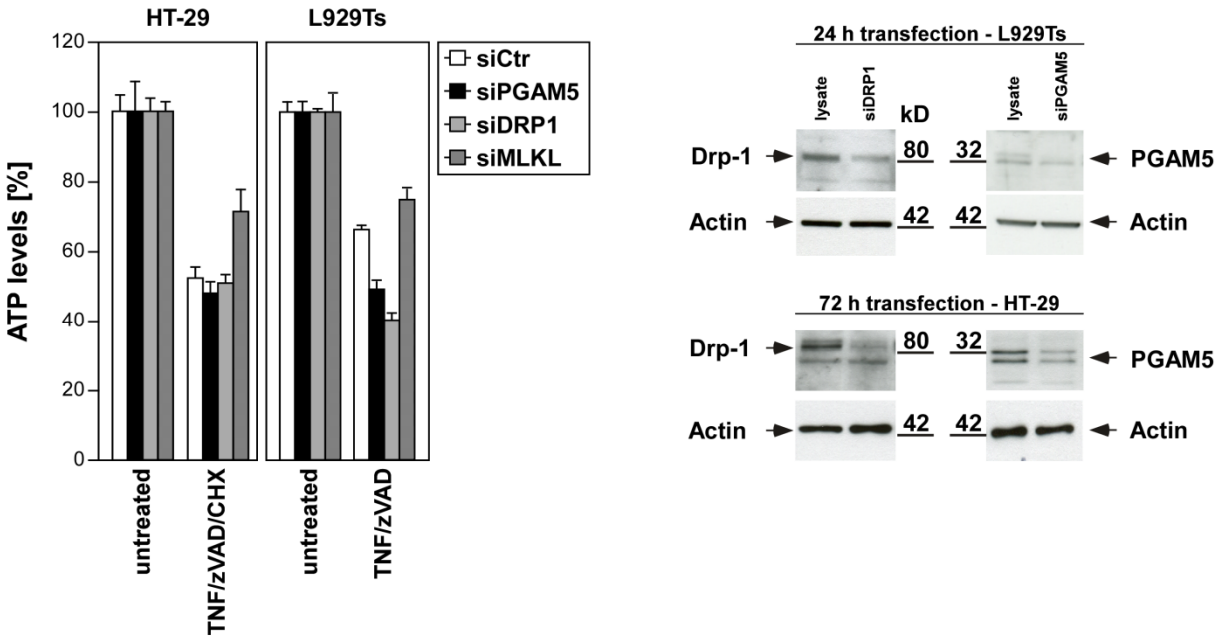

Figure 37: MLKL is a mediator of TNF-induced necroptosis. Left panel: HT-29 and L929Ts cells were transfected with siRNAs specific for human or murine PGAM5, Drp-1 and MLKL, respectively. As a negative control, cells were transfected with non-targeting siRNA. After 24 h (L929Ts) or 72 h (HT-29) of transfection, cells were left untreated or were incubated with 100 ng/mL TNF in combination with 20 µM (L929Ts) or 50 µM (HT-29) zVAD-fmk and 5 µg/mL (HT-29) CHX. After 5 h (L929Ts) or 20 h (HT-29), necroptosis was analyzed by measuring the decrease of intracellular ATP levels as a marker for cell death. ATP levels are shown relative to control-transfected cells. Error bars indicate the SD from five parallel determinations. **Right panel:** Control Western blots of transfected but untreated cells were performed to verify down-regulation of the endogenous protein levels. Detection of actin served as a loading control.

Wang and coworkers (2012) suggested that upon phosphorylation of MLKL by RIPK3, the long splice variant PGAM5L binds to the necrosome followed by binding of the short form of PGAM5 (PGAM5S). Furthermore, they proposed that PGAM5L might be proteolyzed before binding to PGAM5S which then leads to a possible dephosphorylation and activation of Drp-1 and subsequent mitochondrial fragmentation (Wang *et al.* 2012). To further study a possible role of PGAM5 in TNF-induced necroptosis in cells with strong expression of PGAM5, L929Ts cells were stably transfected with a PGAM5-FLAG construct. After induction of cell death by TNF/zVAD, all stably transfected clones showed similar cell death rates, when compared to wild-type L929Ts cells (Figure 38). The treatment with TNF/zVAD/Nec-1 blocked cell death in all clones, confirming the induction of necroptosis. In Western blots, the strongest PGAM5-FLAG expression was detected in clones B11 and C47. Therefore, clone C47 (further named L929Ts PGAM5-FLAG cells) was used for all further experiments which aimed to characterize the role of PGAM5 in necroptosis.

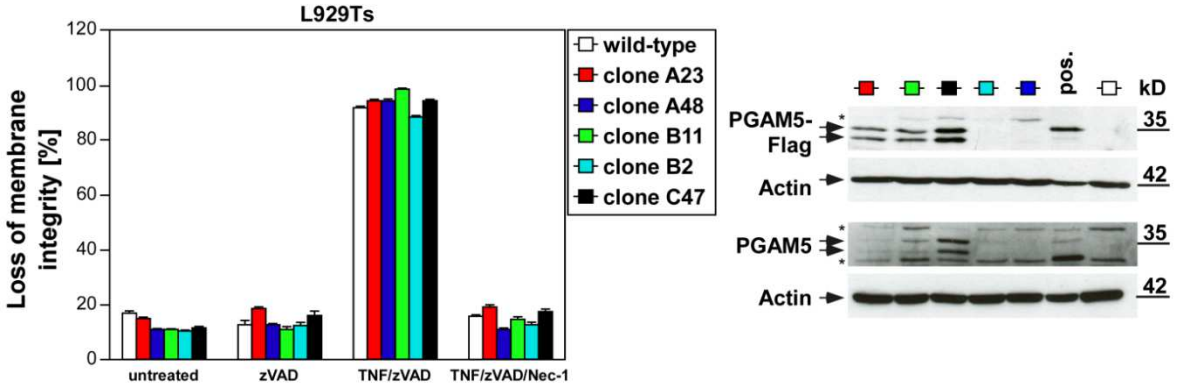

Figure 38: L929Ts cell lines overexpressing PGAM5-FLAG. Left panel: Five different L929Ts cell lines from isolated cell clones harboring and expressing the protein PGAM5 coupled to a FLAG tag were treated with 20 µM zVAD-fmk alone or in combination with 100 ng/mL TNF as well as 50 µM necrostatin 1 (Nec-1) for 5 h and loss of membrane integrity was compared to non-transfected wild-type L929Ts cells. One out of two experiments is shown. Error bars show the SD of three parallel measurements of 10,000 cells each. **Right panel:** Western blot of the stably transfected L929Ts cell clones, wild-type L929Ts and a positive control (HEK293 cells transient over-expressing PGAM5-FLAG (pos.)) shows the expression of PGAM5-FLAG either detected with anti-FLAG or anti-PAGM5 antibodies at 35 kDa. Detection of actin served as a loading control. Asterisk: nonspecific band.

Time kinetics of PGAM5 expression during necroptosis of wild-type L929Ts cells and L929Ts PGAM5-FLAG cells showed that both endogenous and overexpressed PGAM5-FLAG protein levels increased upon induction of necroptosis with TNF/zVAD (Figure 39A). This observation clearly demonstrated that the increased expression of PGAM5 is not due to transcriptional or translational modifications because expression of PGAM5-FLAG relies on a different promoter than the endogenous PGAM5 gene. Rather, the increase of PGAM5 protein levels is possibly caused by an inhibition of proteolysis. This possible regulation of PGAM5 by proteases was substantiated by the observation that increased levels of PGAM5 were observed when cells were treated with a protease inhibitor cocktail alone or in combination with zVAD-fmk to avoid unspecific activation of caspases by the inhibitors (Figure 39B). The treatment of cells with the proteasome inhibitor MG-132 and zVAD also showed increased PGAM5 levels in Western blots (Figure 39B). This suggests a constitutive degradation of the potentially pro-necroptotic protein PGAM5 by unknown proteases in

healthy cells, which is blocked upon induction of necroptosis (elevating PGAM5 levels and thus possibly facilitating mitochondrial fragmentation). Consistent with this assumption, the TNF/zVAD-induced increase of PGAM5 was diminished when necroptosis was blocked by Nec-1 (Figure 39B). Induction of apoptosis (TNF/CHX treatment) resulted also in an increase of PGAM5 levels indicating similar mechanism of the inhibition of the constitutive degradation of PGAM5 after induction of apoptosis (Figure 39B). To further narrow down possible protease candidates involved in the constitutive degradation of PGAM5, cells were treated with serine protease inhibitors (AEBSF and TFCK; Figure 39C) alone or in combination with zVAD-fmk. Western blots of PGAM5 revealed a similar increase in PGAM5 protein levels when serine protease as well as caspase activity was inhibited. Since the mitochondrial serine protease HtrA2/Omi was shown to be crucial for TNF-induced necroptosis, PGAM5 expression was also analyzed in the presence of the HtrA2/Omi inhibitor Ucf-101 alone or in combination with zVAD-fmk. Western blot analysis revealed a similar increase in PGAM5 protein levels when HtrA2/Omi was inhibited by Ucf-101 or Ucf-101/zVAD as in TNF/zVAD-treated cellular extracts (Figure 39C), indicating that HtrA2/Omi might be a potential physiological regulator of PGAM5.

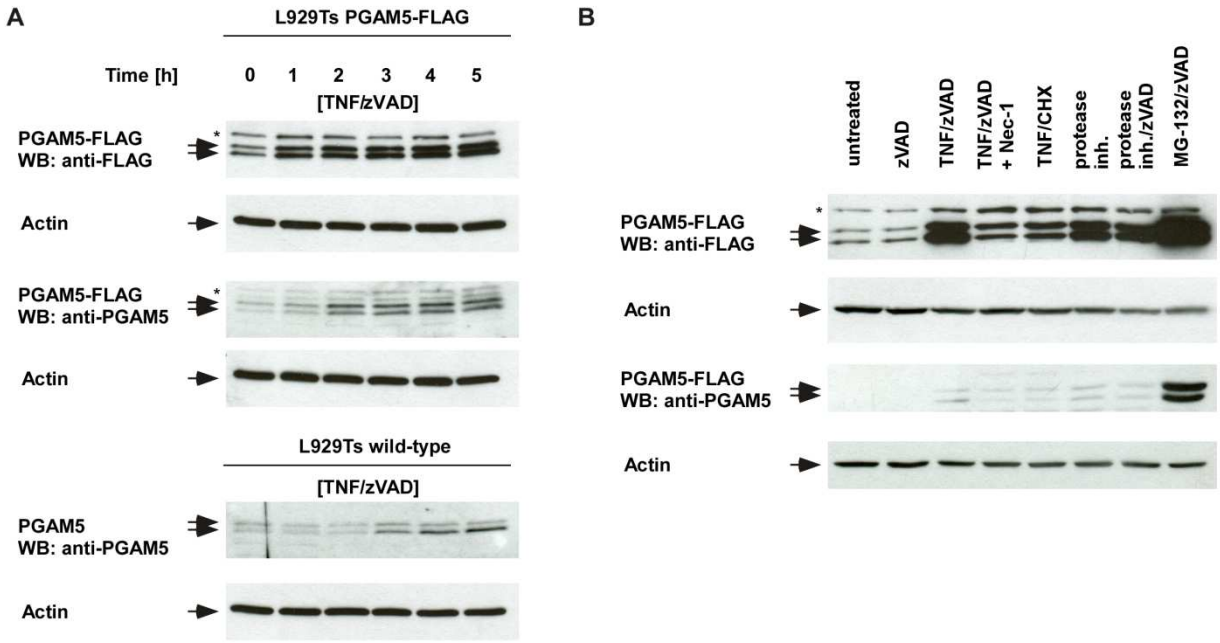

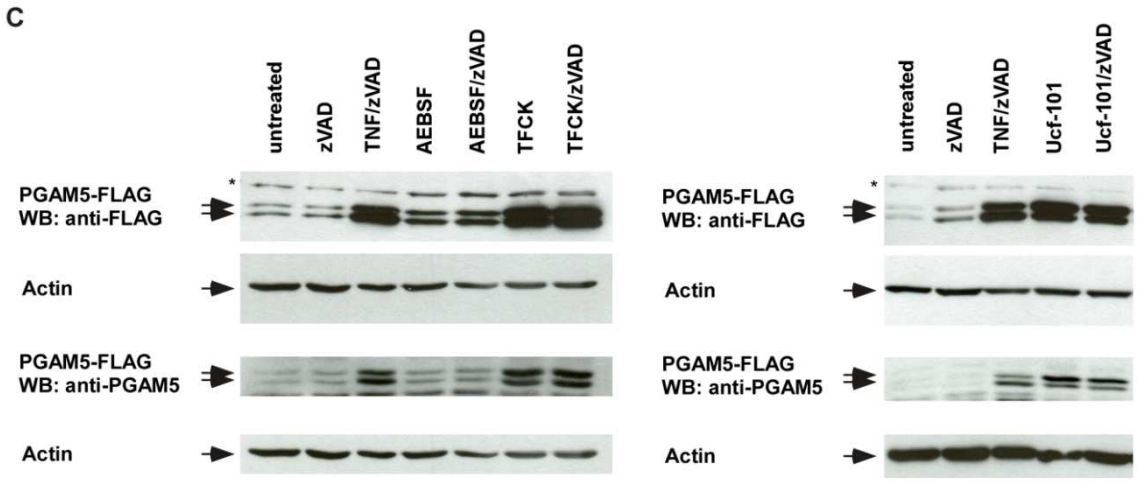

Figure 39: Serine proteases (HtrA2/Omi) and the proteasome are physiological regulators of PGAM5. (A) L929Ts wild-type cells and cells stably expressing the protein PGAM5 coupled to a Flag tag were treated with 100 ng/mL TNF and 20 µM zVAD-fmk for the indicated time-points. Western blots show the expression of PGAM5-FLAG and PGAM5 at 35 kDa. **(B)** L929Ts PGAM5-FLAG cells were left untreated or treated as above for 4 h with TNF/zVAD, TNF/zVAD and 50 µM necrostatin 1 (Nec-1) or TNF and 2 µg/mL CHX. Furthermore, cells were treated for 24 h with either 20 µM zVAD-fmk alone, 10 µg/mL protease inhibitor cocktail (protease inh.), with a combination of zVAD and protease inhibitor cocktail, or the proteasome inhibitor MG-132 (50 µM) in combination with zVAD-fmk. **(C)** L929Ts PGAM5-Flag cells were left untreated or were treated with zVAD or TNF/zVAD as in **(B)**. Stimulation with 100 µM AEBSF/(zVAD), 50 µM TFCK/(zVAD), or 50 µM Ucf-101/(zVAD) was stopped after 24 h. Western blots of cellular extracts were performed using anti-FLAG and anti-PGAM5 antibodies. Expression of actin served as a loading control. Asterisk: unspecific band.

Conclusion: Serine proteases (e.g. HtrA2/Omi) and the proteasome are physiological regulators of PGAM5

In the study presented here, it could be demonstrated that the potentially pro-necroptotic protein PGAM5 is constitutively degraded by yet unknown proteases in healthy cells. The levels of both endogenous and overexpressed PGAM5 increased upon induction of necroptosis. A similar increase in PGAM5 levels was induced by treatment of cells with protease inhibitors such as AEBSF, TFCK and MG-132, pointing to serine proteases and the proteasome as physiological regulators of PGAM5. Moreover, Ucf-101-treated cells also showed increased PGAM5 levels, suggesting that HtrA2/Omi may be involved in the constitutive degradation of PGAM5 in healthy cells. Furthermore, the important role of MLKL during necroptosis could be confirmed and was further analyzed during TRAIL-induced regulated necrosis in clinically relevant tumor cell lines (see 5.3).

5.2.5 Acid sphingomyelinase is proteolytically activated during TNF-induced necroptosis

Activation of A-SMase by TNF/zVAD correlates with the appearance of a 57-kDa proteolytic cleavage fragment in L929Ts cells

Unlike in apoptosis, where caspase-7 and -8 are responsible for the activation of A-SMase (Edelmann *et al.* 2011), the proteolytic maturation and activation of A-SMase in necroptosis must by definition occur in a caspase-independent manner and must therefore be mediated by distinct non-caspase proteases. In an initial experiment, murine L929Ts, NIH3T3 and human Jurkat I42 and U-937 cells were stimulated with TNF/zVAD to induce necroptosis. Afterwards, cells were immediately placed on ice and cellular extracts from each time-point were prepared and analyzed for their levels of endogenous A-SMase protein (Figure 40A). As a limitation of the analysis, commercially available antibodies for A-SMase were only able to detect an A-SMase fragment of approximately 57 kDa which corresponds to the cleaved, active form of A-SMase (Ferlinz *et al.* 1994). Western blot analysis revealed a time-dependent increase of the active A-SMase fragment in L929Ts cells (Figure 40A), providing first hints that A-SMase cleavage may also occur during necroptosis. Treatment of NIH3T3, Jurkat I42 and U-937 cells with TNF/zVAD, showed also effects on endogenous cleaved A-SMase levels (Figure 40A), confirming that A-SMase cleavage occurs during necroptosis in a cell-type unrelated manner.

In order to test whether this detected 57-kDa A-SMase fragment was derived from proteolytic cleavage of the 72 kDa A-SMase pro-form, murine L929Ts cells were stably transfected with a construct coding for a V5-tagged version of the full-length A-SMase. Figure 40B shows that overexpression of A-SMase had no positive or negative impact on TNF/zVAD-induced necroptosis. Furthermore, stimulation of stably transfected L929Ts cells with TNF/zVAD also revealed a time-dependent processing of overexpressed A-SMase (72 kDa) to a cleaved 57-kDa form in Western blots (Figure 40B).

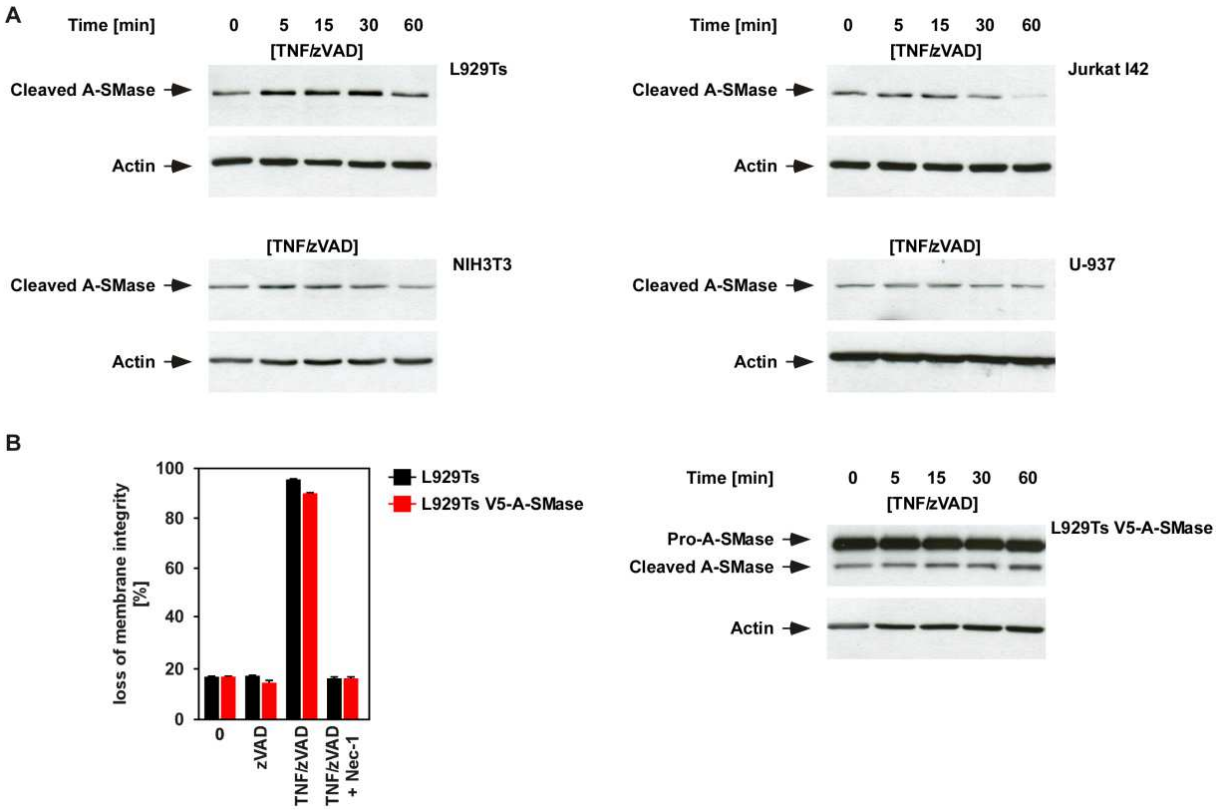

Figure 40: A-SMase is cleaved after TNF/zVAD stimulation. (A) Cells were incubated with 100 ng/mL TNF and 20 µM (L929Ts, NIH3T3) or 50 µM (Jurkat I42, U-937) zVAD-fmk on ice and stimulation was stopped immediately (0 min) (control) or were stimulated at 37 °C for the indicated time-points. Cell lysates were analyzed for endogenous A-SMase by means of Western blot using anti-A-SMase antibodies, which however only recognize the 57-kDa A-SMase cleavage product. **(B) Left panel:** Untransfected and L929Ts cells expressing recombinant V5-A-SMase were stimulated with 100 ng/mL TNF and 20 µM or in combination with 50 µM necrostatin 1 (Nec-1, to inhibit necroptosis) for 5 h before loss of membrane integrity was measured by flow cytometry. 10,000 cells were analyzed in triplicates. The error bars show SD from one out of three independent experiments. **Right panel:** Cells were stimulated as in **(A)** and a Western blot was performed using anti-V5 antibodies, detecting pro-A-SMase-V5 at 72 kDa and the cleavage product of A-SMase-V5 at 57 kDa. Actin served as a loading control.

To analyze if the appearance of the cleaved fragment of overexpressed as well as endogenous A-SMase was an indicator for activation of A-SMase, cell lysates were analyzed in parallel by Western blot for A-SMase cleavage and for A-SMase activity. In stably transfected (V5-A-SMase L929Ts cells) as well as untransfected L929Ts cells, induction of necroptosis with TNF/zVAD led to a time-dependent processing of either overexpressed A-SMase or endogenous pro-A-SMase to a 57-kDa fragment (Figure 41; upper panel), which was accompanied by a corresponding increase in enzymatic activity (Figure 41, lower panel), suggesting that the proteolytic cleavage after induction of necroptosis results in the activation of the A-SMase.

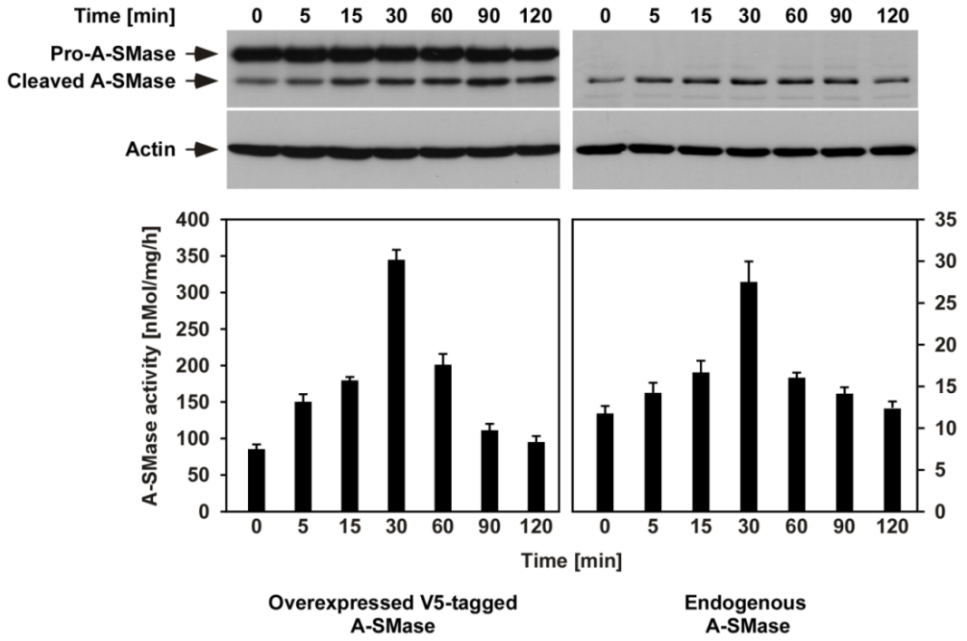

Figure 41: Proteolytic activation of A-SMase in necroptosis. V5-A-SMase L929Ts cells (left) or untransfected L929Ts cells (right) were treated with TNF/zVAD to induce necroptosis for the indicated time-points. **The upper panels** show anti-V5 Western blots for both tagged full length form (pro-A-SMase) and the cleaved active A-SMase form **(left)**. Parallel Western blot of endogenous A-SMase from untransfected L929Ts cells showed only the cleaved, active form of endogenous A-SMase at 57 kDa **(right)**. **Lower panels:** In parallel, A-SMase activity was measured. The data shown were obtained from three experiments each performed in triplicates. Error bars show the respective SD. Protein levels from one representative out of three experiments are shown. A-SMase activity measurements were performed by Supandi Winoto-Morbach (Christian-Albrechts-University, Kiel, Germany).

Treatment of untransfected L929Ts cells with Nec-1, Arc39 (an A-SMase-specific inhibitor; Roth *et al.* 2009; Samapati *et al.* 2012), as well as with TFCK inhibited the proteolytic processing as well as the activation of A-SMase during necroptosis (Figure 42).

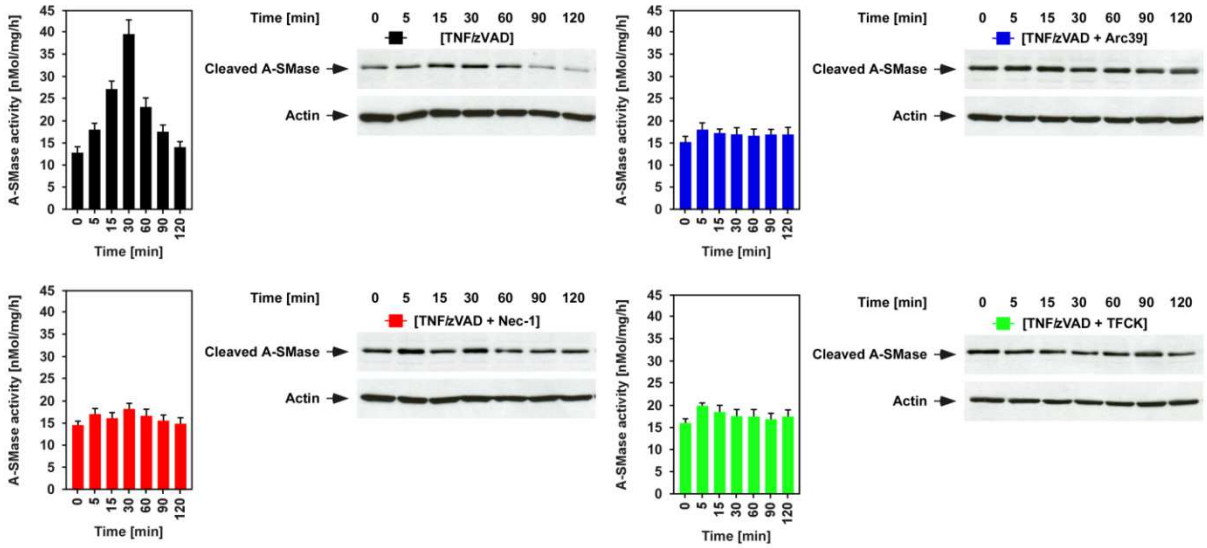

Figure 42: TNF/zVAD-induced A-SMase cleavage and activation occurs downstream of RIPK1. L929Ts cells were stimulated with TNF/zVAD or in combination with 50 µM necrostatin-1 (Nec-1), 10 µM Arc39 or 50 µM TFCK for the indicated time-points. Cell lysates were analyzed for A-SMase activity using N-methyl-[^{14}C]-sphingomyelin as substrate. Data were obtained from four independent experiments performed in triplicates. Error bars show SD. The same lysates were analyzed for endogenous cleaved A-SMase protein levels by Western blots. Western blots were performed to detect the cleaved, active A-SMase at 57 kDa. Detection of actin served as a loading control. Protein levels from one representative out of four experiments are shown. A-SMase activity measurements were performed by Supandi Winoto-Morbach (Christian-Albrechts-University, Kiel, Germany).

In further experiments to extend the inhibitor repertoire, L929Ts cells were treated with NSA, a pharmacological inhibitor of MLKL (Wu *et al.* 2013), or with the internalization inhibitor dynasore in combination with TNF/zVAD. Both inhibitors fully blocked the activation of A-SMase. Parallel Western blots to detect the active, cleaved A-SMase product revealed an inhomogeneous distribution pattern (Figure 43). To rule out that this was due to the solvent the inhibitors were dissolved in, cells were treated with TNF/zVAD in combination with DMSO. As shown in Figure 43, treatment with DMSO had no impact on TNF/zVAD-induced A-SMase activity as well as on the cleavage pattern of A-SMase when compared to protein extracts from cells treated with TNF/zVAD alone. This observation led to the assumption that the inhomogeneous distribution pattern of cleaved A-SMase in extracts from cells treated with NSA or with the internalization inhibitor dynasore in combination with TNF/zVAD is not due to the solvent of the inhibitor but is rather a direct effect of the inhibitors used. In summary, the obtained results suggest that A-SMase is activated downstream of the internalization of the TNF-R1 and downstream of the RIPK1-RIPK3-MLKL complex. Furthermore, the blockage of A-SMase activity after treatment with TFCK suggests the possible involvement of serine proteases in the regulation of A-SMase activity.

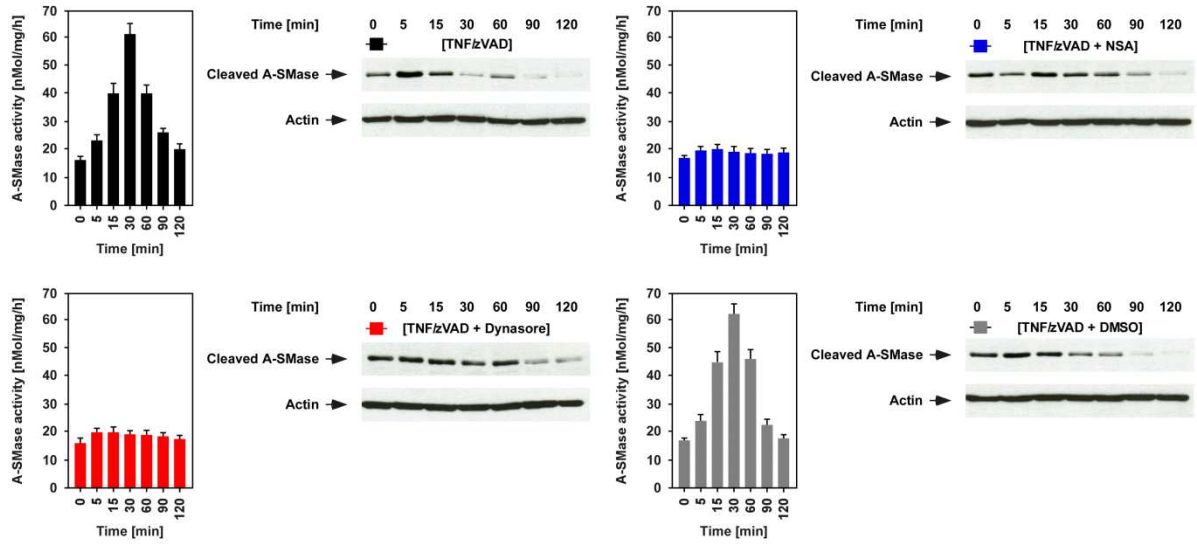

Figure 43: A-SMase cleavage and activation in L929Ts cells occurs downstream of MLKL and is inhibited by dynasore. L929Ts cells were stimulated with TNF/zVAD alone or in combination with 50 µM dynasore or 1 µM necrosulfonamide (NSA) or 5 µL DMSO (as solvent control) for 0 to 120 min. Cell lysates were analyzed for A-SMase activity. Error bars show standard deviations. The same lysates were analyzed for endogenous A-SMase expression. Western blots were performed using anti-A-SMase antibodies, detecting the cleaved, active A-SMase at 57 kDa. Protein levels from one representative out of two (TNF/zVAD/DMSO), three /TNF/zVAD/NSA) or four (TNF/zVAD and TNF/zVAD/dynasore) experiments are shown. A-SMase activity measurements were performed by Supandi Winoto-Morbach (Christian-Albrechts-University, Kiel, Germany).

The effector caspase-7 directly interacts with and mediates A-SMase activation during apoptosis (Edelmann *et al.* 2011). To investigate whether caspase-7 has an impact on necroptosis-induced proteolytic cleavage and activation of A-SMase, caspase-7 deficient MEFs and wild-type MEFs were characterized for A-SMase cleavage and activity under necroptotic conditions. MEFs were incubated with TNF/zVAD/CHX to induce necroptosis and as a control with TNF/CHX to induce apoptosis.

Treatment with TNF/zVAD/CHX revealed increased sensitivity of MEFs devoid of caspase-7 compared to wild-type cells. Addition of Nec-1 decreased cell death rates, confirming that TNF/zVAD/CHX induces necroptosis in these MEFs (Figure 44A). Furthermore, the results obtained showed increased cell death rates of MEFs deficient in caspase-7 compared to their wild-type counterparts after induction of apoptosis (TNF/CHX), suggesting that MEFs devoid of caspase-7 a generally more sensitive towards cell death. In contrast to L929Ts cells treated with TNF/zVAD (see Figures 41, 42, 43) and to wild-type MEFs (Figure 44B), MEFs deficient of caspase-7 did not show an increase of A-SMase activity in response to induction of necroptosis (Figure 44B). However, Western blot analysis showed increased protein levels of cleaved A-SMase after induction of necroptosis in wild-type MEFs whereas only a marginal cleavage of A-SMase was detectable in MEFs deficient in caspase-7 (Figure 44C). These observations suggest that the presence of caspase-7 protein might be needed for activation of A-SMase during TNF-induced necroptosis and that the caspase-7-deficient MEFs utilized in this study might undergo TNF-induced necroptosis via additional effector mechanisms independent from A-SMase activation and subsequent ceramide generation.

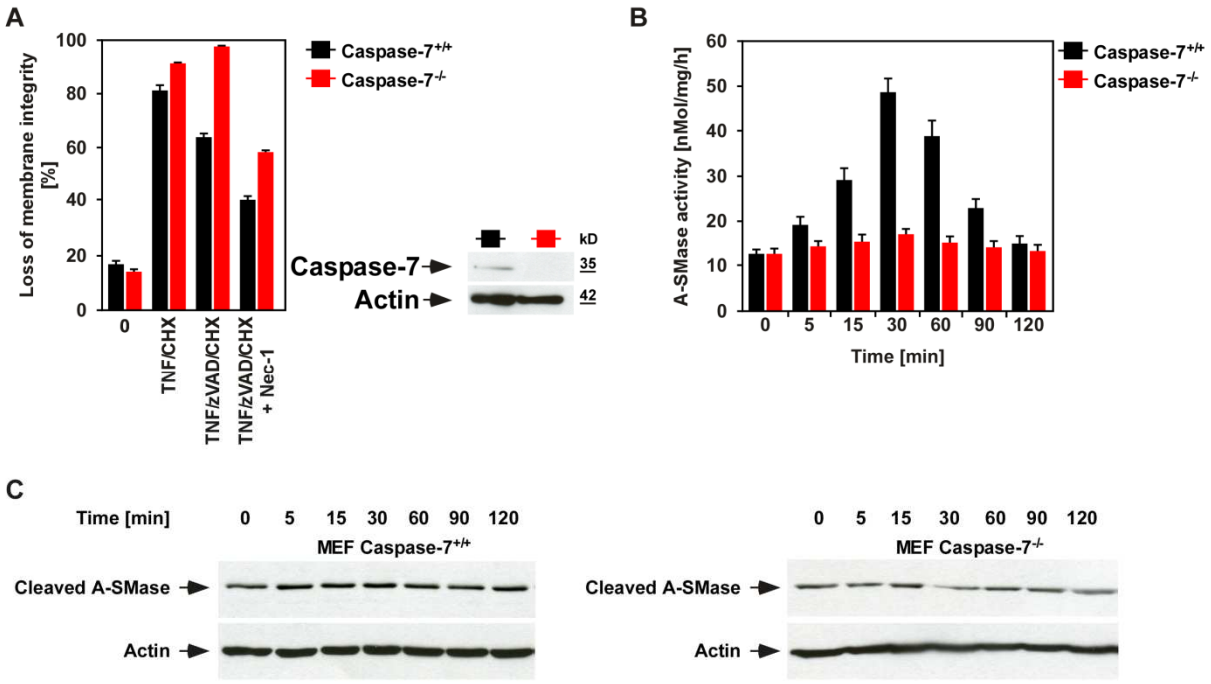

Figure 44: A-SMase activity after TNF-induced necroptosis in wild-type and caspase-7 deficient MEFs. (A) Left panel: Wild-type MEFs (Caspase-7 $^{+/+}$) and MEFs devoid of caspase-7 (Caspase-7$^{-/-}$) were treated with 100 ng/mL TNF and 1 µg/mL CHX (to induce apoptosis) or in combination with 20 µM zVAD-fmk (to induce necroptosis) for 16 h before loss of membrane integrity was measured by PI staining and flow cytometry. 10,000 cells were analyzed for each measurement. One out of three experiments is shown. Error bars show the SD from triplicate measurements. **Right panel:** Western blot to detect full length caspase-7 in cellular extracts of wild-type MEFs and caspase-7$^{-/-}$ MEFs. **(B)** Wild-type MEFs or caspase-7 deficient MEFs treated with 100 ng/mL TNF, 20 µM zVAD-fmk and 1 µg/mL CHX for 16 h were analyzed for A-SMase activity. A-SMase activity measurements were performed by Supandi Winoto-Morbach (Christian-Albrechts-University, Kiel, Germany). **(C)** The same lysates were analyzed for endogenous A-SMase protein levels. Western blots were performed using anti-A-SMase antibodies, detecting the cleaved, active A-SMase at 57 kDa. Protein levels from one out of three experiments are shown. Detection of actin served as a loading control.

Characterization of the 57 kDa A-SMase cleavage product

To define the proteolytic cleavage site where A-SMase is processed from its precursor to the 57-kDa active form, L929Ts cells overexpressing a fusion protein of pro-A-SMase (72 kDa) and the V5 tag (2 kDa), pretreated over night with zVAD-fmk to prevent any apoptotic cleavage of A-SMase, were stimulated with TNF/zVAD for 30 min to induce necroptosis and processing of A-SMase. Unprocessed and processed V5-tagged A-SMase was enriched by immunoprecipitation and lysates were separated by SDS-PAGE following Western blots. As shown in Figure 45, there was an enrichment of V5-A-SMase protein after immunoprecipitation of A-SMase with its V5-tag. Moreover, processed (59 kDa) fragments as well as unprocessed (74 kDa), full-length V5-A-SMase were clearly visible. This cleaved 59-kDa protein corresponds to the 57-kDa active A-SMase molecule after subtraction of the 2-kDa V5-tag.

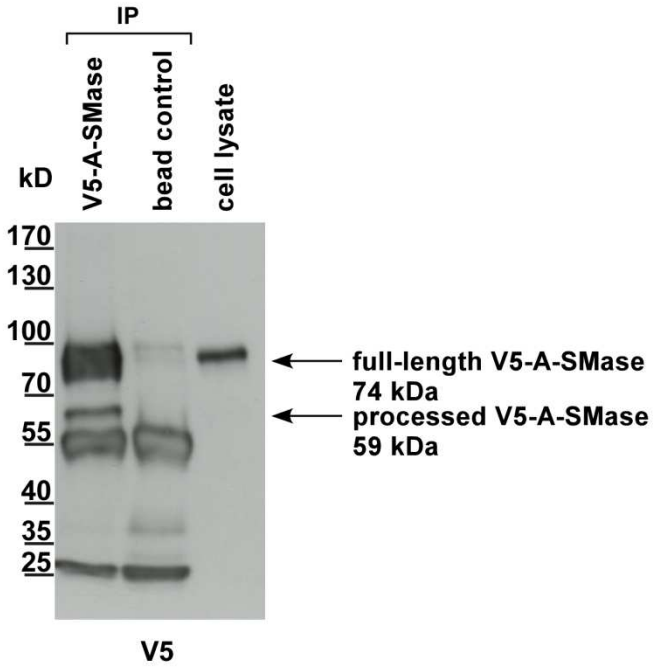

Figure 45: Enrichment of full-length and processed V5-A-SMase. L929Ts cells stably transfected with V5-tagged A-SMase were lysed and anti-V5 or anti-RACK antibodies (as a control for specificity, bead control) were used for immunoprecipitation (IP). Western blot was performed using anti-V5 antibodies detecting V5-tagged full-length V5-A-SMase and processed V5-A-SMase fragment (left). As an additional control, V5-A-SMase was also detected in total cell lysates.

To further analyze full-length and processed V5-A-SMase, preparative SDS-gels were loaded with immunoprecipitated A-SMase fragments and stained with Flamingo™ Fluorescent gel stain. In collaboration with the group of Andreas Tholey (Christian-Albrechts-University, Kiel, Germany) the bands corresponding in size to full-length and processed V5-A-SMase were isolated and half of the samples were labeled at their N-termini and the other half was left un-labeled. All samples were then digested with trypsin and analyzed by means of LC-MS/MS (see 4.2.15.2). Since the N-terminus of full-length and processed V5-A-SMase was labeled before digestion with trypsin, peptides identified with a labeling can be considered as peptides starting from the N-terminus of either full-length or

processed V5-A-SMase. The analyses of extracted V5-A-SMase fragments identified the N-terminus of full-length V5-A-SMase with the N-terminus being at A(59)/(60)H (Figure 46; red box). No labeled peptides were identified for processed V5-A-SMase products in this first set of experiments (Figure 46). However, one unlabeled peptide was identified for cleaved A-SMase starting at the proline at position P(219)/(220)D, providing evidence that A-SMase is cleaved N-terminal to the site identified for cleavage of A-SMase in apoptosis (residue C(250)/(251)D (D253; Edelmann *et al.* 2011)).

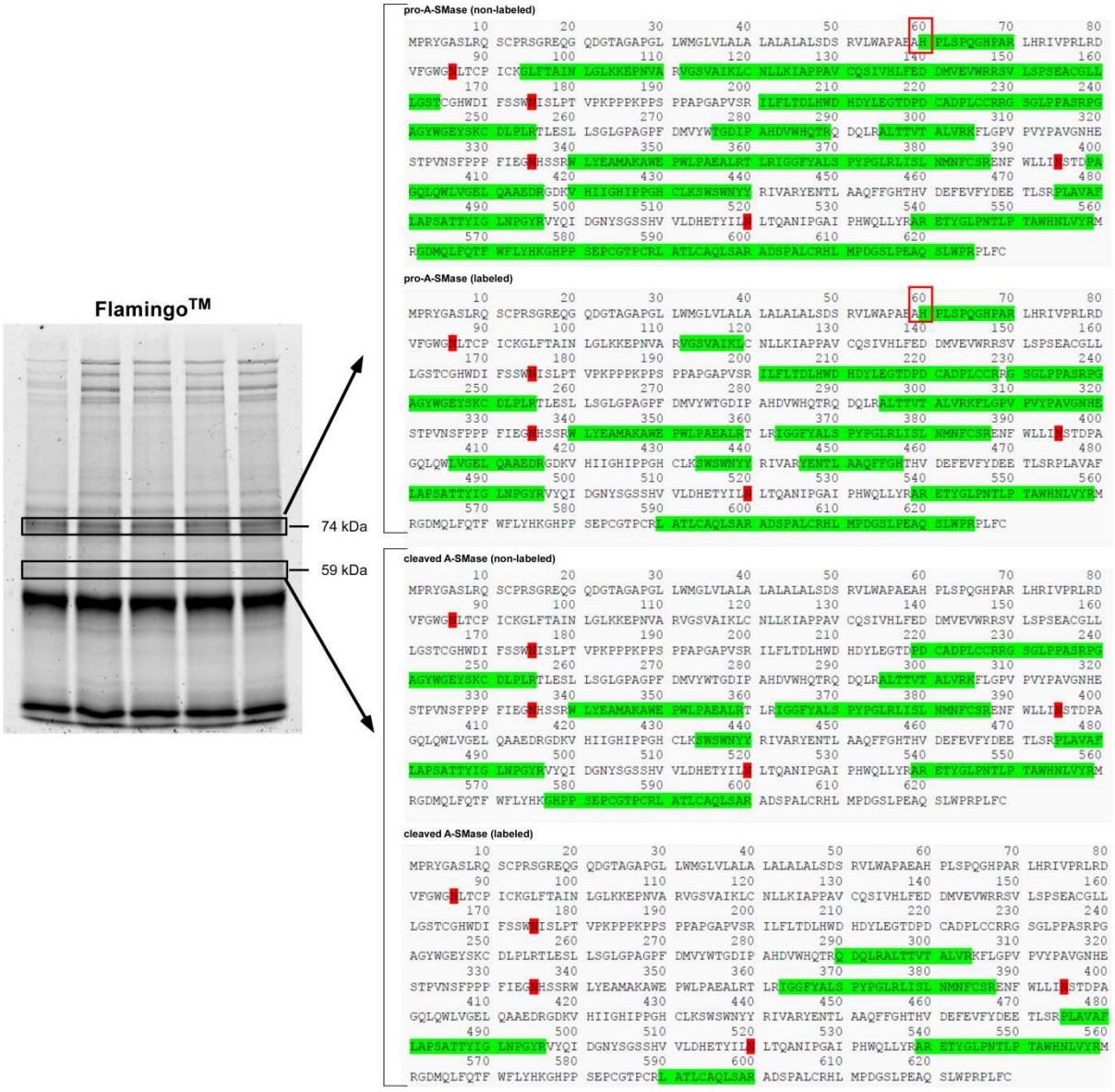

Figure 46: Sequence coverage of full-length and processed A-SMase during TNF-induced necroptosis. Left panel: L929Ts cells stably transfected with V5-tagged A-SMase were treated for 30 min with 100 ng/mL TNF in combination with 20 µM zVAD-fmk to induce necroptosis. Subsequently, cells were lysed and anti-V5 antibodies were used for immunoprecipitation of V5-A-SMase. An SDS-PAGE gel was used for separation of immunoprecipitated proteins (which were loaded in five parallel lanes). The gel was stained with Flamingo™ Fluorescent gel stain to visualize protein bands. Bands at 74 kDa and 59 kDa were excised and combined, respectively. **Right panel:** The sequence coverage of full-length (pro-A-SMase, upper part) and processed (cleaved A-SMase; lower part) V5-A-SMase is shown. Half of the excised material was digested with trypsin (non-labeled; top panel) while the other half was first labeled (at the protein N-terminus and at lysine residues, bottom panel) and then digested with trypsin. Green marked sequences are peptides identified with high confidence. Red marked amino acids represent known N-linked glycosylation sites. The red box marks the identified N-terminus of pro-A-SMase at A(59)/(60)H.

Since the above described analysis of processed V5-A-SMase under necroptotic conditions provided evidence that A-SMase is cleaved at a position distinct from that cleaved during apoptosis, the proteolytic processing of V5-A-SMase under apoptotic and necroptotic condition was compared in a second set of experiments. For this purpose, full-length V5-A-SMase and processed V5-A-SMase fragments were enriched after inducing either apoptosis (TNF/CHX) or necroptosis (TNF/zVAD) and were analyzed as above. The preparative SDS-gels stained with Flamingo™ Fluorescent gel stain revealed that full-length V5-A-SMase and processed V5-A-SMase fragments isolated from cells either undergoing apoptosis or necroptosis had the same molecular weight (Figure 47, left panel). However, in the subsequent LC-MS/MS analyses, the reported cleavage site for apoptosis at residue D253 (Figure 47; blue box; Edelmann *et al.* 2011) was not detected. In spite of this, un-labeled N-terminal peptides starting from L(202)/(203)F were identified, suggesting that the cleavage site of A-SMase under apoptotic conditions might be more upstream than previously reported. In contrast to samples from apoptotic cells, the analysis of processed V5-A-SMase isolated from necroptotic cells revealed un-labeled N-terminal peptides starting from I(201)/(202)L. Overall, the sequence coverage and peptides identified in samples from apoptotic and necroptotic cells were very similar (Figure 47, right panel), suggesting that cleavage of A-SMase during apoptosis and necroptosis might occur at the same sequence or in immediate vicinity. Again, no labeled peptides were identified for processed V5-A-SMase products in this set of experiments due to detection limits and have so far prevented the identification of the exact cleavage site of mature, active A-SMase.

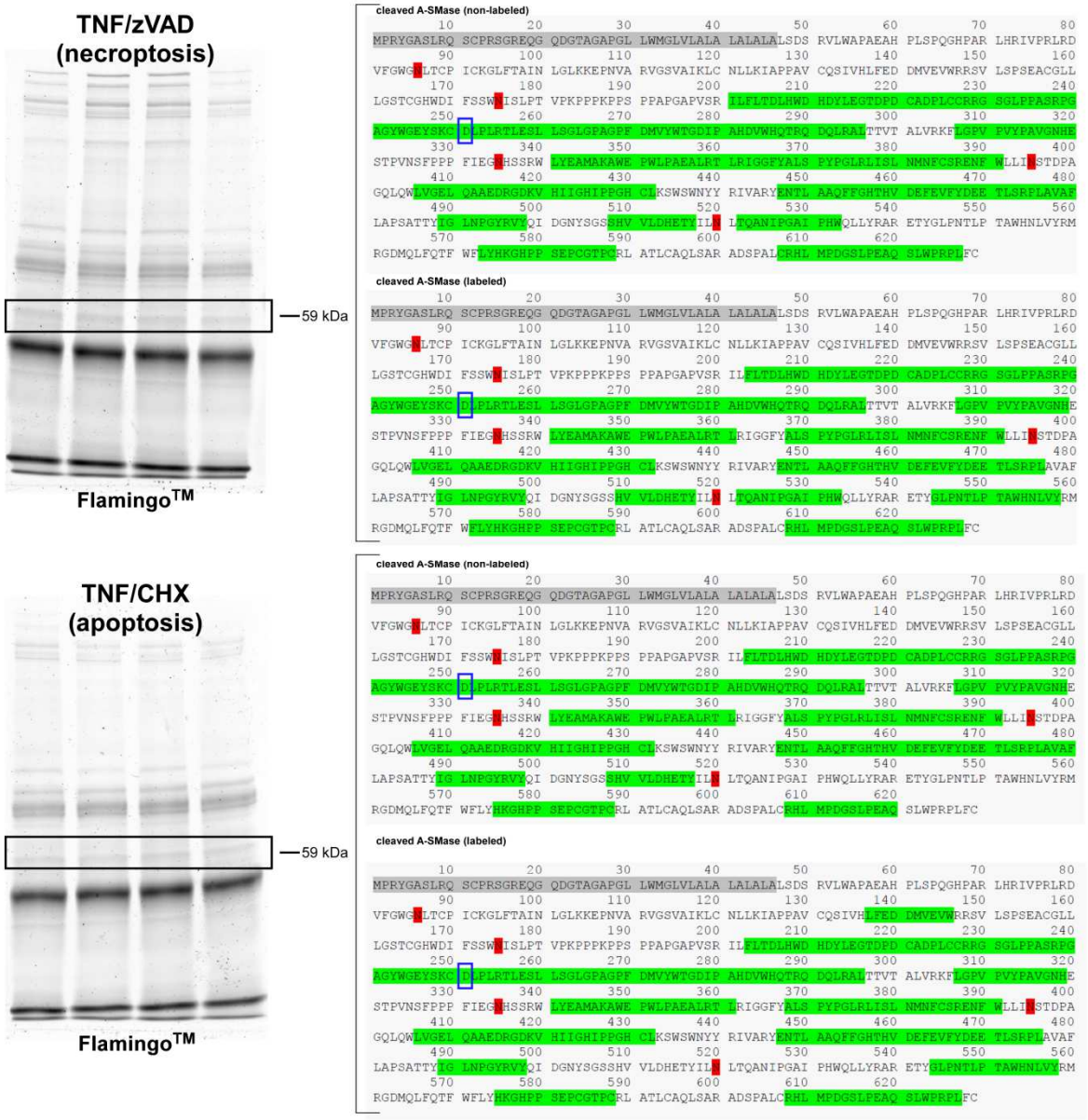

Figure 47: Comparison of sequence coverage of processed V5-A-SMase isolated from cells undergoing TNF-induced necroptosis or TNF-induced apoptosis. Left panel: L929Ts cells stably transfected with V5-tagged A-SMase were treated for 30 min with either 100 ng/mL TNF in combination with 20 µM zVAD-fmk to induce necroptosis **(top panel)** or with 5 µg/mL CHX to induce apoptosis **(bottom panel)**. Subsequently, cells were lysed and anti-V5 antibodies were used for immunoprecipitation of V5-A-SMase. SDS-PAGE gels were used for separation of immunoprecipitated proteins (which were loaded in four parallel lanes). The gels were stained with Flamingo™ Fluorescent gel stain to visualize protein bands. Bands at 57 kDa were excised and combined. **Right panel:** The sequence coverage of processed (cleaved A-SMase) V5-A-SMase is shown. Half of the excised material was digested with trypsin (non-labeled; top panel) while the other half was first labeled (at the protein N-terminus and at lysine residues, bottom panel) and then digested with trypsin. Green marked sequences are peptides identified with high confidence. Red marked amino acids represent known N-linked glycosylation sites. Signal peptide of A-SMase is highlighted in grey. The blue box indicates the reported cleavage site of caspase-7 at D253 confirmed for apoptosis (Edelmann *et al*. 2011).

Conclusion: A-SMase is proteolytically cleaved and activated during necroptosis

In summary, it was shown for the first time that the levels of the 57-kDa fragment of both endogenous and overexpressed A-SMase increased upon induction of necroptosis in multiple cell lines. The processing of overexpressed and endogenous A-SMase to a 57-kDa form during necroptosis was accompanied by a corresponding increase in its enzymatic activity. Moreover, the study presented here shows that Nec-1, NSA as well as TFCK and dynasore inhibit the proteolytic processing as well as the

activation of A-SMase during necroptosis, suggesting that A-SMase is activated downstream of the RIPK1-RIPK3-MLKL complex, and possibly also downstream of serine proteases. The study of caspase-7-deficient MEFs revealed that these cells are able to undergo TNF-induced necroptosis, but A-SMase is not activated, suggesting a possible role of non-enzymatic functions of caspase-7 during necroptosis. The analysis of the pro- and cleaved form of A-SMase identified the N-terminus of pro-A-SMase (Figure 46, red arrow), although detection limits have so far prevented the identification of the exact cleavage site of mature, active A-SMase. As mentioned above, this cleavage site must be distinct from the reported cleavage site where caspase-7 cleaves A-SMase during apoptosis (Edelmann *et al.* 2011; Figure 47, black arrow), because the MS analysis identified peptides that extend N-terminal of this cleavage site. Interestingly, the comparison of the sequence coverage and peptides identified in samples from apoptotic and necroptotic cells suggest that cleavage of A-SMase during apoptosis and necroptosis might nevertheless occur within the same sequence or in immediate vicinity.

5.2.6 The role of presenilin and the presenilin homologue signal-peptide-peptidase-like (SPPL) during TNF-induced necroptosis

To investigate if other peptidases are potential regulators of necroptosis induced by TNF, two established SPP/SPPL (signal-peptide-peptidase [-like]; Weihofen *et al.* 2003; Friedmann *et al.* 2006) inhibitors (inhibitor X and $(Z\text{-}LL)_2$-ketone), were applied to L929Ts and U-937 cells. Cells were pre-treated with inhibitor X or $(Z\text{-}LL)_2$-ketone for 5 h to ensure optimal inhibitory effects before cell death was induced with TNF/zVAD. Treatment with $(Z\text{-}LL)_2$-ketone showed no inhibitory effect on TNF-induced necroptosis in L929Ts and U-937 cells (Figure 48A). On the other hand, the addition of inhibitor X slightly diminished TNF-induced necroptosis in murine L929Ts as well as human U-937 cells (Figure 48A). To further investigate whether SPPL proteins are functionally involved in the execution of TNF-induced necroptosis, MEFs from SPPL2a-, SPPL2b- and SPPL2a/b-deficient mice were analyzed. Depending on the MEF batches analyzed, MEFs deficient for either SPPL2a or SPPL2b or both showed effects on TNF-induced necroptosis (Figure 48B). The analysis of the first batch of MEFs showed that SPPL2b- and SPPL2a/b-deficient MEFs were protected from TNF-induced necroptosis compared to their wild-type counterparts. Unlike batch number one, MEFs from SPPL2b- and SPPL2a/b-deficient mice from two additional, distinct batches showed sensitivity towards TNF-induced necroptosis (Figure 48B). In spite of this, SPPL2a-deficient MEFs showed slight protection from TNF-induced necroptosis compared to the treated wild-type counterparts in batch number two and three (Figure 48B). In conclusion, the above described results did not allow to define a potential role for SPPLs in TNF-induced necroptosis.

Inhibitor X is known to specifically bind and inhibit presenilin proteins, which are part of the γ-secretase protease complex (Dörfler *et al.* 2001). Based on the effects of inhibitor X on TNF-induced necroptosis observed in Figure 48A, MEFs derived from presenilin-1/2-deficient mice were therefore included in the characterization of TNF-induced necroptosis. As shown in Figure 48C, in assays

investigating TNF-induced necroptosis, presenilin 1/2-deficient cells were fully protected from TNF-induced necroptosis, confirming the above described results with inhibitor X and pointing to a possible role of presenilin in this form of regulated necrosis.

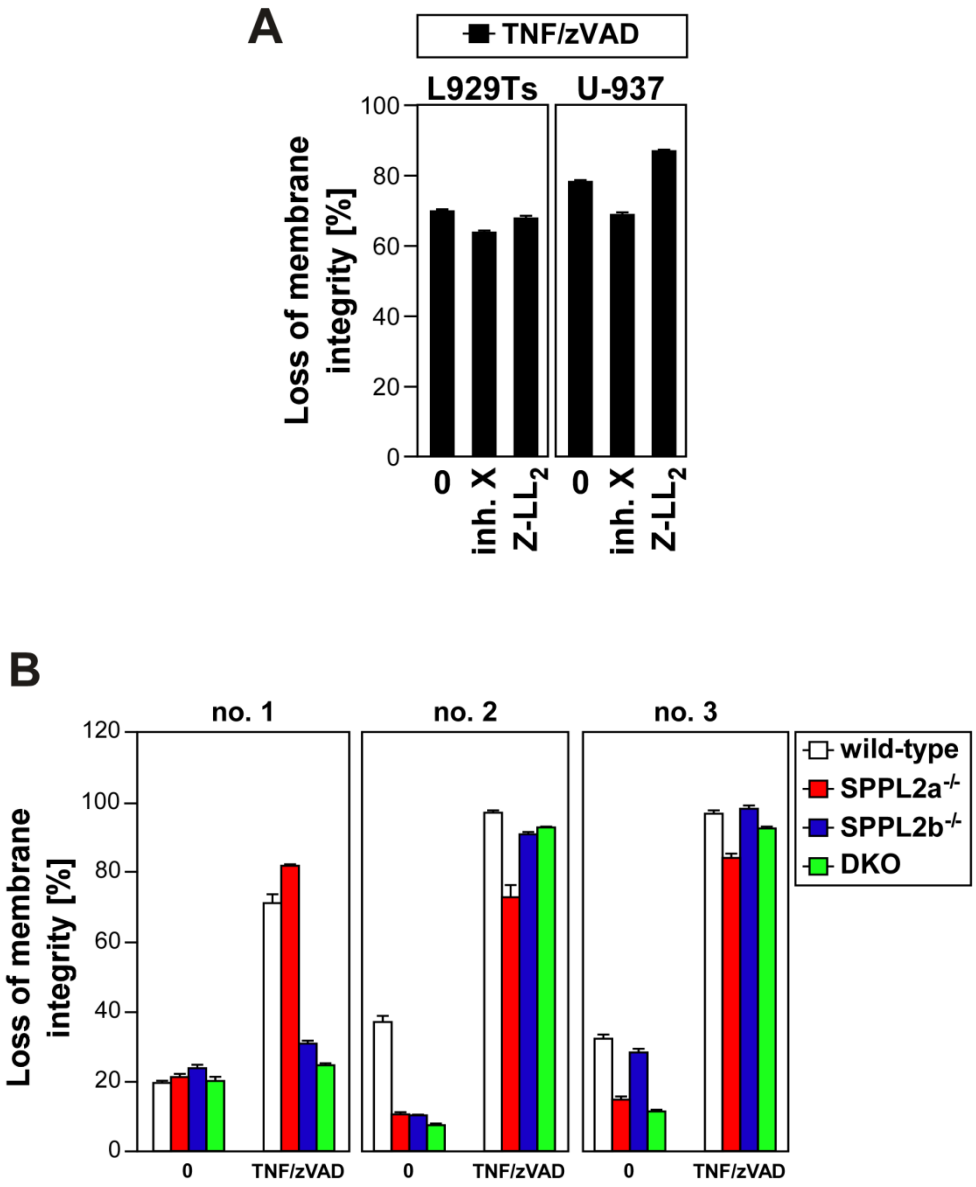

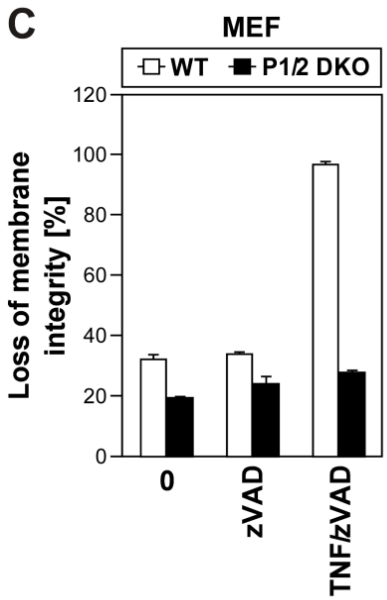

Figure 48: The role of SPPLs and presenilin in TNF-induced necroptosis. (A) Cells were left without, or were pretreated for 5 h with 1 µM inhibitor X or 10 µM $(Z\text{-}LL)_2$-ketone. Subsequently, cells were further incubated for 2 (L929Ts) or 24 h (U-937) in the presence of 100 ng/mL TNF and 20 (L929Ts) or 50 µM (U-937) zVAD-fmk before cell death was analyzed by flow cytometry. **(B)** Wild-type MEFs and MEFs deficient for SPPL2a ($SPPL2a^{-/-}$), SPPL2b ($SPPL2b^{-/-}$) and SPPL2a/b (DKO) from three different batches (no. 1-3) were treated with 100 ng/mL TNF and 20 µM zVAD-fmk for 16 h and were analyzed as in **(A)**. **(C)** Wild-type and presenilin-1/2-deficient (P1/2 DKO) MEFs were stimulated for 16 h as in **(B)** before cell death was determined. One out of three experiments is shown. Error bars indicate the SD from three parallel measurements.

5.3 TRAIL-induced necroptosis is a novel approach to eliminate tumor cells

TRAIL can induce regulated necrosis in human tumor cells

In this part of the study, the ability of TRAIL to induce regulated necrosis in a panel of 14 distinct human cancer cell lines of diverse origin was analyzed. To initially characterize the human cancer cell lines with regard to their sensitivity to TRAIL-induced regulated necrosis, cells were treated with TRAIL/zVAD/CHX. Since treatment with TRAIL normally activates caspase-dependent apoptosis, apoptosis was actively inhibited by addition of zVAD-fmk. Furthermore, all cells were additionally sensitized with non-toxic concentrations of CHX. As depicted in Figure 49, treatment with TRAIL/zVAD/CHX induced regulated necrosis in eight out of 14 tested tumor cell lines. The tumor cell lines U-937, Mz-ChA-1, BxPC-3 and HT-29 exhibited the highest sensitivity, followed by Colo357, Panc89, PancTu-I and A818-4 cells with decreasing sensitivity levels towards TRAIL-induced regulated necrosis. The remaining cell lines (CCRF-CEM, MKN-28, SK-OV-3, KNS-62, Pt45P1, and SK-MEL-28) displayed only a marginal or no response to treatment with TRAIL/zVAD/CHX. The same results were obtained in control assays when regulated necrosis was induced with TNF/zVAD/CHX (see Voigt *et al.* 2014).

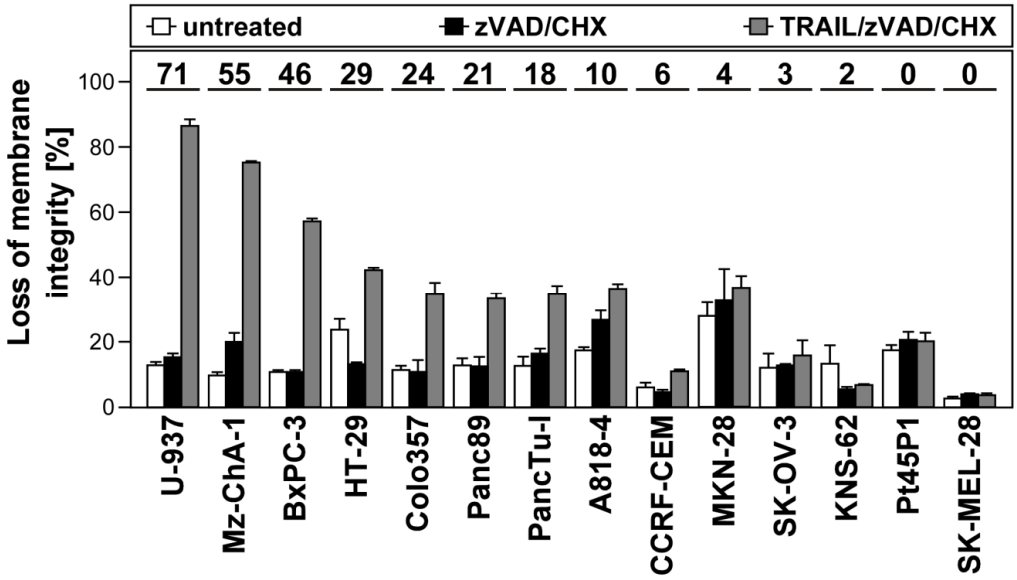

Figure 49: Induction of regulated necrosis by TRAIL in human tumor cell lines. Cells were treated with 100 ng/ml TRAIL in combination with 50 µM zVAD-fmk and non-toxic concentrations of CHX (U-937 0.1 µg/mL; Mz-ChA-1 2 µg/mL; BxPC-3 1 µg/mL; HT-29 5 µg/mL; Colo357 5 µg/mL; Panc89 1 µg/mL; PancTu-I 10 µg/mL; A818-4 10 µg/mL; CCRF-CEM 0.0625 µg/mL; MKN-28 5 µg/mL; SK-OV-3 1 µg/mL; KNS-62 5 µg/mL; Pt45P1 0.1 µg/mL; SK-MEL-28 10 µg/mL). After 24 h, loss of membrane integrity was measured as a marker for cell death by flow cytometric detection of PI-positive cells. Values above the respective columns represent the specific percentage of regulated necrosis (stimulus-induced minus zVAD/CHX-induced regulated necrosis). The spontaneous cell death in untreated cells is shown for comparison. Each bar represent the means of two independent experiments with three parallel determinations each, error bars indicate the corresponding SD. Experiments for Mz-ChA-1, BxPC-3, HT-29, Colo357, Panc89, PancTu-I, A818-4, CCRF-CEM, MKN-28, KNS-62, Pt45P1 and SK-MEL-28 were performed by Stephan Philipp (Christian-Albrechts-University, Kiel, Germany).

Birinapant enhances TRAIL-induced regulated necrosis in human tumor cells

It has been reported that Smac mimetics can act as enhancers of TNF-induced regulated necrosis (He *et al.* 2009). To test whether Smac mimetics can also enhance TRAIL-mediated regulated necrosis in the tested tumor cell lines, five arbitrarily selected sensitive tumor cell lines (U-937, Mz-Cha-1, BxPC-3, HT-29 and Panc89) and as a control one resistant tumor cell line (KNS-62) were stimulated with TRAIL/zVAD/CHX or TNF/zVAD/CHX (as internal control) in the presence of the Smac mimetic birinapant. As shown in Figure 50, the addition of birinapant led to a further enhancement of both TRAIL- and TNF-induced regulated necrosis in the set of five sensitive tumor cell lines, but not in the resistant tumor cell line KNS-62. Furthermore, a ten-fold increase in the concentration of birinapant did not further enhance regulated necrosis in the sensitive cell lines or overcome resistance in KNS-62 cells, indicating that TRAIL- and TNF-induced regulated necrosis is mediated by molecular mechanisms which are likewise responsive to Smac mimetics

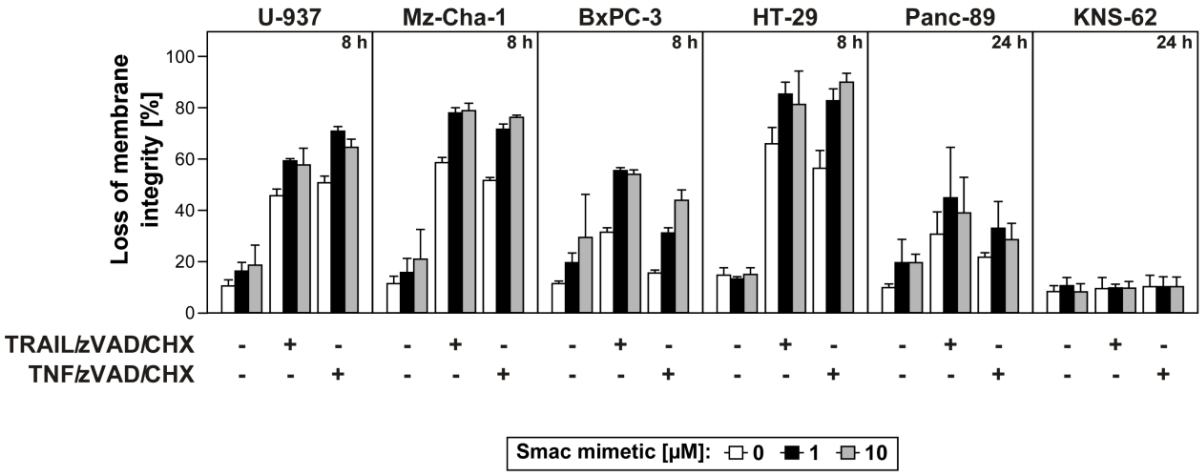

Figure 50: Birinapant enhances TRAIL-induced necroptosis. Cells were treated with 100 ng/ml TRAIL or TNF in combination with 50 µM zVAD-fmk and non-toxic concentrations of CHX (U-937 0.1 µg/mL; Mz-ChA-1 2 µg/mL; BxPC-3 1 µg/mL; HT-29 5 µg/mL; Panc89 1 µg/mL; KNS-62 5 µgmL) in the presence of the indicated concentrations of the Smac mimetic birinapant. After 8 or 24 h of stimulation, regulated necrosis was analyzed by flow cytometric analysis of PI-positive cells. Each bar represents the means of two independent experiments with three parallel determinations each, error bars indicate the corresponding SD.

RIPK1, RIPK3 and MLKL are mediators of TRAIL-induced regulated necrosis in the examined tumor cell lines

As described in the introduction (2.2.1.1), regulated necrosis elicited through DRs critically depends on the protein kinase RIPK1 and the related downstream kinase RIPK3 (Vanden Berghe *et al.* 2014). To this end, the role of RIPK1 was next validated by pharmacological inhibition in the above selected tumor cell lines. The pharmacological inhibition of RIPK1 by Nec-1 protected U-937, Mz-Cha-1, BxPC-3, HT-29 and Panc89 cells from both TRAIL- and TNF-induced regulated necrosis (Figure 51A). Furthermore, the down-regulation of RIPK3 by RNA interference in U-937 and HT-29 cells as two sensitive tumor cell lines that express relatively high levels of RIPK3 (see Voigt *et al.* 2014) significantly blocked TRAIL- as well as TNF-induced killing (Figure 51B), suggesting that TRAIL-induced regulated necrosis likewise occurs via the necroptosis pathway.

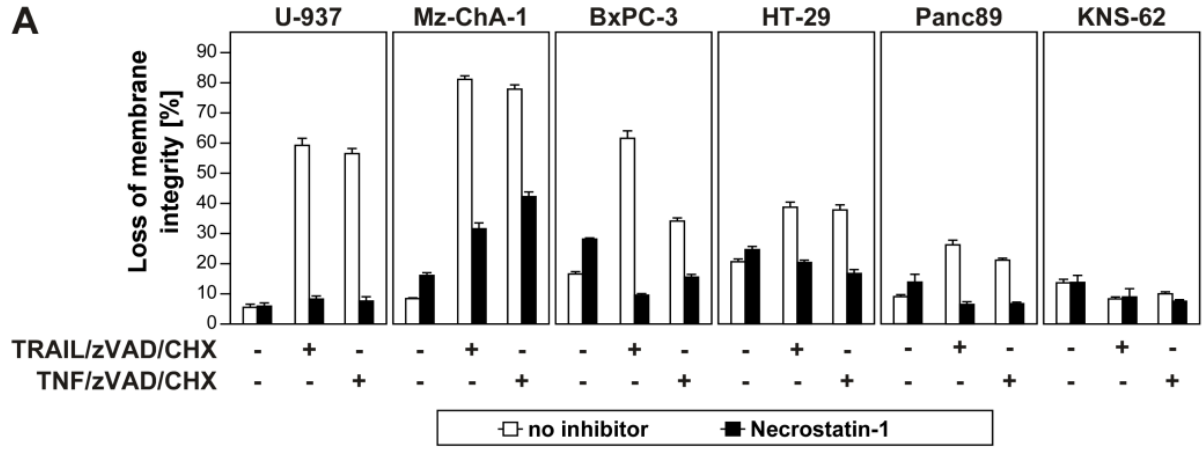

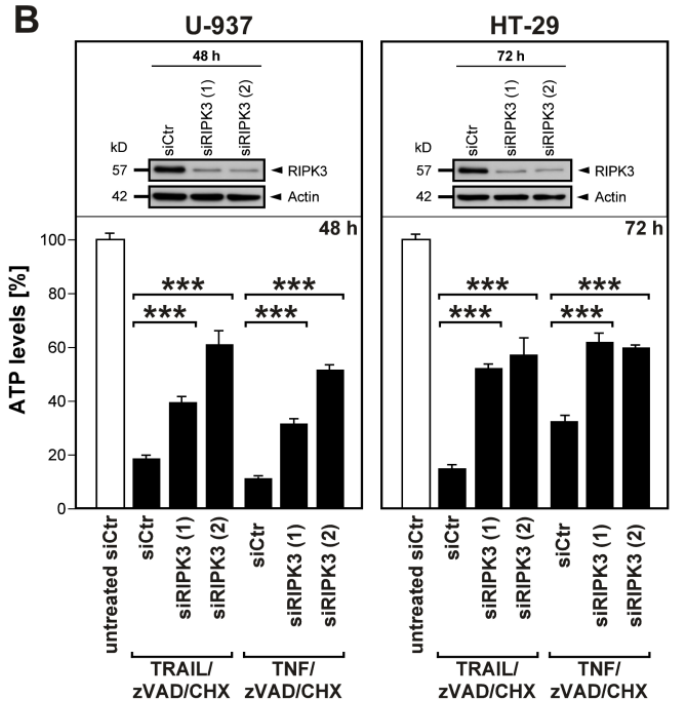

Figure 51: RIPK1 and RIPK3 are mediators of TRAIL-induced regulated necrosis. (A) Cells were left untreated or preincubated with 50 µM necrostatin-1 for 2 h before addition of 100 ng/ml TRAIL or TNF in combination with 50 µM zVAD-fmk and non-toxic concentrations of CHX (U-937 0.1 µg/mL; Mz-ChA-1 2 µg/mL; BxPC-3 1 µg/mL; HT-29 5 µg/mL; Panc89 1 µg/mL; KNS-62 5 µg/mL). After 24 h of stimulation, regulated necrosis was analyzed by flow cytometric analysis of PI-positive cells. Each bar represents the means of two independent experiments with three parallel determinations each. Error bars indicate the corresponding SD. **(B)** U-937 and HT-29 cells were transfected with siRNAs specific for human RIPK3. As a negative control, cells were transfected with an siRNA that does not elicit an RNAi response (siCtr). 48 or 72 h after transfection, cells were left untreated or incubated with TRAIL/zVAD/CHX or TNF/zVAD/CHX as above. After 24 h of stimulation, regulated necrosis was analyzed by measuring the decrease of intracellular ATP levels as a marker for cell death. ATP levels are shown relative to cells transfected with the negative control siRNA but not treated (untreated siCtr). Control Western blots of transfected but untreated cells were performed to verify down-regulation of endogenous RIPK3. Detection of actin served as a loading control. One out of two experiments with similar results is shown. Error bars indicate the SDs from three parallel determinations. Asterisks indicate statistical significance (t-test), $***P \leq 0.001$.

It has been reported that phosphorylation of MLKL by RIPK3 is required for RIPK3-dependent necroptosis (Vanden Berghe *et al.* 2014). To clarify whether MLKL is also involved in the TRAIL-induced killing of tumor cells, MLKL was down-regulated exemplarily in U-937 and HT-29 cells. Similar to down-regulation of RIPK3, down-regulation of MLKL significantly reduced TRAIL- as well as TNF-induced regulated necrosis in both cell lines (Figure 52A). Furthermore, treatment with the MLKL inhibitor NSA resulted in comparable protection from TRAIL- or TNF-induced regulated necrosis in the analyzed human tumor cell lines (Figure 52B).

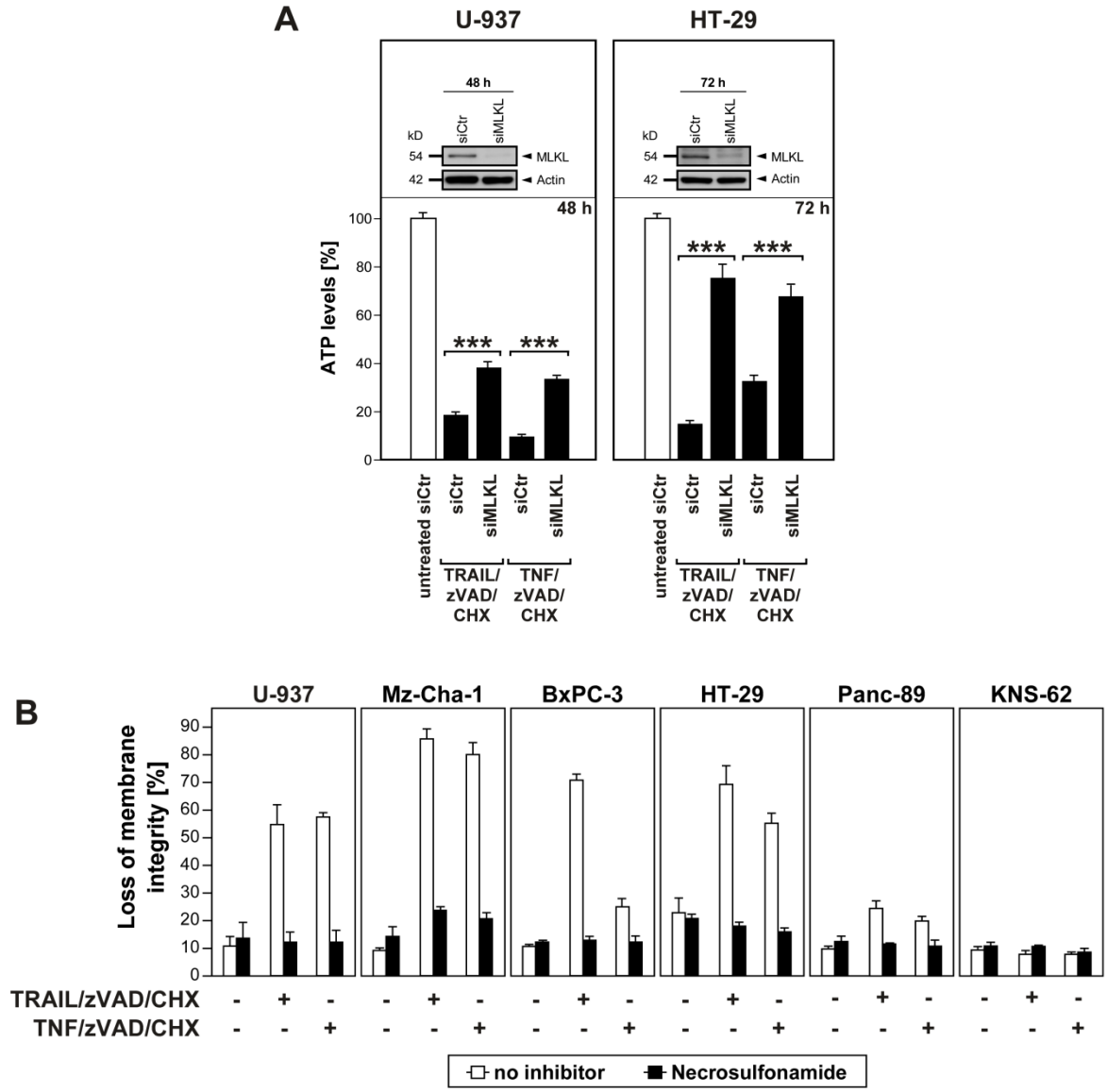

Figure 52: MLKL is a mediator of TRAIL-induced regulated necrosis. (A) U-937 and HT-29 cells were transfected with an siRNA specific for human MLKL. As a negative control, cells were transfected with non-targeting siRNA (siCtr). 48 or 72 h after transfection, cells were left untreated or incubated with 100 ng/ml TRAIL or TNF in combination with 50 µM zVAD-fmk and non-toxic concentrations of CHX (U-937 0.1 µg/mL; HT-29 5 µg/mL). After 24 h of stimulation, regulated necrosis was analyzed by measuring the decrease of intracellular ATP levels. ATP levels are shown relative to cells transfected with the negative control siRNA but not treated (untreated siCtr). Control Western blots of transfected but untreated cells were performed to verify down-regulation of endogenous MLKL. Detection of actin served as a loading control. One out of two experiments with similar results is shown. Error bars indicate the SDs from three parallel determinations. Asterisks indicate statistical significance (t-test), $***P \leq 0.001$. **(B)** Cells were treated with 100 ng/ml TRAIL or TNF in combination with 50 µM zVAD-fmk and non-toxic concentrations of CHX (U-937 0.1 µg/mL; Mz-ChA-1 2 µg/mL; BxPC-3 1 µg/mL; HT-29 5 µg/mL; Panc89 1 µg/mL; KNS-62 5 µg/mL) in the presence or absence of 1 µM necrosulfonamide. After 24 h of stimulation, regulated necrosis was analyzed by flow cytometric analysis of PI-positive cells. Each bar represents the means of two independent experiments with triplicate measurements. Error bars indicate the corresponding SD.

In summary, RIPK1, RIPK3 and MLKL were identified as mediators of not only TNF-, but also of TRAIL-induced regulated necrosis.

Ceramide mediates TRAIL/zVAD/CHX- and TNF/zVAD/CHX-induced regulated necrosis downstream of RIPK3

As described above, the lipase A-SMase is activated during necroptosis downstream of the RIPK1-RIPK3-MLKL complex. Furthermore, recent studies implicated ceramide generated by A-SMase as an important mediator of regulated necrosis induced by TRAIL (Thon *et al.* 2006). However, information on the impact of ceramide as a mediator of regulated necrosis in clinically more relevant tumor cell systems is currently unavailable. To further substantiate the established role of ceramide, tumor cells were treated with Arc39 to inhibit ceramide generation by A-SMase. Arc39 treatment inhibited regulated necrosis in U-937, Mz-ChA-1, BxPC-3, HT-29 and Panc89 cancer cells but not in the necroptosis-resistant cell line KNS-62 when treated with either TNF- or TRAIL/zVAD/CHX (Figure 53).

To investigate the role of RIPK3 not only for TNF-, but also for TRAIL-induced regulated necrosis and to study the position of ceramide in the RIPK3-mediated necroptotic signaling cascade, primary wild-type MEFs and RIPK3-deficient MEFs were treated with TNF/zVAD/CHX or TRAIL/zVAD/CHX to induce regulated necrosis. RIPK3-deficient MEFs but not wild-type MEFs were protected from TNF/zVAD/CHX- and TRAIL/zVAD/CHX-induced regulated necrosis. Likewise, Arc39 treatment protected wild-type MEFs from TNF- or TRAIL-induced necroptosis as did the deletion of RIPK3 in RIPK3-deficient MEFs (Figure 53). Furthermore, RIPK3-deficient MEFs were not further protected by Arc39 (Figure 53).

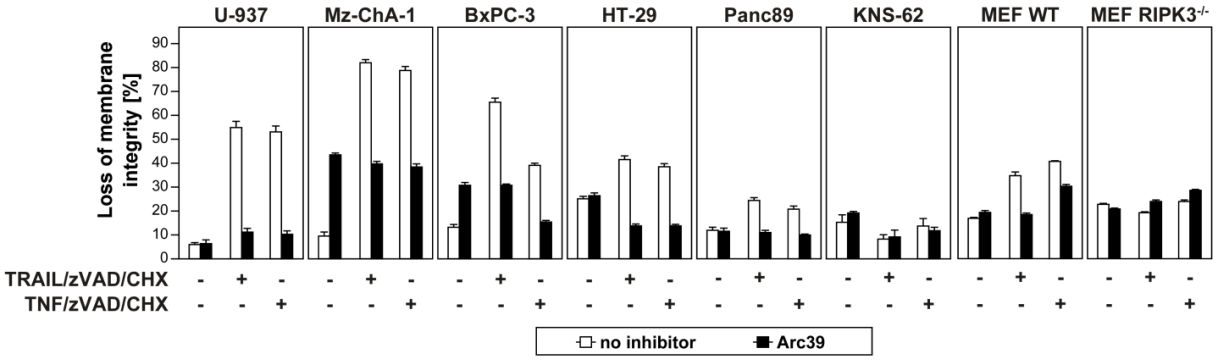

Figure 53: A-SMase activity is crucial for TRAIL- and TNF-induced regulated necrosis in human tumor cell lines. Cells were left untreated or were pre-incubated with 10 µM Arc39 for 2 h before 100 ng/ml of TRAIL or TNF in combination with 20 µM (wild-type (WT) or RIPK3-deficient (RIPK3-/-) primary MEFs) or 50 µM zVAD-fmk and non-toxic concentrations of CHX (U-937 0.1 µg/ml; Mz-ChA-1 2 µg/ml; BxPC-3 1 µg/ml; HT-29 5 µg/ml; Panc89 1 µg/ml; KNS-62 5 µg/ml; MEFs 1 µg/mL) were added. After 16 h (MEFs) or 24 h (all other cell lines) stimulation, cell death was analyzed by flow cytometry of PI-positive cells. Each bar represents the means of two independent experiments with three parallel measurements each. Error bars indicate the corresponding SD.

Moreover, after induction of necroptosis by TNF/zVAD, NIH3T3 cells naturally lacking RIPK3 ($RIPK3^{-/-}$) showed a diminished accumulation of intracellular ceramide levels when compared to NIH3T3 cells that are stably retransfected with wild-type RIPK3 ($RIPK3^{+/+}$). Almost identical results were obtained in TNF/zVAD-treated NIH3T3 cells stably retransfected with kinase-defective RIPK3 ($RIPK3^{D161N}$) (Figure 54). Altogether, the data obtained here suggest that ceramide generated by A-SMase acts downstream of RIPK3 as part of the same signal transduction pathway. The remaining ceramide accumulation after TNF/zVAD treatment in $RIPK3^{-/-}$ and $RIPK3^{D161N}$ NIH3T3 cells is possibly a result of the induction of apoptotic-like caspase-independent cell death pathways rather than an induction of necroptosis, because Newton and coworkers recently claimed that the absence of RIPK3 drives the signaling pathway towards apoptosis (Newton *et al.* 2014).

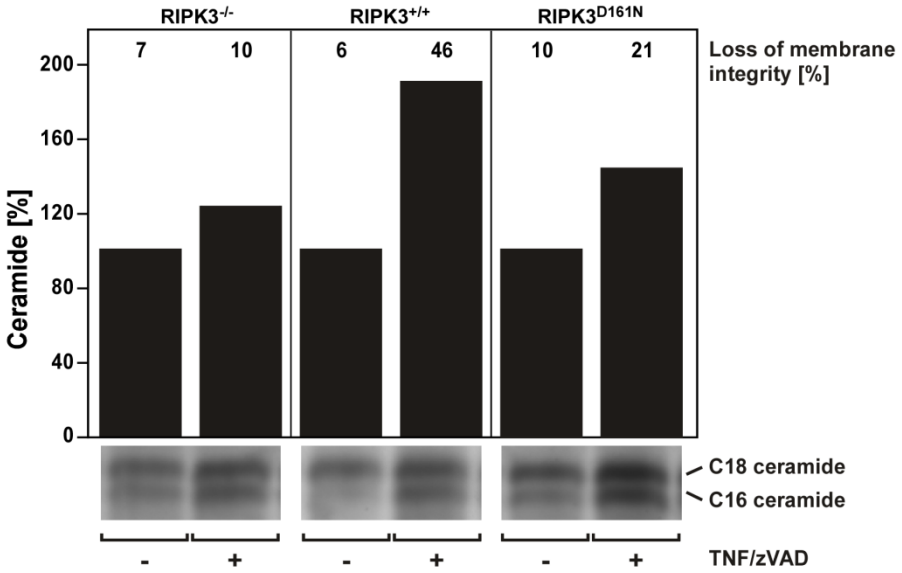

Figure 54: Ceramide mediates TNF/zVAD-induced regulated necrosis downstream of RIPK3. NIH3T3 cells naturally deficient of RIPK3 ($RIPK3^{-/-}$), NIH3T3 cells stably expressing transfected murine wild-type RIPK3 ($RIPK3^{+/+}$) or kinase-defective RIPK3 ($RIPK3^{D161N}$) were left untreated or were stimulated with 100 ng/mL TNF and 20 µM zVAD-fmk for 18 h before intracellular ceramide levels were determined in duplicate. Raw data from the charred thin layer chromatography plate (C16 and C18 ceramide species) are shown below the bar graphs. Loss of membrane integrity was determined by trypan blue staining and is shown above the respective bars. One out of three representative experiments is shown.

Induction of regulated necrosis by TRAIL/zVAD/CHX or TNF/zVAD/CHX reduces the clonogenic survival of tumor cells

To determine whether induction of regulated necrosis also can block the capacity of tumor cells for unlimited proliferation, measurements of the clonogenic survival were employed for the above selected tumor cell lines. As shown in Figure 55, treatment with TRAIL/zVAD/CHX reduced clonogenic survival with statistical significance in four out of the five sensitive cell lines (U-937 cells showed reduced clonogenic survival which was only slightly above the significance threshold of 0.05 with P=0.059). Surprisingly, even in the control cell line KNS-62, which had shown resistance to TRAIL-induced regulated necrosis in cytotoxicity assays conducted above (see Figure 49), the treatment with TRAIL/zVAD/CHX significantly reduced their clonogenic survival. Likewise, treatment with TNF/zVAD/CHX led to a reduction of clonogenicity in five out of the six tested tumor

cell lines. U-937, HT-29 and Panc89 cells showed a statistically significant reduction. KNS-62 cells were only slightly above the significance threshold with *P*=0.057. Altogether, these data confirm that induction of regulated necrosis by TRAIL or TNF can reduce the proliferative potential and thus the clonogenicity of tumor cells.

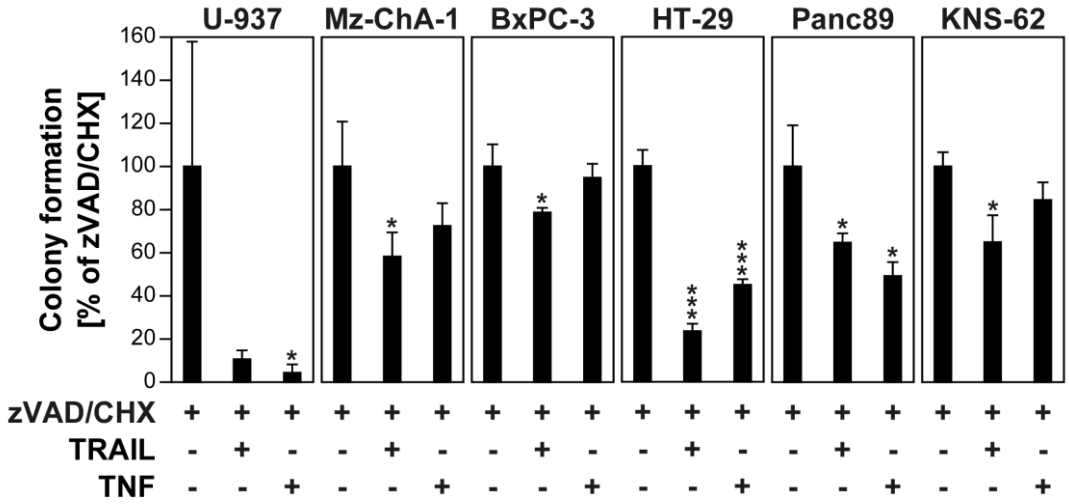

Figure 55: TRAIL- and TNF-induced regulated necrosis reduces clonogenic survival of tumor cells. Tumor cells were treated with 100 ng/ml of TRAIL or TNF in combination with 50 µM zVAD-fmk and non-toxic concentrations of CHX (U-937 0.1 µg/ml; Mz-ChA-1 2 µg/ml; BxPC-3 1 µg/ml; HT-29 5 µg/ml; Panc89 1 µg/ml; KNS-62 5 µg/ml). Subsequently, their ability to form colonies was analyzed by staining with crystal violet (or by soft agarose cloning for the non-adherent cell line U-937) after 7 days (see 4.2.2). Values represent the means from three independently counted wells per condition and error bars represent the corresponding SD. Treatment with zVAD/CHX (negative control) served as reference for calculation of colony formation as well as of *P* values. Asterisks indicate statistical significance (t-test), * $P \leq 0.05$, *** $P \leq 0.001$.

TRAIL-induced regulated necrosis synergizes with chemotherapy in the elimination of tumor cells

The application of TRAIL in combination with chemotherapeutic agents to induce apoptosis in tumor cells has been comprehensively investigated (Hellwig and Rehm, 2012). In contrast, a corresponding study for the induction of regulated necrosis in synergism with chemotherapeutic agents is not available. To alleviate this lack of information, four TRAIL-resistant (Colo357, PancTu-I, MKN-28, SK-Mel-28) and the tumor cell line A818-4 which showed only marginal induction of regulated necrosis (Figure 49) were analyzed in viability assays after treatment with the chemotherapeutic agents cisplatin, etoposide, trichostatin A, 5-fluorouracil, irinotecan, doxorubicin, camptothecin, or paclitaxel in combination with TRAIL/zVAD/CHX. The addition of chemotherapeutic agents significantly enhanced the cytotoxic effect of TRAIL/zVAD/CHX in four out of five tumor cell lines and in 28 out of a total of 40 chemotherapeutic/TRAIL/zVAD/CHX combinations (Figure 56). Notably, the cytotoxic response of the cell line A818-4 which had proven only marginally sensitive to TRAIL/zVAD/CHX treatment alone (Figure 49) was clearly further enhanced by the addition of chemotherapeutics (Figure 56). In summary, the results obtained here demonstrate that TRAIL synergizes with chemotherapeutic agents in the induction of regulated necrosis and that this treatment can overcome resistance against TRAIL-induced regulated necrosis.

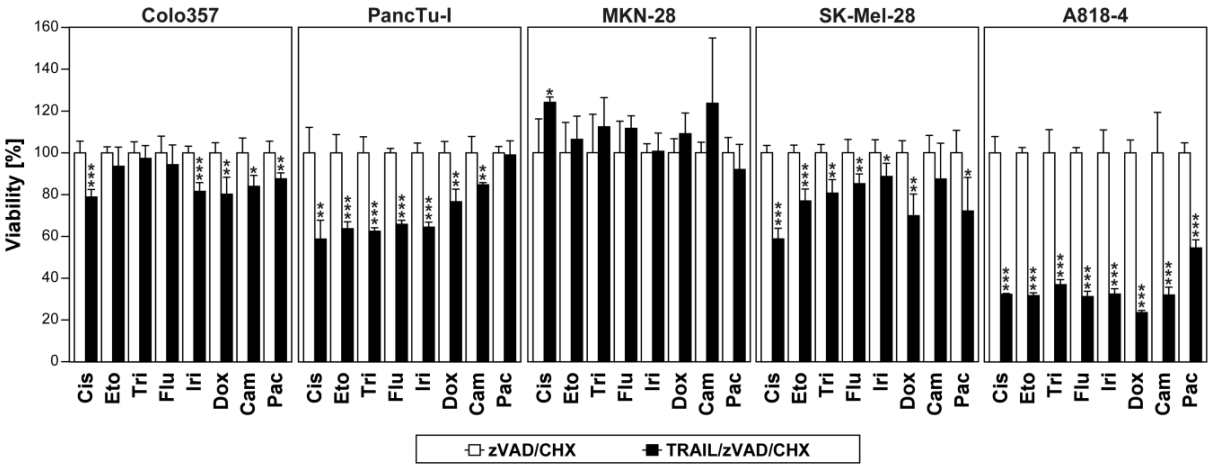

Figure 56: TRAIL-induced regulated necrosis synergizes with chemotherapy in the elimination of tumor cells. Cells were treated with 100 ng/mL TRAIL, 50 µM zVAD-fmk and non-toxic concentrations of CHX (Colo357, MKN-28 5 µg/mL, PancTu-I, SK-Mel-28, A818-4 10µg/mL) with additional application of cisplatin (Cis, 50 µM), etoposide (Eto, 20 µg/ml), trichostatin A (Tri, 100 ng/ml), 5-fluorouracil (Flu, 50 µg/ml), irinotecan (Iri, 1 µM), doxorubicin (Dox, 5 µg/ml), camptothecin (Cam, 10 µM), or paclitaxel (Pac, 1 µM). After 24 h of incubation, viability was measured by crystal violet staining. Treatment with zVAD/CHX (control) served as a reference for the calculation of p values. Viability is shown relative to cells treated with zVAD/CHX in combination with the respective chemotherapeutic agent. Asterisks indicate statistical significance (t-test), * $P \leq 0.05$, ** $P \leq 0.01$, *** $P \leq 0.001$. For each cell line, one out of two experiments with similar results is shown. Error bars indicate the SD from four parallel determinations.

Conclusion: TRAIL can induce regulated necrosis in human tumor cells

The obtained results demonstrate that TRAIL-induced regulated necrosis causes death in eight out of 14 tumor cell lines and that RIPK1, RIPK3 and MLKL are mediators of not only TNF-, but also of TRAIL-induced regulated necrosis. Furthermore, ceramide represents a pivotal factor downstream of RIPK3 in the execution of TRAIL- and TNF-induced regulated necrosis because the interference with the production of ceramide protected tumor cell lines from necroptosis. The findings also demonstrate that the induction of regulated necrosis impairs clonogenic survival of the clinically more relevant tumor cell systems employed here and that TRAIL synergizes with chemotherapeutics in killing tumor cell lines via regulated necrosis.

6. Discussion

The impact of caspase-independent, non-apoptotic PCD such as necroptosis/regulated necrosis has become the focus of international research over the last years. This is particularly true for pathological processes which are linked to regulated necrosis, such as hyperacute shock (Cauwels *et al.* 2003), pancreatitis (He *et al.* 2009; Zhang *et al.* 2009), cerebral and myocardial ischemia-reperfusion injury (Linkermann *et al.* 2013), Crohn's disease (Günther *et al.* 2011), Alzheimer's disease (Lin and Beal, 2006) and photoreceptor cell loss (Viringipurampeer *et al.* 2014). Moreover, pathogens such as HIV, vaccinia virus, Shigella and Salmonella (Festjens *et al.* 2006; Cho *et al.* 2009) can destruct cells via regulated necrosis. The possibility of therapeutic interference with necroptosis/regulated necrosis has raised great expectations for the near future. In consequence, a better knowledge of the still incompletely understood signaling pathways of the different modes of regulated necrosis, the associated components and the distinct executioner mechanisms will facilitate future strategies to interfere with damage induced by necroptosis/regulated necrosis (e.g. in shock, pancreatitis, ischemic damage or neurodegenerative diseases) to eliminate apoptosis resistant cancers.

6.1 TNF-induced necroptosis and PARP-1-mediated necrosis elicit distinct routes to regulated necrosis

Future therapeutic interventions, however, require a better knowledge of the signaling pathways of regulated necrosis. In previous studies, it was reported that the PARP pathway represents an integral part of TNF-induced necroptosis (Los *et al.* 2002, Vandenabeele *et al.* 2010). The results obtained in the study presented here, however, clearly indicate that TNF-induced necroptosis and the PARP pathway represent two distinct routes to regulated necrosis and that they operate separately from each other. This was substantiated by the observations that PARP-1 inhibition did not alter TNF-induced necroptosis, whereas the MNNG-induced PARP pathway was blocked.

Furthermore, the hyperactivation of PARP-1 involves the activation of JNK (Vandenabeele *et al.* 2010) and in this thesis, the interference with JNK as a further component of the PARP pathway revealed that JNK have no role in TNF-induced necroptosis. The revalidated concept that TNF-induced necroptosis and PARP-1-mediated regulated necrosis are distinct and independent routes to regulated necrosis is additionally supported by data of Seok and coworkers who demonstrated that JNK activation by DNA-alkylating agents occurs in a TNF-independent manner (Seok *et al.* 2008). Two other and independent studies were also not able to show a link of JNK activation to TNF-induced necroptosis in multiple cell systems (Lin *et al.* 2003; Wicovsky *et al.* 2007). On the other hand, a role of JNK in the PARP pathway was recently described based on genetic knockouts and pharmacological inhibition studies (Xu *et al.* 2006).

AIF a downstream factor of the PARP pathway was reported to be cleaved by calpains and/or cathepsins to yield truncated AIF (tAIF). Subsequently, tAIF relocates from the mitochondria to the cytosol and nucleus, where it evokes chromatinolysis and PCD (Artus *et al.* 2010). The results obtained here showed that calpain or cathepsin proteases are not crucial for the induction of TNF-induced necroptosis in U-937 cells which is in line with previous findings obtained in other cell lines (Thon *et al.* 2005, Sosna and Voigt *et al.* 2013; Sosna, Voigt *et al.* 2014). Identical to the results presented here, the inhibition of cathepsins B, L, H, or D as further components of the PARP pathway (Artus *et al.* 2010) did not affect TNF-induced necroptosis in murine hepatocytes (Dünstl *et al.* 2007). Furthermore, this thesis shows that cathepsin D-deficient MEFs can undergo TNF-induced necroptosis. Of note, cathepsin D-deficient MEF were not protected from MNNG-induced regulated necrosis in comparison to their wild-type counterparts or to cathepsin D-deficient MEFs ectopically re-expressing cathepsin D in the study presented here, suggesting that cathepsin D plays also no role in either TNF-induced necroptosis or in the PARP pathway.

On the other hand, interference with components of the necroptosis pathway (e.g. RIPK3) did not impair regulated necrosis elicited by the PARP pathway. In reverse approaches interfering with components of TNF-induced necroptosis Xu and coworkers reported that treatment with Nec-1 did not protect murine hippocampal HT-22 cells from MNNG-induced regulated necrosis (Xu *et al.* 2010). Furthermore, necroptosis-resistant HeLa cells were still sensitive to MNNG-induced necrosis (Andrabi *et al.* 2006). Moreover, the results obtained in the study presented here and further independent work in the laboratory by Sosna and coworkers (Sosna, Voigt *et al.* 2014) demonstrated that any role of RIPK1 or RIPK3 in the PARP pathway cannot depend on signals mediated by TNF-R1. The described contribution of RIPK1 and RIPK3 was rather cell-type specific and only of limited impact which is in contrast to the essential function of RIPK1 and RIPK3 in TNF-induced necroptosis. These observations are also consistent with the studies by Xu *et al.* (2010) and Chiu *et al.* (2011) but nevertheless, this additional function of RIPK1 and RIPK3 in PARP-1-induced cell death is independent from TNF-induced necroptosis. In summary, in TNF-induced necroptosis, RIPK1 and RIPK3 play an essential and cell-type-independent role in the initial steps of the death response. In contrast to that, their contribution to MNNG-induced regulated necrosis is of limited importance and cell-type-specific, and does not occur at the initial, but rather in the late steps of the PARP-pathway.

In conclusion, this thesis provides a first answer to the question whether there is one core program or several independent pathways of regulated necrosis. As a consequence of the results obtained in the study presented here, a simultaneous rather than an individual application of highly specific necroptosis (e.g. Nec-1 or NSA) and PARP-1 inhibitors (e. g. olaparib) might be the approach of choice for the future possibly resulting in an improved treatment of damage induced by regulated necrosis (e.g. in shock, pancreatitis, ischemic damage or neurodegenerative diseases).

6.2 Identification of proteases and proteolytic substrates involved in TNF-induced necroptosis

The results obtained in the study presented here demonstrated that the inhibitor of chymotrypsin-like serine proteases TFCK significantly protected murine L929Ts and NIH3T3 cells, human Jurkat cells and its subline I42 as well as HT-29 and U-937 cells from TNF-induced necroptosis. This is in line with a previous study by Vercammen and coworkers showing a protective effect of TFCK on TNF-induced regulated necrosis in L929 cells (Vercammen *et al.* 1997), and in summary clearly shows that proteolytic processes participate in TNF-induced necroptosis.

However, the inhibitors of the cysteine proteases cathepsin L (zFF-fmk), cathepsin B/L (zFA-fmk), and the broad spectrum calpain/cysteine protease inhibitor E-64 did not protect U-937 cells from TNF-induced necroptosis. This is in line with previous studies showing that inhibitors of cysteine proteases and of calpain/cysteine proteases did not protect L929Ts cells from TNF-induced necroptosis (Thon *et al.* 2005, 2006; Sosna and Voigt *et al.* 2013). However, during regulated necrosis, cytotoxic hydrolases such as Ca^{2+}-dependent calpains destabilize lysosomal membranes (Vanlangenakker *et al.* 2008), suggesting that these proteases nevertheless contribute to some extent to cellular events associated with regulated necrosis but maybe not specifically in necroptosis.

In contrast to the other cysteine protease inhibitors utilized, the cathepsin B inhibitor Ca-074Me showed protection from necroptosis in U-937 cells. So far this was not observed in other cell lines undergoing necroptosis (Sosna and Voigt *et al*. 2013). Previous studies examining cathepsin B functions found that cathepsin B is a component of the TNF-induced apoptotic cell death pathway (Guicciardi *et al.* 2000) and under caspase-inhibiting conditions, cathepsin B was shown to process cellular proteins leading to regulated necrosis (Hentze *et al.* 2003). Furthermore, it was shown that the inhibitor Ca-074Me abrogated staurosporine-induced necrotic cell death in leukemia cells and that this is independent of its inhibitory effect on cathepsin B (Mihalik *et al.* 2004). This indicates that the inhibitor Ca-074Me has a cathepsin B-independent target that may play a role in necroptosis upstream of lysosomal breakdown. The same group found that Ca-074Me protected U-937 cells from staurosporine-mediated regulated necrosis by stabilizing the lysosomal compartment and thereby preventing rupture of the plasma membrane of the cells (Dunai *et al.* 2012).

Treatment of U-937 cells with the proteasome inhibitor MG-132 and the acid protease inhibitor pepstatin A did not protect cells from necroptosis elicited by TNF but rather enhanced regulated necrosis. MG-132 was shown to reduce the degradation of ubiquitin-conjugated proteins and to potentiate TRAIL-induced apoptosis (Sung *et al.* 2012). In contrast to that, a study by Volbracht and coworkers showed that proteasome inhibitors reduce regulated necrosis in neurons (Volbracht *et al.* 2001) suggesting that the inhibition of the proteasome has distinct effects in different tissues or cell types. Pepstatin A is a well-known inhibitor of aspartic proteases such as pepsin, cathepsin D and

cathepsin E. Shacka and coworkers showed that cathepsin D-deficiency induces caspase-independent neuron death resulting from the disruption of lysosome function (Shacka *et al.* 2007). A study investigating photoreceptor cell loss showed protective functions of cathepsin D during photoreceptor degradation (Chahory *et al.* 2004). These studies provide indications that non-toxic concentrations of MG-132 and pepstatin A have an impact on degradation processes and may therefore potentiate necroptotic cell death by inhibiting, e.g. subunits of the proteasome or the aspartic acid protease cathepsin D.

Although metalloproteases are involved in early tumorigenesis and are used as prognostic marker, for e.g., lung, colorectal, breast and prostate cancer (Hadler-Olsen *et al.* 2013), broad spectrum metalloproteases inhibitors utilized in this study did not protect from TNF-induced necroptosis, suggesting a minor impact of metalloproteases during necroptosis.

6.2.1 HtrA2/Omi, Lon protease 1, PSA1 and PMPCA are TFCK-sensitive serine proteases identified during necroptosis

The proteomic screen to discover the TFCK-sensitive serine protease(s) responsible for TNF-dependent necroptosis identified HtrA2/Omi as a possible mediator of TNF-induced necroptosis. This is corroborated by additional results linking HtrA2/Omi and the cysteine protease UCH-L1 to TNF-induced necroptosis (Sosna and Voigt *et al.* 2013). The HtrA2/Omi protein is highly conserved and is the mammalian homologue of the bacterial HtrA2 endoprotease. Degradation of proteins misfolded during cellular stress (e.g. ER stress, heat shock and ischemia/reperfusion) was found to be HtrA2/Omi-dependent (Gray *et al.* 2000). In mouse models, the deletion of HtrA2/Omi has been associated with neurodegeneration and Parkinson's disease (Martins *et al.* 2004). Neurodegeneration was also found in patients harboring mutations in the HtrA2/Omi gene affecting the activity of this enzyme (Vande Walle *et al.* 2008). During apoptosis, HtrA2/Omi is released from the mitochondria into the cytoplasm. HtrA2/Omi promotes apoptosis by interacting with the caspase-inhibitor XIAP and thereby induces enhanced caspase activity (van Loo *et al.* 2002). Together with members of the IAPs family, the caspase-8 inhibitor phosphoprotein enriched in astrocytes 15 (Pea-15; Trencia *et al.* 2004) and the anti-apoptotic protein HCLS1-associated protein X-1 (HAX-1; Cilenti *et al.* 2004) are substrates of HtrA2/Omi and are cleaved during apoptosis. HtrA2/Omi can not only induce apoptosis but it was also reported that HtrA2/Omi can mediate regulated necrosis by its serine protease activity upon interleukin-3 deprivation of the mouse pro-B cell line Ba/F3 (Vande Walle *et al.* 2010), or in cytomegalovirus infection (McCormick *et al.* 2008) and in imatinib mesylate-treated human leukemic cells (Okada *et al.* 2004). However, the molecular details how HtrA2/Omi participates in and which substrates are cleaved by HtrA2/Omi during necroptosis are unknown. Only one study, investigating substrates cleaved by HtrA2/Omi during regulated necrosis, reports the cleavage and inactivation of the substrate RIPK1 by HtrA2/Omi (Vande Walle *et al.* 2010). Other reports show that, in contrast to apoptosis, HtrA2/Omi is not released from mitochondria during TNF-induced necroptosis (van Loo *et*

al. 2002; Blink *et al.* 2004). This is also consistent with preliminary experiments not detecting HtrA2/Omi as part of the necroptotic TNF-R1 signaling complex (data not shown; experiments by Vladimir Tchikov, Christian-Albrechts-University, Kiel, Germany). Furthermore, the data in the study presented here showed that the pharmacological inhibition of HtrA2/Omi by Ucf-101 or genetic deletion of HtrA2/Omi fully protects from TNF-induced necroptosis in a panel of murine and human cell lines. In HT-29 cells, protection from TNF-induced necroptosis was less pronounced but nevertheless visible when incubated with Ucf-101, suggesting a cell line-specific alteration in the signaling pathway. Because HT-29 cells were significantly protected from necroptosis elicited by TNF when treated with TFCK, a distinct serine protease might substitute for HtrA2/Omi activity in HT-29 cells. In addition, the parallel incubation of L929Ts cells with TFCK and Ucf-101 did not result in a complete protection of the cells from TNF-induced necroptosis. These observations suggest that both inhibitors function by the same signaling pathway and may both bind to HtrA2/Omi or further serine proteases are involved in regulated necrosis. Altogether, the above described findings not only identified the TFCK-sensitive serine protease HtrA2/Omi as a possible mediator of TNF-induced necroptosis but also substantiate the crucial role of HtrA2/Omi in the execution of TNF-dependent necroptosis.

Furthermore, a second TFCK-sensitive serine protease was identified. The mitochondrial Lon protease 1 plays a role in protein quality control and in stress response signaling pathways (Venkatesh *et al.* 2012). Furthermore, Lon protease serves as a chaperone for mitochondrial protein complex assembly (Rep *et al.* 1996) and it can bind to DNA or RNA and can thereby modulate transcription or translation (Liu *et al.* 2004). In a previous study, Lon protease down-regulation in human lung fibroblasts caused massive apoptosis in the early phase of transfection and this was accompanied by ATP depletion caused by severe mitochondrial defects. Subsequently, the cells underwent a necrotic type of cell death (Bota *et al.* 2005). Moreover, Lon protease has already been associated with tumorigenesis by ROS production (Cheng *et al.* 2013). However, in the study presented here, the down-regulation of human Lon protease did not result in an increase of TNF-induced necroptosis in HT-29 and U-937 cells. One possible explanation for this result could be that the achieved reduction of Lon protease expression was not sufficient to enhance the death response. The characterization of Lon protease action during TNF-induced necroptosis should be further investigated by applying specific inhibitors for Lon protease or by utilizing cells completely deficient of Lon protease.

The proteasomal protein proteasome subunit alpha type-1 (PSA1) was also identified as a TFCK-sensitive serine protease in murine L929Ts cells. Consistent with this finding, several serine protease inhibitors, among them TFCK and Pefabloc, have been shown to non-selectively inhibit the proteasome which has two chymotrypsin-like active sites (Kisselev *et al.* 1999; King *et al.* 2004). The identification of proteasomal proteins is in line with a study by Egger and coworkers who found

different proteasomal subunits in the TFCK-enriched fraction during a screen for serine proteases responsible for ER stress-induced cell death. Moreover, PSA1 was also identified in proteasomal pull-down experiments performed by Egger and coworkers (Egger *et al.* 2007), suggesting that the identification of PSA1 in this thesis was specific. Down-regulation of PSA1 did not result in inhibition or enhancement of TNF-induced necroptosis in HT-29 cells. This is in contrast to U-937 cells where down-regulation of PSA1 lead to an increased loss of membrane integrity compared to control transfected cells. PSA1 was recently described to be involved in sensitization of bortezomib-resistant leukemia cells (Fang *et al.* 2012), suggesting cell-type and species-specific functions of PSA1 during TNF-induced necroptosis.

The results of the experiments to isolate TFCK-sensitive serine proteases performed during this thesis, however also showed that most of the labeled protein spots were non-proteases. This might be due to the limited specificity of the chymotrypsin-like serine protease inhibitor TFCK. Notably, the mitochondrial-processing metallopeptidase subunit alpha (PMPCA, also abbreviated as MPP-A) was also found during the identification of serine proteases responsible for TNF-induced necroptosis, although the metallopeptidase PMPCA should not be bound by the serine protease-specific inhibitor TFCK. So far, it is unclear whether the identification of PMPCA was unspecific or not. Nevertheless, down-regulation of PMPCA in HT-29 and U-937 cells showed an increase in cell death, thus suggesting that PMPCA might be a novel protease participating in TNF-induced necroptosis. A connection between PMPCA and Lon protease might be possible, because unassembled PMPCA subunits are degraded by mitochondrial Lon protease (Ondrovicova *et al.* 2005). Like Lon protease, PMPCA is a quality control enzyme completely degrading misfolded proteins. On the other hand, PMPCA can also act as a processing enzyme specifically cleaving mitochondrial proteins with regulatory functions during cell death, such as processing of the dynamin-like GTPase optic atrophy 1 protein (OPA1; Ishihara *et al.* 2006).

6.2.2 Five novel proteases enhance TNF-induced necroptosis

A complementary siRNA screen of all proteases encoded by the human genome identified 10 proteases with pronounced (and six candidates with less pronounced) effects (see Table 4) which were distinct from the identified in 5.2.1 as TFCK-sensitive serine protease(s) responsible for TNF-dependent necroptosis. Remarkably, the best candidates were caspase-8, CYLD and c-FLIP, proteins that represent key regulators of necroptosis (Kaczmarek *et al.* 2013). The other proteases (DESC, GGT1, DPYL4, PRPF8, MMP3) investigated in this study showed enhanced necroptosis upon down-regulation in HT-29 cells and in U-937 cells. The identification of the above proteases as regulators of necroptosis is consistent with the reported functions of these proteases in anti-apoptotic or pro-tumorigenic processes. In particular, the transmembrane serine protease DESC1 confers tumorigenic properties and is upregulated in tumors of different origin (Viloria *et al.* 2007). The threonine protease GGT1 is upregulated by the oncogene K-Ras (and also by TNF). GGT1 enhances the expression of

pro-apoptotic molecules and down-regulates the expression of anti-apoptotic molecules, and can thereby overcome apoptotic signals (Boonyanugomol *et al.* 2012). The metalloprotease DPYL4 is a target of the tumor suppressor p53 in the apoptotic response to DNA damage (Kimura *et al.* 2011). The metalloprotease PRPF8 shares high homology with ARP2, involved in cell death (Tapia-Vieyra *et al.* 2005) and the matrix metalloproteinase MMP3 participates in tumor initiation (Sternlicht *et al.* 1999) and is involved in cancer progression and tissue remodeling (Si-Tayeb *et al.* 2008). Moreover, nuclear MMP3 can induce apoptosis via its catalytic activity (Si-Tayeb *et al.* 2008). Although down-regulation of YME1L1 showed no effect in both cell systems (as detected by ATP level measurements and flow cytometry), YME1L1 might play a role in regulated necrosis. Like Lon protease 1, YME1L1 is part of the mitochondrial ATPases associated with diverse cellular activities (AAA) complex. The AAA complex exerts peptidase, chaperone-like and translocase activities on the intermembrane space side of the inner mitochondrial membrane (Stiburek *et al.* 2012). One substrate of YME1L1 is the dynamin-like GTPase OPA1 (Griparic *et al.* 2007) which can also be processed by PMPCA (Ishihara *et al.* 2006). OPA1 is localized in the mitochondrial intermembrane space side and during apoptosis OPA1 is proteolytically cleaved by AAA, released into the cytosol and causes fragmentation of mitochondria (Griparic *et al.* 2007). However, the precise role of YME1L1 and of the other proteases identified here in regulated necrosis, and in particular, in necroptosis is unknown and should be investigated in the future.

Surprisingly, the data obtained by the siRNA screen indicate a differential proteolytic regulation of necroptosis by caspase-8 in humans. In the study presented here, caspase-8 down-regulation resulted in a protection of human HT-29 cells from TNF-induced necroptosis. Furthermore, the down-regulation of caspase-8 was also protective in human U-937 cells measuring ATP levels. However, protection of U-937 cells after down-regulation of caspase-8 was not observed after PI-staining. This observation was not in line with later experiments using individual siRNAs (data not shown), suggesting off-target effects of the used mixture of four siRNAs targeting caspase-8 in U-937 cells. Nevertheless, the observation that caspase-8 down-regulation protects rather than enhances necroptotic cell death elicited by TNF is in contrast to the overall view that caspase-8 suppresses necrosome-dependent necroptosis (Holler *et al.* 2000; Cho *et al.* 2009; He *et al.* 2009, Zhang *et al.* 2009). In mice, FADD, caspase-8 and $FLIP_L$ counteract RIPK1- and RIPK3-dependent necroptosis during development, because embryonic lethality in mice lacking FADD or caspase-8 can be rescued by RIPK1 or RIPK3 deletion (Kaiser *et al.* 2011; Oberst *et al.* 2011; Zhang *et al.* 2011). Down-regulation of caspase-8 or FADD in L929Ts cells potentiated necroptosis elicited by TNF (Vanlangenakker *et al.* 2011b). However, interpretation of these studies has to be performed with caution, because they present work from murine systems. Unlike mice, humans have two initiator caspases, caspase-8 and caspase-10. Human caspase-10 has close homology to human caspase-8 (Fernandes-Alnemri *et al.* 1996) and functions as an initiator caspase in DR-mediated signaling (Sprick *et al.* 2002). Caspase-10 has overlapping substrate specificities with caspase-8 (Fischer *et al.* 2006) and similar to caspase-8,

caspase-10 was reported to play a role in viral infection (Takahashi *et al.* 2006). Kischkel and coworkers showed that both caspase-8 and caspase-10 can function independently of each other during ligand-induced apoptosis (Kischkel *et al.* 2001). The reported observations together with the results obtained in the study presented here raise the question whether the roles of these two related enzymes are redundant or whether they have distinct or complementary functions during necroptosis. Another issue which has to be discussed is the fact that the broad spectrum inhibitor of caspases zVAD-fmk was always present raising the question why loss of caspase-8 expression still has an impact on necroptosis. A study by Kadohara and coworkers could demonstrate that caspase-8 is able to mediate the mitochondrial release of pro-apoptotic proteins in a proteolysis-independent manner (Kadohara *et al.* 2008). Accordingly, the protective effect of caspase-8 down-regulation in human cancer cell lines during necroptosis might be due to novel scaffolding functions of caspase-8, and maybe caspase-10.

To investigate the contribution of the identified proteases in regulated necrosis, the metalloprotease MEP1B was further characterized. However, in preliminary experiments in the study presented here, no effects of the two broad-spectrum metalloprotease inhibitors GM6001 and marimastat were observed during TNF-induced necroptosis. Nevertheless, in the study presented here, cell death levels were decreased after down-regulation of MEP1B in U-937 cells. On the other hand, this was not observed in HT-29 cells, suggesting a cell-type-specific involvement of MEP1B during TNF-induced necroptosis. In contrast to that, HT-29 cells transiently transfected with wild-type MEP1B showed enhanced cell death rates compared to non-transfected cells after TNF/zVAD/CHX stimulation. Cells expressing a catalytically inactive MEP1B mutant also showed increased cell death levels during necroptosis. In conclusion, the analysis of MEP1B function suggests that MEP1B plays a role in the execution of TNF-induced necroptosis. Nevertheless, these preliminary data should be substantiated by loss of gene function studies and by studying the effects of MEP1B-specific inhibitors. Furthermore, the role of MEP1B in mediating ischemia-reperfusion injury under caspase-independent conditions should be investigated, because meprin inhibition is protective from renal hypoxia-reoxygenation injury (Carmago *et al.* 2002) and regulated necrosis is linked to ischemia-reperfusion injury (Linkermann *et al.* 2013).

6.2.3 Newly identified signaling components of TNF-induced necroptosis

Cell surface receptors are activated after binding to their ligands, transmit intracellular signals and generate a signaling cascade. In the last decade, it has become clear that signal transduction pathways may require receptor internalization for signal transduction (McPherson *et al.* 2001). TNF-R1 internalization was shown to be essential for the initiation of apoptosis (Schütze *et al.* 1999; Schneider-Brachert *et al.* 2004). In the presented thesis, the internalization capability of TNF-R1 under conditions of caspase-inactivity was confirmed in U-937 cells by flow cytometry. Immunofluorescence detection of TNF-R1 in L929Ts and U-937 cells revealed a time-dependent appearance of endocytic vesicles harboring the TNF-R1 molecules. In the presented study, immuno-

magnetic isolation of cell surface TNF-R1 was performed to detect new or known proteins differentially expressed or even cleaved during necroptosis. The method allows the monitoring of the temporary maturation and distribution of specific proteins involved in intracellular signaling from intracellular compartments (Tchikov *et al.* 2014). The receptors are isolated in their native membrane environment in the absence of any detergent and the gentle physical homogenization procedure should preserve the morphology and functional integrity of the compartments (Tchikov *et al.* 2014). The analysis of the immuno-magnetically enriched necroptotic TNF-R1 containing vesicles from L929Ts and U-937 cells revealed the accumulation of the proteins RIPK1 and RIPK3 to the receptor during necroptosis. This is in line with the reported signaling cascade of TNF-induced necroptosis (Vanden Berghe *et al.* 2014). Isolated magnetic TNF-R1 fractions contained Rab5, a marker of early endosomes, and accumulated lysosomal proteins. In contrast to apoptosis, TNF/zVAD stimulation revealed early accumulation of LAMP proteins within the magnetic TNF-R1 containing vesicles, suggesting an early fusion of lysosomes with TNF-R1 containing vesicles during necroptotic cell death. However, to clearly prove that the isolated magnetic fractions are intact subcellular compartments and are fused at early time-points to lysosomes, the fractions should be analyzed by electron microscopy.

Next, to find protease targets during necroptosis, a 2D-DIGE approach following MS analysis was performed. This approach revealed that cofilin-1 (CFL-1) protein levels were consistently increased in cellular extracts of U-937 cells undergoing necroptosis. The actin-binding protein CFL-1 disassembles actin filaments and reorganizes the cytoskeleton. During cell death, cytoskeleton-associated proteins play a role in connecting TNF signaling to actin reorganization. For example, the death-associated protein kinase (DAPK) phosphorylates LIM domain kinase 1 and its downstream target CFL-1. Upon phosphorylation, CFL-1 possibly acts as a scaffold and as a trigger for actin reorganization and detachment of the cell (Ivanovska *et al.* 2013). During oxidative stress in T cells, CFL-1 is oxidized and provokes a stiff actin cytoskeleton and T-cell death. Oxidation of CFL-1 leads to its translocation/accumulation to the mitochondria and with that to the execution of regulated necrosis (Wabnitz *et al.* 2010) which possibly explains the finding of increased protein levels of CFL-1 during TNF-induced necroptosis in the 2D-DIGE analysis. Furthermore, Wabnitz and coworkers assume that oxidized CFL-1 interferes with mitochondrial functions and thus energy depletion does not involve the Bcl-2 family (Wabnitz *et al.* 2010). The 2D-DIGE analysis showed that the major constituent of microtubules tubulin alpha-1B chain (TUBA1B) and the glycolytic enzyme pyruvate kinase isozymes M1/M2 (PKM) showed decreased protein levels in cells undergoing necroptosis. TUBA1B was found to be upregulated in small cell lung cancer tissues (Jeong *et al.* 2011), suggesting a protective role of TUBA1B during cell death. To overcome this protective role, protein levels of TUBA1B might be therefore decreased during necroptosis. It was reported that upon translocation of the tumor marker PKM to the nucleus, PCD is induced in a caspase-independent manner (Stetak *et al.* 2007). This might explain the low protein levels of PKM after induction of necroptosis in the isolated TNF-containing

vesicles (because PKM is already in the nucleus). The protein levels of the two dehydrogenases inosine-5'-monophosphate dehydrogenase 2 (IMPDH2) and D-3-phosphoglycerate dehydrogenase (PHGDH) were found to be increased in magnetic TNF-R1 fractions isolated from cells undergoing necroptosis. Mantle cell lymphoma cells, a rare aggressive type of B-cell non-Hodgkin's lymphoma, are resistant to TRAIL treatment which is associated with a decreased expression of three key enzymes of purine nucleotide metabolism, namely purine nucleoside phosphorylase, adenine phosphoribosyltransferase and IMPDH2 (Pospisilova *et al.* 2013). These enzymes have profound effects on nucleotide homeostasis and IMPDH2 among others might have pro-necrotic functions during regulated necrosis. Resistance to cell death and an increased glucose catabolism are hallmarks of cancer. Moreover, cancer cells adapt their metabolic processes to induce rapid cell growth and proliferation. PHGDH is involved in the serine biosynthesis pathway and PHGDH protein levels are elevated in 70 % of estrogen receptor-negative breast cancers patients. The suppression of PHGDH does not affect intracellular serine levels but causes increased α-ketoglutarate levels (Possemato *et al.* 2011). However, in the study presented here, PHGDH was found to be upregulated in U-937 cells undergoing necroptosis. This is in contrast to the observations that, for example, GLUD1, a mitochondrial enzyme converting glutamate into α-ketoglutarate, is hyperactivated by RIPK3 and the execution of necroptosis is dependent on the excessive generation of α-ketoglutarate (Mates *et al.* 2009). Therefore, the role of PHGDH has to be substantiated by loss of gene function studies and by studying the effects of PHGDH-specific inhibitors. The 2D-DIGE analysis revealed that the peroxisome enzyme catalase (CAT) showed lower protein levels in necroptotic cells. The rapid decomposition of harmful H_2O_2, a byproduct of many metabolic processes within the cell, is an important physiological process to prevent damage of cells and tissues. Yu and coworkers reported that caspase inhibition induces catalase degradation and thereby ROS accumulation and non-apoptotic PCD (Yu *et al.* 2006). Since the accumulation of ROS is crucial for the execution of regulated necrosis, catalase might be an important substrate for proteolytic cleavage during necroptosis. The 2D-DIGE proteomic approach provided evidence that the structural constituent of the cytoskeleton moesin is a target of proteolytic cleavage. However, at present there are no studies available showing moesin cleavage as a result of PCD. Similar to moesin, the cleavage of the protein stathmin should be verified by Western blot analysis of cleavage fragments.

However, only two cleaved proteins were identified and already known protease substrates during regulated necrosis such as RIPK1 or Bid (Mocarski *et al.* 2011; Heibein *et al.* 2000; Lorenzo and Susin, 2007) were not detected by the analysis conducted here. One explanation can be given by the kinetics of proteolysis. In response to TNF-induced necroptosis, proteolysis might vary from protein to protein and certain proteomic changes might not be detected at the 20 min time-point studied here, but could occur earlier or later. Furthermore, some changes in molecular weight of proteins due to proteolysis might be masked by other proteins over-represented in the 2D gel and small peptide fragments resulting from proteolytic cleavage might be under-represented and excluded.

Consequently, the 2D-DIGE analysis should be repeated for further time-points and different protein levels, and also should be confirmed by means of quantitative real-time PCR or Western blot. Alternatively, the non-gel-based technique iTRAQ (isobaric tag for relative and absolute quantification; Ross *et al.* 2004) could be conducted to study proteomic changes simultaneously at different time-points of TNF-induced regulated necrosis.

In summary, the use of the 2D-DIGE approach revealed insight into cellular events leading to necroptosis and identified proteins whose aberrant regulation may contribute to the induction and execution of regulated necrosis. The proteins identified here provide exciting new resources to further unravel the mechanisms of regulated necrosis caused by TNF stimulation.

6.2.4 PGAM5 is constitutively degraded under physiological conditions

Necroptosis critically relies upon the signaling molecule MLKL (Sun *et al.* 2012, Wu *et al.* 2013) which promotes necroptosis by activating PGAM5 and Drp-1, leading to mitochondrial fragmentation (Wang *et al.* 2012). Remarkably, in the study presented here, down-regulation of PGAM5 and Drp-1 did not affect necroptosis. This is in line with a study by Remijsen and coworkers showing that down-regulation of RIPK1, RIPK3 or MLKL diminishes TNF-induced necroptosis in murine cells, whereas repression of PGAM5 and Drp-1 has no or only marginal effects on the induction of necroptosis (Remijsen *et al.* 2014). These observations suggest that Drp-1 and PGAM5 are no essential factors for TNF-induced necroptosis but may support i.e. mitochondrial fragmentation during necroptosis.

In apparent contrast to this is the observation that PGAM5 protein levels increased upon induction of necroptosis, visualized in the study presented here by Western blot. A similar enrichment of PGAM5 levels was observed when protease inhibitors were applied, suggesting a constitutive degradation of the potentially pro-necroptotic protein PGAM5 by unknown proteases in healthy cells. In further experiments, the identity of these proteases could be narrowed down to the family of serine proteases. For example, PGAM5 protein levels were increased when HtrA2/Omi was inhibited, indicating that HtrA2/Omi is a potential physiological regulator of PGAM5. The proteasome inhibitor MG-132 also elevated PGAM5 protein levels, indicating that the proteasome is another physiological regulator of PGAM5. A possible explanation for the constitutive degradation of PGAM5 under physiological conditions might be that in healthy cells, keeping PGAM5 at low levels most likely prevents inadvertent induction of mitochondrial fragmentation and thus necroptosis. In consequence, the induction of necroptosis may lead to an increased susceptibility of cells to mitochondrial fragmentation by inhibiting PGAM5 degradation. In addition, a recent study by Zhuang and coworkers suggested that PGAM5 is cleaved by a non-caspase protease during apoptosis thereby releasing PGAM5 from the mitochondria. Once in the cytosol, PGAM5 is shown to be an antagonistic IAP substrate (Zhuang *et al.* 2013).

Additionally, the important role of MLKL in necroptosis could be shown in U-937 and HT-29 cells and could be extended to clinically relevant tumor cell lines. In this thesis, it could further be demonstrated that MLKL is not only involved in TNF-induced necroptotic killing of tumor cells, but that it is also involved in TRAIL-induced regulated necrosis.

6.2.5 A-SMase is proteolytically cleaved during necroptosis

While there is much evidence implicating ceramide in apoptosis, the question whether ceramide represents an essential inducer or is generated in consequence of necroptosis is still subject to debate. The study presented here shows for the first time that TNF-induced necroptosis results not only in A-SMase activation but also in generation of a 57-kDa protein band in L929Ts cells and a 59-kDa V5-tagged A-SMase protein in L929Ts cells expressing V5-A-SMase. The occurrence of two molecular forms of A-SMase, a 72 kDa polypeptide and a 57-kDa form, was already described in 1994 (Ferlinz *et al.* 1994). The 57-kDa protein bands obtained in the study presented here correlated with A-SMase induction/activation and this observation is in line with findings by Edelmann and coworkers investigating A-SMase cleavage during TNF-induced apoptosis (Edelmann *et al.* 2011). Furthermore, the 59-kDa recombinant cleavage product of V5-A-SMase still carried the C-terminal V5-tag, suggesting that A-SMase is proteolytically cleaved to its enzymatically active product at the N-terminus of the protein. A study by Jenkins and coworkers reported the proteolytic processing of V5-A-SMase to a 65 kDa form of A-SMase lacking the C-terminal V5-tag (Jenkins *et al.* 2011). This observation is in direct contrast to the results obtained in the study presented here. In the study by Jenkins and coworkers, the C-terminal cleavage of A-SMase was detected in unstimulated cells whereas, in the study presented here, cells were stimulated with TNF to induce necroptosis. Furthermore, the MS analyses of extracted V5-A-SMase fragments clearly showed that V5-A-SMase is cleaved at the N-terminus after TNF-induced necroptosis. Therefore, the detection of a C-terminal cleavage fragment of lysosomal A-SMase (Jenkins *et al.* 2011) might represent a process required for lysosomal A-SMase maturation rather than a process involved in TNF-induced activation of A-SMase. The observation that A-SMase is cleaved and activated during necroptosis could be further substantiated: both necroptosis inhibitors Nec-1 and NSA prevented the proteolytic processing as well as the activation of A-SMase during necroptosis. A-SMase activity was also decreased when TFCK or dynasore were applied, suggesting that the internalization of the TNF-R1 is required for A-SMase cleavage and thus for necroptosis (see 5.2.3). Moreover, cleaved A-SMase was not found in the necroptotic TNF-R1 fractions, suggesting that A-SMase is activated downstream of the necrosome complex, and possibly cleaved and activated by a yet unknown serine protease. Surprisingly, necroptosis-sensitive caspase-7 deficient MEFs did not show A-SMase activity after induction of necroptosis. During apoptosis, caspase-8 and caspase-7 sequentially mediate proteolytic activation of A-SMase after TNF stimulation (Edelmann *et al.* 2011). Since overall caspase activity was suppressed by the addition of zVAD-fmk in every experimental set-up, the presence of caspase-7 protein rather

than its activity might be essential for the activation of A-SMase during TNF-induced necroptosis. Caspase-7 plays a crucial role in the execution of apoptosis whereas non-apoptotic functions of caspase-7 are, so far, not described (Fan *et al.* 2005; Lamkanfi *et al.* 2007). However (although A-SMase is the main enzyme responsible for induction of ceramide-mediated necroptosis, see below), cell death can be induced by increased ceramide levels also in an A-SMase-independent manner. A report by Lafont and coworkers showed that CD95-induced sphingomyelin synthase inhibition leads to sphingomyelin decrease and ceramide increase, contributing to cell death. Furthermore, the authors could show that sphingomyelin synthase 1 is a putative target for caspase-7 (Lafont *et al.* 2010). To unravel the putative function of caspase-7 during necroptotic activation of A-SMase, ceramide levels of caspase-7 deficient MEFs and their wild-type counterparts should be measured after induction of necroptosis. Furthermore, the effect on A-SMase activation after re-transfection of recombinant caspase-7 in caspase-7 deficient MEFs should be analyzed in the future.

Under conditions where the classical apoptosis machinery fails, the generation of ceramide may be an important backup system enabling a cell to commit suicide by regulated necrosis. In particular, it was shown that ceramide consistently accumulates before the onset of necroptosis (Thon *et al.* 2005). Inhibition of ceramide generation by overexpression of acid ceramidase, pharmacological intervention, down-regulation or genetic ablation of A-SMase resulted in protection of L929Ts, NIH3T3 and Jurkat T cells (Strelow *et al.* 2000; Thon *et al.* 2005). A-SMase deficient lung fibroblasts were re-sensitized for necroptosis by reconstitution of A-SMase, implicating A-SMase as the main enzyme responsible of the accumulation of ceramide after induction of necroptosis (Thon *et al.* 2005).

The isolation and analysis of bands corresponding in size to unprocessed and processed A-SMase from preparative gels identified the N-terminus of pro-A-SMase being at A(59)/(60)H. The N-terminal proteolytic processing at histidine 60 of pro-A-SMase was already described (Schissel *et al.* 1998). Although detection limits have, so far, prevented the identification of the exact cleavage site of mature, active A-SMase in necroptosis, the analysis of the 57 kDa band of cleaved A-SMase demonstrated that the necroptotic A-SMase fragment extends beyond the putative N-terminal apoptotic cleavage site (Edelmann *et al.* 2011). This suggests that during necroptosis, the cleavage of A-SMase must be distinct from the site where caspase-7 cleaves A-SMase during apoptosis. Surprisingly, results of the study presented here, revealed that processed A-SMase fragments after induction of apoptosis include N-terminal peptides starting from L(202)/(203)F which are upstream of the putative cleavage site at D253 found by Edelmann and coworkers (Edelmann *et al.* 2011). In contrast to the suggestion that A-SMase is cleaved during necroptosis at a distinct site, the sequence coverage and peptides identified between apoptotic and necroptotic cleaved A-SMase fragments were very similar in the study presented here. The putative cleavage site of pro-A-SMase at D253 was identified by mutation analysis (Edelmann *et al.* 2011). However, this cleavage site does not match the canonical consensus sequence of caspase-7 and should be revalidated with further analysis of the

cleavage fragments by novel MS analysis such as terminal amine isotopic labeling of substrates (TAILS; Kleifeld *et al.* 2011) like processed A-SMase to define the termini of A-SMase via quantitative proteomic analyses.

In summary, a proteolytic activation of A-SMase in response to necroptosis could be confirmed. However, the questions which protease cleaves pro-A-SMase during necroptosis and the precise location of the N-terminus of cleaved A-SMase still remain open.

6.2.6 Presenilins are indispensable for TNF-induced necroptosis

Presenilin proteins belong to a family of multi-pass transmembrane proteins. They are part of the catalytic core of the γ-secretase protease complex located in the plasma membrane (Zhang *et al.* 2013). Mice deficient for presenilin-1 show severe defects and die after birth (Shen *et al.* 1997). Patients with familial Alzheimer disease show mutations in their presenilin-1 gene (Menendez, 2004). Down-regulation of presenilin-1 sensitizes human Hep G2 cells to ER stress-dependent cell death (Száraz *et al.* 2013). In the study presented here, MEFs derived from presenilin 1/2-deficient mice were fully protected from TNF-induced necroptosis. This is in line with the observation that the γ-secretase protease complex inhibitor X diminished TNF-induced necroptosis in L929Ts and U-937 cells. So far no data are available which links presenilins to necroptosis. However, recent studies reported that HtrA2/Omi can interact with presenilin-1 in the active γ-secretase protease complex in mitochondria (Gupta *et al.* 2004; Behbahani *et al.* 2010). This observation is in line with the association of HtrA2/Omi protease activity and neurodegenerative disorder, e.g. with a parkinsonian phenotype (Martins *et al.* 2004). Based upon the preliminary results obtained in this thesis, presenilins might represent a missing link between HtrA2/Omi activation and execution of necroptosis.

The Alzheimer's disease-associated presenilins, the signal peptide peptidase (SPP) and, its homologues, the SPP-like peptidases (SPPL) are intramembrane-cleaving proteases (I-CLIPs; Wolfe and Kopan, 2004) and members of a group of the GxGD-type aspartyl protease family (Weihofen and Martoglio, 2003). Although SPP/SPPLs and presenilins share very limited sequence homologies, they exhibit similarities in the cleavage pattern of their substrates, suggesting a common concept of intramembrane proteolysis (Fluhrer and Haass, 2007). In the thesis presented here, studying MEFs from SPPL2a-, SPPL2b- and SPPL2a/b-deficient mice revealed no conclusive evidence that SPPL2 proteins play a role in TNF-induced necroptosis, because depending on the MEF batches analyzed, the knock-out of either SPPL2a or SPPL2b as well as the double knock-out showed protective effects on TNF-induced necroptosis or not. Furthermore, the inhibitor $(Z\text{-}LL)_2$-ketone, an established SPP/SPPL inhibitor (Friedmann *et al.* 2006) had no inhibitory effect on TNF-induced necroptosis in L929Ts and U-937 cells. The inconclusive results of the different MEF batches might be due to phenotypic alterations during immortalization. For example, mutations of the growth-suppressive protein p53 seem to be a common event in the formation of permanent cell lines (Harvey and Levine, 1991). The

p53 tumor suppressor pathway is a central link for nearly all cellular stress responses this include, for example, DNA repair, cell cycle arrest, cell death and senescence. Furthermore, p53 regulates PARP-1 dependent necrosis (Elkholi and Chipuk, 2014). Thus immortalized cell lines with an altered p53 pathway might have different sensitivities to TNF- or TRAIL-induced cell death pathways. Consequently, further experiments have to be conducted investigating other cell systems by down-regulating or over-expressing SPPL2 proteins to unravel the involvement of SPPL2 proteins during necroptosis. A possible link between SPPL proteins and regulated necrosis might be the Mg^{2+} transport pathway within the cell. Preliminary data showed an altered Mg^{2+} homeostasis in SPPL2a-deficient mice, possibly as a result in altered cleavage of a member of the transient receptor potential channels of the melastatin-like family (TRPM; unpublished observations by Bernd Schröder, Christian-Albrechts-University, Kiel, Germany). These ion channels were recently associated with cell death. For example, TRPM2 is activated by free radicals and TNF as well as H_2O_2 stimulation cause cell death through a TRPM2-dependent mechanism (Hara *et al.* 2002). TRPM7 was shown to be a downstream target of MLKL, leading to Ca^{2+} influx and TNF-induced necroptosis (Cai *et al.* 2014). The ion channel TRPM6 is one prominent key player in Mg^{2+} homeostasis (Ferre *et al.* 2011) and a study by Schmitz and coworkers showed that TRPM7 and its closest homologue, TRPM6 are functionally non-redundant but can influence each other's biological activity (Schmitz *et al.* 2005). Furthermore, deletion of TRPM7 caused growth arrest, Mg^{2+} deficiency, and cell death in B-lymphocytes (Schmitz *et al.* 2005). TRPM6, being a potential substrate of SPPL2a, has not yet been implicated in cell death. The interplay of pro-necroptotic TRPM7 and TRPM6 may also contribute to cell death through as yet uncharacterized pathways or through dimerization with either TRPM2 or TRPM7.

6.3 TRAIL induces regulated necrosis in clinically relevant tumor cell lines

The third part of the study presented here provides strong evidence for the suitability of TRAIL-induced regulated necrosis as a tool to eliminate tumor cells from a wide range of sources. In contrast to regulated necrosis, the efficacy of TRAIL in the apoptotic elimination of tumor cells has been already demonstrated in clinical trials in patients (Hellwig and Rehm, 2012). Nevertheless, intrinsic resistance of tumors against TRAIL-induced apoptosis was found to limit the therapeutic success. Therefore, the induction of regulated necrosis by TRAIL would be an additional option to eliminate tumor cells that are intrinsically resistant to TRAIL-induced apoptosis. This has, however, been investigated only in a very limited number of studies so far. One of those studies has recently reported that TRAIL induces necroptosis in the tumor cell lines HT-29 (which was also used in the study presented here) and Hep G2 (Jouan-Lanhouet *et al.* 2012). However, unlike in the study presented here, necroptosis occurred only under acidified but not physiologic conditions. Moreover, Jouan-Lanhouet and coworkers reported that in their system caspase activity is required for cell death (Jouan-

Lanhouet *et al.* 2012). This is in contrast to the common molecular mechanisms described for necroptosis (Vanden Berghe *et al.* 2014) and to the observations of the study presented here. Furthermore, the study by Jouan-Lanhouet and coworkers showed that their above described findings for necroptosis induced by TRAIL do not apply to necroptosis induced by either TNF or CD95 ligand (Jouan-Lanhouet *et al.* 2012), suggesting that conclusions from their study have to be interpreted with a certain caution and cannot be generalized for physiologic conditions. Another more encouraging study by Hunter and coworkers showed that TRAIL is able to kill small cell lung cancer cells in synergy with paclitaxel through a caspase-independent mechanism (Hunter *et al.* 2011). Furthermore, the treatment with TRAIL in combination with lobaplatin, an antitumor platinum drug, had effects on the growth of breast cancer cells *in vitro* by inducing regulated necrosis (Engel *et al.* 2012). Independently, Katz and coworkers reported that combining sorafenib therapy with TRAIL results in augmented caspase-independent cell death of malignant pleural mesothelioma cell lines. Furthermore, pilot *in vivo* studies demonstrated promising evidence of the therapeutic efficacy in a xenograft mouse model (Katz *et al.* 2009). The results obtained in the study presented here show that TRAIL-induced regulated necrosis is even more effective under conditions that more closely resemble the *in vivo* situation, because TRAIL-induced regulated necrosis clearly interfered with the capacity of the tested tumor cell lines for unlimited proliferation in clonogenic survival assays. These observations may represent promising new options for the development of future combination therapies for the elimination of apoptosis-resistant cancers. Furthermore, the data presented here demonstrate that TRAIL-induced regulated necrosis synergized with chemotherapeutic agents such as cisplatin, etoposide, trichostatin A, 5-fluorouracil, irinotecan, doxorubicin, camptothecin and paclitaxel and enhances the cytotoxic response in the tumor cell lines. In summary, the data obtained here and the above mentioned studies provide additional encouragement for the development of future combination therapies.

With regard to unraveling the molecular pathways of TRAIL-induced regulated necrosis, the results obtained in the study presented here identified RIPK1, RIPK3 and MLKL as crucial components. Furthermore, RIPK3 may represent a possible determinant of susceptibility or resistance of tumor cells to TRAIL-induced regulated necrosis (Voigt *et al.* 2014). In line with this observation, also MLKL protein expression was reported to be a prognostic biomarker in patients with pancreatic adenocarcinoma, where low expression of MLKL was associated with decreased overall survival of the patients (Colbert *et al.* 2013). Finally, the study presented here confirmed and extended the role of ceramide as one of the key mediators of regulated necrosis downstream of RIPK1 and RIPK3 to the clinically more relevant tumor cell systems investigated, because treatment with Arc39 suppressed TNF- or TRAIL-induced necroptosis in U-937, Mz-ChA-1, BcPC-3, HT-29 and Panc89 cancer cells and in MEFs but not in a necroptosis-resistant cell line. There is emerging evidence that A-SMase could serve as an important drug target for a variety of diseases. For example, increased A-SMase concentrations were found in atherosclerosis, chronic heart failure and depression (Uhlig and

Gulbins, 2008). Therefore, the regulation of A-SMase by Arc39 may represent a novel mechanism for pharmacological inhibition of the enzyme and the development of combination therapies with TRAIL could help to design future strategies to interfere with damage induced by necroptosis/regulated necrosis. In line with the crucial function of the kinase RIPK3 in necroptosis, NIH3T3 cells naturally lacking RIPK3 displayed a decreased accumulation of intracellular ceramide levels when undergoing necroptosis, whereas the stable re-expression of RIPK3 in wild-type cells restored the elevated ceramide levels in cells dying by necroptosis. Cells harboring kinase-defective RIPK3 showed slightly elevated ceramide levels upon induction of necroptosis. This is possibly a result of the induction of apoptotic-like caspase-independent cell death pathways rather than an induction of necroptosis, because Newton and coworkers recently claimed that the absence of RIPK3 drives the signaling pathway towards apoptosis (Newton *et al.* 2014).

With regard to a future application of TRAIL-induced regulated necrosis, still further research is required. For future therapeutic application of TRAIL-induced regulated necrosis to eliminate tumor cells in patients, strategies for the induction of regulated necrosis need to be adapted to the *in vivo* situation, because the sensitizer CHX used in the study presented here is cytotoxic also to healthy tissue. Therefore, future therapies based on the treatment of patients with CHX are not suitable. As a possible alternative, He and coworkers showed that Smac mimetics can similarly sensitize cell culture models for TRAIL- and TNF-induced regulated necrosis (He *et al.* 2009). This could be confirmed with results obtained in the study presented here showing that the Smac mimetic birinapant similarly can act as enhancer of TRAIL- as well as TNF-induced regulated necrosis in tumor cell lines. However, *in vivo* studies showing the efficacy or toxicity of Smac mimetics under conditions of regulated necrosis are not available so far. A second possible alternative to CHX might be the application of the protein biosynthesis inhibitor homoharringtonine together with TRAIL/zVAD to induce regulated necrosis. Clinical studies have already indicated that homoharringtonine is effective in treating leukemia such as acute myeloid leukemia or chronic myeloid leukemia (Zhou *et al.* 1995) and in consequence, homoharringtonine has been approved for the treatment of chronic myeloid leukemia in patients (Narayanan *et al.* 2013). Apart from the problems of cytotoxicity of CHX, it must also be clarified whether TRAIL or zVAD-fmk treatment is indeed non-toxic *in vivo*. The study by Hellwig and Rehm demonstrated that TRAIL was well tolerated in preclinical models at serum concentrations (Hellwig and Rehm, 2012). Furthermore, in two independent studies, the application of zVAD-fmk did not show toxicity *in vivo*, either in a transgenic mouse model of Huntington disease (Chen *et al.* 2000) or a transgenic mouse model of amyotrophic lateral sclerosis (Li *et al.* 2000). As a next step, the possible *in vivo* toxicity of a joint application of TRAIL and zVAD-fmk has to be clarified, as well as in additional combination with chemotherapeutic agents.

Rapid plasma permeabilization due to necrotic triggers leads to the release of DAMPs from the cell. These necrosis-dependent DAMPs can trigger inflammatory responses (Kaczmarek *et al.* 2013).

Accordingly, the release of DAMPs has to be addressed with regard to future therapies, because regulated necrosis has been associated with inflammation in several diseases, such as kidney ischemia reperfusion or systemic inflammatory response syndrome (Kaczmarek *et al.* 2013). Hence, it has to be addressed whether the death of tumor cells by regulated necrosis is immunogenic. It is also unknown whether regulated necrosis as a result may elicit an immune response that might eliminate residual and neighboring tumor cells (Vandenabeele *et al.* 2010). Resolving these questions for TRAIL-induced necrosis could thus contribute to an even more effective treatment for cancer patients in the future.

6.4 Conclusions and biological relevance of the above observations

Programmed cell death stands out as a critical process for multicellular organisms. This is demonstrated by the highly interconnected machinery that ensures its induction, regulation and execution. In this present study, it was confirmed that TNF-induced necroptosis and the PARP pathway represent two distinct and independent routes to regulated necrosis (Figure 57; see Sosna, Voigt *et al.* 2014). These findings have profound therapeutic implications, because they suggest that inhibiting just one of the signaling pathways that lead to regulated necrosis (including e.g. TNF-induced necroptosis or PARP-1-dependent regulated necrosis) or apoptosis may exert only limited cytoprotective effects. As a consequence, a combinatorial strategy that simultaneously inhibits multiple signal transduction cascades rather than an individual application of highly specific necroptosis (e.g. Nec-1 or NSA) or PARP-1 inhibitors (e.g. olaparib) might be the approach of choice for the future, possibly resulting in an improved treatment of damage induced by regulated necrosis (e.g. in shock, pancreatitis, ischemic damage or neurodegenerative diseases). Still, future studies should address the decryption of the different modes of regulated necrosis to generate profound insights into molecular mechanisms of e.g. necroptosis and thus paving the way for its pharmacological modulation in the clinic.

The data presented in this thesis help to decode at least some parts of the molecular pathways involved primarily in TNF-mediated necroptosis. Based upon the results obtained in the study presented here, the following extensions to the already established models can be proposed. HtrA2/Omi can be integrated as a key regulator into the known general signaling pathways of TNF-induced necroptosis (see Sosna and Voigt *et al.* 2013). In this model, binding of TNF to TNF-R1 induces activation of the kinases RIPK1, RIPK3, and of MLKL as components of the necrosomal core complex. HtrA2/Omi is activated indirectly within the mitochondria and presenilins might represent a missing link between HtrA2/Omi activation and execution of necroptosis. As another likely mechanism, MLKL has been found to activate the phosphatases PGAM5L/S, which in turn couple to the mitochondrial protein Drp-1, and as a mitochondrial attack complex, may cause the subsequent intramitochondrial activation of HtrA2/Omi. Furthermore, PGAM5 is constitutively degraded by yet unknown proteases in healthy cells. Upon induction of necroptosis, this constitutive proteolysis is inhibited, leading to an increase in PGAM5 levels, which may facilitate the fragmentation of mitochondria during necroptosis. In the

proteomic screen for serine proteases relevant in necroptosis, in addition to HtrA2/Omi, the proteases Lon protease 1, PMPCA and PSA1 were found to be potential candidates (Figure 57). The complementary siRNA screen of all proteases encoded by the human genome identified the anti-apoptotic or pro-tumorigenic proteases DESC, MMP3, GGT1, PRPF8 and DPYL4 in addition to caspase-8, CYLD and c-FLIP. However, all identified proteases have to be further investigated with regard to their exact function and position in the signaling pathways of necroptosis. The 2D-DIGE approach unraveled an enrichment of proteins involved in the cellular energy metabolism (PHGDH, IMPDH2) or involved in the structural organization of the cell (CFL-1) during necroptosis. On the other hand, the levels of proteins involved in the structural organization of the cell (TUBA1B) or involved in the energy metabolism (PKM, CAT) were also decreased. Moreover, moesin, a component of the cytoskeleton was identified as a proteolytic substrate during necroptosis (Figure 57). However, these results should be further validated in additional biological replicates, and in the future the obtained candidates have to be analyzed for their impact on TNF-induced necroptosis. Apart from this, the proteolytic activation of A-SMase in response to TNF-induced necroptosis could be confirmed. However, the questions which protease cleaves pro-A-SMase and where the N-terminus of cleaved A-SMase is precisely localized still remain open.

The characterization of TRAIL-induced regulated necrosis revealed that it is effective for the elimination of various types of tumor cells and that A-SMase and ceramide are critical mediators also in this system (Figure 57; Voigt *et al.* 2014). Similar to TNF-induced necroptosis, studies should aim at unraveling the detailed signaling pathways of TRAIL-induced regulated necrosis, as they might be a promising target for novel anti-tumor treatments. To this end, more information is needed to fill in the "gap" between receptor activation, RIPK1, RIPK3 and MLKL interaction and the observed activation of A-SMase and the resulting increase in intracellular ceramide levels.

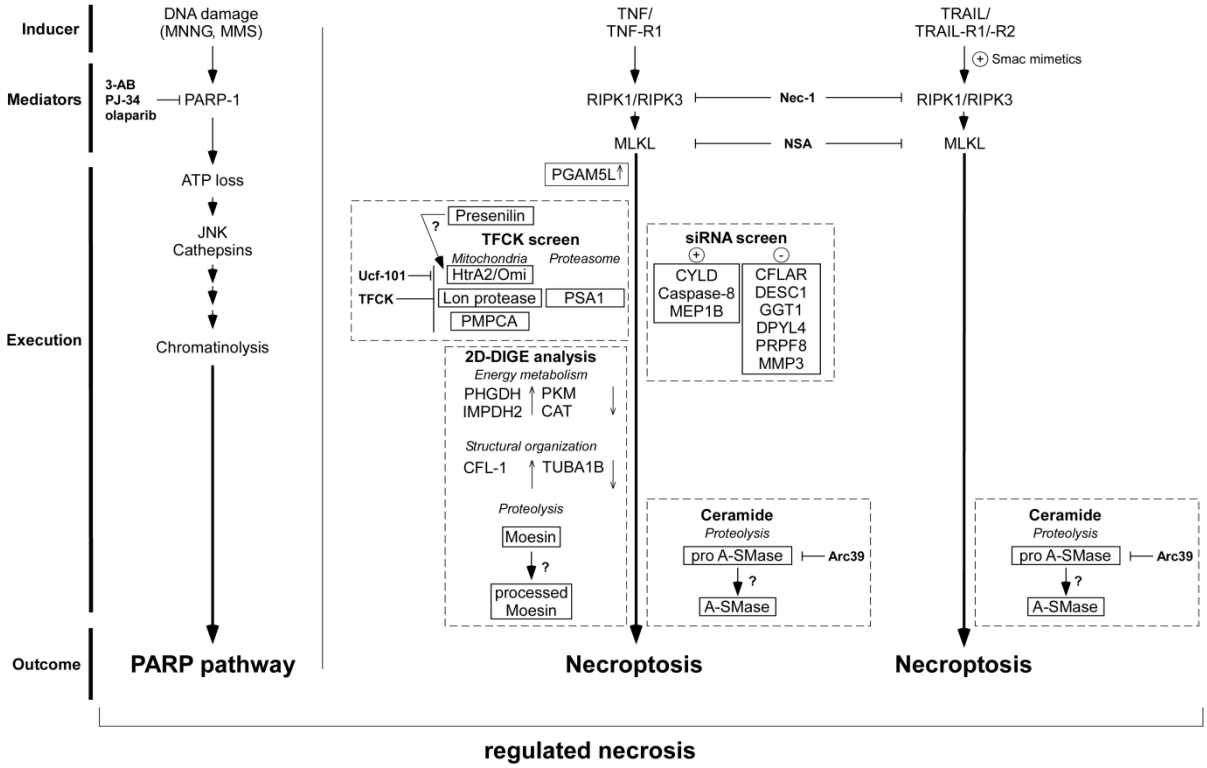

Figure 57: A general model of selected signaling pathways in regulated necrosis based on the results obtained in the study presented here. Left: DNA damage induced by DNA alkylating agents such as MNNG or MMS lead to the activation of the PARP pathway. The resulting activation of PARP-1 can be efficiently blocked by the specific PARP-1 inhibitors 3-AB, PJ-34 or olaparib. The activation of PARP-1 culminates in the rapid loss of ATP levels, accompanied by the activation of JNK and cathepsins, and subsequently resulting in chromatinolysis and the death of the cell via regulated necrosis. **Middle:** Another distinct pathway of regulated necrosis is necroptosis which can be mediated by e.g. TNF or TRAIL. After activation of TNF-R1 by binding of TNF under caspase inhibitory conditions, the necrosome containing phosphorylated and activated RIPK1 and RIPK3 is formed. Subsequently, the protein MLKL is activated. This signaling cascade then culminates in a yet unknown way in different executioner mechanisms. PGAM5 was shown to be constitutively degraded in healthy cells and thus upregulated during TNF-induced necroptosis. During a TFCK-sensitive serine protease screen, the serine protease HtrA2/Omi was identified which may be activated by novel mechanisms that involve the activity of presenilins. The TFCK-sensitive serine protease Lon protease 1 as well as the TFCK-sensitive metalloproteinase PMPCA might also be involved in the execution of TNF-induced necroptosis, similar to the proteasomal protein PSA1. The siRNA screen identified, among CYLD, caspase-8 and CFLAR, proteases whose down-regulation potentiates (DESC1, GGT1, DPYL4, PRPF8, MMP3) or protects (MEP1B) from TNF-induced necroptosis and who thus may be negative or positive regulators of the execution of necroptosis. Furthermore, 2D-DIGE analyses of soluble proteins and magnetically enriched TNF-R1-containing vesicles revealed that levels of proteins involved in regulating the energy metabolism were either increased (PHGDH, IMPDH2) or decreased (PKM, CAT) during TNF-induced necroptosis. Moreover, protein levels of components of the structural organization of the cell were increased (CFL-1) or decreased (TUBA1B) or proteins were substrates for proteolytic cleavage (moesin). Ceramide generation as another executioner mechanism of TNF-induced necroptosis is initiated by the proteolytic maturation/activation of A-SMase by a yet unknown protease. TNF-induced necroptosis can be efficiently blocked by the RIPK1 inhibitor Nec-1, the MLKL inhibitor NSA, the serine protease inhibitor TFCK and/or by the HtrA2/Omi inhibitor Ucf-101. **Right:** Likewise, TRAIL-induced necroptosis can be blocked by the addition of Nec-1 or NSA. The addition of Smac mimetics can potentiate and thereby positively regulate TRAIL-induced necroptosis in clinically relevant tumor cells. Here, ceramide generation is also an important executioner mechanism and recent studies also point to a proteolytic maturation/activation of A-SMase during TRAIL-induced regulated necrosis (M. Kähler, Master Thesis, 2013). Question marks indicate unknown signaling pathways of proteins. **Abbreviations:** acid sphingomyelinase (A-SMase), adenosine-5'-triphosphate (ATP), catalase (CAT), caspase-8 and FADD-like apoptosis regulator (CFLAR), cofilin-1 (CFL-1), cylindromatosis (CYLD), transmembrane protease serine 11E (DESC1), dihydropyrimidinase-like 4 (DPYL4), gamma-glutamyltransferase 1 (GGT1), inosine-5'-monophosphate dehydrogenase 2 (IMPDH2), c-Jun N-terminal kinases (JNK), meprin beta (MEP1B), mixed-lineage kinase domain-like (MLKL), metalloproteinase 3 (MMP3), methyl methanesulfonate (MMS), 1-methyl-3-nitro-1-nitrosoguanidine (MNNG), necrostatin 1 (Nec-1), necrosulfonamide (NSA), poly(ADP-ribose) polymerase (PARP), phosphoglycerate mutase family member (PGAM), D-3-phosphoglycerate dehydrogenase (PHGDH), pyruvate kinase isozymes M1/M2 (PKM), mitochondrial processing peptidase alpha (PMPCA), pre-mRNA processing factor 8 (PRPF8), proteasome subunit alpha type-1 (PSA1), receptor-interacting protein kinase (RIPK), tumor necrosis factor (TNF), TNF-receptor 1 (TNF-R1), TNF-related apoptosis inducing ligand (TRAIL), TRAIL-receptor (TRAIL-R), tubulin alpha-1B chain (TUBA1B), two-dimensional difference gel electrophoresis (2D-DIGE).

7. References

Aggarwal BB (2003) Signaling pathways of the TNF superfamily: a double-edged sword. *Nat Rev Immunol* 2, 745-756

Aggarwal BB and Natarajan K (1996) Tumor necrosis factors: Developments during the last decade. *Eur Cytokine Netw* 7, 93-124

Ameloot P, Fiers W, De Bleser P, Ware CF, Vandenabeele P, Brouckaert P (2001) Identification of tumor necrosis factor (TNF) amino acids crucial for binding to the murine p75 TNF receptor and construction of receptor-selective mutants. *J Biol Chem* 276, 37426-37430

Andrabi SA, Kim NS, Yu SW, Wang H, Koh DW, Sasaki M, Klaus JA, Otsuka T, Zhang Z, Koehler RC, Hurn PD, Poirier GG, Dawson VL, Dawson TM (2006) Poly(ADP-ribose) (PAR) polymer is a death signal. *Proc Natl Acad Sci USA* 103, 18308-18313

Andrabi S, Dawson T, Dawson V (2008) Mitochondrial and nuclear cross talk in cell death: parthanatos. *Ann NY Acad Sci* 1147, 233-241

Antolin AA, Jalencas X, Yelamos J, Mestres J (2012) Identification of Pim kinases as novel targets for PJ34 with confounding effects in PARP biology. *ACS Chem Biol* 7, 1962-1967

Artus C, Boujrad H, Bouharrour A, Brunelle MN, Hoss S, Yuste VJ, Lenormand P, Rousselle JC, Namane A, England P, Lorenzo HK, Susin SA (2010) AIF promotes chromatinolysis and caspase-independent programmed necrosis by interacting with histone H2AX. *EMBO J* 29, 1585-1599

Ashkenazi A, Herbst RS (2008) To kill a tumor cell: the potential of proapoptotic receptor agonists. *J Clin Invest* 118, 1979-1990

Barkla DH, Gibson PR (1999) The fate of epithelial cells in the human large intestine. *Pathology* 31, 230-238

Behbahani H, Bavlov PF, Wiehager B, Nishimura T, Winblad B, Ankarcrona M (2010) Association of Omi/HtrA2 with γ-secretase in mitochondria. *Neurochem Int* 57, 668-675

Bertrand MJ, Milutinovic S, Dickson KM, Ho WC, Boudreault A, Durkin J, Gillard JW, Jaquith JB, Morris SJ, Barker PA (2008) cIAP1 and cIAP2 facilitate cancer cell survival by functioning as E3 ligases that promote RIP1 ubiquitination. *Mol Cell* 30, 689-700

Bidere N, Lorenzo HK, Carmona S, Laforge M, Harper F, Dumont C, Senik A (2003) Cathepsin D triggers Bax activation, resulting in selective apoptosis-inducing factor (AIF) relocation in T lymphocytes entering the early commitment phase to apoptosis. *J Biol Chem* 278, 31401-31411

Bligh EG and Dyer WJ (1959) A rapid method of total lipid extraction and purification. *Can J Biochem Physiol* 37, 911-917

Blink E, Maianski NA, Alnemri ES, Zervos AS, Roos D, Kuijpers TW (2004) Intramitochondrial serine protease activity of Omi/HtrA2 is required for caspase-independent cell death of human neutrophils. *Cell Death Differ* 11, 937-939

Boonyanugomol W, Chomvarin C, Song JY, Kim KM, Kim JM, Cho MJ, Lee WK, Kang HL, Rhee KH, Sripa B, Hahnvajanawong C, Baik SC (2012) Effects of *Helicobacter pylori* gamma-glutamyltransferase on apoptosis and inflammation in human biliary cells. *Dig Dis Sci* 57, 2615-2624

Bota DA, Ngo JK, Davies KJA (2005) Downregulation of human Lon protease impairs mitochondrial structure and function and causes cell death. *Free Radic Biol Med* 38, 665-677

Brenner B, Ferlinz K, Grassmé H, Weller M, Koppenhoefer U, Dichgans J, Sandhoff K, Lang F, Gulbins E (1998) Fas/CD95/Apo-I activates the acidic sphingomyelinase via caspases. *Cell Death Differ* 5, 29-37

Brenner C, Cadiou H, Vieira HL, Zamzami N, Marzo I, Xie Z, Leber B, Andrews D, Duclohier H, Reed JC, Kroemer G (2000) Bcl-2 and Bax regulate the channel activity of the mitochondrial adenine nucleotide translocator. *Oncogene* 19, 329-336

Brenner D and Mak TW (2009) Mitochondrial cell death effectors. *Curr Opin Cell Biol* 21, 871-877

Burke JE, Dennis EA (2009) Phospholipase A_2 biochemistry. *Cardiovasc Drugs Ther* 23, 49-59

Cai Z, Jitkaew S, Zhao J, Chiang HC, Choksi S, Liu J, Ward Y, Wu LG, Liu ZG (2014) Plasma membrane translocation of trimerized MLKL protein is required for TNF-induced necroptosis. *Nat Cell Biol* 16, 55-65

Carmago SH, Shah SV, Walker PD (2002) Meprin, a brush-border enzyme, plays an important role in hypoxic/ischemic acute renal tubular injury in rats. *Kidney Int* 61, 959-966

Cauwels A, Janssen B, Waeytens A, Cuvelier C, Brouckaert P (2003) Caspase inhibition causes hyperacute tumor necrosis factor-induced shock via oxidative stress and phospholipase A2. *Nat Immunol* 4, 387-393

Chahory S, Padron L, Courtois Y, Torriglia A (2004) The LEI/L-DNase II pathway is activated in light-induced retinal degeneration in rats. *Neurosci Lett* 367, 205–209.

Chan FKM, Shisler J, Bixby JG, Felices M, Zheng L, Appel M, Orenstein J, Moss B, Lenardo MJ (2003) A role of tumor necrosis factor receptor-2 and receptor-interacting protein in programmed necrosis and antiviral responses. *J Biol Chem* 278, 51613-51621

Chen M, Ona VC, Li M, Ferrante RJ, Fink KB, Zhu S, Bian J, Guo L, Farrell LA, Hersch SM, Hobbs W, Vonsattel JP, Cha JH, Friedlander RM (2000) Minocycline inhibits caspase-1 and caspase-3 expression and delays mortality in a transgenic mouse model of Huntington disease. *Nat Med* 6, 797-801

Chen X, Li W, Ren J, Huang D, He WT, Song Y, Yang C, Li W, Zheng X, Chen P, Han J (2014) Translocation of mixed lineage kinase domain-like protein to plasma membrane leads to necrotic cell death. *Cell Res* 24, 105-121

Cheng CW, Kuo CY, Fan CC, Fang WC, Jiang SS, Lo YK, Wang TY, Kao MC, Lee AY (2013) Overexpression of Lon contributes to survival and aggressive phenotype of cancer cells through mitochondrial complex I-mediated generation of reactive oxygen species. *Cell Death Dis* 20, e681

Chiarugi A (2005) Intrinsic mechanisms of poly (ADP-ribose) neurotoxicity: three hypotheses. *Neurotoxicology* 26, 847-55

Chiu LY, Ho FM, Shiah SG, Chang Y, Lin WW (2011) Oxidative stress initiates DNA damager MNNG-induced poly(ADP-ribose) polymerase-1-dependent parthanatos cell death. *Biochem Pharmacol* 81, 459-470

Cho YS, Challa S, Moquin D, Genga R, Ray TD, Guildford M, Chan FK (2009) Phosphorylation-driven assembly of the RIP1-RIP3 complex regulates programmed necrosis and virus-induced inflammation. *Cell* 137, 1112-1123

Cilenti L, Lee Y, Hess S, Srinivasula S, Park KM, Junqueira D, Davis H, Bonventre JV, Alnemri ES, Zervos AS (2003) Characterization of a novel and specific inhibitor for the pro-apoptotic protease Omi/HtrA2. *J Biol Chem* 278, 11489-11494

Cilenti L, Soundarapandian MM, Kyriazis GA, Stratico V, Singh S, Gupta S, Bonventre JV, Alnemri ES, Zervos AS (2004) Regulation of HAX-1 anti-apoptotic protein by Omi/HtrA2 protease during cell death. *J Biol Chem* 279, 50295-50301

Colbert LE, Fisher SB, Hardy CW, Hall WA, Saka B, Shelton JW, Petrova AV, Warren MD, Pantazides BG, Gandhi K, Kowalski J, Kooby DA, El-Rayes BF, Staley CA 3rd, Adsay NV, Curran WJ Jr, Landry JC, Maithel SK, Yu DS (2013) Pronecrotic mixed lineage kinase domain-like protein expression is a prognostic biomarker in patients with early-stage resected pancreatic adenocarcinoma. *Cancer* 119, 3148-3155

Degterev A, Huang Z, Boyce M, Li Y, Jagtap P, Mizushima N, Cuny GD, Mitchison TJ, Moskowitz MA, Yuan J (2005) Chemical inhibitor of nonapoptotic cell death with therapeutic potential for ischemic brain injury. *Nat Chem Biol* 1, 112-119

Degterev A, Hitomi J, Germscheid M, Ch'en IL, Korkina O, Teng X, Abbott D, Cuny GD, Yuan C, Wagner G, Hedrick SM, Gerber SA, Lugovskoy A, and Yuan J (2008) Identification of RIP1 kinase as a specific cellular target of necrostatins. *Nat Chem Biol* 4, 313-321

Degterev A, Yuan J (2008) Expansion and evolution of cell death programmes. *Nat Rev Mol Cell Biol* 9, 378-390

Dixon SJ, Lemberg KM, Lamprecht MR, Skouta R, Zaitsev EM, Gleason CE, Patel DN, Bauer AJ, Cantley AM, Yang WS, Morrison B, Stockwell BR (2012) Ferroptosis: an iron-dependent form of nonapoptotic cell death. *Cell* 149, 1060-1072

Dörfler P, Shearman MS, Perlmutter RM (2001) Presenilin-dependent gamma-secretase activity modulates thymocyte development. *Proc Natl Acad Sci USA* 98, 9312-9317

Dünstl G, Weiland T, Schlaeger C, Nüssler A, Künstle G, Wendel A (2007) Activation of an alternative death receptor-induced signaling pathway in human hepatocytes under caspase arrest. *Arch Biochem Biophys* 462, 140-149

Dunai ZA, Imre G, Barna G, Korcsmaros T, Petak I, Bauer PO, Mihalik R (2012) Staurosporine induces necroptotic cell death under caspase-compromised conditions in U937 cells. *PLoS ONE* 7, e41945

Edelmann B, Bertsch U, Tchikov V, Winoto-Morbach S, Perrotta C, Jakob M, Adam-Klages S, Kabelitz D, Schütze S (2011) Caspase-8 and caspase-7 sequentially mediate proteolytic activation of acid sphingomyelinase in TNF-R1 receptosomes. *EMBO J* 30, 379-394

Egberts JH, Schniewind B, Schafmayer C, Kruse ML, Sipos B, Fändrich F, Kalthoff H, Tepel J (2007) Establishment of a novel orthotopic xenograft model of human gallbladder carcinoma. *Clin Exp Metastasis* 24, 141-148

Egger L, Madden DT, Rheme C, Rao RV, Bredesen DE (2007) Endoplasmatic reticulum stress-induced cell death mediated by the proteasome. *Cell Death Differ* 14, 1172-1180

Eldering JA, Grünberg J, Hahn D, Croes HJE, Fransen JAM, Sterchi EE (1997) Polarised expression of human intestinal *N*-benzoyl-L-tyroxyl-*p*-aminobenzoic acid hydrolase (human meprin) α and β subunits in Madin-Darby canine kidney cells. *Eur J Biochem* 247, 920-932

Elkholi R, Chipuk JE (2014) How do I kill thee? Let me count the ways: p53 regulates PARP-1 dependent necrosis. *Bioessays* 36, 46-51

Ellis HM, Horvitz HR (1986) Genetic control of programmed cell death in the nematode *C. elegans*. *Cell* 44, 817-829

Emery JG, McDonnell P, Brigham Burke M, Deen KC, Lyn S, Silverman C, Dul E, Appelbaum ER, Eichman C, DiPrinzio R, Dodds RA, James IE, Rosenberg M, Lee JC, Young PR (1998) Osteoprotegerin is a receptor for the cytotoxic ligand TRAIL. *J Biol Chem* 273, 14363-14367

Enesa K, Zakkar M, Chaudhury H, le Luong A, Rawlinson L, Mason JC, Haskard DO, Dean JL, Evans PC (2008) NF-kappaB suppression by the deubiquitinating enzyme cezanne: a novel negative feedback loop in pro-inflammatory signaling. *J Biol Chem* 283, 7036-7045

Engel JB, Martens T, Hahne JC, Häusler SF, Krockenberger M, Segerer S, Djakovic A, Meyer S, Dietl J, Wischhusen J, Honig A (2012) Effects of lobaplatin as a single agent and in combination with TRAIL on the growth of triple-negative p53-mutated breast cancers in vitro. *Anticancer Drugs* 23, 426-436

Fan TJ, Han LH, Cong RS, Liang J (2005) Caspase family proteases and apoptosis. *Acta Biochim Biophys Sin* 37, 719-727

Fang J, Rhyasen G, Bolanos L, Rasch C, Varney M, Wunderlich M, Goyama S, Jansen G, Cloos J, Rigolino C, Cortelezzi A, Mulloy JC, Oliva EN, Cuzzoly M, Starczynowski DT (2012) Cytotoxic effects of bortezomib in myelodysplastic syndrome/acute myeloid leukemia depend on autophagy-mediated lysosomal degradation of TRAF6 and repression of PSMA1. *Blood* 120, 858-867

Feng S, Yang Y, Mei Y, Ma L. Zhu DE, Hoti N, Castanares M, Wu M (2007) Cleavage of RIP3 inactivates its caspase-independent apoptosis pathway by removal of kinase domain. *Cell Signal* 19, 2056-2067

Feoktistova M, Geserick P, Kellert B, Panayotova Dimitrova D, Langlais C, Hupe M, Cain K, MacFarlane M, Häcker G, Leverkus M (2011) cIAPs block ripoptosome formation, a RIP1/caspase-8 containing intracellular cell death complex differentially regulated by c-FLIP isoforms. *Mol Cell* 43, 1-15

Ferlinz K, Hurwitz R, Vielhaber G, Suzuki K, Sandhoff K (1994) Occurrence of two molecular forms of human acid sphingomyelinase. *Biochem J* 301, 855-862

Ferlinz K, Hurwitz R, Moczall H, Lansmann S, Schuchmann EH, Sandhoff K (1997) Functional characterization of the N-glycosylation site of human acid sphingomyelinase by site-directed mutagenesis. *Eur J Biochem* 243, 511-517

Fernandez-Alnemri T, Armstrong RC, Krebs J, Srinivasula SM, Wang L, Bullrich F, Fritz LC, Trapani JA, Tomaselli KJ, Litwack G, Alnemri ES (1996) In vitro activation of CPP32 and Mch3 by Mch4, a novel human apoptotic cysteine protease containing two FADD-like domains. *Proc Natl Acad Sci USA* 93, 7464-7469

Ferre S, Hoenderop JG, Bindels RJ (2011) Insight into renal Mg^{2+} transporters. *Curr Opin Nephrol Hypertension* 20, 169-176

Festjens N, Vanden Berghe T, Vandenabeele P (2006) Necrosis, a well-orchestrated form of cell demise: signalling cascades, important mediators and concomitant immune response. *Biochim Biophys Acta* 1757, 1371-1387

Fischer U, Jänicke RU, Schulze-Osthoff K (2003) Many cuts to ruin: a comprehensive update of caspase substrates. *Cell Death Differ* 10, 76-100

Fischer U, Stroh C, Schulze-Osthoff K (2006) Unique and overlapping substrate specificities of caspase-8 and caspase-10. *Oncogene* 25, 152-159

Fluhrer R, Haass C (2007) Signal peptide peptidases and gamma-secretase: cousins of the same protease family? *Neurodegener Dis* 4, 112-116

Franken NA, Rodermond HM, Stap J, Haveman J, van Bree C (2006) Clonogenic assay of cells in vitro. *Nat Protoc* 1, 2315-2319

Friedmann E, Hauben E, Maylandt K, Schleeger S, Vreugde S, Lichtenthaler SF, Kuhn PH, Stauffer D, Rovelli G, Martoglio B (2006) SPPL2a and SPPL2b promote intramembrane proteolysis of TNF-alpha in activated dendritic cells to trigger IL-12 production. *Nat Cell Biol* 8, 843-848

Galluzzi L, Vanden Berghe T, Vanlangenakker N, Buettner S, Eisenberg T, Vandenabeele P, Madeo F, Kroemer G (2011) Programmed necrosis: from molecules to health and disease. *Int Rev Cell Mol Biol* 289, 1-35

Galluzzi L, Vitale I, Abrams JM, Alnemri ES, Baehrecke EH, Blagosklonny MV, Dawson TM, Dawson VL, El-Deiry WS, Fulda S, Gottlieb E, Green DR, Hengartner MO, Kepp O, Knight RA, Kumar S, Lipton SA, Madeo F, Malorni W, Mehlen P, Nunez G, Peter ME, Piacentini M, Rubinsztein DC, Shi Y, Simon HU, Vandenabeele P, White E, Yuan J, Zhivotovsky B, Melino G, Kroemer G (2012a) Molecular definitions of cell death subroutines: recommendations of the Nomenclature Committee on Cell Death 2012. *Cell Death Differ* 19, 107-120

Galluzzi L, Kepp O, Trojel-Hansen C, Kroemer G (2012b) Mitochondrial control of cellular life, stress, and death. *Circ Res* 111, 1198-1207

Galluzzi L, Kepp O, Krautwald S, Kroemer G, Linkermann A (2014a) Molecular mechanisms of regulated necrosis. *Semin Cell Dev Biol*, doi: 10.1016/j.semcdb.2014.02.006 [Epub ahead of print]

Galluzzi L, Kepp O, Kroemer G (2014b) MLKL regulates necrotic plasma membrane permeabilization. *Cell Res* 24, 139-140

Gassmann NR, Stefanick DF, Kedar PS, Horton JK, Wilson SH (2012) Hyperactivation of PARP triggers nonhomologous end-joining in repair-deficient mouse fibroblasts. *PLoS ONE* 7, e49301

Grassmé H, Cremesti A, Kolesnick R, Gulbins E (2003) Ceramide-mediated clustering is required for CD95-DISC formation. *Oncogene* 22, 5457-5470

Gray CW, Ward RV, Karran E, Turconi S, Rowles A, Viglienghi D, Southan C, Barton A, Fantom KG, West A, Savopoulos J, Hassan NJ, Clinkenbeard H, Hanning C, Amegadzie B, Davis JB, Dingwall C, Livi GP, Creasy CL (2000) Characterization of human HtrA2, a novel serine protease involved in the mammalian cellular stress response. *Eur J Biochem* 267, 5699-5710

Griparic L, Kanazawa T, van der Bliek AM (2007) Regulation of the mitochondrial dynamin-like protein Opa1 by proteolytic cleavage. *J Cell Biol* 178, 757-764

Günther C, Martini E, Wittkopf N, Amann K, Weigmann B, Neumann H, Waldner MJ, Hedrick SM, Tenzer S, Neurath MF, Becker C (2011) Caspase-8 regulates TNF-alpha-induced epithelial necroptosis and terminal ileitis. *Nature* 477, 335-339

Guicciardi ME, Deussing J, Miyoshi H, Bronk SF, Svingen PA, Peters C, Kaufmann SH, Gores GJ (2000) Cathepsin B contributes to TNF-α-mediated hepatocyte apoptosis by promoting mitochondrial release of cytochrome c. *J Clin Invest* 106, 1127-1137

Gulbins E, Szabo I, Baltzer K, Lang F (1997) Ceramide-induced inhibition of T lymphocyte voltage-gated potassium channel is mediated by tyrosine kinases. *Proc Natl Acad Sci USA* 94, 7661-7666

Gulbins E, Drescher S, Wilker B, Grassmé H (2004) Ceramide, membrane rafts and infections. *J Mol Med (Berl)* 82, 357-363

Gulbins E, Li PL (2006) Physiological and pathophysiological aspects of ceramide. *Am J Physiol Regul Integr Comp Physiol* 290, R11-R26

Guo Y, Chen C, Zheng Y, Zhang J, Tao X, Liu S, Zheng D, Liu Y (2005) A novel anti-human DR5 monoclonal antibody with tumoricidal activity induces caspase-dependent and caspase-independent cell death. *J Biol Chem* 280, 41940-41952

Gupta S, Singh R, Datta P, Thang Z, Orr C, Lu Z, Dubios G, Zervos AS, Meisler MH, Srinivasula SM, Fernandes-Alnemri T, Alnemri ES (2004) The C-terminal tail of presenilin regulates Omi/HtrA2 protease activity. *J Biol Chem* 279, 45844-45854

Hadler-Olsen E, Winberg JO, Uhlin-Hansen L (2013) Matrix metalloproteinases in cancer: their value as diagnostic and prognostic markers and therapeutic targets. *Tumor Biol* 34, 2041-2051

Hahn-Windgassen A, Noqueira V, Chen CC, Skeen JE, Sonnenberg N, Hay N (2005) Akt activates the mammalian target of rapamycin by regulating cellular ATP level and AMPK activity. *J Biol Chem* 280, 32081-32089

Haimovitz-Friedmann A, Kan CC, Ehleiter D, Persaud RS, McLoughlin M, Fuks Z, Kolesnick RN (1994) Ionizing radiation acts on cellular membranes to generate ceramide and initiate apoptosis. *J Exp Med* 180, 525-535

Han WQ, Xia M, Xu M, Boini KM, Ritter JK, Li NJ, Li PL (2012) Lysosome fusion to the cell membrane is mediated by the dysferlin C2A domain in coronary arterial endothelial cells. *J Cell Sci* 125, 1225-1234

Hannun YA, Obeid LM (2008) Principles of bioactive lipid signaling: lessons from sphingolipids. *Nat Rev Mol Cell Biol* 9, 139-150

Hara Y, Wakamori M, Ishii M, Maeno E, Nishida M, Yoshida T, Yamada H, Shimizu S, Mori E, Kudoh J, Shimizu N, Kurose H, Okada Y, Imoto K, Mori Y (2002) LTRPC2 Ca2+-permeable channel activated by changes in redox status confers susceptibility to cell death. *Mol Cell* 9, 163-173

Harlow E, Lane D (1988) Antibodies. A laboratory manual. *Cold Spring Harbor Laboratory Press*, USA

Harvey DM, Levine AJ (1991) p53 alteration is common event in the spontaneous immortalization of primary BALB/c murine embryo fibroblasts. *Genes Dev* 5, 2375-2385

He S, Wang L, Miao L, Wang T, Du F, Zhao L, Wang X (2009) Receptor interacting protein kinase-3 determines cellular necrotic response to TNF-α. *Cell* 137, 1100-1111

Heibein JA, Goping IS, Barry M, Pinkoski MJ, Shore GC, Green DR, Bleackley RC (2000) Granzyme B-mediated cytochrome c release is regulated by the Bcl-2 family members Bid and Bax. *J Exp Med* 192, 1391-1402

Heinrich M, Wickel M, Schneider-Brachert W, Sandberg C, Gahr J, Schwandner R, Weber T, Saftig P, Peters C, Brunner J, Krönke M, Schütze S (1999) Cathepsin D targeted by acid sphingomyelinase-derived ceramide. *EMBO J* 18, 5252-5263

Heinrich M, Neumeyer J, Jakob M, Hallas C, Tchikov V, Winoto-Morbach S, Wickel M, Schneider-Brachert W, Trauzold A, Hethke A, Schütze S (2004) Cathepsin D links TNF-induced acid sphingomyelinase to Bid-mediated caspase-9 and -3 activation. *Cell Death Differ* 11, 550-563

Hellwig CT, Rehm M (2012) TRAIL signaling and synergy mechanisms used in TRAIL-based combination therapies. *Mol Cancer Ther* 11, 3-13

Hentze H, Lin XY, Choi MSK, Porter AG (2003) Critical role for cathepsin B in mediating caspase-1-dependent interleukin-18 maturation and caspase-1-independent necrosis triggered by the microbial toxin nigericin. *Cell Death Differ* 10, 956-968

Herreman A, Hartmann D, Annaert W, Saftig P, Craessaerts K, Serneels L, Umans L, Schrijvers V, Checler F, Vanderstichele H, Baekelandt V, Dressel R, Cupers P, Huylebroeck D, Zwijsen A, Van Leuven F, De Strooper B (1999) Presenilin 2 deficiency causes a mild pulmonary phenotype and no changes in amyloid precursor protein processing but enhances the embryonic lethal phenotype of presenilin 1 deficiency. *Proc Natl Acad Sci USA* 96, 11872-11877

Hitomi J, Christofferson DE, Ng A, Yao J, Degterev A, Xavier RJ, Yuan J (2008) Identification of a molecular signaling network that regulates a cellular necrotic cell death pathway. *Cell* 135, 1311-1323

Holler N, Zaru R, Micheau O, Thome M, Attinger A, Valitutti S, Bodmer JL, Schneider P, Seed B, and Tschopp J (2000) Fas triggers an alternative, caspase-8-independent cell death pathway using the kinase RIP as effector molecule. *Nat Immunol* 1, 489-495

Hunter TB, Manimala NJ, Luddy KA, Catlin T, Antonia SJ (2011) Paclitaxel and TRAIL synergize to kill paclitaxel-resistant small cell lung cancer cells through a caspase-independent mechanism mediated through AIF. *Anticancer Res* 31, 3193-3204

Hurwitz R, Ferlinz K, Vielhaber G, Moczall H, Sandhoff K (1994) Processing of human sphingomyelinase in normal and I-cell fibroblasts. *J Biol Chem* 269, 5440-5445

Huwiler A, Fabbro D, Pfeilschifter J (1998) Selective ceramide binding to protein kinase C-alpha and -delta isoenzymes in renal mesangial cells. *Biochemistry* 37, 14556-14562

Huwiler A, Johansen B, Skarstad A, Pfeilschifter J (2001) Ceramide binds to the CaLB domain of cytosolic phospholipase A2 and facilitates its membrane docking and arachidonic acid release. *FASEB J* 15, 7-9

Ishihara N, Fujita Y, Oka T, Mihara K (2006) Regulation of mitochondrial morphology through proteolytic cleavage of OPA1. *EMBO J* 25, 2966-2977

Ivanovska J, Trequbova A, Mahadevan V, Chakilam S, Gandesiri M, Benderska N, Ettle B, Hartmann A, Söder S, Ziesche E, Fischer T, Lautschaum L, Fabry B, Segrer G, Gohla A, Schneider-Stock (2013) Identification of DAPK as a scaffold for the LIMK/cofilin complex in TNF-induced apoptosis. *Int J Biochem Cell Biol* 45, 1720-1729

Jäättelä M, Tschopp J (2003) Caspase-independent cell death in T lymphocytes. *Nat Immunol* 4, 416-423

Jenkins RW, Idkowiak-Baldys J, Simbari F, Canals D, Roddy P, Riner CD, Clarke CJ, Hannun YA (2011) A novel mechanism of lysosomal acid sphingomyelinase maturation: requirement for carboxy-terminal proteolytic processing. *J Biol Chem* 286, 3777-3788

Jeong HC, Kim GI, Cho SH, Lee KH, Ko JJ, Yang JH, Chung KH (2011) Proteomic analysis of human small cell lung cancer tissues: up-regulation of coactosin-like protein-1. *J Proteome Res* 10, 269-276

Jouan-Lanhouet S, Arshad MI, Piquet-Pellorce C, Martin-Chouly C, Le Moigne-Muller G, Van Herreweghe F, Takahashi N, Sergent O, Lagadic-Gossmann D, Vandenabeele P, Samson M, Dimanche-Boitrel MT (2012) TRAIL induces necroptosis involving RIPK1/RIPK3-dependent PARP-1 activation. *Cell Death Differ* 19, 2003-2014

Juhl H, Helmig F, Baltzer K, Kalthoff H, Henne-Bruns D, Kremer B (1997) Frequent expression of complement resistance factors CD46, CD55, and CD59 on gastrointestinal cancer cells limits the therapeutic potential of monoclonal antibody 17-1A. *J Surg Oncol* 64, 222-230

Kaczmarek A, Vandenabeele P, Krysko DV (2013) Necroptosis: the release of damage-associated molecular patterns and its physiological relevance. *Nat Rev Mol Cell Biol* 11, 700-714

Kadohara K, Nagumo M, Asami S, Tsukumo Y, Sugimoto H, Igarashi M, Nagai K, Kataoka T (2008) Caspase-8 mediates mitochondrial release of pro-apoptotic proteins in a manner independent of its proteolytic activity in apoptosis induced by the protein synthesis inhibitor acetoxycycloheximide in human leukemia Jurkat cells. *J Biol Chem* 284, 5478-5487

Kähler M (2013) TRAIL-induced caspase-independent cell death: Impact of receptor localization, interacting proteins and proteolytic events. *Master Thesis*, Christian-Albrechts-Universität zu Kiel, Kiel

Kagedal K, Zhao M, Svensson I, Brunk UT (2001) Sphingosine-induced apoptosis is dependent on lysosomal proteases. *Biochem J* 359, 335-343

Kaiser WJ, Upton JW, Long AB, Livingston-Rosanoff D, Daley-Bauer LP, Hakem R, Caspary T, Mocarski ES (2011) RIP3 mediates the embryonic lethality of caspase-8-deficient mice. *Nature* 471, 368-372

Karasuyama H and Melchers F (1988) Establishment of mouse cell lines which constitutively secrete large quantities of interleukin 2, 3, 4, or 5, using modified cDNA expression vectors. *Eur J Immunol* 18, 97-104

Katz SI, Zhou L, Chao G, Smith CD, Ferrara T, Wang W, Dicker DT, El-Deiry WS (2009) Sorafenib inhibits ERK1/2 and MCL-1(L) phosphorylation levels resulting in caspase-independent cell death in malignant pleural mesothelioma. *Cancer Biol Ther* 8, 2406-2416

Kerr JF, Wyllie AH, Currie AR (1972) Apoptosis: a basic biological phenomenon with wide-ranging implications in tissue kinetics. *Br J Cancer* 26, 239-257

Kimura J, Kudoh T, Miki Y, Yoshida K (2011) Identification of dihyropyrimidase-related protein 4 as a novel target of the p53 tumor suppressor in the apoptotic response to DNA damage. *Int J Cancer* 128, 1524-1531

King MA, Halicka HD, Darzynkiewicz Z (2004) Pro- and anti-apoptotic effects of an inhibitor of chymotrypsin-like serine proteases. *Cell Cycle* 3, 1566-1571

Kischkel FC, Lawrence DA, Tinel A, LeBlanc H, Virmani A, Schow P, Gazdar A, Blenis J, Arnott D, Ashkenazi A (2001) Death receptor recruitment of endogenous caspase-10 and apoptosis initiation in the absence of caspase-8. *J Biol Chem* 276, 46639-46646

Kisselev AF, Akopian TN, Castillo V, Goldberg AL (1999) Proteasome active sites allosterically regulate each other, suggesting a cyclical bite-chew mechanism for protein breakdown. *Mol Cell* 4, 395-402

Kleifeld O, Doucet A, Prudova A, auf dem Keller U, Kizhakkedathu JN, Overall CM (2011) Identifying and quantifying proteolytic events and the natural N terminome by terminal amine isotopic labeling of substrates. *Nat Protoc* 22, 1578-1611

Kolesnick RN, Krönke M (1998) Regulation of ceramide production and apoptosis. *Annu Rev Physiol* 60, 643-665

Kurdow R, Schniewind B, Zoefelt S, Boenicke L, Boehle AS, Dohrmann P, Kalthoff H (2005) Apoptosis by gemcitabine in non-small cell lung cancer cell line KNS62 is induced downstream of caspase 8 and is profoundly blocked by Bcl-xL overexpression. *Langenbecks Arch Surg* 390, 243-248

Laemmli UK (1970) Cleavage of structural proteins during the assembly of the head of bacteriophage T4. *Nature* 227, 680-685

Lafont E, Milhas D, Carpentier S, Garcia V, Jin ZX, Umehara H, Okazaki T, Schulze-Osthoff K, Levade T, Benoist H, Sequi B (2010) Caspase-mediated inhibition of sphingomyelin synthesis is involved in FasL-triggered cell death. *Cell Death Differ* 17, 642-654

Lamkanfi M, Festjens N, Declercq W, Vanden Berghe T, Vandenabeele P (2007) Caspases in cell survival, proliferation and differentiation. *Cell Death Differ* 14, 44-55

Lazebnik YA, Kaufmann SH, Desnoyers S, Poirier GG, Earnshaw WG (1994) Cleavage of poly(ADP-ribose) polymerase by a proteinase with properties like ICE. *Nature* 371, 346-347

Leist M, Jäättelä M (2001) Four deaths and a funeral: from caspases to alternative mechanisms. *Nat Rev Mol Cell Biol* 2, 589-598

Li J, McQuade T, Siemer AB, Napetschnig J, Moriwaki K, Hsiao YS, Damko E, Moquin D, Walz T, McDermott A, Chan FKM, Wu H (2012) The RIP1/RIP3 necrosome forms a functional amyloid signaling complex required for programmed necrosis. *Cell* 150, 339-350

Li M, Ona VO, Guégan C, Chen M, Jackson-Lewis V, Andrews LJ, Olszewski AJ, Stieg PE, Lee JP, Przedborski S, Friedlander RM (2000) Functional role of caspase-1 and caspase-3 in ALS transgenic mouse model. *Science* 288, 335-339

Lim SY, Davidson SM, Mocanu MM, Yellon DM, Smith CC (2007) The cardioprotective effect of necrostatin requires the cyclophilin-D component of the mitochondrial permeability transition pore. *Cardiovasc Drugs Ther* 21, 467-469

Lin MT, Beal MF (2006) Mitochondrial dysfunction and oxidative stress in neurodegenerative diseases. *Nature* 443, 787-798

Lin Y, Devin A, Rodriguez Y, Liu ZG (1999) Cleavage of the death domain kinase RIP by caspase-8 prompts TNF-induced apoptosis. *Genes Dev* 13, 2514-2526

Lin Y, Choski S, Shen HM, Yang QF, Hur GM, Kim YS, Tran JH, Nedospasov SA, Liu ZG (2003) TNF-induced non-apoptotic cell death requires RIP-mediated cellular reactive oxygen species accumulation. *J Biol Chem* 279, 10822-10828

Linkermann A, Bräsen JH, Darding M, Kyung Jin M, Sanz AB, Heller JO, De Zen F, Weinlich R, Ortiz A, Walczak H, Weinberg JM, Green DR, Kunzendorf U, Krautwald S (2013) Two independent pathways of regulated necrosis mediate ischemia-reperfusion injury. *Proc Natl Acad Sci USA* 110, 12024-12029

Lipinski S, Grabe N, Jacobs G, Billmann-Born S, Till A, Häsler R, Aden K, Paulsen M, Arlt A, Kraemer L, Hagemann N, Erdmann KS, Schreiber S, Rosenstiel P (2012) RNAi screening identifies mediators of NOD2 signaling: Implications for spatial specificity of MDP recognition. *Proc Natl Acad Sci USA* 109, 21426-21431

Liu T, Lu B, Lee I, Ondrovicova G, Kutejova E, Suzuki CK (2004) DNA and RNA binding by the mitochondrial lon protease is regulated by nucleotide and protein substrate. *J Biol Chem* 279, 13902-13910

Lockshin RA, Williams CM (1964) Programmed cell death. II. Endocrine potentiation of the breakdown of the intersegmental muscles of silkmoths. *J Insect Physiol* 10, 643-649

Lorenzo HK, Susin SA (2007) Therapeutic potential of AIF-mediated caspase-independent programmed cell death. Drug Resist. *Updates* 10, 235-255

Los M, Mozuluk M, Ferrari D, Stepczynska A, Stroh C, Renz A, Herceg Z, Wang ZQ, Schulze-Osthoff K (2002) Activation and caspase-mediated inhibition of PARP: a molecular switch between fibroblast necrosis and apoptosis in death receptor signaling. *Mol Biol Cell* 13, 978-988

Madison DL, Stauffner D, Lundblad JR (2011) The PARP inhibitor PJ34 causes a PARP1-independent, p21-dependent mitotic arrest. *DNA Repair* 10, 1003-1013

Mahmood Z, Shukla Y (2010) Death receptors: Targets for cancer therapy. *Exp Cell Res* 316, 887-899

Martins LM, Morrison A, Klupsch K, Fedele V, Moisoi N, Teismann P, Abuin A, Grau E, Geppert M, Livi GP, Creasy CL, Martin A, Hargreaves I, Heales SJ, Okada H, Brandner S, Schulz JB, Mak T, Downward J (2004) Neuroprotective role of the Reaper-related serine protease HtrA2/Omi revealed by targeted deletion in mice. *Mol Cell Biol* 24, 9848-9862

Mates JM, Segura JA, Campos-Sandoval JA, Lobo C, Alonso L, Alonso FJ, Marquez J (2009) Glutamine homeostasis and mitochondrial dynamics. *Int J Biochem Cell Biol* 41, 2051-2061

McCormick AL, Roback L, Mocarski ES (2008) HtrA2/Omi terminates cytomegalovirus infection and is controlled by the viral mitochondrial inhibitor of apoptosis (vMIA). *PLoS Pathog* 4, e1000063

McPherson PS, Kay BK, Hussain NK (2001) Signaling on the endocytic pathway. *Traffic* 2, 375-384

Menendez M (2004) Pathological and clinical heterogeneity of presenilin 1 gene mutations. *J Alzheimers Dis* 6, 475-482

Merino D, Lalaoui N, Morizot A, Schneider P, Solary E, Micheau O (2006) Differential inhibition of TRAIL-mediated DR5-DISC formation by decoy receptors 1 and 2. *Mol Cell Biol* 26, 7046-7055

Micheau O, Tschopp J (2003) Induction of TNF receptor I-mediated apoptosis via two sequential signaling complexes. *Cell* 114, 181-190

Mihalik R, Imre G, Petak I, Szende B, Kopper L (2004) Cathepsin B-independent abrogation of cell death by CA-074-OMe upstream of lysosomal breakdown. *Cell Death Differ* 11, 1357-1360

Mocarski ES, Upton JW, Kaiser WJ (2011) Viral infection and the evolution of caspase 8-regulated apoptotic and necrotic death pathways. *Nat Rev Immunol* 12, 79-88

Morgan MJ, Kim YS, Liu ZG (2008) TNFα and reactive oxygen species in necrotic cell death. *Cell Res* 18, 343-349

Moriwaki K, Chan FK (2013) Necrosis-dependent and independent signaling of the RIPK kinases in inflammation. *Cytokine Growth Factor Rev* 25, 167-174

Narayanan V, Gutman JA, Pollyea DA, Jimeno A (2013) Omacetaxine mepesuccinate for the treatment of chronic myeloid leukemia. *Drugs Today (Barc)* 49, 447-456

Newton K, Dugger DL, Wickliffe KE, Kapoor N, De-Almagro MC, Vucic D, Komuves L, Ferrando RE, French DM, Webster J, Roose-Girma M, Warming S, Dixit VM (2014) Activity of protein kinase RIPK3 determines whether cells die by necroptosis or apoptosis. *Science* 343, 1357-1360

Oberst A, Dillon CP, Weinlich R, McCormick LL, Fithgerald P, Pop C, Hakem R, Salvesen GS, Green DR (2011) Catalytic activity of the caspase-8-FLIPL complex inhibits RIPK3-dependent necrosis. *Nature* 471, 363-367

O'Donnell MA, Legarda-Addison D, Skountzos P, Yeh WC, Ting AT (2007) Ubiquitination of RIP1 regulates an NF-kappaB-independent cell-death switch in TNF signaling. *Curr Biol* 17, 418-424

O'Farrell PH (1975) High resolution two-dimensional electrophoresis of proteins. *J Biol Chem* 250, 4007-4021

Okada M, Adachi S, Imai T, Watanabe K, Toyokuni S, Ueno M, Zervos AS, Kroemer G, Nakahata T (2004) A novel mechanism for imatinib mesylate-induced cell death of BCR-ABL-

positive human leukemic cells: caspase-independent, necrosis-like programmed cell death mediated by serine protease activity. *Blood* 103, 2299-2307

Ondrovicova G, Liu T, Singh K, Tian B, Li H, Gakh O, Perecko D, Janata J, Granot Z, Orly J, Kutejova E, Suzuki CK (2005) Cleavage site selection within a folded substrate by the ATP-dependent lon protease. *J Biol Chem* 280, 25103-25110

Perrotta C, Bizzozero L, Cazzato D, Morlacchi S, Assi E, Simbari F, Zhang Y, Gulbins E, Bassi MT, Rosa P, Clementi E (2010) Syntaxin 4 required for acid sphingomyelinase activity and apoptotic function. *J Biol Chem* 285, 40240-40251

Pettus BJ, Chalfant CE, and Hannun YA (2002) Ceramide in apoptosis: an overview and current perspectives. *Biochim Biophys Acta* 1585, 114-125

Pospisilova J, Vit O, Lorkova L, Klanova M, Zivny J, Klener P, Petrak J (2013) Resistance to TRAIL in mantle cell lymphoma cells is associated with the decreased expression of purine metabolism enzymes. *Int J Mol Med* 31, 1273-1279

Possemato R, Marks KM, Shaul YD, Pacold ME, Kim D, Birsoy K, Sethumadhavan S, Woo HK, Jang HG, Jha AK, Chen WW, Barrett FG, Stransky N, Tsun ZH, Cowley GS, Barretina J, Kalaany NY, Hsu PP, Ottina K, Chan AM, Yuan B, Garraway LA, Root DE, Mino-Kenudson M, Brachtel EF, Driggers EM, Sabatini DM (2011) Functional genomics reveal that the serine synthesis pathway is essential in breast cancer. *Nature* 476, 346-350

Pukac L, Kanakaraj P, Humphreys R, Alderson R, Bloom M, Sung C, Riccobene T, Johnson R, Fiscella M, Mahoney A, Carrell J, Boyd E, Yao XT, Zhang L, Zhong L, von Kerczek A, Shepard L, Vaughan T, Edwards B, Dobson C, Salcedo T, Albert V (2005) HGS-ETR1, a fully human TRAIL-receptor 1 monoclonal antibody, induces cell death in multiple tumor types *in vitro* and *in vivo*. *Br J Cancer* 92, 1430-1441

Remijsen Q, Kuijpers TW, Wirawan E, Lippens S, Vandenabeele P, Vanden Berghe T (2011) Dying for a cause: NETosis mechanisms behind an antimicrobial cell death modality. *Cell Death Differ* 18, 581-588

Remijsen Q, Goossens V, Grootjans S, Van den Haute C, Vanlangenakker N, Dondelinger Y, Roelandt R, Bruggeman I, Goncalves A, Bertrand MJ, Baekelandt V, Takahashi N, Vanden Berghe T, Vandenabeele P (2014) Depletion of RIPK3 or MLKL blocks TNF-driven necroptosis and switches towards a delayed RIPK1 kinase-dependent apoptosis. *Cell Death Dis* 16, e1004

Rep M, Van Dijl JM, Suda K, Schatz G, Grivelli LA, Suzuki CK (1996) Promotion of mitochondrial membrane complex assembly by a proteolytically inactive yeast Lon. *Science* 274, 103-106

Rhein C, Tripal P, Seebahn A, Konrad A, Kramer M, Nagel C, Kemper J, Bode J, Mühle C, Gulbins E, Reicher M, Becker CM, Kornhuber J (2012) Functional implications of novel human acid sphingomyelinase splice variants. *PLoS ONE* 7, e35467

Roach HI, Clarke NM (2000) Physiological cell death of chondrocytes *in vivo* is not confined to apoptosis. New observations on the mammalian growth plate. *J Bone Joint Surg Br* 82, 601-613

Rokhlin OW, Guseva NV, Taghiyev AF, Glover RA, Cohen MB (2004) Multiple effects of N-α-tosyl-L-phenylalanyl chloromethyl ketone (TPCK) on apoptotic pathways in human prostatic carcinoma cell lines. *Cancer Biol Ther* 3, 761-768

Ross PL, Huang YN, Marchese JN, Williamson B, Parker K, Hattan S, Khainovski N, Pillai S, Dey S, Daniels S, Purkayastha S, Juhasz P, Martin S, Bartlet-Jones M, He F, Jacobson A, Pappin DJ (2004) Multiplexed protein quantification in Saccharomyces cerevisiae using amine-reactive isobaric tagging reagents. *Mol Cell Proteomics* 3, 1154-1169

Roth AG, Drescher D, Yang Y, Redmer S, Uhlig S, Arenz C (2009) Potent and selective inhibition of acid sphingomyelinase by bisphosphonates. *Angew Chem Int Ed Engl* 48, 7560-7563

Rotolo JA, Zhang J, Donepudi M, Lee H, Fuks Z, Kolesnick R (2005) Caspase-dependent and -independent activation of acid sphingomyelinase signaling. *J Biol Chem* 280, 26425-26434

Saddoughi SA, Gencer S, Peterson YK, Ward KE, Mukhopadhyay A, Oaks J, Bielawski J, Szulc ZM, Thomas RJ, Selvam SP, Senkal CE, Garrett-Mayer E, De Palma RM, Fedarovich D, Liu A, Habib AA, Stahelin RV, Perrotti D, Ogretmen B (2013) Sphingosine analogue drug FTY720 targets I2PP2A/SET and mediates lung tumor suppression via activation of PP2A-RIPK1-dependent necroptosis. *EMBO J* 5, 105-121

Samapati R, Yang Y, Yin J, Stoerger C, Arenz C, Dietrich A, Gudermann T, Adam D, Wu S, Freichel M, Flockerzi V, Uhlig S, Kuebler WM (2012) Lung endothelial Ca^{2+} and permeability response to platelet-activating factor is mediated by acid sphingomyelinase and transient receptor potential classical 6. *Am J Resp Crit Care Med* 185, 160-170

Santana P, Pena LA, Haimovitz-Friedmann A, Martin S, Green D, McLoughlin M, Cordon-Cardo C, Schuchmann EH, Fuks Z, Kolesnick R (1996) Acid sphingomyelinase-deficient human lymphoblasts and mice are defective in radiation-induced apoptosis. *Cell* 86, 189-199

Savill J, Fadok V (2000) Corpse clearance defines the meaning of cell death. *Nature* 407, 784-788

Scaffidi C, Fulda S, Srinivasan A, Friesen C, Li F, Tomaselli KJ, Debatin KM, Krammer P, and Peter ME (1998) Two CD95 (APO-1/Fas) signaling pathways. *EMBO J* 17, 1675-1687

Scandroglio F, Venkata JK, Loberto N, Prioni S, Schuchmann EH, Chigorno V, Prinetti A, Sonnino S (2008) Lipid content of brain, brain membrane lipid domains, and neurons from acid sphingomyelinase deficient mice. *J Neurochem* 107, 329-338

Schissel SL, Keesler GA, Schuchmann EH, Williams KJ, Tabas I (1998) The cellular trafficking and zinc dependence of secretory and lysosomal sphingomyelinase, two products of the acid sphingomyelinase gene. *J Biol Chem* 273, 18250-18259

Schneider-Brachert W, Tchikov V, Neumeyer J, Jakob M, Winoto-Morbach S, Held-Feindt J, Heinrich M, Merkel O, Ehrenschwender M, Adam D, Mentlein R, Kabelitz D, Schütze S (2004) Compartmentalization of TNF receptor 1 signaling; internalized TNF receptosomes as death signaling vesicles. *Immunity* 21, 415-428

Schmidt H, Gelhaus C, Lucius R, Nebendahl M, Leippe M, Janssen O (2009) Enrichment and analysis of secretory lysosomes from lymphocyte populations. *BMC Immunol* 10, 1471-2172

Schmitz C, Dorovkov MV, Zhao X, Davenport BJ, Ryazanov G, Perraud AL (2005) The channel kinases TRPM6 and TRPM7 are functionally nonredundant. *J Biol Chem* 280, 37763-37771

Schrader K, Huai J, Jöckel L, Oberle C, Borner C (2010) Non-caspase proteases: triggers or amplifiers of apoptosis? *Cell Mol Life Sci* 67, 1607–1618

Schütze S, Potthoff K, Machleidt T, Berkovic D, Wiegmann K, Krönke M (1992) TNF activates NF-kappa-B by phosphatidylcholine-specific phospholipase-C-induced acidic sphingomyelin breakdown. *Cell* 71, 765-776

Schütze S, Machleidt T, Adam D, Schwandner R, Wiegmann K, Kruse LM, Heinrich M, Wickel M, Krönke M (1999) Inhibition of receptor internalization by monodansylcadaverine selectively blocks p55 TNF receptor death domain signaling. *J Biol Chem* 274, 10203-10212

Schuchmann EH (2010) Acid sphingomyelinase, cell membranes and human disease: lessons from Niemann-Pick disease. *FEBS Lett* 584, 1895-1900

Schulze-Osthoff K, Bakker AC, Vanhaesebroeck B, Beyaert R, Jacob WA, Fiers W (1992) Cytotoxic activity of tumor necrosis factor is mediated by early damage of mitochondrial functions. Evidence for the involvement of mitochondrial radical generation. *J Biol Chem* 267, 5317-5323

Seok JH, Park KA, Byun HS, Won M, Shin S, Choi BL, Lee H, Kim YR, Hong JH, Park J, Hur GM (2008) Long-term activation of c-Jun N-terminal kinase through receptor interacting protein is associated with DNA damage-induced cell death. *Korean J Physiol Pharmacol* 12, 185-191

Sevrioukova IF (2011) Apoptosis-inducing factor: structure, function, and redox regulation. *Antioxid Redox Signal* 14, 2545-2579

Shacka JJ, Klocke BJ, Young C, Shibata M, Olney JW, Uchiyama Y, Saftig P, Roth KA (2007) Cathepsin D deficiency induces persistent neurodegeneration in the absence of Bax-dependent apoptosis. *J Neurosci* 27, 2081-2090

Shembade N, Ma A, Harhaj EW (2010) Inhibition of NF-kappaB signaling by A20 through disruption of ubiquitin enzyme complexes. *Science* 327, 1135-1139

Shen J, Bronson RT, Chen DF, Xia W, Selkoe DJ, Tonegawa S (1997) Skeletal and CNS defects in presenilin-1-deficient mice. *Cell* 89, 629-639

Simpson WL Jr, Medelson D, Wasserstein MP, McGovern MM (2010) Imaging manifestations of Niemann-Pick disease type B. *AJR Am J Roentgenol* 194, W12-W19

Sipos B, Möser S, Kalthoff H, Török V, Löhr M, Klöppel G (2003) A comprehensive characterization of pancreatic ductal carcinoma cell lines: towards the establishment of an in vitro research platform. *Virchows Arch* 442, 444-452

Siskind LJ, Colombini M (2000) The lipids C2- and C16-ceramide form large stable channels. Implications for apoptosis. *J Biol Chem* 275, 38640-38644

Si-Tayeb K, Monvoisin A, Mazzocco C, Lepreux S, Decossas M, Cubel G, Taras D, Blanc JF, Robinson DR, Rosenbaum J (2006) Matrix metalloproteinase 3 is present in the cell nucleus and is involved in apoptosis. *Am J Pathol* 169, 1101-1103

Sosna J, Voigt S, Mathieu S, Lange A, Thon L, Davarnia P, Herdegen T, Linkermann A, Rittger A, Chan FK, Kabelitz D, Schütze S, Adam D (2014) TNF-induced necroptosis and PARP-1-mediated necrosis represent distinct routes to programmed necrotic cell death. *Cell Mol Life Sci* 71, 331-348

Sosna J, Voigt S, Mathieu S, Kabelitz D, Trad A, Janssen O, Meyer-Schwesinger C, Schütze S, Adam D (2013) The proteases HtrA2/Omi and UCH-L1 regulate TNF-induced necroptosis. *Cell Commun Signal* 11, 76

Sprick MR, Rieser E, Stahl H, Grosse-Wilde A, Weigand MA, Walczak H (2002) Caspase-10 is recruited to and activated at the native TRAIL and CD95 death-inducing signaling complexes in a FADD-dependent manner but cannot functionally substitute caspase-8. *EMBO J* 21, 4520-4230

Stancevic B, Kolesnick R (2010) Ceramide-rich platforms in transmembrane signaling. *FEBS Lett* 584, 1728-1740

Sternlicht MD, Lochter A, Sympson CJ, Huey B, Rougier JP, Gray JW, Pinkel D, Bissel MJ, Werb Z (1999) The stromal proteinase MMP3/stromelysin-1 promotes mammary carcinogenesis. *Cell* 98, 137-146

Stetak A, Veress R, Ovadi J, Csermely P, Keri G, Ullrich A (2007) Nuclear translocation of the tumor marker pyruvate kinase M2 induces programmed cell death. *Cancer Res* 67, 1602-1608

Stiburek L, Cesnekova J, Kostkova O, Fornuskova D, Vinsova K, Wenchich L, Houstek J, Zeman J (2012) YME1L controls the accumulation of respiratory chain subunits and is required for apoptotic resistance, critae morphogenesis, and cell proliferation. *Mol Biol Cell* 23, 1010-1023

Strelow A, Bernardo K, Adam-Klages S, Linke T, Sandhoff K, Krönke M, Adam D (2000) Overexpression of acid ceramidase protects from tumor necrosis factor-induced cell death. *J Exp Med* 192, 601-611

Sun L, Wang H, Wang Z, He S, Chen S, Liao D, Wang L, Yan J, Liu W, Lei X, Wang X (2012) Mixed Lineage Kinase Domain-like Protein Mediates Necrosis Signaling Downstream of RIP3 Kinase. *Cell* 148, 213-227.

Sun X, Yin J, Starovasnik MA, Fairbrother WJ, Dixit VM (2002) Identification of a novel homotypic interaction motif required for the phosphorylation of receptor-interacting protein (RIP) by RIP3. *J Biol Chem* 277, 9505-9511

Sung ES, Park KJ, Choi HJ, Kim CH, Kim YS (2012) The proteasome inhibitor MG-132 potentiates TRAIL receptor agonist-induced apoptosis by stabilizing tBid and Bik in human and neck squamous cell carcinoma cells. *Exp Cell Res* 318, 1564-1576

Száraz P, Banhegyi G, Marcolongo P, Benedetti A (2013) Transient knockdown of presenilin-1 provokes endoplasmic reticulum stress related formation of autophagosomes in HepG2 cells. *Arch Biochem Biophys* 538, 57-63

Tait SM, Oberst A, Quarato G, Milasta S, Haller M, Wang R, Karvela M, Ichim G, Yatim N, Albert ML, Kidd G, Wakefield R, Frase S, Krautwald S, Linkermann A, Green DR (2013) Widespread mitochondrial depletion via mitophagy does not compromise necroptosis. *Cell Rep* 5, 878-885

Takahashi K, Kawai T, Kumar H, Sato S, Yonehara S, Akira S (2006) Cutting edge: roles of caspase-8 and caspase-10 in innate immune responses to double-stranded RNA. *J Immunol* 176, 4520-4524

Tapia-Vieyra JV, Arellano RO, Mas-Oliva J (2005) ARP2 a novel protein involved in apoptosis of LNCaP cells shares a high degree homology with splicing factor Prp8. *Mol Cell Biochem* 269, 189-201

Tartaglia LA, Pennica D, Goeddel DV (1993) Ligand passing: the 75-kDa tumor necrosis factor (TNF) receptor recruits TNF for signaling by the 55-kDa TNF receptor. *J Biol Chem* 268, 16542-16548

Taylor RC, Cullen SP, Martin SJ (2008) Apoptosis: controlled demolition at the cellular level. *Nat Rev Mol Cell Biol* 9, 231-241

Tchikov V, Schütze S (2008) Immunomagnetic isolation of tumor necrosis factor receptosomes. *Methods Enzymol* 442, 101-123

Tchikov V, Fritsch J, Schütze S (2014) Separation of magnetically isolated TNF receptosomes from mitochondria. *Methods Enzymol* 535, 327-349.

Temkin V, Huang Q, Liu H, Osada H, Pope RM (2006) Inhibition of ADP/ATP exchange in receptor-interacting protein-mediated necrosis. *Mol Cell Biol* 26, 2215-2225

Thon L, Möhlig H, Mathieu S, Lange A, Bulanova E, Winoto-Morbach S, Schütze S, Bulfone-Paus S, and Adam D (2005) Ceramide mediates caspase-independent programmed cell death. *FASEB J* 19, 1945-1956

Thon L, Mathieu S, Kabelitz D, Adam D (2006) The murine TRAIL receptor signals caspase-independent cell death through ceramide. *Exp Cell Res* 312, 3808-3821

Trencia A, Fiory F, Maitan MA, Vito P, Barbagallo AP, Perfetti A, Miele C, Ungaro P, Oriente F, Cilenti L, Zervos AS, Formisano P, Beguinot F (2004) Omi/HtrA2 promotes cell death by binding and degrading the anti-apoptotic protein ped/pea-15. *J Biol Chem* 279, 46566-46572

Trichonas G, Murakami Y, Thanos A, Morizane Y, Kayama M, Debouck CM, Histomi T, Miller JW, Vavvas DG (2010) Receptor interacting protein kinases mediate retinal detachment-induced photoreceptor necrosis and compensate for inhibition of apoptosis. *Proc Natl Acad Sci USA* 107, 21695-21700

Uhlig S, Gulbins E (2008) Sphingolipids in the lung. *Am J Respir Crit Care Med* 178, 1100-1114

Unlü M, Morgan ME, Minden JS (1997) Difference gel electrophoresis: a single gel method for detecting changes in protein extracts. *Electrophoresis* 18 (11), 2071-2077

Upton J, Kaiser W, Mokarski E (2010) Virus inhibition of RIP3-dependent necrosis. *Cell Host Microbe* 7, 302-313

Van Herreweghe F, Mao J, Chaplen FW, Grooten J, Gevaert K, Vandekerckhove J, Vancompernolle K (2002) Tumor necrosis factor-induced modulation of glyoxylase I activities through phosphorylation by PKA results in cell death and is accompanied by the formation of a specific methylglyoxal AGE. *Proc Natl Acad Sci USA* 99, 949-954

Van Loo G, Van Gurp M, Depuydt B, Srinivasula SM, Rodriguez I, Alnemri ES, Gevaert K, Vandekerckhove J, Declercq W, Vandenabeele P (2002) The serine protease Omi/HtrA2 is released from mitochondria during apoptosis. Omi interacts with caspase-inhibitor XIAP and induces enhanced caspase activity. *Cell Death Differ* 9, 20-26

Vande Walle L, Lamkanfi M, Vandenabeele P (2008) The mitochondrial serine protease HtrA2/Omi: an overview. *Cell Death Differ* 15, 453-460

Vande Walle L, Wirawan E, Lamkanfi M, Festjens N, Verspurten J, Saelens X, Vanden Berghe T, Vandenabeele P (2010) The mitochondrial serine protease HtrA2/Omi cleaves RIP1 during apoptosis of Ba/F3 cells induced by growth factor withdrawal. *Cell Res* 20, 421-433

Vandenabeele P, Galluzzi L, Vanden Berghe T, Kroemer G (2010) Molecular mechanisms of necroptosis: an ordered cellular explosion. *Nature Rev Mol Cell Biol* 11, 700-714

Vanden Berghe T, Linkermann A, Jouan-Lanhouet S, Walczak H, Vandenabeele P (2014) Regulated necrosis: the expanding network of non-apoptotic cell death pathways. *Nat Rev Mol Cell Biol* 15, 135-147

Vanhaesebroeck B, Decoster E, Van Ostade X, Van Bladel S, Lenaerts A, Van Roy F, Fiers W (1992) Expression of an exogenous tumor necrosis factor (TNF) gene in TNF-sensitive cell lines confers resistance to TNF-mediated cell lysis. *J Immunol* 148, 2785-2794

Vanlangenakker N, Vanden Berghe T, Krysko DV, Festjens N, Vandenabeele P (2008) Molecular mechanisms and pathophysiology of necrotic cell death. *Curr Mol Med* 8, 207-220

Vanlangenakker N, Vanden Berghe T, Bogaert P, Laukens B, Zobel K, Deshayes K, Vucic D, Fulda S, Vandenabeele P, Bertrand MJ (2011a) cIAP1 and TAK1 protect cells from TNF-induced necrosis by preventing RIP1/RIP3-dependent reactive oxygen species production. *Cell Death Differ* 18, 656-6654

Vanlangenakker N, Bertrand MJ, Bogaert P, Vandenabeele P, Vanden Berghe T (2011b) TNF-induced necroptosis in L929 cells is tightly regulated by multiple TNFR1 complex I and II members. *Cell Death Dis* 2, e230

Vanlangenakker N, Vanden Berghe T, Vandenabeele P (2012) Many stimuli pull the necrotic trigger, an overview. *Cell Death Differ* 19, 75-86

Varfolomeev E, Blankenship JW, Wayson SM, Fedorova AV, Kayagaki N, Garg P, Zobel K, Dynek JN, Elliott LO, Wallweber HJ, Flygare JA, Fairbrother WJ, Deshayes K, Dixit VM, Vucic D (2007) IAP antagonists induce autoubiquitination of c-IAPs, NF-kappaB activation, and TNFalpha-dependent apoptosis. *Cell* 131, 669-681

Venkatesh S, Lee J, Singh K, Lee I, Suzuki CK (2012) Multitasking in the mitochondrion by the ATP-dependent Lon protease. *Biochim Biophys Acta* 1823, 56-66

Vercammen D, Vandenabeele P, Beyaert R, Declercq W, Fiers W (1997) Tumour necrosis factor-induced necrosis versus anti-Fas-induced apoptosis in L929 cells. *Cytokine* 9, 801-808

Vercammen D, Beyaert R, Denecker G, Goossens V, van Loo G, Declercq W, Grooten J, Fiers W, Vandenabeele P (1998a) Inhibition of caspases increases the sensitivity of L929 cells to necrosis mediated by tumor necrosis factor. *J Exp Med* 187, 1477-1485

Vercammen D, Brouckaert G, Denecker G, Van de Craen, Declercq W, Fiers W, Vandenabeele P (1998b) Dual signaling of the Fas receptor: initiation of both apoptotic and necrotic cell death pathways. *J Exp Med* 188, 919-930

Viloria CG, Peinado JR, Astudillo A, Garcia-Suarez O, Gonzaalez MV, Suarez C, Cal S (2007) Human DESC1 serine protease confers tumorigenic properties to MDCK cells and it is upregulated in tumors of different origin. *Br J Cancer* 97, 201-209

Viringipurampeer IA, Shan X, Gregory-Evans K, Zhang JP, Mahammadi Z, Gregory-Evans CY (2014) Rip3 knockdown rescues photoreceptor cell death in blind pde6c zebrafish. *Cell Death Differ* 21, 665-675

Vogt C (1842) Untersuchungen über die Entwicklungsgeschichte der Geburtshelferkröte (*Alytes obstetricans*). *Solothurn: Jent und Gassmann*

Voigt S (2009) Characterisation of TRAIL-induced caspase-independent programmed cell death. *Bachelor Thesis*, Brandenburgische Technische Universität Cottbus-Senftenberg, Senftenberg

Voigt S (2010) Characterisation of caspase-independent programmed cell death in clinically relevant tumour cell lines. *Master Thesis*, Brandenburgische Technische Universität Cottbus-Senftenberg, Senftenberg

Voigt S, Philipp S, Davarnia P, Winoto-Morbach S, Röder C, Arenz C, Trauzold A, Kabelitz D, Schütze S, Kalthoff H, Adam D (2014) TRAIL-induced programmed necrosis as a novel approach to eliminate tumor cells. *BMC Cancer* 14, 74

Volbracht C, Leist M, Kolb SA, Nicotera P (2001) Apoptosis in caspase-inhibited neurons. *Mol Med* 7, 36-48

von Moltke J, Ayres JS, Kofoed EM, Chavarria-Smith J, Vance RE (2013) Recognition of bacteria by inflammasomes. *Annu Rev Immunol* 31, 73-106

Wabnitz GH, Goursot C, Jahraus B, Kirchgessner H, Hellwig A, Klemke M, Konstandin MH, Samstag Y (2010) Mitochondrial translocation of oxidized cofilin induces caspase-independent necrotic-like programmed cell death of T cells. *Cell Death Dis* 1, e58

Walczak H, Miller RE, Ariail K, Gliniak B, Griffith TS, Kubin M, Chin W, Jones J, Woodward A, Le T, Smith C, Smolak P, Goodwin RG, Rauch CT, Schuh JC, Lynch DH (1999) Tumoricidal activity of tumor necrosis factor-related apoptosis-inducing ligand *in vivo*. *Nat Med* 5, 157-163

Walczak H (2011) TNF and ubiquitin at the crossroads of gene activation, cell death, inflammation, and cancer. *Immunol Rev* 244, 9-28

Wang S, El-Deiry WS (2003) TRAIL and apoptosis induction by TNF-family death receptors. *Oncogene* 22, 8628-8633

Wang Z, Jiang H, Chen S, Du F, Wang X (2012) The mitochondrial phosphatase PGAM5 functions at the convergence point of multiple necrotic death pathways. *Cell* 148, 228-243

Wartha F, Henriques-Normark B (2008) ETosis: a novel cell death pathway. *Sci Signal* 1, pe25

Weihofen A, Lemberg MK, Friedmann E, Rügger H, Schmitz A, Paganetti P, Rovelli G, Martoglio B (2003) Targeting presenilin-type aspartic protease signal peptide peptidase with gamma-secretase inhibitors. *J Biol Chem* 278, 16528-16533

Weihofen A, Martoglio B (2003) Intramembrane-cleaving proteases: controlled liberation of proteins and bioactive peptides. *Trends Cell Biol* 13, 71-78

Wicovsky A, Müller N, Daryab N, Marienfeld R, Kneitz C, Kavuri S, Leverkus M, Baumann B, Wajant H (2007) Sustained JNK activation in response to tumor necrosis factor is mediated by caspases in a cell type-specific manner. *J Biol Chem* 282, 27174-2183

Wicovsky A, Henkler F, Salzmann S, Scheurich P, Kneitz C, Wajant H (2009) Tumor necrosis factor receptor-associated factor-1 enhances proinflammatory TNF receptor-2 signaling and modifies TNFR1-TNFR2 cooperation. *Oncogene* 28, 1769-1781

Wiley SR, Schooley K, Smolak PJ, Din WS, Huang CP, Nicholl JK, Sutherland GR, Smith TD, Rauch C, Smith CA, Goodwin RG (1995) Identification of a new member of the TNF family that induces apoptosis. *Immunity* 3, 673-682

Willingham SB, Bergstralh DT, O'Connor W, Morrison AC, Taxman DJ, Duncan JA, Barnoy S, Venkatesan MM, Flavell RA, Deshmukh M, Hoffman HM, Ting JP (2007) Microbial pathogen-induced necrotic cell death mediated by the inflammasome components CIAS1/cryopyrin/NLRP3 and ASC. *Cell Host Microbe* 2, 147-159

Wolfe MS, Kopan R (2004) Intramembrane proteolysis: theme and variations. *Science* 305, 1119-1123

Wu CJ, Conze DB, Li X, Ying SX, Hanover JA, Ashwell JD (2005) TNF-alpha induced c-IAP1/TRAF2 complex translocation to a Ubc6-containing compartment and TRAF2 ubiquitination. *EMBO J* 24, 1886-1898

Wu G, Chai J, Suber TL, Wu JW, Du C, Wang X, Shi Y (2000) Structural basis of IAP recognition by Smac/DIABLO. *Nature* 408, 1008-1012

Wu GS, Burns TF, Zhan Y, Alnemri ES, El-Deiry WS (1999) Molecular cloning and functional analysis of the mouse homologue of the KILLER/DR5 tumor necrosis factor-related apoptosis-inducing ligand (TRAIL) death receptor. *Cancer Res* 59, 2770-2775

Wu J, Huang Z, Ren J, Zhang Z, He P, Li Y, Ma J, Chen W, Zhang Y, Zhou X, Yang Z, Wu SQ, Chen L, Han J (2013) Mlkl knockout mice demonstrate the indispensable role of Mlkl in necroptosis. *Cell Res* 23, 994-1006

Xie T, Peng W, Yan C, Wu J, Gong X, Shi Y (2013) Structural insights into RIP3-mediated necroptotic signaling. *Cell Rep* 17, 70-78

Xu X, Chua CC, Zhang M, Geng D, Liu CF, Hamdy RC, Chua BH (2010) The role of PARP activation in glutamate-induced necroptosis in HT-22 cells. *Brain Res* 1343, 206-212

Xu Y, Huang S, Liu ZG, Han J (2006) Poly(ADP-ribose) polymerase-1 signaling to mitochondria in necrotic cell death requires RIP1/TRAF2-mediated JNK1 activation. *J Biol Chem* 281, 8788-8795

Yu L, Wan F, Dutta S, Welsh S, Liu ZH, Freundt E, Baehrecke EH, Lenardo M (2006) Autophagic programmed cell death by selective catalase degradation. *Proc Natl Acad Sci USA* 103, 4952-4957

Yu SW, Wang HM, Poitras MF, Coombs C, Bowers WJ, Federoff HJ, Poirier GG, Dawson TM, Dawson VL (2002) Mediation of poly(ADP-ribose) polymerase-1-dependent cell death by apoptosis-inducing factor. *Science* 297, 259-263

Yuan J, Lipinski M, Degterev A (2003) Diversity in the mechanisms of neuronal cell death. *Neuron* 40, 401-413

Zeidan YH, Hannun YA (2007) Activation of acid sphingomyelinase by protein kinase C delta-mediated phosphorylation. *J Biol Chem* 282, 11549-11561

Zhang DW, Shao J, Lin J, Zhang N, Lu BJ, Lin SC, Dong MQ, Han J (2009) RIP3, an energy metabolism regulator that switches TNF-induced cell death from apoptosis to necrosis. *Science* 325, 332-336

Zhang H, Zhou X, McQuade T, Li J, Chan FKM, Zhang J (2011) Functional complementation between FADD and RIP1 in embryos and lymphocytes. *Nature* 471, 373-376

Zhang S, Zhang M, Cai F, Song W (2013) Biological function of presenilin and its role in AD pathogenesis. *Transl Neurodegener* 2, 15

Zhang Y, Yao B, Delikat S, Bayoumy S, Lin XH, Basu S, McGinley M, Chan-Hui PY, Lichenstein H, Kolesnick R (1997) Kinase suppressor of Ras is ceramide-activated protein kinase. *Cell* 89, 63-72

Zhao J, Jitkaew S, Cai Z, Choksi S, Li Q, Luo J, Liu ZG (2012) Mixed lineage kinase domain-like is a key receptor interacting protein 3 downstream component of TNF-induced necrosis. *Proc Natl Acad Sci USA* 109, 5322-5327

Zhou DC, Zittoun R, Marie JP (1995) Homoharringtonine: an effective new natural product in cancer chemotherapy. *Bull Cancer* 82, 987-995

Zhuang M, Guan S, Wang H, Burlingame AL, Wells JA (2013) Substrates of IAP ubiquitin ligases identified with a designed orthogonal E3 ligase, the NEDDylator. *Mol Cell* 49, 273-282

8. Appendix

Table S1: The 40 candidate proteases identified in the first siRNA screen whose down-regulation either positively or negatively affects TNF-induced necroptosis in HT-29 cells. These proteases meet rules for candidates as follows: **(a)** protease genes, represented by two or three siRNAs, which after down-regulation either enhanced or reduced TNF-induced necroptosis compared to control transfected cells by at least 1.5-fold, or **(b)** protease genes, represented by a single siRNA, whose down-regulation either enhanced or reduced necroptosis by at least 1.5-fold and for which the effects after down-regulation by the two other siRNAs had the same enhancing or reducing effect on necroptosis (but with fold-induction below 1.5 and thereby not passing the threshold). Highlighted proteases were also found as candidate hits in the second siRNA screen (see 5.2.2). For all proteins, the related reference sequence from the National Center of Biotechnology Information is listed.

		Meeting rules for positive candidates			
		(a)		(b)	
		positive	negative	positive	negative
Protease	Reference sequence	effect after stimulation			
ADAM33	NM_025220			x	
ADAMTS18	NM_199355			x	
aminopeptidase Q	NM_173800			x	
archaemetzincin1	NM_133463			x	
ATPGTP binding proteinlike 2	NM_024783			x	
ATPGTP binding proteinlike 3	NM_178563				x
carboxypeptidase A5	NM_080385			x	
caspase-8	NM_001228		x		
casperFLIP	NM_003879	x			
cathepsin W	NM_001335				x
chymotrypsin C	NM_007272				x
cylindromatosis protein	NM_015247				x
DESC1 protease	NM_014058			x	
dihydropyrimidinase-related protein 3	NM_001387		x		
dihydropyrimidinase-related protein 4	NM_006426	x			
dipeptidylpeptidase 8	NM_197960				x
DNAdamage inducible protein 2	NM_032341			x	
epoxide hydrolase	NM_000120				x
gammaglutamyltransferase 1	NM_005265	x			
gelatinase A	NM_004530				x
glutamine-fructose-6-phosphate transamidase 2	NM_005110			x	
granzyme A	NM_006144			x	
insulysin	NM_004969			x	
kallikrein hK4	NM_004917				x
kallikrein hK6	NM_002774				x
MAP1D methione aminopeptidase 1D	NM_199227			x	
MASP13	NM_001879			x	
meprin beta subunit	NM_005925			x	
methionyl aminopeptidase I	NM_015143			x	
neutrophil elastase	NM_001972			x	
pancreatic elastase II form B	NM_015849				x
plasma Glucarboxypeptidase	NM_016134				x
polyserase 2	NM_173502				x
PRPF8	NM_006445	x			
rhomboid 5 homolog 2	NM_001005498			x	
S2P protease	NM_015884				x
stromelysin 1	NM_002422			x	
thimet oligopeptidase	NM_003249			x	
tryptase gamma 1	NM_012467	x			
YME1like 1	NM_139312			x	

Table S2: Soluble proteins differentially regulated after induction of necroptosis which were identified by MS analysis. For differential proteome analysis, soluble proteins were extracted from U-937 cells stimulated with TNF60-Fc and zVAD-fmk on ice (0 min) and 20 min at 37 °C to induce necroptosis. Protein extracts from cells stimulated for 20 min were labeled with the fluorescent dye Cy 3, and control extracts were labeled with the fluorescent dye Cy 5 and separated by 2D-DIGE. All differentially expressed protein spots were analyzed by means of MALDI-TOF/TOF, and in the first experiment 30 proteins were identified with high confidence classified based on their x-fold increased or decreased protein levels after induction of necroptosis. In the repetition (second experiment) of the above experiment, 89 differentially expressed protein spots were detected. For 29 protein spots, increased protein levels after 20 min TNF/zVAD stimulation were detected whereas 60 proteins spots showed decreased levels compared to untreated (0 min) samples. Positive values in average ratio mean increased amounts of protein levels after induction of necroptosis, compared to untreated samples. Negative average ratios indicate decreased protein levels after induction of necroptosis. The accession number for the reference sequence of each protein is listed. The protein stathmin with the spot number 2467 and 2469 is a candidate for proteolytic cleavage during necroptosis (see Figure S1). The 2D-DIGE experiment was performed with technical assistance of Melanie Nebendahl and Benjamin Schönbeck (Christian-Albrechts-University, Kiel, Germany). The mass spectrometry analysis of isolated proteins was performed by Tomas Koudelka (Christian-Albrechts-University, Kiel, Germany).

spot no.	identified proteins	accession number	average ratio
Experiment 1			
1145	Probable ATP-dependent RNA helicase	P17844	1.2293
1162	Heterogenous nuclear ribonucleoprotein L	P14866	1.5268
1170	ATPase family AAA domain-containing protein 3B	Q5T9A4	1.2437
1193	Heterogeneous nuclear ribonucleoprotein K	P61978	-1.2687
1291	Tubulin alpha-1C	Q9BQE3	-1.2605
1294	Tubulin alpha-1B chain	P68363	-1.308
1303	Tubulin alpha-1B chain	P68363	-1.2671
1325	Tubulin alpha-1B chain	P68363	-1.2107
1418	Pyruvate kinase isozymes M1/M2	P14618	-1.7399
1428	cAMP-dependent protein kinase type II-alpha regulatory subunit	P13861	1.2019
1488	Protein disulfide-isomerase A6	Q15084	1.3049
1639	Actin, cytoplasmic 2	P63261	-1.3389
1724	Heterogenous nuclear ribonucleoprotein A3	P51991	1.2382
1897	Heterogenous nuclear ribonucleoproteins A2/B1	P22626	1.2153
1927	S-formylglutathione hydrolase	P10768	-1.282
1947	Heterogenous nuclear ribonucleoprotein A1	P09651	1.214
1951	Heterogenous nuclear ribonucleoprotein A1	P09651	1.3069
1974	ELAV-like protein 1	Q15717	1.3073
2036	40S ribosomal protein S3	P23396	-1.268
2076	Rho GDP-dissociation inhibitor 2	P52566	-1.2841
2110	Phosphoglycerate mutase 1	P18669	1.3754
2123	Heat shock protein beta-1	P04792	1.9526
2126	Heat shock protein beta-1	P04792	-1.8452
2211	Adenine phosphoribosyltransferase	P07741	-1.2185
2261	Peptidyl-prolyl cis-trans isomerase B	P23284	1.2811
2272	Cofilin-1	P23528	1.3971
2273	Cofilin-1	P23528	1.2384
2283	Stathmin	P16949	-1.2725
2294	Peptidyl-prolyl cis-trans isomerase A	P62937	1.2322
2295	Nucleoside diphosphate kinase B	P22392	1.2404

Table S2: Continued.

spot no.	identified proteins	accession number	average ratio
Experiment 2			
601	Heterogenous nuclear ribonucleoprotein U	Q00839	-1.331
791	Alpha-actinin-1	P12814	-1.2283
853	DNA replication licensing factor MCM4	P33991	-1.2152
859	Elongation factor 2	P13639	-1.2129
917	Glycogen phosphorylase, brain form	P11216	1.378
1080	Protein transport protein Sec23A	Q15436	1.2614
1100	Procollagen galactosyltransferase 1	Q8NBJ5	1.2913
1105	TATA-binding protein-associated factor 2N	Q92804	-1.302
1125	Moesin	P26039	-1.2084
1226	Plastin-2	P13796	-1.4327
1322	Heterogenous nuclear ribonucleoprotein K	P61978	1.3104
1322	Tubulin beta chain	P07437	1.3104
1346	Heterogenous nuclear ribonucleoprotein K	P61978	-1.2407
1349	Heterogenous nuclear ribonucleoprotein K	P61978	-1.377
1355	Heterogenous nuclear ribonucleoprotein K	P61978	-1.2114
1366	Phosphoglucomutase-1	P36871	-1.9062
1366	Acyl-CoA synthetase family member 2	Q96CM8	-1.9062
1396	Splicing factor U2AF 65 kDa subunit	P26368	-1.2887
1396	Cytoplasmic dynein 1 light intermediate chain	Q9Y6G9	-1.2887
1446	Tubulin alpha-1B chain	P68363	-1.2435
1465	Pyruvate kinase isozymes M1/M2	P14618	-1.3968
1465	Nicalin	Q969V3	-1.3968
1467	Tubulin beta chain	P07437	-1.288
1472	Tubulin beta-2C chain	P68371	-1.2712
1493	Serine beta-lactamase-like protein LACTB, mitochondrial	P83111	-1.3182
1503	Tubulin beta-2B chain	Q9BVA1	-1.4021
1504	Tubulin beta chain	P07437	-1.2213
1510	Adenylyl cyclase-associated protein 1	Q01518	-1.218
1512	Adenylyl cyclase-associated protein 1	Q01518	-1.4225
1516	Adenylyl cyclase-associated protein 1	Q01518	1.2287
1530	Tubulin beta-2C chain	P68371	-1.2569
1532	Pyruvate kinase isozymes M1/M2	P14618	-1.3317
1565	Pyruvate kinase isozymes M1/M2	P14618	-1.2241
1573	cAMP-dependent protein kinase type II-alpha regulatory subunit	P13861	-1.2236
1573	Histone-binding protein RBBP4	Q09028	-1.2236
1580	Glutaminase kidney isoform, mitochondrial	O94925	-1.2558
1580	Pyruvate kinase isozymes M1/M2	P14618	-1.2558
1583	SWI/SNF-related matrix-associated actin-dependent regulator of chromatin subfamily E member 1	Q969G3	-1.0381
1583	Tubulin beta chain	P07437	-1.0381
1583	Serine/arginine-rich splicing factor 6	Q13247	-1.0381
1583	cAMP-dependent protein kinase type II-alpha regulatory subunit	P13861	-1.0381
1591	Pyruvate kinase isozymes M1/M2	P14618	-1.4774
1688	Septin-7	Q16181	-1.7378
1699	Pyruvate kinase isozymes M1/M2	P14618	1.2977
1738	DAZ-associated protein 1	Q96EP5	-1.9626
1738	Elongation factor 1-alpha 2	Q05639	-1.9626
1783	Flap endonuclease 1	P39748	-1.2501

Table S2: Continued.

spot no.	identified proteins	accession number	average ratio
Experiment 2			
1800	Actin, cytoplasmic 2	P36261	-1.3143
1911	Heterogenous nuclear ribonucleoprotein D0	Q14103	-1.2239
1913	Serine-threonine kinase receptor-associated protein	Q9Y3E4	1.2256
1950	Heterogeneous nuclear ribonucleoproteins A2/B1	P22626	-1.2348
1950	Replication factor C subunit	P40938	-1.2348
1979	Heterogeneous nuclear ribonucleoproteins C1/C2	P07910	-1.2041
1979	Glyoxylate reductase/hydroxypyruvate reductase	Q9UBQ7	-1.2041
1981	Annexin A2	P07355	-1.2043
1981	Casein kinase II subunit alpha	P19784	-1.2043
2001	Glyceraldehyde-3-phosphate dehydrogenase	P04406	-1.4635
2023	Ribonuclease H2 subunit B	Q5TBB1	-1.2017
2023	Heterogeneous nuclear ribonucleoprotein A1	P09651	-1.2017
2062	Guanine nucleotide-binding G(I)/G(S)/G(T) subunit beta 1	P62879	1.215
2062	Guanine nucleotide-binding G(I)/G(S)/G(T) subunit beta 2	P62873	1.215
2080	Serine/arginine-rich splicing factor 1	Q07955	1.2787
2087	Prohibitin-2	Q99623	1.2682
2128	Phosphatidylinositol transfer protein beta isoform	P48739	-1.4339
2128	Phosphatidylinositol transfer protein alpha isoform	Q00169	-1.4339
2128	S-formylglutathione hydrolase	P10763	-1.4339
2149	Cytochrome c-type heme lyase	P53701	1.3478
2149	Cyclin-dependent kinase 1	P06493	1.3478
2164	Proteasome assembly chaperone 2	Q969U7	-1.0069
2165	Translation initiation factor eIF-2B subunit alpha	Q14232	1.3218
2165	Actin-related protein 2/3 complex subunit 2	O15144	1.3218
2165	Glucosamine-6-phosphate isomerase 1	P46926	1.3218
2181	Complement component 1 Q subcomponent-binding protein	Q07021	-1.3724
2197	Putative elongation factor 1-alpha-like	Q5VTE0	-1.2226
2223	Peflin	Q9UBV8	1.2091
2223	Acidic leucine-rich nuclear phosphoprotein 32 family member B	Q92688	1.2091
2251	Galectin-3	P17931	-1.3358
2277	High mobility group protein B2	P26583	-1.0863
2284	Adenylate kinase 2	P54819	1.6237
2294	Protein NipSnap homolog 1	Q9BPW8	-1.211
2309	Eukaryotic translation initiation factor 4H	Q15056	2.6146
2311	Heat shock protein beta-1	P04792	1.6897
2311	NADH dehydrogenase [ubiquinone] iron-sulfur protein 3, mitochondrial	O75489	1.6897
2313	Heat shock protein beta-1	P04792	-2.8604
2329	Metaxin-2	O75431	-1.2695
2337	GrpE protein homolog 1, mitochondrial	Q9HAV7	-2.5753
2351	Translationally-controlled tumor protein	P13693	-1.2034
2361	Cysteine and glycine-rich protein 1	P21291	-1.279
2365	NADH dehydrogenase [ubiquinone] 1 beta subcomplex subunit 10	O96000	-1.7841
2373	Mps one binder kinase activator-like 1B	Q9H859	2.4766
2373	Rho GDP-dissociation inhibitor 2	P52566	2.4766
2374	Ubiquitin-40S ribosomal protein S27a	P62979	-1.3271
2374	Histone H2A type 1-H	Q96KK5	-1.3271
2374	Nucleophosmin	P06748	-1.3271
2376	40S ribosomal protein S3a	P61247	-1.3644
2430	Uncharacterized protein KIAA1143	Q96AT1	1.2517
2442	Cofilin-1	P23528	1.4223
2447	Sorting nexin-3	O60493	-1.176
2447	Sorting nexin-12	Q9UMY4	-1.176
2449	Destrin	P60981	1.3217
2455	Tumor necrosis factor alpha-induced protein 8-like protein 2	Q6P589	-1.404
2460	Nucleoside diphosphate kinase A	P15531	-1.3189
2461	Ubiquitin-conjugating enzyme E2 L3	P68036	-1.0153
2463	Eukaryotic translation initiation factor 5A-2	Q9GZV4	1.6478
2467	Stathmin	P16949	2.3271
2469	Stathmin	P16949	-1.4405
2489	60S ribosomal protein L22	P35268	-1.2124
2489	Dual specificity protein phosphatase 23	Q9BVJ7	-1.2124

Table S3: Proteins differentially regulated during necroptosis identified by MS analysis. For differential proteome analysis, in the first experiment magnetically enriched TNF-R1 containing vesicles of U-937 cells stimulated with TNF60-Fc/zVAD for 0 and 20 min were isolated without depletion of mitochondria and compared by 2D-DIGE. All differentially expressed protein spots were analyzed by means of MALDI-TOF/TOF. The mass spectrometric analysis identified 21 proteins with increased and 25 with decreased protein levels in the fraction of U-937 cells treated with TNF60-Fc/zVAD for 20 min. In the repetition (second experiment), prior to 2D-DIGE analysis, the magnetic TNF-R1 fractions stimulated as above were subjected to density-gradient centrifugation to avoid contamination with mitochondria. The protein spots were again analyzed by MALDI-TOF/TOF. The mass spectrometric analysis identified 6 proteins with increased and 4 proteins with decreased levels in the fraction containing TNF-R1 vesicles which were isolated from cells stimulated with TNF60-Fc/zVAD for 20 min. Positive values in average ratio mean increased amounts of protein levels after induction of necroptosis, compared to untreated samples. Negative average ratios indicate decreased protein levels after induction of necroptosis. The accession number for the reference sequence of each protein is listed. The 2D-DIGE experiment was performed with technical assistance of Melanie Nebendahl and Benjamin Schönbeck (Christian-Albrechts-University, Kiel, Germany). The mass spectrometry analysis of isolated proteins was performed by Tomas Koudelka (Christian-Albrechts-University, Kiel, Germany).

spot no.	identified proteins	accession number	average ratio
Experiment 1	*with mitochondria fraction*		
349	Hypoxia up-regulated protein 1	Q9Y4L1	1.4146
592	C-1-tetrahydrofolate synthase, cytoplasmic	P11586	-1.2063
601	Moesin	P26038	1.2082
714	Heat shock protein HSP 90-beta	P08238	1.4239
830	Ezrin	P15311	-1.2443
845	Moesin	P26038	-1.2421
922	Trifunctional enzyme subunit alpha, mitochondrial	P40939	1.2192
996	Plastin-2	P13796	-1.2863
1008	Plastin-2	P13796	-1.3026
1009	Plastin-2	P13796	-1.2483
1106	T-complex protein 1 subunit alpha	P17987	1.2315
1193	Catalase	P04040	-1.2924
1195	Catalase	P04040	-1.2491
1203	Calreticulin	P27797	1.0358
1272	Prenylcysteine oxidase 1	Q9UHG3	-1.217
1274	D-3-phosphoglycerate dehydrogenase	O43175	1.2025
1278	Tubulin beta chain	P07437	-1.4212
1280	Inosine-5'-monophosphate dehydrogenase 2	P12268	2.0197
1316	T-complex protein 1 subunit beta	P78371	1.204
1329	ATP synthase subunit alpha, mitochondrial	P25705	1.2206
1344	ADP-dependent glucokinase	Q9BRR6	1.1363
1354	Eukaryotic translation initiation factor 2 subunit 3	P41091	1.2255
1369	ATP synthase subunit beta, mitochondrial	P06576	1.2251
1371	ATP synthase subunit beta, mitochondrial	P06576	1.3572
1416	Actin-related protein 3	P61158	-1.2959
1440	Protein-disulfide-isomerase A6	Q15084	1.5891
1456	Protein-disulfide isomerase A6	Q15084	-1.4015
1478	Alpha-enolase	P06733	-1.6507
1567	Heterogeneous nuclear ribonucleoprotein K	P61978	1.2578
1598	Actin, cytoplasmic 2	P63261	-1.2056
1606	Actin, cytoplasmic 2	P63261	-1.3595
1607	Actin, cytoplasmic 2	P63261	-1.2551
1608	Actin, cytoplasmic 2	P63261	-1.3179
1681	Fructose-bisphosphate aldolase A	P04075	-1.2993
1775	Annexin A1	P04083	-1.8544
1821	Keratin, type II cytoskeletal 2 epidermal	P35908	1.0087
1821	Pyruvate dehydrogenase E1 component subunit beta, mitochondrial	P11177	1.0087
1821	Keratin, type II cytoskeletal 1 epidermal	P04264	1.0087
1829	L-lactate dehydrogenase B chain	P07195	-1.2598
1858	Guanine nucleotide-binding protein G(I)/G(S)/G(T) subunit beta-2	P62879	-1.3633
1883	Voltage-dependent anion-selective channel protein	P45880	-1.5461
1888	Prohibitin-2	Q99623	1.3515
1939	Annexin A4	P09525	-1.4519
1960	Prohibitin	P35232	1.3244
1965	D-beta-hydroxybutyrate dehydrogenase, mitochondrial	Q02338	-1.2161
2100	Keratin, type II cytoskeletal 2 epidermal	P35908	-1.5863
Experiment 2	*without mitochondria fraction*		
381	Catalase	P04040	-2.3861
589	Inosine-5'-monophosphate dehydrogenase 2	P12268	1.7859
710	D-3-phosphoglycerate dehydrogenase	O43175	1.677
836	Myosin-lg	B0I1T2	1.6536
1271	Protein-disulfide-isomerase A6	Q15084	-2.1127
1319	Septin-7	Q16181	1.6205
1333	Alpha-enolase	P06733	1.0232
1340	Alpha-enolase	P06733	-1.2494
1348	Alpha-enolase	P06733	1.015
1607	Annexin A2	P07355	-1.8261

9. List of publications

Parts of the presented doctoral thesis have been published previously:

Sosna J*, Voigt S*, Mathieu S, Kabelitz D, Trad A, Janssen O, Meyer-Schwesinger C, Schütze S, Adam D (2013) The proteases HtrA2/Omi and UCH-L1 regulate TNF-induced necroptosis. *Cell Commun Signal* 11, 76 (* authors contributed equally)

Voigt S, Philipp S, Davarnia P, Winoto-Morbach S, Röder C, Arenz C, Trauzold A, Kabelitz D, Schütze S, Kalthoff H, Adam D (2014) TRAIL-induced programmed necrosis as a novel approach to eliminate tumor cells. *BMC Cancer* 14, 74

Sosna J, Voigt S, Mathieu S, Lange A, Thon L, Davarnia P, Herdegen T, Linkermann A, Rittger A, Chan FK, Kabelitz D, Schütze S, Adam D (2014) TNF-induced necroptosis and PARP-1-mediated necrosis represent distinct routes to programmed necrotic cell death. *Cell Mol Life Sci* 71, 331-348

10. Eidesstattliche Erklärung

Hiermit erkläre ich, Susann Voigt, dass ich die vorliegende wissenschaftliche Abhandlung mit dem Titel:

„Induction, execution and clinical relevance of TNF- and TRAIL-induced necroptosis"

nach den Regeln guter wissenschaftlicher Praxis eigenständig verfasst und keine anderen als die angegebenen Hilfsmittel und Quellen benutzt habe. Dabei habe ich keine Hilfe, außer der wissenschaftlichen Beratung durch meinen Doktorvater Prof. Dr. rer. nat. Dieter Adam und durch die namentlich erwähnten Kooperationspartner in Anspruch genommen.

Diese Arbeit wurde bisher an keiner Stelle im Rahmen eines Prüfungsverfahrens vorgelegt. Teile dieser Arbeit wurden bereits publiziert.

Kiel, im Mai 2014

Susann Voigt

11. Danksagung

Besonderer Dank gebührt meinem Betreuer Prof. Dr. rer. nat. Dieter Adam für die Bereitstellung des interessanten Themas, für das Vertrauen und die Wertschätzung, die er mir in den vergangenen Jahren entgegen gebracht hat. Vielen Dank für die motivierenden und kritischen wissenschaftlichen Diskussionen im Rahmen dieser Zusammenarbeit, die maßgeblich zum erfolgreichen Voranschreiten des Projektes und meiner wissenschaftlichen Entwicklung beigetragen haben.

Herrn Prof. Dr. Dr. h.c. Thomas Bosch danke ich für seine Bereitschaft, die Begutachtung dieser Arbeit zu übernehmen und für seine Ratschläge für die Disputation.

Ebenfalls möchte ich dem Direktor des Institutes für Immunologie Prof. Dr. med. Dieter Kabelitz für die Möglichkeit danken, diese Arbeit anzufertigen. Weiterhin bedanke ich mich herzlich bei allen Mitarbeitern am Institut für Immunologie für die freundschaftliche Atmosphäre, sowie allen genannten Kooperationspartnern im Rahmen des Sonderforschungsbereiches 877.

Mein besonderer Dank gilt Parvin Davarnia und Sabine Mathieu, für ihre exzellente technische Unterstützung und die sehr gute Zusammenarbeit. Ein herzlicher Dank sei in diesem Zusammenhang auch an die jetzigen und ehemaligen Kollegen der Arbeitsgruppe von Prof. Dr. rer. nat. Dieter Adam gerichtet. Ihnen danke ich für die gute Atmosphäre, die wissenschaftlichen Dialoge und Unterstützung im Laboralltag.

Der gesamten Arbeitsgruppe von Prof. Dr. rer. nat Stefan Schütze, insbesondere Dr. Supandi Winoto-Morbach, Dr. Vladimir Tchikov und Dr. Jürgen Fritsch danke ich für die experimentelle Mitwirkung und Unterstützung im Rahmen dieser Arbeit. Meinen Arbeitskollegen und Freunden Dr. Bärbel Edelmann und Dr. Mario Stephan danke ich für ihre immerwährende Hilfe in allen Lebenslagen und ihre Unterstützung beim Korrekturlesen meiner Arbeit.

Besonders erwähnen möchte ich auch meine Kolleginnen und Freundinnen Susann Hüttl, Dr. Susanne Quabius, Henriette Ebsen und Dr. Josephine Tauer für die fruchtbaren wissenschaftlichen Gespräche und die großartige Unterstützung im Laboralltag und privat.

Im Rahmen dieser Doktorarbeit betreute ich unter anderem die Master-Arbeit von Meike Kähler und die Projekt-Arbeit von Jihyen Ha, denen ich hiermit für die Zusammenarbeit danken möchte.

Mein tiefer Dank gilt meiner Familie, meinen Eltern Steffi und René und meinem Freund Daniel, für ihre Liebe, ihr Vertrauen und ihren Rückhalt. Insbesondere danke ich meinen Großeltern Rosemarie und Walter, die den Verlauf dieser Arbeit immer mit Spannung verfolgt und ihr ganzes Vertrauen in mich gesetzt haben.

Vielen Dank.

12. Wissenschaftlicher Werdegang

Zur Person:

Name:	Susann Voigt
Wohnort:	Nußbaumkoppel 4 in 24119 Kronshagen
Geburtsdatum:	21. Februar 1987
Geburtsort:	Dresden
Staatsangehörigkeit:	deutsch

Promotion:

seit 11.2010	Promotions-Arbeit im Rahmen des Sonderforschungsbereich 877 („Proteolysis as a regulatory event in pathophysiology“) in der Arbeitsgruppe von Prof. Dr. Dieter Adam, Christian-Albrechts-Universität zu Kiel

Hochschulstudium:

03.2010 – 10.2010	Master-Arbeit zum Thema „Characterisation of TRAIL-induced caspase-independent programmed cell death in clinically relevant tumour cell lines“ in der Arbeitsgruppe von Prof. Dr. Dieter Adam, Christian-Albrechts-Universität zu Kiel
03.2009 – 10.2010	Master-Studium in Biotechnology (englischsprachig) an der Brandenburgischen Technischen Universität Cottbus-Senftenberg Abschluss: Master of Science
08.2008 – 02.2009	Bachelor-Arbeit zum Thema „Characterisation of TRAIL-induced caspase-independent programmed cell death“ in der Arbeitsgruppe von Prof. Dr. Dieter Adam, Christian-Albrechts-Universität zu Kiel
09.2005 – 02.2009	Bachelor-Studium der Biotechnologie an der Brandenburgischen Technischen Universität Cottbus-Senftenberg Abschluss: Bachelor of Science

Schulbildung:

08.1997 – 07.2005	Gymnasium Dresden-Cotta Abschluss: Allgemeine Hochschulreife
08.1993 – 07.1997	41. Grundschule Dresden